Decadal to millennial time scale climate variability in the Central Mediterranean during the Holocene:

a reconstruction based on geochemical proxies from high resolution sedimentary records

Utrecht Studies in Earth Sciences

No. 56

Promotor:

Prof. Dr. G.J. de Lange

Co-promotor:

Dr. G.J. Reichart

Members of the dissertation comitee:

Prof. Dr. J.B.M. Middelburg, Utrecht University.

Prof. Dr. L.J. Lourens, Utrecht University.

Prof. Dr. H. Brinkhuis, Utrecht University / Royal Netherlands Institute for Sea Research (NIOZ).

Prof. Dr. E. Bard, Collége de France, CEREGE Aix-en-Provence CNRS IR

Prof. Dr. F.C. Martínez-Ruiz, Granada University, CSIC.

Marie-Louise S. Goudeau

marielouise.goudeau@gmail.com

This research was funded by by the Nederlandse Organisatie voor Wetenschappelijk Onderzoek (NWO) as part of the MOCCHA- project funded by the European Science Foundation (ESF) Eurocores Programme EuroMARC.

ISBN: 90-6266-361-3

Printed by Wöhrmann Print Service Zutphen

Cover: Compilation of pictures of the Eastern Mediterranean Sea taken by participants of the Machiatto, Ristretto e Lungo and Cortado cruises.

Cover design and layout: M.S. Goudeau and M.Stoete

Decadal to millennial time scale climate variability in the Central Mediterranean during the Holocene:

a reconstruction based on geochemical proxies from high resolution sedimentary records

Klimaatfluctuaties met een tijdsduur van tientallen tot duizenden jaren in het Centrale Middellandse Zeegebied gedurende het Holoceen :

een hoge resolutie reconstructie gebaseerd op geochemische proxies in sediment- archieven

(met een samenvatting in het Nederlands)

Proefschrift

Ter verkrijging van de graad van doctor aan de Universiteit Utrecht op gezag van de rector magnificus, prof. Dr. G.J. van der Zwaan, ingevolge het besluit van het college voor promoties in het openbaar te verdedigen op woensdag 21 mei 2014 des middags te 2.30 uur

door

Marie-Louise Sophie Goudeau

Geboren op 14 oktober 1983

te Sapulpa, Oklahoma, Verenigde Staten van Amerika

Promotor:

Prof. Dr. G.J. de Lange

Co-promotor:

Dr. G.J. Reichart

I've looked at clouds from both sides now,
From up and down, and still somehow
It's cloud illusions I recall.
I really don't know clouds at all.

*'Both Sides, Now', Joni Mitchel**

**Joni Mitchel never lies. – 'Got 'Til It's Gone', Janet Jackson feat. Q-Tip*

Contents

Chapter 1: General Introduction and Summary

1.1 Future climate

Since the 1950s global temperature has risen, which is partly attributed to anthropogenic forced emissions of amongst others the greenhouse gas CO_2 (Stocker et al., 2013). With continuing emissions of such greenhouse gases, global climate models predict an ongoing increase of global temperature during the next few decades, which would inevitably lead to enhanced melting of continental ice sheets and major changes in precipitation patterns (Stocker et al., 2013). Pluvial events as well as extreme aridity will be more frequent during specific seasons and for distinctive regions. Although most models predict a comparable long-term trend, differences exist between 1) amplitude, 2) global trend and specific regions and 3) between simulations and observations on a decadal scale (Stocker et al., 2013). Insufficient comprehension of natural climate variability causes uncertainties in models. A better understanding of the natural climate background is needed to improve the quality of forecast of future climate.

Instrumental registrations of temperature and precipitation usually comprise not more than a century, and are not available for all areas. Studying natural variability on multi-decadal or longer time scales, therefore, demands for a more extensive kind of record of past climate variability. Sediments deposited in lakes, seas and ocean floor, accumulated ice from glaciers and ice sheets, corals and speleothems can all be used as archives of past climate variability on longer time scales. Reading such past climate archives, however, requires the use of so-called proxies. Proxies are measurable chemical or physical parameters of the sediments, ice, coral or speleothem, that are related to and that may represent the targeted environmental parameters such as temperature or precipitation (see 1.4). Reconstructions of past climate based on such archives have made clear that climate has varied considerably in the past. Even since the last major glaciation, when major continental ice sheets disappeared and therefore present-day boundary conditions prevailed, climate did not remain stable (e.g. Mayewski et al., 2004; Wanner et al., 2008, 2011). Comprehension of climate variability during this period (11,500 cal yr BP to the present), the Holocene, is vital for understanding future climate variability as it can be considered the natural background of today's climate, with similar boundary conditions as today.

1.2 From the Glacial into the Holocene, and Holocene climate variability

Climate variability on time scales of 20.000 to 400.000 yrs, such as the glacial/interglacial cycles, have been primarily related to regular changes in the Earth's axis and its orbit around the sun, the so-called Milankovitch cycles (Milankovitch, 1941). These

'Who am I to disagree? I traveled the world and the seven seas. Everybody is looking for something'
(Sweet dream are made of this; Eurytmics)

parameters have a high influence on the solar insulation received at the Earth's surface. The transition from the Last Glacial Maximum into the present Interglacial, the Holocene, was however, not gradual but rather stepwise. Melt water pulses originating from continental icesheets, during amongst others the Younger Dryas (Fairbanks, 1989, Bard et al., 2010) and the associated shutdown of the Atlantic thermohaline circulation resulted in cold and dry conditions in the Northern Hemisphere (e.g. Broecker et al., 1998, 2010; Alley et al., 2007). Intermittently, warmer conditions prevailed (e.g. Bølling-Allerød). After the last glacial, in response to the precession cycle, the so-called Inter Tropical Convergence Zone (ITCZ) moved to a more northward position in summer (e.g. Hilgen, 1991; Bosmans et al., 2011). The ITCZ is the zone where the Northern and Southern hemisphere Hadley cells collide. It is a low pressure zone, where rising air results in massive rainfall and release of latent heat (Fig. 1). The annual shift of the ITCZ between the tropics of Capricorn and Cancer underlies the monsoon. A more northward position of the ITCZ during boreal summer resulted in moist conditions in northern Africa from ~ 14.8 the 5.5 cal. ka BP (the African Humid Period (AHP), e.g. DeMenocal et al., 2000), tropical South America (Haug et al., 2001) and Asia (Reichart et al., 1998; Fleitmann et al., 2003, Wang et al., 2005).

During the Holocene several periods of rapid climate change (RCC) can be identified across the globe (Mayewski et al., 2004). Amongst these RCC events are the 8.200 yr event, Medieval Warm Period (MWP) and the Little Ice Age (LIA). Although these RCC events are not of the same amplitude as the Glacial/Interglacial transition, on a regional scale their impact is considerable. Asynchronous expression of these abrupt events has been explained by variance in atmospheric circulation patterns.

Whereas moisture transport at low latitudes is related to the ITCZ, the moisture-rich westerlies control precipitation patterns on the European mainland (Fig. 1, e.g. Hurell et al., 1995). Variance in the pathway of the westerlies is closely linked to the North Atlantic Oscillation (NAO, Hurell et al., 1995). The NAO index is defined as the atmospheric pressure difference between the subpolar Icelandic low (IL) and the subtropical Azores high (AH). When the NAO is in a positive mode, (NAO+ , a large difference between IL and AH) , the westerlies are blocked and deflected to the north, causing cold and warm conditions in northern Europe (Fig. 1). During a negative NAO mode (NAO-) the westerlies bring more moisture to southern Europe, resulting in more humid climate conditions for that region. Climate in the polar region is related to variability in the Arctic Oscillation (AO, Fig. 1). A positive mode of the AO (AO+) exist when there is a relatively high pressure zone between ~37° and -45°N and a relatively low pressure zone over the polar region. During the opposite pressure difference a negative AO mode (AO-) prevails. When in a positive mode, colder conditions prevail in the Arctic, while during an AO- the potential for outbreaks of cold air to northern America, Europe, and Asia is enhanced (Fig. 1, e.g. Thompson et al., 1998).

During most of the RCC events polar cooling and tropical aridity indicates that variance in these atmospheric patterns are drivers for climate variability (Mayewski et al., 2004). This was not restricted to the poles and tropics, but also extended into the mid-

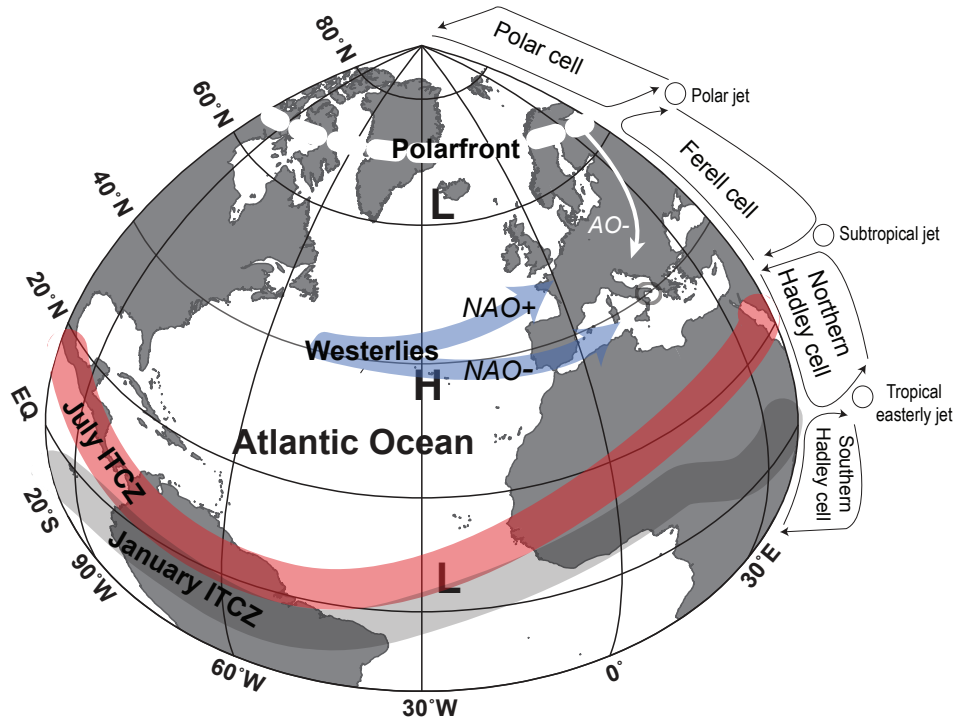

Fig. 1: Atmospheric circulation patterns in the Northern Hemisphere influencing the study area. AO-= negative Arctic Oscillation, NAO= North Atlantic Oscillation, NAO- is the negative mode, NAO+ the positive mode. ITCZ stands for Inter Tropical Convergence Zone.

latitudes. For example, the transition from the wet and warm MWP to the cold and dry LIA in northern Europe is attributed to a shift from a persistent NAO+ to a more NAO- during the LIA (Mann et al., 2009; Trouet et al., 2009). Denton et al., (2005) suggested that cooling at higher latitudes was restricted to the winter season. Although not affecting the interannual variability in climate, it would have affected the seasonal contrast severely. The changes in atmospheric circulation patterns, and associated regional climate variability are suggested to have had a profound impact on human civilisation (e.g. Zhang et al., 2011). A centennial time scale southward shift of the ITCZ and the associated extreme aridity is coherent with the collapse of the Maya civilisation (Haug et al., 2003). Similarly, the demise of the Western Roman Empire and the turmoil of the migration period coincided with a relatively wet period in northern and central Europe (Büntgen et al., 2011). However, it is still heavily debated what exactly drives climate change at decadal to millenial time scales (Mayewski et al., 2004; Wanner et al., 2008).

Solar variability is one of the possible drivers of climate variability on centennial time scales (e.g. Bard and Frank, 2006; Gray et al., 2010). The amount of solar irradiance is correlated to the occurrence of so-called sun spots. The more sun spots, the higher the Total Solar Irradiance (TSI). Irregular cycles of ~11 yr, but also of multidecadal and

centennial periods, of varying sunspots have been recognised (Gray et al., 2010). The LIA, for example, was concomitant with a centennial period of low solar irradiance, the so-called Maunder minimum. Numerous paleoclimate studies indicated changes in solar irradiance as a major forcer of climate change, although its direct contribution to the global heat budget is minor (<1 %, e.g. Bard and Frank, 2006). However, changes in UV light are large (~10%), which may have had a pronounced effect on the lower stratosphere. Positive feedback mechanisms as cloud formation, affecting atmospheric patterns, may subsequently lead to a more significant impact on regional climate variability (Gray et al., 2010).

Also changes in heat budget of the Atlantic and Pacific Ocean played a major role in shaping Holocene climate variability (e.g., Wanner et al., 2008). During years of relatively warm surface waters of the Pacific Ocean, so-called El Niño years, major flooding occurs in the Andes, while major droughts impacts Australia. However, it has been shown that patterns in Pacific sea surface temperatures (SSTs) known as El Nino Southern Oscillation (ENSO) through teleconnections could also have a global impact (e.g. Diaz et al., 2001). In the Atlantic Ocean another oscillation of SST patterns has been recognised, the Atlantic Multi-decadal Oscillation (AMO). The AMO has a typical periodicity of about 70 years and has been invoked to explain changes in amongst others Sahel drought, i.e. ITCZ dynamics (Kerr et al., 2000; Knight et al., 2000, Shanahan et al., 2009). Its impact on higher latitude atmospheric patterns of the NAO, however, appears less straightforward (Hurrel et al., 1995, Hoerling et al., 2001, Sutton and Hudson, 2003, Knudsen et al., 2011).

1.3 Sediments from the Central Mediterranean sea as a climate archive

Unravelling the many unknowns in extent of climate variability on decadal to millennial time scales and possible forcing requires paleo-records from areas sensitive to changes in atmospheric climate patterns and that allow a high temporal resolution (~10 years). The Mediterranean Sea is located on the boundary between tropical and mid-latitude climate zones (Fig. 1). In summer, the Mediterranean region is dry as a result of the northward extension of the high pressure zone of the Hadley cell (Alpert et al., 2006 and references therein). A more southward position of the Hadley cell in winter, allows the moisture-rich westerlies to enter the Mediterranean region, leading to humid winters during NAO- modes (Trigo et al. 2006 and references therein). Winter temperatures in the Adriatic and Aegean region regularly drop as a consequence of outbreaks of cold, polar air from the north, the so-called Bora winds (Theocharis and Georgopoulos, 1993, Poulos et al., 1997) .In summary, Mediterranean climate variability is linked to high- and low- latitude atmospheric circulations patterns. This region is, therefore, ideal for Holocene climate studies.

Sensitivity of the Eastern Mediterranean to both high- and low- latitude climate variability is probably best demonstrated by the typical repetitive occurrence of distinct

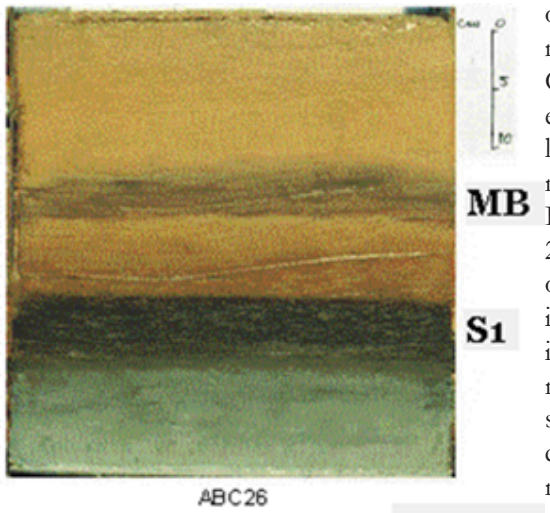

Fig. 2: Typical organic rich layer of Sapropel S1. S1=sapropel S1, MB= Manganese layer. (Picture from core ABC 26, courtesy of Gert J. de Lange)

organic-rich black layers in its sediments, the so-called sapropels (Fig. 2, Olausson, 1961, Hilgen, 1991; Lourens et al., 1996; Marino et al., 2009). The latest sapropel was formed synchronously with a northward shift of the ITCZ, the AHP (e.g. De Lange et al., 2008). A more northward placement of the ITCZ increased precipitation in the Nile catchment area, increasing its discharge into the Mediterranean. Increased Nile discharge, possibly accompanied by increased river discharge from other southern and northern borderlands into the Mediterranean, presumably resulted in substantially increased primary productivity (PP) and/or decreased ventilation (Olausson, 1961; Rohling and Hilgen, 1991; Emeis et al., 2000; Thomson et al., 2004; De Lange et al., 2008; Gallego-Torres et al., 2010). High PP and low ventilation resulted in oxygen-free bottom water, thus encouraging preservation of organic matter. These conditions have been interrupted during the 8.2 kyr event, which divides sapropel S1 into two parts S1a and S1b. This 8.2 kyr event is generally assumed to be related to increased outbreaks of cold winds from the north (Bora) over the Adriatic and Aegean Seas (e.g. Rohling et al., 1997; De Rijk, et al., 1999; Marino et al., 2009). These regions are instrumental for Eastern Mediterranean deep water formation. Cooling of surface waters in these regions could have enhanced convective turnover, and subsequently have lead to a more ventilated Eastern Mediterranean.

Most areas in the Mediterranean Sea, however, are characterized by low sedimentation rates and, therefore, do not record climate variability at a sufficiently high resolution for centennial or multi-decadal studies. The Adriatic mudbelt is an exception (Fig. 3). Rivers draining the Italian hinterland, of which the Po River is the largest, bring high sediment loads to the Adriatic Sea (Trincardi et al., 1994; Raicich, 1996; Cattaneo et al., 2003; Frignani et al., 2005; Syvitski and Kettner, 2007;). The anti-cyclonic circulation in the Adriatic Sea pushes the discharged water into a small relatively fresh water band, the West Adriatic Current (WAC), which can be located southwards all the way into the Gulf of Taranto (Fig. 3, Poulain et al., 2001). This WAC disperses the high sediment loads forming a narrow mudbelt, leading to high sedimentation rates in the study area. Cores taken from this area, therefore, have a sufficient resolution for detailed Holocene paleoclimate studies (e.g. Cini Castagnoli et al., 1992a,b, Versteegh et al., 2007, see **chapter 2**). The region is essential for Eastern Mediterranean deep water formation and possible changes in ventilation should be reflected in its sediments. Sediments at the end of

the WAC plume originate from locations spread across the entire Italian peninsula and thus capture supra regional on-land climate variability (Fig. 3). Previous studies from the Gulf of Taranto, covering the last 2000 years, suggest short-time scale climate variability, possibly correlated to changes in TSI (e.g. Cini Castagnoli et al., 1992a,b; Versteegh et al., 2007). Although these sediments are ideal for high resolution paleoclimate studies, sediment pathways in the southern Adriatic and Gulf of Taranto are insufficiently known, in contrast to the Northern Adriatic (Faganeli et al., 1994; Buccolieri et al., 2005, 2006; Spagnoli et al., 2010; Perri et al., 2012). A better understanding of sediment dispersal processes is necessary for reliable geochemical-based reconstructions of past

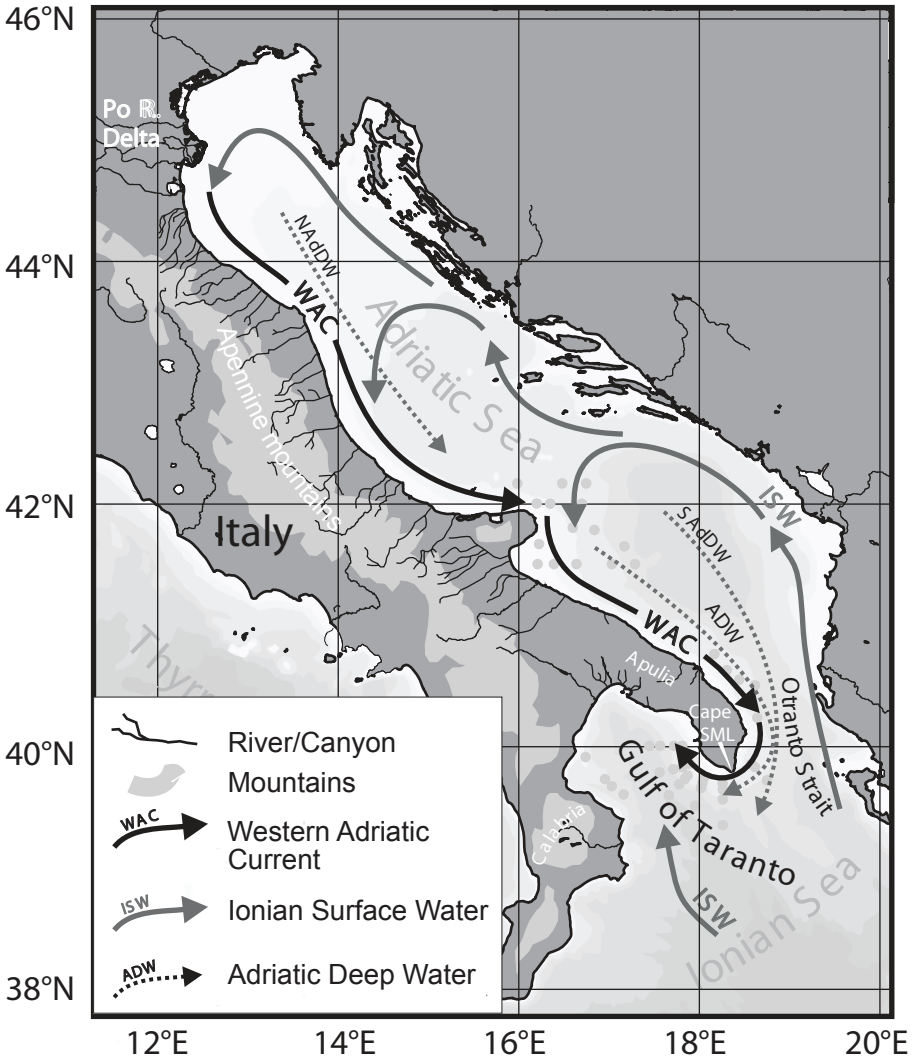

Fig. 3: Map of the area studied in this thesis (Adriatic Sea, Ionian Sea and Gulf of Taranto) and the most important rivers and currents.

circulation in this region and thus of past climate at a larger scale (see **chapter 2, 3**).

1.4 Geochemical proxies of environmental variability

1.4.1 Geochemistry, grainsize and colour of sediments

The elemental composition of sediments depends on the origin of the deposited sediments, the environment in which they accumulated, and potential early diagenetic modifications (for trace elements in particular) that may have occurred. Sediments have initially been eroded from a certain source rock and have subsequently been transported by rivers or wind before they finally settle. The geochemical composition of the sediments accumulated at any site, therefore, contains original source rock information: if the elemental composition of possible sources is known, then potentially the provenance of marine sediments can be identified. Environmental conditions during weathering and transport may modify the initial provenance signature. Sediments eroded under more humid conditions have a different chemistry than those eroded under more arid conditions. For example, the K/Al ratio of the sediments can be used to indicate relative humid conditions (Bonatti and Gartner, 1973, Yarincik et al., 2004), while Ti/Al and Zr/Al ratios can indicate dust (Wehausen and Brumsack, 2000). Different transportation mechanisms have different energetic conditions, which underlie particle size fractionation of the sediments carried. As some minerals erode easier than others, the elemental composition differs between sand, silt and clay particles. Sediment samples consisting of mostly sand generally have elevated quartz content and thus high Si values. Hence, for an accurate use of the elemental composition as a proxy for climate change some knowledge of the effect of grainsize is needed. Part of the sediment is produced also in the sea itself. Increased PP in the surface waters brings high amounts of organic carbon, carbonate, and opal to the seafloor. Preservation of organic carbon depends not only on this flux, but also on the amount of oxygen available at the sea floor. Anoxic conditions enhance the potential preservation of organic matter, which can result in distinctive black laminations. Past changes in anoxia, can be detected by the pattern in redox sensitive elements as vanadium (V) and Molybdenum (Mo) in the sediments (e.g., Calvert and Pederson, 1993). As organic matter is usually darker than the more carbonate-rich, organic-poor sediments, changes in colour can also be applied as proxies for changes in PP or anoxia. Past changes in provenance, river discharge and dust transport, primary productivity and anoxia, are all impacted by changes in climate. Hence, if we know the elemental composition of our sediments and we understand the different pathways leading to their deposition, then these can be used to reconstruct past climate change.

To determine sediment elemental composition, a variety of methods exists. Discrete samples are analysed using, for example, Inductively Coupled Plasma-Atomic Emission Spectroscopy (ICP-AES), which is the most reliable and traditional method (Hennekam and de Lange, 2013; see **chapters 2-6;**). X-ray fluorescence (XRF) core scanning is non-destructive and less time consuming (e.g. Tjallingi et al., 2007, see **chapter 3**). For

this method, the flat surface of core sediments is excited with X-rays, after which the characteristic fluorescent X-rays emissions are used to determine the elemental composition. This rapid method, however, is considered semi-quantitative, and possible absorption by a water film on top of the sediments may affect some elements, mainly the lighter ones such as aluminium (Tjallingi et al., 2007; Weltje and Tjallingi, 2008; Hennekam and De Lange, 2013). These limitations have to be taken into consideration when applying this method for paleo-climatic studies.

For higher resolution studies, sediments frequently need to be analysed for their elemental composition on intervals spanning less than a millimetre. For such studies, discrete sampling and XRF core scanning are not an option. Resin embedded blocks from the sediment, however, can be studied using Laser ablation ICP-MS (LA-ICP-MS) and μXRF mapping (e.g. Haug et al., 2003; Jilbert et al.,2008, Jilbert et al., 2010a,b; see **chapter 6**). These novel techniques allow investigating elemental compositions on a millimetre and even micrometre scale, ideal for high resolution paleoclimate studies. For LA-ICP-MS the embedded block is placed in a vacuum chamber on a moving stage. While moving, it is targeted with a laser beam, allowing closely spaced analysis. The ablated sediments are subsequently transported to an ICP-Mass spectrometer (ICP-MS) on a He carrier gas, before being mixed with Ar to analyse major and minor elements. For μXRF the same principal is used as for XRF-core scanning, but with a spatial resolution that is orders of magnitude higher. As the sediments are embedded in blocks, the analysis is not affected by the formation of a possible water film on top of the sediments. The high spatial resolution makes it possible to create high resolution maps, creating a 2D elemental concentration picture of the sediments in which the chemical differences between but also within laminations can be made visible.

1.4.2 Foraminiferal test chemistry

Part of the carbonate flux to the sea floor consists of shells of foraminifera. Foraminifera (Protista) are single-celled organisms, occupying a wide variety of habitats in the marine realm. Planktonic foraminifera (Fig. 4a) are found in the water column while benthic foraminifera (Fig. 4b) live near the sediment water interface, and even within the sediments. A large group of foraminiferal species 'build' an external test around their cell, that consist of sediment particles (agglutinated foraminifera), organic compounds (allogromid foraminifera) or calcium carbonate (calcareous foraminifera). During the calcification process, calcareous foraminifera also incorporate trace elements and oxygen and carbon isotopes into their test. The uptake of these elements by the foraminifera and the degree of incorporation into the test depend on environmental variables as nutrient availability, seawater isotope values, temperature and salinity. Hence the chemical composition resulting from analyses of the test can be used as a proxy for past environmental conditions.

The oxygen isotope composition of the foraminferal test depends on the oxygen isotope composition of the sea water under which it calcifies, and can therefore be applied as a proxy for temperature (Emiliani, 1954, Shackleton, 1967). The oxygen isotope

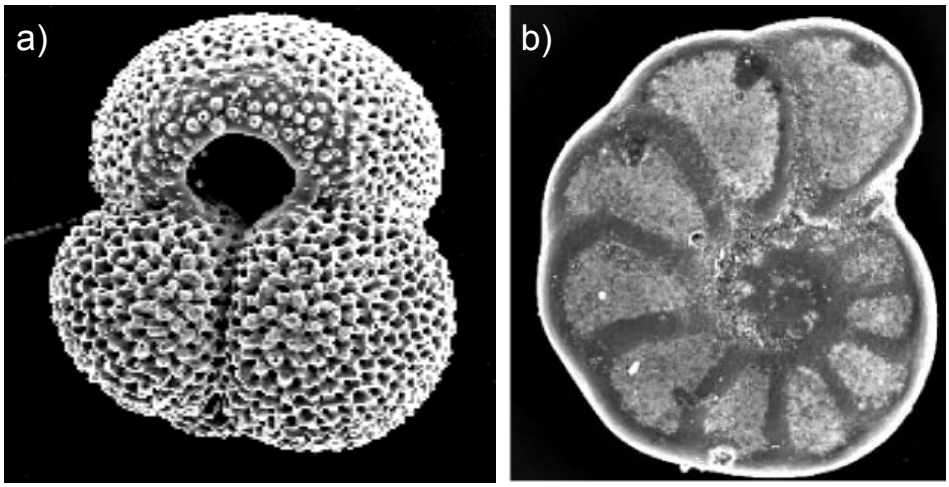

Fig 4: Two species of foraminifera:
a) Fossil test of Globigerinoides ruber, a planktonic foraminifer.
b) Fossil test of Hyalinea balthica, a benthic foraminifer
(source : http://palaeo-electronica.org/2002_2/guide/rota.htm).

composition itself depends on environmental conditions as evaporation and salinity. In the region studied in this thesis, changes in salinity, and thus sea water oxygen isotope composition, occur as the influence of the low-saline WAC varies. This influence is clearly visible in the oxygen isotopic analysis on the fossil tests of *Globigerinoides ruber* (white) (Fig. 4a) retrieved from core top samples in the study area (Grauel and Bernasconi, 2010). Not only the oxygen isotopes of *G. ruber* (white) depend on changes in the influence of the WAC, also the carbon isotope test chemistry is affected. When the WAC increases, more nutrients are brought to the region, causing high PP. Under a high PP, light conditions are reduced, which restricts the photosynthesing symbiont carrying *G ruber* (white) to the upper water column. The higher PP in the upper surface waters affects tand the lower light intensities effect the carbon isotope composition of the sea water and symbiontactivity and, therefore, also that of the foraminferal test which calcifies higher in the water collumn.

Besides the isotopic composition of the test also its trace elemental composition can be used as a proxy. Mg/Ca test chemistry of foraminifera has been successfully correlated to temperature (e.g. Elderfield and Ganssen, 2000, Anand et al., 2003). In 'normal' calcareous foraminifera this correlation is less steep than for the Mg-rich test of *Hyalinea balthica* (Rosenthal et al. 2011; Fig. 4b).This steep correlation implies that small changes in temperature have a large effect on test chemistry of *H balthica*. As annual changes in temperature are relatively minor during the Holocene, this sensitivity makes *H. balthica* ideal to reconstruct Holocene climate variability (See **chapter 4, 5**). In recent years, LA-ICP-MS made it possible to determine the Mg/Ca of a single specimen of foraminifera (Reichart et al., 2003). Studying the chemistry for a suite of single foraminiferal tests from within the same sample allows the reconstruction of seasonality, provided that the species used for this analysis produces carbonate test throughout the year. Wit et al.

(2010) showed that seasonality can be reconstructed in the Mediterranean Sea using *G. ruber* (white) specimens (see **chapter 5**). Moreover, after LA-ICP-MS elemental analysis, the same individual can be analysed for its isotopic contents. This allows the reconstruction of the past seawater stable oxygen isotopic composition. This derived stable oxygen isotopic seawater composition can then be applied to reconstruct paleo-salinity. However, the error of the Mg/Ca based temperatures and the variety of other environmental parameters affecting oxygen isotopes of seawater can lead an accumulation of errors (Schmidt et al., 1999, Rohling, 2000). To reduce the accumulation of errors, a recently introduced direct proxy for salinity, the Na/Ca values of the foraminifer's tests, can be used (Wit et al., 2013, **chapter 4**).

1.5 Objectives and summary

In this thesis decadal to millennial and seasonal Holocene climate variability has been reconstructed for sediments from the Southern Adriatic and Gulf of Taranto using a multi-proxy geochemical approach. This multi-proxy approach combines the results from the chemical composition, grainsize and colour of the sediments with test chemistry of foraminifera. Understanding of this variability will improve comprehension of changes in climate patterns from high- and low-latitudes during rapid climate change events.

To do so, first more knowledge is needed on present provenance and sediment pathways in the studied areas. In **chapter 2** pathways and provenance are discussed on the basis of surface samples from the southern Adriatic and Gulf of Taranto and a variety of samples from the Italian rivers and lakes while integrating a variety of proxies. The elemental composition of the sediments indicates that Ce/Ni and Zr/Cr are valuable provenance indicators, independent of grainsize. The origin of organic matter is determined using bulk carbon isotopes and the C/N ratio. Integrating these results with those from complementary studies reveals that:

- Sediments from the northwestern Adriatic are transported as far southward as the Gallipoli shelf (eastern Gulf of Taranto) by the Western Adriatic Current (WAC);
- Along the WAC, there is a consistent southward decrease in Po River / northern Apennines provenance and a concomitant decrease in terrestrial (soil) organic matter (OM), whereas the percentage of marine OM increases;
- The provenance for Gallipoli shelf sediments is for ~80% attributed to Po River / northern Apennines sources and for ~20% to southern Italian sources;
- OM in the eastern Gulf of Taranto contains more marine OM than other areas within the WAC, whereas OM and sediments from the western part of the Gulf of Taranto have a more local, riverine provenance;

To understand more about the sediment transport mechanism and its evolution over time an extensive, high-resolution, sedimentological-geochemical survey is presented in **chapter 3**. For this purpose the sediments from 11 cores from the Gulf of Taranto, the southern Adriatic Sea, and the central Ionian Sea spanning the last 16 cal. ka BP were studied using geoacoustics, XRF-core scans, ICP-AES, AMS ^{14}C-dating and grain size analyses. Although sedimentation rates and composition appear to be rather different between regions, comparable results were obtained for cores from the Gallipoli shelf (eastern Gulf of Taranto), and the southern Adriatic Sea. This implies, in line with results from **chapter 2**, that the Gallipoli Shelf sediments have a similar origin as sediments within the western Adriatic mud belt. The sedimentary composition along with AMS ^{14}C-dating was used for a stratigraphic framework to accurately correlate and date the cores of Gallipoli Shelf. Subsequently, the Glacial/Interglacial transition and Holocene environmental variability was reconstructed using the elemental composition. This reconstruction suggests that:

- A warm interval during the late Younger Dryas is characterized by sediments from a more southern origin suggesting increased precipitation in southern Italy, in contrast to northern Italy.

- Coincident with the end of sapropel formation, sea level rise and the onset of deep water formation in the Adriatic Sea, detrital input from an Adriatic mud belt provenance is found in the Gulf of Taranto at approximately ~7 cal. ka BP.

- Millennial scale events of increased detrital input concording with a more negative NAO mode are found during the mid-to late Holocene

In **chapter 4** the elemental composition of Gallipoli sediments is combined with the carbonate test chemistry of the planktonic foraminiferal species *Globigerinoides ruber* (white) and the benthic foraminifer *Hyalinea balthica* for a full palaeoclimatic reconstruction. Carbon isotope test chemistry of *G. ruber* (white) primarily records summer conditions and thus can be used as a proxy for shifts of the Hadley cells, and therefore the ITCZ. In contrast, the Na/Ca of *H. balthica* reflects salinity variability during winter and thus reflects the NAO. Similar centennial scale variability is found in records of the test chemistry of *G. ruber* and *H. balthica*. It is shown that the coupling between the reconstructed high and low latitude centennial climate variability alternates. During periods of high North Atlantic SST and/ or ENSO activity a periodicity of ~70 yr, similar to the characteristic period of the AMO, appears in the NAO reconstruction. As shifts in the summer ITCZ are assumed to be continuously linked to variability of the AMO, this implies that during these events both NAO and the ITCZ were driven by changes in Atlantic SST.

In **chapter 5** the test chemistry (Mg/Ca, δ^{18}O and δ^{13}C) of individual *G. ruber* is used to reconstruct seasonality in the Gulf of Taranto. This method is applied on samples from selected depth intervals, coinciding with the Bronze Age (BA), Roman Humid Period (RHP), MWP and LIA. These results are combined with high resolution (<15yr/

sample) SST reconstructions based on average *G. ruber* $\delta^{18}O$ and *H. balthica* Mg/Ca, shown to reflect summer and winter SSTs respectively. Precipitation seasonality during the last 3500 years is larger than variability in the seasonal temperature contrast. Still, winter cooling is observed during the BA and LIA. During the BA, winters are dry and accompanied by hot and dry summers, which results in a large range in temperatures and year-round aridity. In contrast, the LIA is characterised by wet and cool, winter like conditions throughout the year.

In **chapter 6** a high-resolution record from a finely laminated (~1 mm) sapropel (S1) from the Southern Adriatic Sea is presented. The core was retrieved from a water depth of 565 m, close to the critical upper depth for sapropel formation during S1. The combination of high sedimentation rates, proximity to the redox cline, and the generally laminated sediment fabric allow investigating short timescale variability in sediment geochemistry. Using high resolution geochemical techniques such as Laser Ablation-ICP-MS, μXRF and Scanning Electron Microscopy (SEM) we characterise the composition of the laminations and infer the environmental conditions responsible for their formation. We then constructed a continuous high-resolution grayscale record. Based on correlation between colour and the redox sensitive geochemical proxy V and the occurrence of framboidal shaped pyrites, this record is used to reconstruct past variance in water column oxygen depletion. A comparison with regional and global climate records of comparable resolution reveals that decadal modulations of anoxia during sapropel S1 formation occurred when outbreaks of cold air initiated convective turnover, and associated water column ventilation.

Chapter 2: Provenance of surface sediments along the southeastern Adriatic coast off Italy: an overview

Marie-Louise S. Goudeau, Anna-Lena Grauel, Stefano M. Bernasconi and Gert J. de Lang

(Published in: Estuarine, Coastal and Shelf Science 134, 45-56)

Multi-proxy studies are necessary to understand sediment composition and related provenance on continental shelfs. Here it is shown that the spatial distribution of geochemical composition and grain size for surface sediments along the southeastern Italian coast is related to provenance and mechanisms influencing sediment pathways. A northern Adriatic/Italian provenance can be distinguished from a southern Apennine River source. This is done independent of grain size using the element ratios Ce/Ni and Zr/Cr. Furthermore, the origin of organic matter is determined using bulk carbon isotopes and the C/N ratio. Integrating these results with those from complementary studies on $\delta^{18}O$ and $\delta^{13}C$ of *Globigerinoides ruber* (white), the BIT index, stable isotopes of plant waxes and dinoflagellate cyst distribution from the same set of samples reveals that:

- Sediments from the northwestern Adriatic are transported as far southward as the Gallipoli shelf (eastern Gulf of Taranto) by the Western Adriatic Current (WAC)
- Along the WAC, there is a consistent southward decrease in Po River / northern Apennines provenance and a concomitant decrease in terrestrial (soil) organic matter (OM), whereas the percentage of marine OM increases.
- The provenance for Gallipoli shelf sediments is for ~80% attributed to Po River / northern Apennines sources and for ~20% to southern Italian sources
- OM in the eastern Gulf of Taranto contains more marine OM than other areas within the WAC, whereas OM and sediments from the western part of the Gulf of Taranto have a more local, riverine provenance
-

1. Introduction

High sedimentation rates in the Gulf of Taranto make this an excellent region for high resolution paleoclimate reconstructions (e.g., Cini Castagnoli et al., 1992a; **chapter 3**). Downcore geochemical elemental and isotope compositions, and grain size have been successfully used as tools in reconstructing past variations in sedimentation and primary productivity in the Mediterranean Sea (e.g. De Lange et al., 1999; Jilbert et al., 2010a; Nieto-Moreno et al., 2011). To fully understand variability in the past, it is necessary to recognise how geochemical elemental, isotope compositions, and grain size are affected by sediment transportation pathways and dispersion mechanisms in the present.

The cyclonic circulation of the surface water and associated particulate matter in the Adriatic Sea has resulted in a narrow band of southward flowing water (Western Adriatic Current, i.e. WAC) and mud belt, that is predominantly influenced by discharge from Po River, Adige- and Apennine Rivers (see below: 3. Study Area, Fig. 1). The sediment load (~39 to ~43 Mt/yr in total) of these rivers, with the Po River (13 Mt/yr) and northern Apennine Rivers (22 Mt/yr) as the main contributors, form the base of the Adriatic mud belt which has been reported to extend from the Po River down to south of the Gargano promontory (Trincardi et al., 1994; Cattaneo et al., 2003; Syvitski and Kettner, 2007). From the rivers south of the Gargano promontory, continental outputs are mostly transported by the Ofanto River, the largest of all southern rivers (Cattaneo et al., 2003). Most of the coarse fraction of Po and other river sediments settles close to the river mouth. During storm events, some of these coarse sediments are transported further southward by the WAC (Cattenao et al., 2003), in particular in winter/ spring when the WAC reaches maximal flow rate and volume, concomitant with maximal river discharge (Poulain, 2001; Sellschopp and Alvarez, 2003). In total approximately $4.6*10^6$ t/yr of sediment of central/northern Adriatic provenance is transported to the southern Adriatic (Frignani et al., 2005).

Dispersal of sediments in these fine grained systems is rather complex, in particular, on a spatial scale due to processes such as re-suspension by bottom currents (e.g., Trincardi et al., 2003; Fain et al. 2007). A better understanding of the dispersal on a spatial scale not only leads to a better comprehension of variations in the past, but also improves our knowledge of sediment pathways from source to sink in fine grained sedimentary systems in general. The latter is of high importance to determine the impact of e.g. the building of sediment barriers, the fate of pollutants from agriculture and industrial waste associated with sediments and organic matter that are transferred to the ocean (e.g., Dolenec et al., 1996; Trincardi et al., 2003). Studies on the geochemistry of core top samples have been successful for reconstructing the spatial provenance not only in the northern and central Adriatic (Amorosi et al., 2002; Dinelli et al., 2007; Weltje and Brommer, 2011) but also offshore other major delta systems such as the Amazon (Vital and Stattegger, 2000), Mississippi (Piper et al., 2006), Pearl River (Qi et al., 2010) and Yellow River (Yang et al., 2006). Additionally, 80% of the burial of organic carbon occurs on continental margins (Berner, 1989; Hedges and Keil, 1995). Hence, for a full comprehension of the global carbon cycle, understanding the fate of organic matter

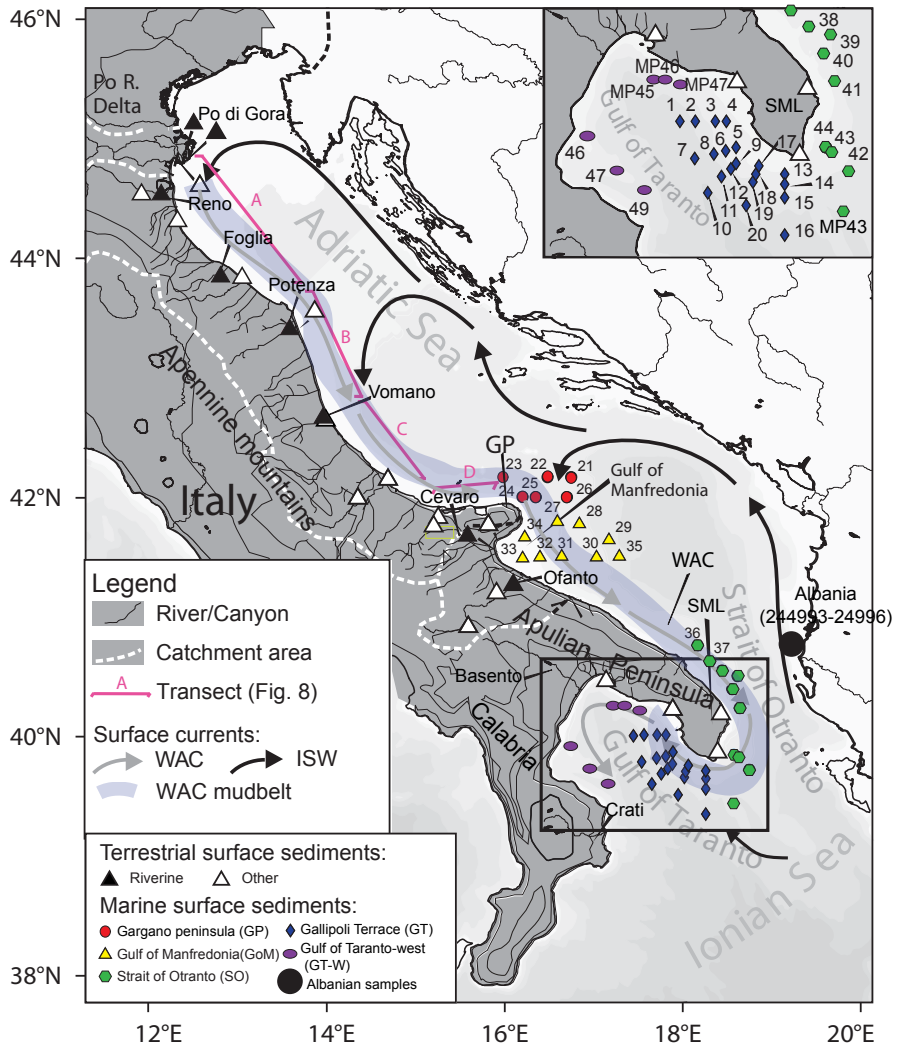

Fig. 1.: Oceanographic setting of the area (WAC = West Adriatic current, ISW = Ionian surface waters, GP= Gargano peninsula, SML= Santa Maria di Leuca). Core locations of all samples are indicated as well as the different marine regions and transects indicated in Fig. 8 (A=Po prodelta, B =Po prodelta-Ancona, C=Ancona-P. Penna, D= P. Penna-Gargano pit) (after Leider et al., 2013).

on continental shelves is essential. In the Adriatic Sea, the WAC is the main supplier of nutrients and, therefore, has a major effect on primary productivity along the western Adriatic shore (e.g., Boldrin et al., 2002; Morovic et al., 2006) and the Gulf of Taranto (Zonneveld et al., 2009; Grauel and Bernasconi, 2010; Leider et al., 2010). In general, waters of the southern Adriatic Sea are more oligotrophic than those of the northern Adriatic Sea (e.g., Civitarese et al., 1998). In winter / early spring, surface water cooling in the Adriatic Sea enhances vertical mixing bringing nutrients from deeper waters to the euphotic zone stimulating primary productivity (Boldrin et al., 2002).

In contrast to the northern and central Adriatic Sea, studies on sediments and OM dispersal from the southern Adriatic Sea and Gulf of Taranto are restricted to limited areas and single parameters (e.g., Faganeli et al., 1994; Buccolieri et al., 2005, 2006; Spagnoli et al., 2010; Perri et al., 2012). Hence, dispersal patterns of OM and sediments transported by the WAC beyond the Gargano peninsula remain largely unknown (Spagnoli et al., 2010). Studies in the northern and central Adriatic Sea have shown the importance of grain size for bulk geochemistry and for the C/N ratio of organic matter (OM) (Faganeli et al., 1994; Spagnoli et al., 2008). Furthermore, it has been reported that it is difficult to determine different provenances based on geochemical composition alone (Weltje and Brommer, 2011). Hence, combining geochemistry with grain size is important for this region. In addition, geochemical elemental and isotope compositions, and grain size distribution integrated with work on other parameters will result in a better comprehension of provenance for sediments in a complex continental shelf area as the Adriatic Sea (Spagnoli et al., 2010).

Such an integrated approach is used in this study using a large set of samples recovered from Italian rivers and lakes, and marine core-top samples from the south Adriatic Sea and the Gulf of Taranto. Not only results and interpretations based on elemental and isotope composition and grain size analyses are reported but these are also integrated with the most relevant results based on $\delta^{18}O$ and $\delta^{13}C$ of *G.ruber* (white) (Grauel and Bernasconi, 2010), BIT index (Leider et al., 2010), stable isotopes of plant waxes (Leider et al.,2013) and dinoflagellate cysts (Zonneveld et al., 2009) from the same set of samples so as to get a full understanding of sediment sources and transport pathways.

2. Study Area

The Adriatic Sea is a semi-enclosed basin bordered by the Italian peninsula in the west and the Balkan Peninsula in the east, which is characterized by a thermohaline cyclonic circulation (Cattaneo et al., 2003). This circulation is seasonally modulated by cold Bora winds from the northeast during winter (e.g., Artegiani et al., 1997). The cyclonic circulation restricts the fresh waters discharged by the Po River and Apennine Rivers to a narrow band along the western side of the basin, also known as the West Adriatic current (WAC) down to the Gulf of Taranto (Poulain, 2001). The WAC consists mostly of discharge from the Po River and northern Apennine Rivers (~70% of all river discharge into the Adriatic Sea; Raicich, 1996). In the Gulf of Taranto, the WAC mixes with Ionian Surface water (ISW) and the more saline Leventine Intermediate water (LIW) from the Ionian Sea (Fig. 1; Savini and Corselli, 2010). Apart from the predominantly southward transport pathway of the WAC, there are a few other small structures that influence sediment dispersal. In the Gulf of Taranto, sediments from rivers of the Basilicata region are transported to the western part of the Gulf of Taranto by a prevailing anti-clockwise current (Buccolieri et al., 2006). In the Gulf of Manfredonia, there is a clockwise current mainly driven by northern winds, transporting sediments of the local Ofanto River in a N-NW direction (Fig.1; Oeltzschner and Sigl, 1970; Spagnoli et al.,

	Gargano Peninsula		Gulf of Manfredonia		Strait of Otranto		Gallipoli Terrace		Gulf of Taranto-west	
	mean	stdev	mean	stdev	mean	stdev	mean	stdev	mean	
Ch	0.3	0.1	0.5	0.3	0.3	0.0	0.3	0.0	0.4	0.1
S	38.3	0.2	37.9	0.7	37.6	0.2	38.3	0.3	34.3	5.4
Depth of O_2 penetration (cm)	4.8	1.6	8.5	8.5	6.0	5.4	7.0	5.4	3.6	1.1
TOC (%)	0.44	0.19	0.5	0.2	0.6	0.2	0.6	0.2	0.6	0.2
C/N	7.3	0.6	7.4	0.7	7.3	0.3	7.3	0.8	6.2	0.4
$\delta 13C_{org}$ (‰)	-23.6	0.6	-23.6	0.6	-23.3	0.4	-23.1	0.7	-23.5	0.2
Ba/Al (ppm/%)	65.1	22.6	64.9	34.9	40.9	8.5	42.2	7.3	39.3	1.9
Ca/Al (% /%)	1.65	1.44	1.87	1.63	1.86	0.80	1.93	1.17	1.07	0.3
Ce/Al (ppm/%)	10.4	2.5	10.6	2.5	9.3	0.7	10.1	1.4	9.1	0.2
Co/Al (ppm/%)	3.2	1.3	3.2	1.6	2.6	0.4	2.7	0.7	2.6	0.4
Cr/Al (ppm/%)	19.1	5.6	18.9	5.3	15.6	1.4	15.4	1.4	13.9	0.4
Cu/Al (ppm/%)	4.2	1.1	4.3	1.1	3.9	0.6	4.6	0.9	4.6	0.3
Fe/Al (%/%)	0.62	0.14	0.65	0.18	0.55	0.04	0.56	0.11	0.52	0.02
K/Al (%/%)	0.38	0.08	0.35	0.08	0.30	0.03	0.30	0.03	0.28	0.01
Li/Al (ppm/%)	7.6	1.3	7.2	1.4	7.7	0.8	7.7	0.6	7.7	0.08
Na/Al (%/%)	0.51	0.08	0.48	0.`09	0.49	0.06	0.44	0.14	0.39	0.03
Ni/al (ppm/ ppm)	13.9	7.5	12.4	6.9	8.9	1.6	8.8	1.6	7.7	0.3
S/Al (%/%)	0.05	0.02	0.05	0.02	0.04	0.00	0.04	0.01	0.03	0.00
Sc /Al (ppm/ppm)	1.8	0.3	1.9	0.3	1.7	0.1	1.7	0.1	1.7	0.0
Sr/Al (ppm/ppm)	241.6	223.8	193.2	253.5	65.6	26.5	110.4	87.9	45.7	14.7
V/Al (ppm/ppm)	19.9	2.4	21.1	4.8	18.3	0.6	17.6	1.6	17.3	0.2
Zn/Al (ppm ppm)	9.7	3.7	10.8	3.4	11.7	1.8	11.6	1.8	12.1	0.4
Zr /Al (ppm/ppm)	12.0	1.9	13.4	2.6	12.3	0.8	12.9	0.8	11.9	0.1
Mg/Ca (%/%)	0.14	0.05	0.16	0.06	0.17	0.04	0.15	0.03	0.23	0.05
Sr/Ca (ppm/%)	38.8	8.4	35.6	7.9	35.5	1.52	42.2	5.3	42.4	2.2

Table 1 : Mean and standard deviation (stdev) of environmental variables (with Ch= chlorophyll-a in spring, S= salinity in winter, and oxygen penetration depth (cm) into the sediment after Zonneveld et al., 2009) and the geochemical composition of the different regions in this study.

2008). Near the Gargano promontory, the WAC also mixes with LIW and ISW. Currents from the eastern side of the Adriatic Sea are driven westward by the gyre of the south Adriatic. In contrast to the major amounts of sediment present and transported along the western Adriatic shores, the eastern coast is steep with very little sediment eroded from its hinterland (Correggiari et al., 1996).

3. Material and Methods

Fifty-three surface samples (0-2 cm) were collected with multicores (52 samples) and box corer (1 sample) from across the southwest Adriatic Sea and Gulf of Taranto area (Fig. 1). Cores GeoB 1070901 – GeoB10709-48 (numbered 1-48 in Fig 1.) were retrieved during the "CAPPUCCINO" cruise with R.V. Poseidon in June 2006; cores MP38MC, MP43BC, MP45MC, MP46MC and MP47MC were taken in December 2009 during the "MACCHIATO" cruise with R.V. Pelagia from now on MP38, MP43, MP45 and MP47); and samples 244993 – 249961 were taken from near the Albanian coast (Fig. 1). Relatively high sedimentation rates (as inferred from ^{210}Pb and radiocarbon dating) in the study area suggest that surface samples represent the last 2 -30 years (Zonneveld et al., 2009; **chapter 3**). All marine samples from the "CAPPUCCINO" cruise were internally mixed and subsequently split into different portions for detailed studies on dinoflagellate cysts (Zonneveld et al., 2009), the isotopes of *G. ruber* (white) (Grauel and Bernasconi, 2010) and organic geochemistry (BIT-index and the isotopes of plant waxes n-alkanes; Leider et al., 2010, 2013), grain size (this study), elemental composition (this study) and organic carbon/nitrogen and carbon isotopes (this study). Prior to analysis for elemental composition and carbon isotopes, samples were freeze dried and powdered with an agate mortar.

Twenty-five land samples were collected by hand drilling from beaches and river beds along the Adriatic coast during the MOCCHA land program in October 2009 (Fig. 1). Land derived samples were analysed for the isotopes of plant waxes n-alkanes (Leider et al., 2013), elemental composition (this study) and organic carbon isotopes (this study). The land samples were oven-dried (60˚C) for two days and powdered with an agate mortar.

Grain size was determined for all marine GeoB surface samples. For a better disaggregation of the sediment, the samples were suspended in Na_3PO_4 (5g l^{-1}) overnight before measurements. Grain size was determined using a Malvern Laser Diffraction Grainsizer 2000 with the dispersing module Hydro 2000S.

Major and minor elemental composition of all samples was measured using Inductively Coupled Plasma-Atomic Emission Spectroscopy (ICP-AES) with a Perkin Optima 3000 at Utrecht University. For this purpose, 125 mg of each sample was dissolved in 2.5 ml HF (40%) and a 2.5 mL 2:3 mixture of concentrated HNO_3 and $HClO_4$ and heated at 90 ˚C in a closed vessel for at least 8 hours (for full methodology see Reitz et al., 2004). Subsequently, the mixture was evaporated at 160˚C until a gel formed. The gel was then dissolved in 25 ml 1 M HNO_3. Relative precision (<5%) and accuracy were established by duplicates and standards (ISE-921).

Furthermore, 300 mg of each sample was decalcified using 1 M HCl. The decalcified sample was dried at 60˚C and finely ground using an agate mortar. For the decalcified sediments, the total organic carbon (TOC) and total nitrogen (TN) contents was determined on a Fisons Instruments NCS NA 1500 analyser using dry combustion at 1030˚C. In addition, the carbon isotope compositions of the organic carbon ($\delta^{13}C_{org}$ (‰)) was

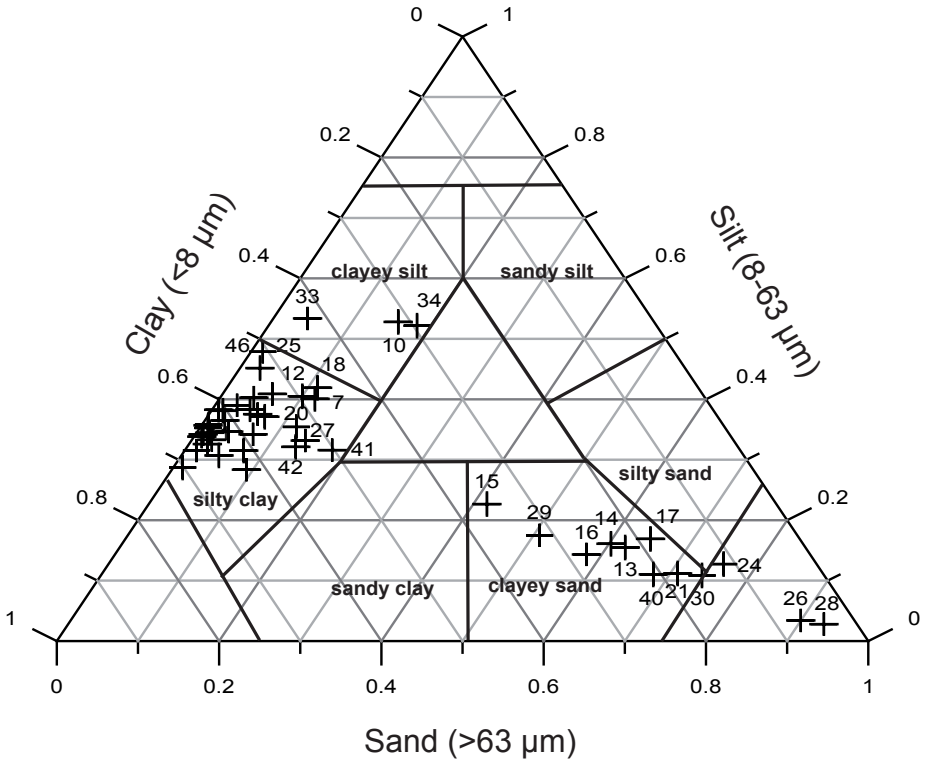

Fig. 2: Shepard ternary diagram, a grain size classification system based on the proportion of sand, silt and clay particles (for locations of samples see Fig. 1).

determined with a VG SIRA 24 mass spectrometer. The isotope data are reported in the conventional delta notation with respect to VPDB. Precision (≤0.1 ‰) and accuracy were established using international (Graphite quartzite standard NAXOS (GQ)), and in-house standards (Ammonium Sulphate (ASS), Acetanilide, and Atropine).

The methods for the data obtained on the same samples as this study that are discussed and integrated with these data, have been outlined in subsequent papers for dinoflagellates (Zonneveld et al., 2009), for foraminifer stable isotopes (Grauel and Bernasconi, 2010), and for organic biomarkers (Leider et al., 2010, 2013). For the latter, the Branched and Isoprenoid Tetraether (BIT) index was determined which is a ratio between the abundance of branched GDGTs (from anaerobic soil bacteria) and chrenarchaeol indicating the relative abundance of soil derived terrestrial organic matter input (e.g., Kim et al., 2006; Weijers et al., 2006 a, b). Besides the BIT-index also the stable isotopic compositions of hydrogen (δD) and carbon ($\delta^{13}C$) of plant- wax derived n-C_{29} and -C_{31} alkanes have been studied (Leider et al.,2013). Plant leaf waxes are well resistant to degradation (e.g., Schimmelmann et al., 2006). Previous studies have shown that their isotopes are not only good proxies for changes in temperature/aridity (e.g., Sachse et al., 2012 and references therein, Horikawa et al., 2010), but also to estimate the C_3 vs. C_4 plant contribution (Rommerskirchen et al., 2006; Vogts et al., 2009).

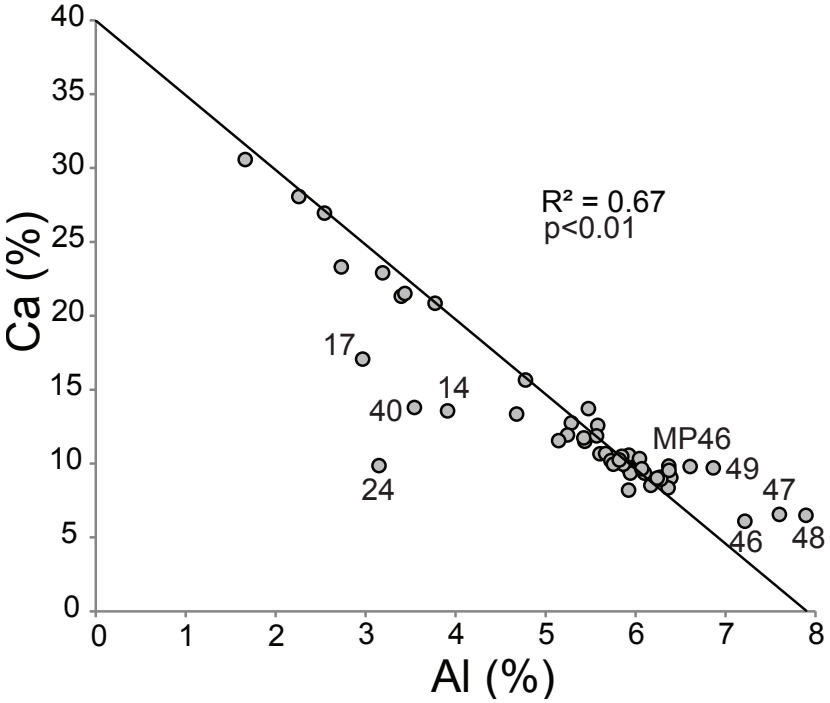

Fig 3 Percentage of Calcium and Aluminium of the marine samples in this study. Numbers correspond to sample numbers. 40% Ca corresponds to 100% $CaCO_3$ if all Ca is associated to carbonate.

4. Results

4.1 Grain size

The majority of the samples consist of silty clay, a mixture of 50% - 75% clay (< 8 μm) and 20% -50% silt (8μm-63μm, Fig. 2). However, samples 33, 34 (Gulf of Manfredonia) and 10 (central Gulf of Taranto) consist of clayey silt, a mixture of 20% -50% clay (< 8μm) and 50 %-75% silt (8μm-63μm). Furthermore, for the samples 13, 14, 15, 16, 17 (Gulf of Taranto), 21, 29 (central Adriatic) and 40 (Strait of Otranto) the grain size distribution is qualified as clayey sand, a mixture of 20-50% clay (< 8 μm) and more than 50% sand (>63μm). Only samples 24, 26, 28 and 30, from the south and central Adriatic Sea, close to the south Adriatic Pit, consist of mostly sand (>63μm).

4.2 Ca and Al

Ca in marine sediments can be considered to be dominantly derived from marine biogenic carbonate and Al to be from detrital aluminosilicates (i.e. clay minerals). Accordingly, most samples fit on a Ca-Al mixing line (R^2=0.67; p<0.01, Fig. 3). Only samples 40, 24, 14 and 17, characterized by a larger grain size, have lower Al than expected, presumably due to dilution with quartz which contains high elemental Si that cannot

	Water depth (m)	Transect	Ch	S	Depth of O_2 penetration (cm)	Clay (%)	Silt (%)	Sand (%)
TOC (%)	-0.25	0.23	**0.53**	-0.25	**-0.51**	**0.55**	**0.82**	**-0.77**
C/N	-0.2	-0.31	-0.03	0.06	-0.12	**-0.56**	-0.45	**0.54**
$\delta 13C_{org}$ (‰)	-0.05	0.3	0.09	0.21	-0.2	0.41	0.38	-0.41
Ba/Al (ppm/ %)	0.11	-0.39	-0.36	0.21	0.36	-0.7	**-0.81**	**0.83**
Ca/Al (%/%)	-0.06	-0.38	-0.34	0.34	0.35	**-0.52**	**-0.79**	**0.79**
Ce/Al (ppm/ %)	0.12	-0.08	-0.33	0.2	0.23	**-0.72**	**-0.7**	**0.81**
Co/Al (ppm/%)	0.44	-0.03	**-0.59**	0.33	0.56	-0.21	**-0.56**	0.43
Cr/Al (ppm/%)	0.21	**-0.5**	-0.36	0.21	0.35	0.14	-0.11	0.01
Cu/Al (ppm/ %)	0.76	0.25	**-0.48**	0.36	**0.46**	0.19	-0.03	-0.05
Fe/Al (%/%)	-0.06	-0.48	-0.32	0.09	0.42	-0.2	-0.41	0.3
K/Al (%/%)	-0.11	**-0.62**	-0.3	0.17	0.39	**-0.63**	**-0.77**	**0.75**
Li/Al (ppm/ %)	0.02	-0.05	0.02	0.12	-0.07	**0.68**	**0.52**	**-0.64**
Na/Al (%/%)	-0.34	-0.43	-0.03	-0.13	0.14	-0.19	-0.24	0.22
Ni/Al(ppm / ppm)	0.45	-0.34	**-0.65**	0.35	**0.55**	0.07	-0.31	0.17
S/Al (%/%)	-0.22	-0.41	-0.18	0.07	0.23	-0.24	-0.3	0.28
Sc/Al(ppm/ ppm)	0.15	-0.38	-0.37	0.26	**0.46**	0.06	-0.16	0.04
Sr/Al (ppm/ ppm)	0.14	-0.17	**-0.51**	**0.54**	**0.42**	**-0.57**	**-0.86**	**0.81**
Zn/Al(ppm/ ppm)	-0.13	0.19	0.38	-0.1	-0.23	**0.71**	**0.76**	**-0.82**
Zr Al(ppm/ ppm)	0.28	0.15	-0.39	0.3	0.11	-0.14	-0.18	0.23
Mg/Ca (%/%)	0.1	0.22	0.28	-0.31	-0.2	**0.55**	**0.76**	**-0.79**
Sr/Ca (ppm/%)	0.21	**0.5**	-0.09	**0.47**	0.05	0	-0.15	0.07
Ce/Ni(ppm/ ppm)	**-0.34**	**0.34**	**0.42**	-0.26	**-0.41**	-0.22	0.05	0.08
Zr/Cr(ppm/ ppm)	-0.09	**0.51**	0.17	-0.03	-0.27	-0.13	0.02	0.08

Table 2 Correlation of the different geochemical parameters with environmental variables (water depth (m), Transect (Regions along the transect from Gargano peninsula towards the Gulf of Taranto-west, see Fig. 1); Ch=chlorophyll-a in spring, S= salinity in winter, and the oxygen penetration depth (cm) into the sediment (after Zonneveld et al., 2009) and grain size (clay, silt and sand). Significant correlations ($p < 0.05$) as tested with an F-test of an oneway ANOVA are in bold.

be detected with the analytical method used in this study. In contrast, samples from the western Gulf of Taranto (MP46, 46, 47, 48 and 49) with smaller grain sizes have higher Ca contents than expected. High input of terrestrial minerals with enhanced Ca/Al ratio (e.g., the Ca-rich plagioclase**)** may cause this offset. In general however, the data validate such a two component system for most of the study area. The few exceptions indicate either an unaccounted for third component or a different detrital source material.

4.3 Elemental composition

In the following discussion the data are normalized to Al to avoid effects related to dilution by biogenic carbonate and to better visualize effects related to non-carbonate thus mainly terrestrial minerals. Ba/Al, Cr/Al, Fe/Al., K/Al, Mg/Al, Ni/Al, Sc/Al have relatively high values in surface samples from the Gargano Peninsula and the Gulf of Manfredonia compared to the other regions considered in this study (Table 1).

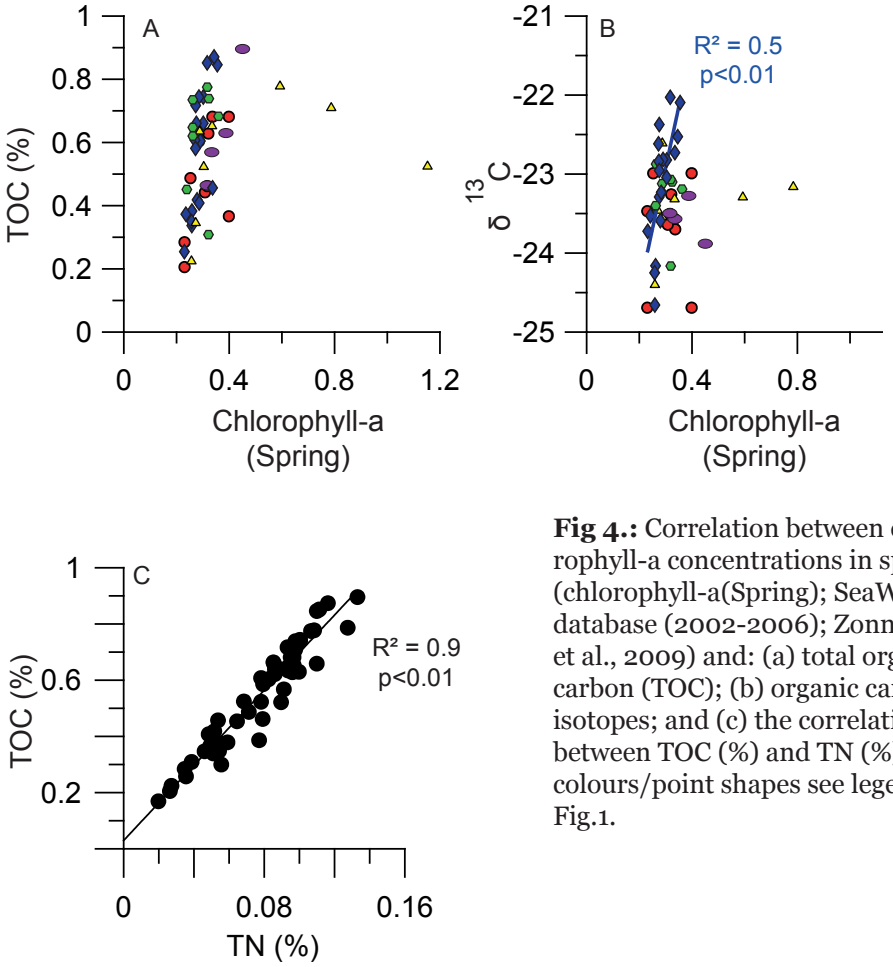

Fig 4.: Correlation between chlorophyll-a concentrations in spring (chlorophyll-a(Spring); SeaWifs database (2002-2006); Zonneveld et al., 2009) and: (a) total organic carbon (TOC); (b) organic carbon isotopes; and (c) the correlation between TOC (%) and TN (%). For colours/point shapes see legend of Fig.1.

	Po di Goro	Reno river	Foglia river	Potenza river	Vomano river	Cevaro river	Ofanto river
Lat.	44°50'08"	44°33'06"	43°52'00"	43°24'55"	42°38'43"	41°34'22"	41°17'06"
Long.	12°20'40"	12°08'26"	12°48'42"	13°39'17"	13°59'25"	15°53'10"	16°06'51"
TOC (%)	1.00	0.33	0.55	1.01	0.37	0.79	1.82
C/N	9.43	5.34	8.99	9.36	8.14	7.36	10.35
$\delta 13C_{org}$(‰)	-27.2	-27.6	-26.5	-26.8	-26.8	-30.2	-22.7
Ba/Al (ppm/%)	52.3	71.3	112.6	82.3	65.1	138.0	80.3
Ca/Al (%/%)	1.50	1.81	3.76	4.47	4.03	5.49	1.56
Ce/Al (ppm/%)	9.1	8.4	8.3	10.8	9.6	7.9	13.1
Co/Al (ppm/%)	2.4	1.7	2.1	1.7	1.4	1.0	1.8
Cr/Al (ppm/%)	27.3	15.8	15.7	15.5	13.0	4.9	10.2
Cu/Al (ppm/%)	6.8	3.6	5.6	5.5	2.5	1.6	8.6
Fe/Al (%/%)	0.54	0.42	0.47	0.43	0.44	0.30	0.50
K/Al (%/%)	0.27	0.34	0.31	0.30	0.35	0.58	0.29
Li/Al (ppm/%)	7.2	5.9	6.3	6.0	6.0	3.9	5.9
Na/Al (%/%)	0.15	0.23	0.19	0.18	0.23	0.38	0.09
Ni/Al (ppm/%)	16.7	9.00	8.6	7.8	6.4	2.4	5.1
S/Al (%/%)	0.01	0.02	0.03	0.01	0.04	0.08	0.01
Sc /Al(ppm/%)	1.8	1.4	1.6	1.6	1.4	0.8	1.5
Sr/Al (ppm/%)	54.3	66.4	109.4	93.0	95.8	363.8	50.5
V/Al (ppm/%)	14.2	9.6	12.2	12.7	11.4	6.8	14.7
Zn/Al (ppm/%)	19.8	12.7	13.4	14.6	10.3	14.2	16.3
Zr /Al (ppm/%)	9.6	11.2	9.3	11.5	7.8	10.5	22.4
Ce/Ni (ppm/ppm)	0.5	0.9	1.0	1.4	1.5	3.3	2.6
Zr/Cr (ppm/ppm)	0.4	0.7	0.6	0.7	0.6	2.2	2.2

Zn/Al ratio show a southward increasing trend from the Gargano Peninsula towards the Gulf of Taranto-west. The Gulf of Manfredonia surface samples contain the highest Zr/Al ratio. The Gulf of Taranto-west has relatively low Ce/Al and Na/Al ratio but a high Mg/Ca ratio. The Sr/Ca and Cu/Al ratio are relatively high in the entire Gulf of Taranto basin compared to samples from the south Adriatic Sea.

Along the transect from the north towards the Gulf of Taranto Cr/Al, K/Al ratios significantly decrease ($R^2>0.5$, $p<0.05$), while the Sr/Ca and Zr/Cr ratio increase ($R^2>0.5$, $p<0.05$). Most elements indicate significant correlation with grain size (Table 2).

	Mean land samples	stdev	**Lat.**
TOC (%)	1.11	2.45	-0.15
C/N	12.8	25.0	-0.3
$\delta 13C_{org}$(‰)	-25.1	2.2	-0.2
Ba/Al (ppm/%)	107.8	63.94	-0.3
Ca/Al (%/%)	3.82	3.83	-0.4
Ce/Al (ppm/%)	17.7	17.15	**-0.6****
Co/Al (ppm/%)	2.1	0.87	-0.1
Cr/Al (ppm/%)	19.5	13.97	-0.2
Cu/Al (ppm/%)	4.1	2.95	-0.2
Fe/Al (%/%)	0.74	1.29	-0.3
K/Al (%/%)	0.39	0.13	**-0.6***
Li/Al (ppm/%)	6.3	2.36	-0.4
Na/Al (%/%)	0.8	1.39	**-0.5****
Ni/Al (ppm/%)	7.4	4.31	**0.6****
S/Al (%/%)	0.2	0.44	**-0.6****
Sc /Al(ppm/%)	2.0	1.29	**-0.5***
Sr/Al (ppm/%)	1596	3939.4	**-0.6****
V/Al (ppm/%)	15.9	11.66	**-0.5****
Zn/Al (ppm/%)	14.5	9.66	-0.3
Zr /Al (ppm/%)	14.5	10.93	**-0.5****
Ce/Ni (ppm/ppm)	2.4	1.86	**-0.7****
Zr/Cr (ppm/ppm)	1.1	0.90	-0.4

Table 3 Geochemical composition of the rivers in this study, mean geochemical composition of all land samples, and the correlation of land samples with latitude (Lat, °N). Significant correlations as tested with an F-test of an oneway ANOVA are in bold, with* = $p < 0.05$, ** =$p < 0.001$.

Po River sediments are characterized by relatively high Co/Al, Cr/Al, Li/Al, Ni/Al, V/Al and Zn/Al ratios. In general, the northern Apennine Rivers (Reno, Foglia, Potenza and Vomano) have more intermediate values for these elemental ratios compared to the Po River and the more southern rivers (Table 3). Furthermore, almost no variation in elemental ratios is found within these rivers sediments. On the other hand, the elemental compositions for the southern Apennine Rivers, Cevaro and Ofanto, appear to have a different signature compared to the other Apennine Rivers and the Po River. The former river sediments are characterized by relatively low Cr/Al, Cu/Al, Fe/Al, Li/Al, and elevated Zr/Al (only for Ofanto River) and Ce/Al values compared to the more northern Italian rivers. The general trend (all $R^2 > 0.5$, $p<0.05$ or $p<0.01$) along the Adriatic coastal area is that some ratios increase southwards (Ce/Al, K/Al, Mg/Al, Na/Al, S/Al, Sc/Al, Sr/Al, V/Al, Zr/Al), whereas Ni/Al significantly decreases ($R^2= 0.6$ $p<0.01$, Table 1, 3).

4.4 Organic matter

Organic carbon and total nitrogen content are highest in the Strait of Otranto (Table 1). The C/N ratio is comparable in all regions, except for the Gulf of Taranto-west, where a relative low TOC and the lowest TN were detected. The $\delta^{13}C_{org}$ shows no significant variations among the different regions. Despite differences between rivers, the organic carbon and nitrogen content and the carbon isotopes show an increasing trend to the south (Table 3). The sediments of the Ofanto River, however, have the highest organic carbon contents and the Vomano River sediments the lowest. The Ofanto River also has the highest C/N ratio, which is generally relatively low in all river sediments

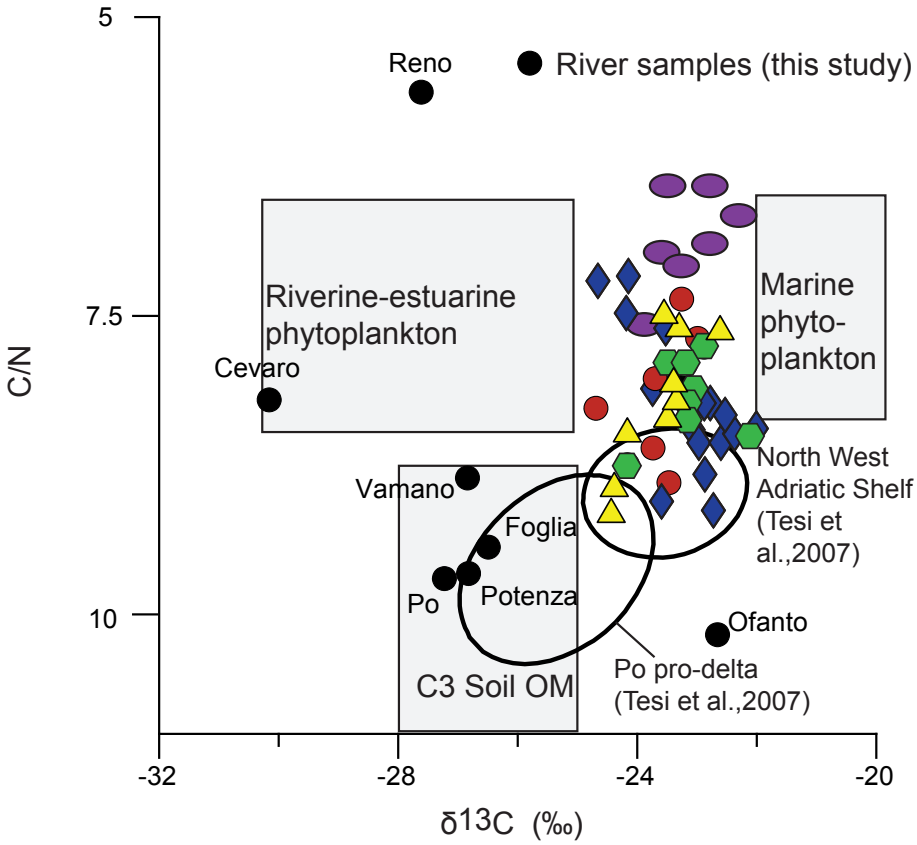

Fig 5. Organic-C/N vs. d13Corg for all samples (shore-and sea-based, from this study), grey boxes correspond to composition of 3 possible organic matter sources, black ellipses correspond to surface sediments in the north west Adriatic shelf, and the Po prodelta (data Tesi et al., 2007). For meaning colours/point shapes see Fig. 1.

compared to other land samples. The $\delta^{13}C_{org}$ varies from -30.2 ‰ (Cevaro River) to -22.6 ‰ (Ofanto River), whereas the $^{13}C_{org}$ of sediments from rivers above the Gargano Peninsula are rather comparable varying only between -27.6 and -26.8 ‰. Spring time chlorophyll-a observations (Zonneveld et al., 2009) correspond reasonably well with $\delta^{13}C_{org}$ and TOC distributions, except in the Gulf of Manfredonia (Fig. 4a, b; Table 2). TOC (%) and TN (%) are correlated ($R^2 = 0.9$, $p<0.01$, Fig. 4c) and have an intercept near zero (TOC (%) = 6.68* TN (%) + 0.03). The $\delta^{13}C_{org}$ values and the C/N ratio (Fig. 5) for most samples lie between those reported for riverine and estuarine phyto-plankton, soil organic matter, and marine phytoplankton (Fig. 5; Tesi et al., 2007 and references therein).

5. Discussion

The various proxies in this study are all affected differently by environmental variables

such as water depth, bottom water currents, and redox conditions (e.g., Faganeli et al., 1994; Dinelli et al., 1999; Tesi et al., 2007; Spagnoli et al., 2008; Weltje and Brommer, 2010). Moreover, knowledge on the grain size in itself is of importance for a correct interpretation of the bulk geochemistry (e.g., Spagnoli et al., 2008; Weltje and Brommer, 2010). Therefore, we will first discuss the spatial distribution of grain size, followed by the provenance of sediments, and the origin of organic matter as revealed by bulk geochemistry. We finalise our discussion by integrating the proxies of this study with those from other studies on the same sample set **(**Zonneveld et al., 2009; Grauel and Bernasconi, 2010; Leider et al., 2010, 2013).

5.1 Grain size and elemental composition

Most of the studied samples consist of silty clay. Coarser, sandy sediments are found at the most western tip of the Gargano Peninsula (GP), around Capo Santa Maria di Leuca (SML) and the steep continental slopes in the southern Adriatic (Fig.1, 2). The steep slopes of these regions are characterized by erosional features, caused by slope failure or strong currents (e.g., Tomadin, 2000; Ridente et al., 2007; Malinverno et al., 2010; Weltje and Brommer, 2010). Deposition of more silty samples has been observed in front and north of the Ofanto and Cevaro River deltas (samples 33, 34 and 25), which is presumably related to transport of relative coarse material by these rivers and shore-ward clockwise currents (Spagnoli et al., 2008; Fig. 1, 2). Accordingly, the silty composition of sample 46 in the northwestern Gulf of Taranto could also be related to local river input (Fig. 1, 2). The most probable source is the Basento River, whose sediments are transported to the west by the anti-clock wise current in the Gulf of Taranto (e.g., Buccolieri et al., 2006). The fine-grained and rather similar grain size distribution of all other samples which are under the influence of the WAC (Fig. 1) indicates that energy conditions and transport mechanisms are similar within the pathway of the WAC, the Adriatic mud belt.

The bulk geochemistry of sediment is usually highly influenced by differences in grain size. This is also the case for the samples in this study, where grain size varies mainly in the clay/silt vs. sand fraction (Table 2). The sand fraction in the Gulf of Manfredonia is characterized by marine biogenic carbonate components (thus high Ca/Al, Sr/Al and Mg/Al), by K-feldspars (high in K/Al and Ba/Al), as well as by heavy mineral fractions like garnet, apatite and barite (high in Zn/Al and Ba/Al; Garcia et al., 2004, Spagnoli et al., 2008) originating from land. This is in accordance with observed elemental ratios for our study area. Notably, all these ratios are significantly correlated to the sand fraction ($p<0.05$, Table 2). In contrast, the Li/Al ratio is mainly bound to the clay and silt fraction. Because of their size fractionation, caution should be taken when using these elements individually as provenance indicator.

5.2 Sediment Provenance and elemental composition

For differentiating sediment provenance using geochemical proxies it is not only neces-

sary to evaluate the influence of grain size and to understand transport pathways, but also to know the composition and weathering products of rock from the hinterland. For the Adriatic and in particular for the western Adriatic mud belt, the predominant source of sediment is from the Italian hinterland, whereas a negligible fraction may originate from the eastern Adriatic coast (see section 3; Trincardi et al., 1994; Syvitski and Kettner, 2007). Zr/Al, Cr/Al, Ni/Al, and Ce/Ni are amongst the elemental ratios that have been reported as useful geochemical tracers for indicating sediment provenance from Po and Ofanto River independent of grain size (Amorosi et al., 2002; Dinelli et. al, 2007; Spagnoli et al., 2008). The selected elemental ratios relate predominantly to the presence of ultramafic rock that occurs in variable amounts in the Italian hinterland. The more southern rivers contain a high proportion of ultramafic rocks in their hinterland (Pigorini et al., 1968) which are enriched in Zr and Cr contributing to elevated levels of these elements in the sediments carried by the Ofanto River (Spagnoli et al., 2008). The ultramafic rock from the Po River drainage area has high Ni/Al and Cr/Al ratio (Amorosi et al., 2002). The Cr/Al ratio is higher in the sediments from the Po River (27.3 ppm %) than found in the Apennine Rivers (4.9-15.8 ppm/%; Table 3). Ni/Al values in the land samples increase significantly with latitude ($p<0.05$), indicating high Ni/Al ratios in the hinterland of the more northern Apennine Rivers (Table 3). Zr/Al and Ce/Al show an opposite pattern (Table 3). To improve the geochemical differentiation between various provenance regions we have made a refined selection of elemental ratios that combines features of the previously mentioned tools. Despite the large range in grain sizes, these two ratios (Ce/Ni and Zr/Cr) are relatively insensitive to differences in grain size ($R^2<0.1$; $p>0.05$; Table 2). Using the sample composition based on these ratios we distinguish three discrete source regions: the Po River, the northern Apennine Rivers, and the southern Apennine Rivers (Fig. 6). All marine surface samples of this study have Ce/Ni and Zr/Cr values between these different provenance sources. The more northern samples have values similar to the more northern sources (lower Ce/Ni and Zr/Cr), whilst the more southern ones have higher Ce/Ni and Zr/Cr ratios in line with a more southern provenance. This pattern is consistent with samples along the WAC to contain a mixture of Po River and Apennine rivers sediments (Fig. 6).

A few samples are deviating from the consistent general picture. In particular, samples 17 and 24 (and to a lower degree also 13, 14, 18, 34, and 40) have a higher Ce/Ni than expected based on their Zr/Cr ratio (Fig. 6). Nearly the same set of samples also deviates in their grain size and their Ca vs. Al being too low (Fig. 2, 3), indicating that local sources or processes have a significant impact. Amongst the local processes that are thought to have played a role are relatively high primary productivity fluxes and related post-depositional diagenesis effecting the Ni/Al ratio (Tribovillard et al., 2006 and references therein) and erosional processes such as winnowing (see *6.1*). As we wish to focus on the main path ways, being of more global importance, we will not further discuss details of these deviating samples.

In addition, the seasonal and interannual variability of the WAC pathway (Poulain et al., 2001;v Selschopp and Alvarez, 2003) as well as its decreasing contribution to sedimentary deposition in more coast-remote areas, all contribute to a high variability and a

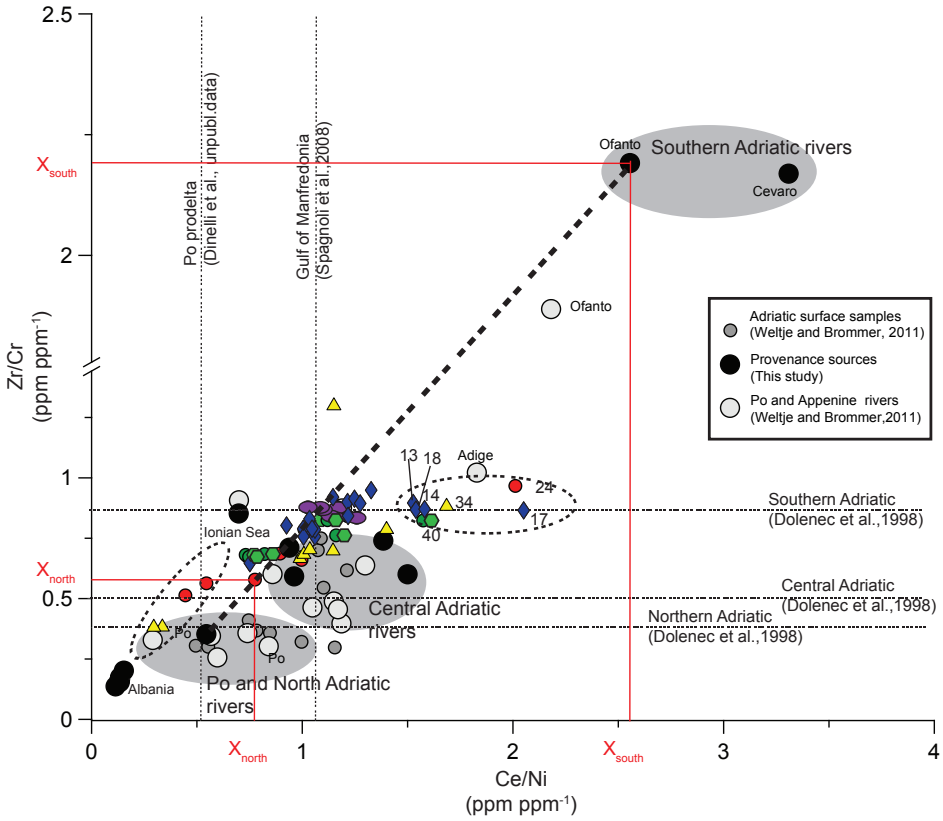

Fig. 6: Zr/Cr (ppm ppm) vs. Ce/Ni (ppm ppm) for all surface sediments (grey shaded ellipses are marine surface samples (data from Weltje and Brommer, 2011) and possible provenance sources (black dots= this study). Thin horizontal and vertical dotted lines indicate ratios reported for different areas in the Adriatic Sea (Dolenec et al., 1998; Spagnoli et al., 2008; Dinelli et al., unpublished data). The thick diagonal dotted line indicates a mixing line between Po river sediments and the Ofanto/Cevaro river sediments, samples within the two dotted ellipses deviate from this mixing line; the one on the lower left indicates some mixing with eastern Adriatic and Ionian sources, whereas the one on the upper right is influenced by local sources (see text). Endmembers used for provenance calculations (X_{north} and X_{south}) are indicated in red lines.

more complex spatial pattern of sediment provenance. For example, samples near the southern river mouths in the Gulf of Manfredonia will have a more southern provenance than samples more distant from the coast that are more influenced by sediments brought from the north by the WAC. Furthermore, even though sediment transport from the east by ISW is thought to be minimal (Trincardi et al., 1994; Syvitski and Kettner, 2007) the rather low Ce/Ni and Zr/Cr ratio of the eastern-most samples (22, 21, 29 and 35) suggest some sediment from eastern and Ionian provenance (see deviating samples in Fig. 6, 7b).

If the WAC is taken to be a closed system with no substantial contributions from the eastern Adriatic and Ionian Sea, then the Zr/Cr and Ce/Ni ratio can be used to calculate the percentage of contribution from the southern Apennine Rivers in comparison with northern sources using equation 1 (see also Fig. 7b).

Southern Adriatic provenance (%) = $100*(X_{sample}-X_{north})/ (X_{south}-X_{north})$

X_{sample} is the ratio of Ce/Ni or Zr/Cr as found in the surface samples. The northernmost sample in our data set that is least influenced by near-coastal, local and eastern Adriatic related provenance, i.e. sample 23, is considered as the best representative for the northern source endmember (X_{north}; Ce/Ni= 0.77 ppm/ppm; Zr/Cr=0.58 ppm/ppm, Fig. 6). For the southern Adriatic endmember (X_{south}) the values of the sample from the Ofanto River, the largest of all southern rivers in the study area, is used (Cattaneo et al., 2003). These sediments have relatively elevated values of Ce/Ni and Zr/Cr of 2.56 and 2.19 ppm/ppm, respectively (Fig. 7a).

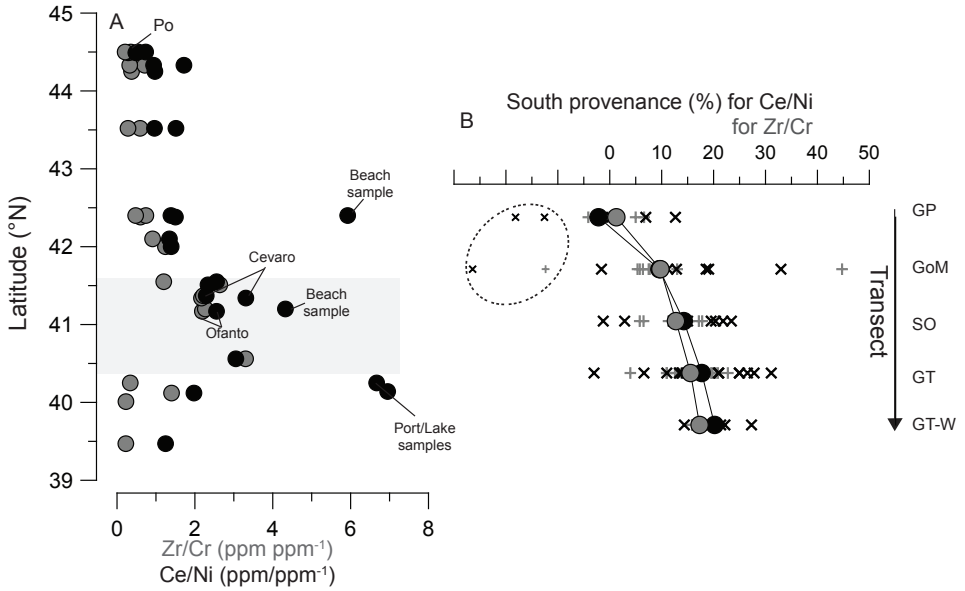

Fig 7 (a) Shore-based samples Zr/Cr (ppm/ppm, grey dots) and Ce/Ni (ppm/ppm, black dots) vs. Latitude. Grey square area indicates the latitudes were the highest Zr/Cr and Ce/Ni ratio are found. (b) Calculated percentage of southern Adriatic river provenance for marine sediments based on Ce/Ni and Zr/Cr (resp. black and grey crosses) plotted per region along the transect from Gargano peninsula towards the Gulf of Taranto-west (see Fig. 1). Average values are indicated in large dots, and regions are ranked vertically, for abbreviations see Fig. 1. Samples with deviating Ce/Ni ratio compared to their Zr/Cr ratio (13, 14, 17, 18, 40, 24 and 34) are not taken into account (see text). Samples in the dotted ellipseare the eastern-most samples, thought to be influenced by contributions from the eastern Adriatic and Ionian Seas (see Fig. 6 and text).

Along the WAC, the calculated average southern river provenance for the marine surface sediments increases from 0 to ~23% (Ce/Ni) and from 0 to ~19% (Zr/Cr) going southwards (Fig. 7b). Comparable values are found if the endmember for southern river provenance is based on the fine fraction of the Ofanto River (data Weltje and Brommer, 2011) or if an average of the Ofanto and Cevaro River is taken (e.g., for the Gallipoli shelf 18-23% versus 19-23%). The values found for the Gulf of Manfredonia (~10% southern Apennine provenance) are lower than those reported by Weltje and Brommer (2011; 40% central-southern Apennine provenance). In our study, the dominant sediment source, the Ofanto River (41.2ºN) is taken rather than all rivers below 42ºN. In addition, the Weltje and Brommer (2011) study has taken the average composition of northern river sediments as possible provenance endmember, whereas in this study the most northern marine sediment is taken as an integrated endmember for sediment coming from north of Gargano Peninsula. An alternative estimate for the southern contribution can be made using total sediment budgets. Approximately ~4.6 * 10^6 t/yr of sediments are exported from the west-central Adriatic, i.e. north of Gargano Peninsula, towards the southern Adriatic (Frignani et al., 2005). If these sediments are well mixed with the total sediment load of the dominant source for southern component sediments, the Ofanto River (~1.5 * 10^6 t/yr; Cattaneo et al., 2003), ~24 % of Ofanto River provenance is expected for the sediments in the Gulf of Manfredonia. Taking into account that the bulk of Ofanto River sediments, i.e. the coarse fraction, will settle close to the river mouth, this number based on total sediment load is rather comparable to the contribution calculated on the basis of geochemical composition of sediments in the Gulf of Manfredonia (~10 %), the approach of our study thus appears to produce consistent and meaningful results.

Despite the variability displayed within some regions, the Ce/Ni and Zr/Cr ratio based estimations both show an increase in southern provenance from the Gargano Peninsula (~0%) towards the Gulf of Taranto (~20 %). The Zr/Cr ratio based estimations most consistently indicate an increase of southern provenance along the transect (R^2=0.51; p<0.01). The south-eastern part of the Gulf of Taranto (Gallipoli Shelf) is at the end of the WAC-mud belt (Fig. 1, 8, Zonneveld et al., 2009). The highest fraction of southern river provenance is found here. Nonetheless, a large amount of material from Northern Adriatic provenance still reaches the Gallipoli shelf, as ~80 % of the sediment is of northern provenance.

The Ce/Ni ratio based southern provenance estimations in the western part of the Gulf of Taranto seems relatively low compared to the eastern Gallipoli shelf sediments (Fig. 1, 6 and 8). Sediments in the Gulf of Taranto-west area are mixed with those from the local rivers as the Basento River and some minor streams (see 5.1; Buccolieri et al., 2006; Medici et al., 2011; Perri et al., 2012). The Basento River located in the central part of the Gulf of Taranto drains the area around Potenza, a highly industrialized area, with sediments high in Ni contents (Medici et al., 2011). Furthermore, the Crati River, draining the Calabrian peninsula into the western Gulf of Taranto, has similar Cr and Ni values as the more central Apennine rivers (Perri et al., 2012). Local influences, therefore, limit the application of this studies approach for southern provenance for sedi-

ments from the western Gulf of Taranto, whereas the calculations are adequate for the sediments along the WAC mud belt from the Gargano Peninsula to the Gallipoli shelf.

5.3 Origin of Organic material

5.3.1. Primary Productivity

The sedimentary TOC content has a good correlation with primary productivity based on chlorophyll-a concentrations (Fig. 4; Table 2), except in the Gulf of Manfredonia. In contrast, the $\delta^{13}C_{org}$ seems to have no direct correspondence with the overall chlorophyll-a concentrations (Table 2; Zonneveld et al., 2009). This generally low correspondence is thought to be related to the multiple sources with distinct $\delta^{13}C$ that can be expected in a coastal setting. In addition, areas with the highest primary productivity due to high riverine nutrient input are often also the areas with the highest input of terrestrial material (Tesi et al., 2007). However, when considering the individual areas, a significant correlation is found between chlorophyll-a concentrations in the water column and $\delta^{13}C_{org}$ in the eastern Gulf of Taranto (Fig. 4). It is only in this area that the $\delta^{13}C_{org}$ clearly correlates with changes in chlorophyll-a concentrations (hence primary productivity). This indicates that the amount of marine- OM compared to terrestrial-OM is substantial. Probably because of the less dominant terrestrial OM contribution there is a clear correlation, permitting the determination of endmember compositions for marine and terrestrial components. Based on this correlation we derive that the main terrestrial organic matter (OM) source has a $\delta^{13}C_{org}$ of approximately -27.5‰. Furthermore, TOC with the highest marine OM component has a $\delta^{13}C_{org}$ of about -22‰. The values of these $\delta^{13}C_{org}$ endmembers (terrestrial and marine) concord with those reported in previous studies in the Adriatic Sea (e.g., Faganeli et al., 1994; Tesi et al., 2007 and references therein). In addition, the terrestrial organic endmember isotope value is similar to that found for the river samples, except for the Cevaro and Ofanto River. The latter suggests a northern origin of the terrestrial OM (Table 3).

5.3.2 Provenance of organic material

The Italian vegetation consists for only 1.5 % of C4 plants ($\delta^{13}C$ = -12 to -15 ‰; Collins and Jones, 1985; Fry and Sherr, 1984; Woodward et al., 2004). Hence, the contribution of the remains of C4 plants to the TOC can be considered as negligible in the Adriatic Sea (Tesi et al., 2007). Accordingly, the combined δD and $\delta^{13}C$ of n-alkanes of plantwaxes from the same set of core top samples reflect typical C3 vegetation (Leider et al., 2013). Therefore, three groups of possible sources of sedimentary OM can be identified: soils with a C3-vegetation, riverine-estuarine phytoplankton, and marine phytoplankton (Tesi et al., 2007 and references therein, Fig. 5).

The carbon isotopic signatures of the marine samples indicate that the sediments are a combination of terrestrial and marine sources (Fig. 5 and Table 2). In the north and

central Adriatic the main source of terrigenous material is from soils transported from the northern Po River and Apennine Rivers to the south (Tesi et al., 2007). Although average C/N values in the samples in southern Adriatic and Gallipoli shelf are lower than those in the central and northern Adriatic (Tesi et al., 2007; Fig. 8), their intermediate values suggest that still a high portion of the OM is derived from soils. Although it is not ruled out that the C/N ratio is somewhat affected by increased preservation of organic nitrogen in this area, the TOC and TN have a low intercept close to zero (TOC is 0.03 at TN is 0), suggesting that nitrogen is related to organic matter and is not clay-bound (Hedges et al., 1986; Tesi et al., 2007; Fig. 4c). In addition, the potential clay-bound organic-N has been reported to be rather modest at most (~0.003%; Mueller, 1977; De Lange, 1992). Furthermore, the higher C/N ratio is in coherence with the relatively high BIT-index, a proxy for the relative abundance of terrestrial organic matter from soils (Kim et al., 2006; Weijers et al., 2006a, b), found in the Gulf of Manfredonia (Leider et al., 2010, Fig. 8). Tesi et al. (2007) argue that only small amounts of organic material from the Po River and Apennine Rivers are transported southward which may partly be due to ongoing organic matter (OM) oxidation. The latter process would also lead to a more rapid decrease in the amount of marine OM and to a concomitant relative increase in more refractory soil-derived OM from Po and Apennine provenance along the western Adriatic shelf down to the Gargano peninsula (Tesi et al., 2007). Input of soil derived material from a northern source is in coherence with the observed pattern of the C/N ratio and the BIT–index and the derived terrestrial OM $\delta^{13}C_{org}$ endmember of the Gallipoli Shelf (see 5.3.1). Furthermore, despite high spatial variability (see 5.2 above), a trend of a southward increasing contribution of marine organic matter (more heavy $\delta^{13}C_{org}$) is observed (Fig. 8 and Table 2), indicating a reduced influence of the WAC.

The western Gulf of Taranto has the lowest C/N ratios showing a lower influence of terrestrial material from soils (Fig. 8, Tesi et al., 2007). The low C/N ratio is in coherence with the relatively low BIT index values (Fig. 8; Leider et al., 2010). The low C/N ratio combined with relatively high δ^{13}Corg values compared to the Gallipoli shelf indicate that the terrestrial organic material transported to the western Gulf of Taranto is mostly from riverine-estuarine phytoplankton origin (Fig. 5).

5.4 Integration of proxies

Large temporal and spatial variability related to natural physical and biogeochemical dynamic processes appear to have an important influence on the sediment composition and distribution in the complex study area. This may partly obscure the statistical verification of patterns for provenance in this study if only a single proxy was used. Therefore, the results from this study for the mainly inorganic geochemical proxies are combined with those obtained on the same samples but for organic geochemical, stable isotope of foraminifera, and dinoflagellate related proxies. In this way, we get a more complete understanding of the complex coastal system sediment distribution patterns

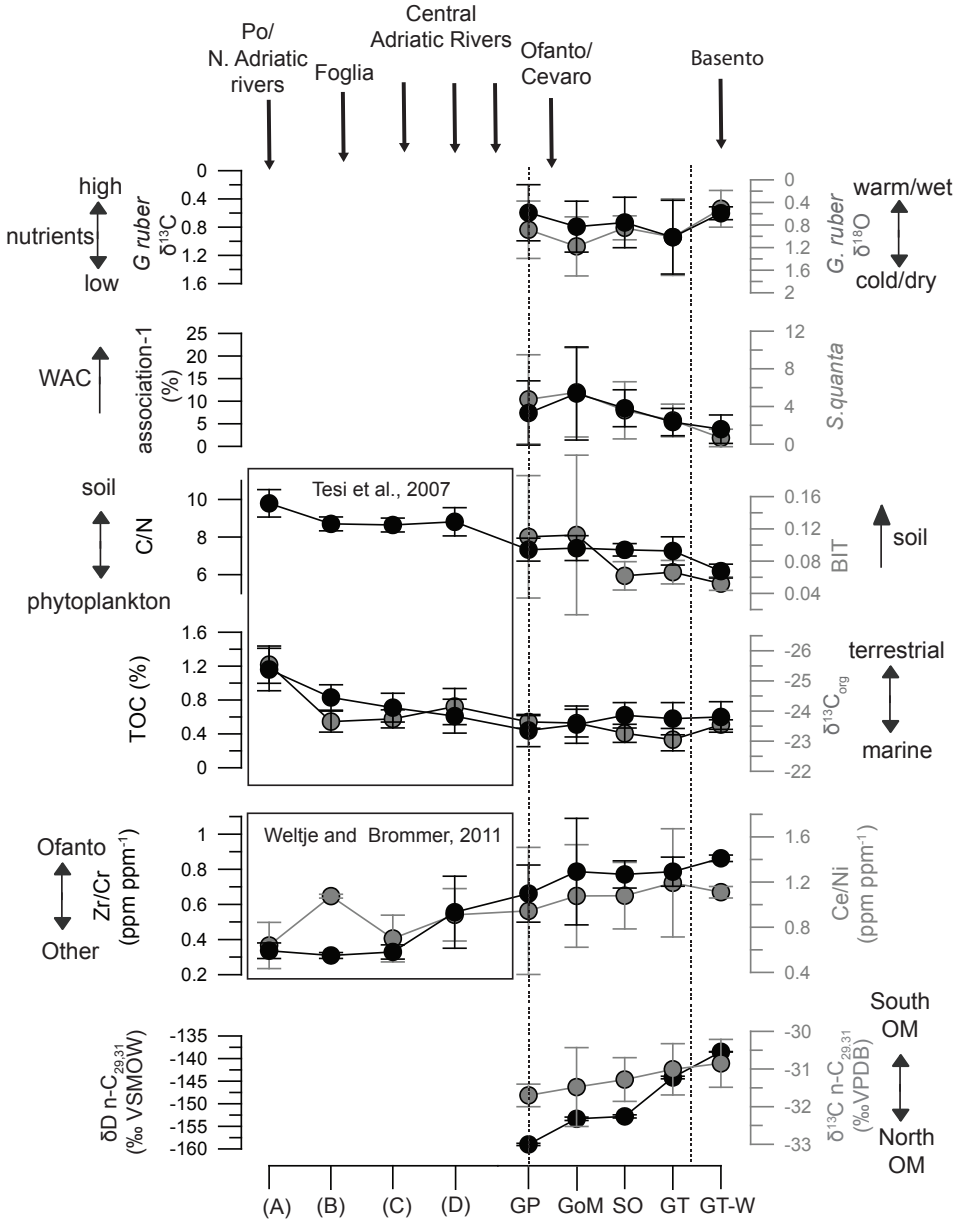

Fig. 8: Integrated representation for data of a suite of proxies in marine surface samples along a transect from the northern Italian coast into the Gulf of Taranto (for transects names and abbreviations: see Fig. 1). From top to bottom: carbon and oxygen isotopes of *G. ruber* (white) (Grauel and Bernasconi, 2010), relative abundance of dinoflagellate species *Selenopemphix quanta,* total relative abundance of species indicators of river plume association-1 (Zonneveld et al., 2009), BIT Index (Leider et al., 2010), TOC (%), C/N, δ^{13}Corg (data Tesi et al., 2007 and this study), Zr/Cr and Ce/Ni ratio (Weltje and Brommer, 2011 and this study) and plant waxes carbon and hydrogen isotopes (Leider et al., 2013). WAC= West Adriatic current.

for the western Adriatic Sea.

Dinoflagellate-cyst associations in the research area reflect environmental conditions (Zonneveld et al., 2009). The most diagnostic association is 'river plume' association-1 (consisting of the cysts of *Echinidimium spp., L. Sabrina, L. machaerophurum, Polykrikos spp., P. stellatum, S.quanta)* that is closely corresponding to river discharge, i.e. to the WAC (Fig. 8; Zonneveld et al., 2009). The relative abundance of *Selenopemphix quanta*, (the most common species in this association) and the total relative abundance of association-1 gradually decrease from the Gulf of Manfredonia towards the Gallipoli shelf and are close to zero in the Gulf of Taranto-west. This pattern indicates that the Gallipoli shelf is connected with the Adriatic Sea by the WAC, but that this influence is gradually being reduced along the transect (Fig. 1, 8). The oxygen isotopes ($\delta^{18}O$) data of *G.ruber* (white) indicate summer temperatures in the region but are also influenced by salinity and nutrients (Grauel and Bernasconi, 2010). Intermediate values are detected in the WAC mud belt (i.e. relatively low salinity, nutrient rich, high temperature), while high values are found in the deeper parts of the Gulf of Otranto, Adriatic Sea and Ionian Sea (i.e. mainly high salinity). Along the path of the WAC, the $\delta^{13}C$ of *G. ruber* (white), an indicator of nutrient availability, increases (gets more heavy; Grauel and Bernasconi, 2010). This corresponds with a decreasing influence of the WAC towards the eastern Gulf of Taranto. Accordingly, a lower BIT-index, a proxy for the input of terrestrial organic matter of mainly soils, and the C/N ratio in combination with increasing, i.e. less negative $\delta^{13}C_{org}$ all indicate that the relative contribution of terrestrial OM also decreases along this transect (Leider et al., 2010). On the base of the C,H- isotopes of plant waxes, Leider et al. (2013) have shown that this terrestrial OM is of a more southern Italian source, going from the Gargano Peninsula to the Gulf of Taranto (Fig. 8). This is coherent with the patterns found for Zr/Cr and Ce/Ni ratios which also indicate that the influence of southern provenance increases from north to south along the WAC (Fig. 8).

Thus, all proxies indicate that the WAC influence extends all the way down to the eastern Gulf of Taranto. In contrast, for the western part of the Gulf of Taranto, a deviating pattern occurs for all proxies, indicating the predominant influence of local river input (e.g. Basento River), thus a much reduced influence of the WAC and a terrestrial source different from the one transported by the WAC (Fig. 8). Along the WAC pathway towards the Gulf of Taranto, the amount of material (sediments and OM) from southern provenance increases. In contrast, the total amount of terrestrial material decreases, indicating a reduced influence of the WAC.

6. Conclusions

The elemental ratios Zr/Cr and Ce/Ni have been used to distinguish a northern Adriatic from a southern Apennine River provenance independent of sediment grain size. On the basis of these elemental ratios, $\delta^{18}O$ and $\delta^{13}C$ of *G.ruber* (white), the BIT index,

stable isotopes of plant waxes, and the dinoflagellate cyst distribution, it is shown that the influence and sediment transport pathway of the Western Adriatic Current (WAC) extends all the way south to the eastern Gulf of Taranto. In contrast, the counter-clockwise current and local river input in the western Gulf of Taranto results in a deviating, predominantly locally derived sediment composition and provenance. For the WAC, an increase in sediments with a southern provenance is found along its southward pathway from the Gulf of Manfredonia, to the Strait of Otranto, and into the Gulf of Taranto. A total of ~80% of the sediment in the eastern Gulf of Taranto appears to originate from the north/central Adriatic Sea and ~20% of the sediments have a southern provenance. Furthermore, organic matter in the WAC mud belt consists mainly of terrestrial organic matter from Apennine Rivers. Along its pathway, the relative contribution of terrestrial-derived organic matter (OM) decreases, whereas that of marine OM increases. This results in sediments with the highest marine component to occur in the Gulf of Taranto compared to other areas within the West Adriatic mud belt.

Acknowledgments

Franziska Lechleitner is thanked for analyzing grain size composition at ETH Zurich. At Utrecht University we thank Arnold van Dijk, Helen de Waard, Dineke van de Meent and Brice Robert for lab assistance with ICP-AES, C/Norg and isotopes analysis. We are grateful for sample collection by: participants onboard of the CAPPUCCINO cruise (coordinated by K.A.F. Zonneveld) and MACHIATTO cruise (coordinated by Gert De Lange), the Albanian samples (coordinated by C. Corselli), and the land sampling team (coordinated by G. Versteegh). Arne Leider, Philippe Goudeau, Marit Brommer, Karin Zonneveld and Fransesca Sangiorgi are thanked for fruitful discussions and contributions that helped to improve the manuscript and E. Dinelli for access to unpublished data. We thank the editor and two anonymous reviewers for their helpful comments and suggestions which have greatly improved the manuscript. This work was supported by the Nederlandse Organisatie voor Wetenschappelijk Onderzoek (NWO) and the Swiss National Science Foundation (SNF Project 20MA21-115934) as part of the MOCCHA- project funded by the European Science Foundation (ESF) Eurocores Programme Euromarc.

Chapter 3: The Glacial-Interglacial transition and Holocene environmental changes in sediments from the Gulf of Taranto, Central Mediterranean

Marie-Louise S. Goudeau, Anna-Lena Grauel*, Chiara Tessarolo, Arne Leider, Liang Chen, Stefano M. Bernasconi, Gerard J.M. Versteegh, Karin A.F. Zonneveld, W. Boer, C. M. Alonso-Hernandez and Gert J. De Lange. * authors contributed equally to this work.*

(Published in: Marine Geology 348, 88–102)

An extensive, high-resolution, sedimentological-geochemical survey was done using geo-acoustics, XRF-core scans, ICP-AES, AMS ^{14}C-dating and grain size analyses of sediments in 11 cores from the Gulf of Taranto, the southern Adriatic Sea, and the central Ionian Sea spanning the last 16 cal. ka BP. Comparable results were obtained for cores from the Gallipoli shelf (eastern Gulf of Taranto), and the southern Adriatic Sea suggesting that the dominant provenance of Gallipoli Shelf sediments is from the western Adriatic mud belt. The ^{210}Pb and ^{14}C-dated high-accumulation-rate sediments permit a detailed reconstruction of climate variability over the last 16 cal. ka BP.

Although, the Glacial-Interglacial transition is generally dry and stable these conditions are interrupted by two phases of increased detrital input during the Bølling-Allerød and the late Younger Dryas. The event during the Younger Dryas period is characterized by increased sediment inputs from southern Italian sources. This suggests that runoff was higher in southern- compared to northern Italy. At approximately ~7 cal. ka BP, increased detrital input from the Adriatic mud belt, related to sea level rise and the onset of deep water formation in the Adriatic Sea, is observed and is coincident with the end of sapropel S1 formation in the southern Adriatic Sea. During the mid-to-late Holocene we observed millennial-scale events of increased detrital input, e.g. during the Roman Humid Period, and of decreased detrital input, e.g., Medieval Warm Period. These dry/wet spells are consistent with variability in the North Atlantic Oscillation (NAO). A negative state of the NAO and thus a more advanced penetration of the westerlies into the central Mediterranean, that result in wet conditions in the research area concord with events of high detrital input e.g., during the Roman Humid Period. In contrast, a positive state of the NAO, resulting in dry conditions in the Mediterranean, dominated during events of rapid climate change such as the Medieval Warm Period and the Bronze Age.

1. Introduction

During the Holocene, millennial-scale climatic events such as the 'Medieval Warm Period' (MWP) and the 'Little Ice Age' (LIA) can be detected across the Northern Hemisphere (NH), and have been associated with changes in atmospheric circulation and solar variability (deMenocal et al., 2000; Bond et al., 2001; Rohling et al., 2002; Mayewski et al., 2004). These events have site-specific expressions, and their controlling factors and natural feedback mechanisms are still not fully understood (Mayewski et al., 2004). Therefore, full comprehension of this millennial-scale climatic variability requires long, continuous, high-resolution records from climate-sensitive areas. The Mediterranean region is situated between the subtropical high-pressure belt and the mid-latitude westerlies, recording both high- and low-latitude climate changes, such as those related to the North Atlantic Oscillation (NAO), El Niño Southern Oscillation (ENSO), and Asian Monsoon (Rossignol-Strick, 1985; Hurrell, 1995; Alpert et al., 2006; Trigo et al., 2006; Brandimarte et al., 2011; Nieto-Moreno et al., 2011).

Orbital-scale climate changes are reflected by organic-rich sapropel layers in Mediterranean sediment that have been related with predominately low-latitude forcing (Rossignol-Strick, 1985; Hilgen, 1991; Lourens et al., 1996; De Lange et al., 2008). High-latitude climate variability has been associated to millennial to decadal changes in dust transport, temperature, precipitation, and deep-water formation in the Mediterranean region (e.g., Cini Castagnoli et al., 1999; Schilman et al., 2001; Sangiorgi et al., 2003; Rohling et al., 2002; Frisia et al., 2005; Piva et al., 2008; Gennari et al., 2009; Jilbert et al., 2010a,b). Climate reconstructions of the Adriatic Sea region suggest that cold events coincide with North Atlantic ice-rafting events (Sangiorgi et al., 2003; Piva et al., 2008). In addition, late Holocene records in particular from the Adriatic area suggest that it was generally wetter and warmer during the 'Roman Humid Period' (RHP), drier and warmer during the MWP, but relatively cold and wet during the LIA (e.g., Sangiorgi et al., 2003; Frisia et al., 2005; Piva et al., 2008; Chen et al., 2011, 2013; Giraudi et al., 2011, Grauel et al., 2013a). Cold and warm spells are thought to affect Adriatic Deep Water (ADW) formation and consequently the general Mediterranean ocean circulation (Sangiorgi et al., 2003; Piva et al., 2008). Late Holocene records in lakes reveal contrasting millennial scale hydrological patterns between northern Italy (>43°N) and southern Italy (<43°N; e.g., Magny et al., 2003; Joannin et al., 2012). This suggests shifts in the extent of the westerlies (i.e. NAO) and indicates that these events are characterized by complex patterns and expressions.

Climate records based on marine sediments from the southern Adriatic and the central Mediterranean Sea that cover the entire Holocene and deglaciation are rare and mostly focus on Sea Surface Temperature (SST) reconstructions based on faunal assemblages or oxygen isotopes (e.g., Rohling et al. 2002; Sangiorgi et al., 2003; Piva et al, 2008). Sub-decadal to centennial scale variability has been observed in the Gallipoli Shelf sediments for carbonate contents (Cini Castagnoli et al., 1992b), stable oxygen isotopes of *Globigerinoides ruber* (e.g., Cini Castagnoli et al., 1999; Grauel et al., 2013a,b), UK'_{37} (Versteegh et al., 2007; Grauel et al., 2013a) and dinoflagellate cysts (Chen et al.,

2011, 2013; Zonneveld et al., 2012). This variability has been related to changes in SST, salinity and eutrophication caused by changes in river discharge, the NAO, and solar variability. Only a few limited studies have been reported on recent sediment transport and geochemical patterns in the Gulf of Taranto indicating a complex and spatially different morphology, sedimentation, and chemical composition as well as a connection with the Adriatic Sea (Rossi, 1983; Buccolieri et al., 2006; Malinverno et al., 2010; **chapter 2**). Surface sediments from the Gulf of Taranto and Southern Adriatic suggest that the geochemical signature of sediments can be used to detect changes in grainsize, productivity, and to distinguish a northern from a more southern Italian provenance (**chapter 2**).

Despite the high potential of this area to reconstruct high-frequency Holocene paleoclimate variability and possible contrasting north/ south hydrological patterns, to date no comprehensive studies covering more than 5500 years exist for the Gallipoli Shelf sediments (Cini Castagnoli et al., 1992b). This highlights the need for a basin-wide sedimentological study in the Gulf of Taranto to better understand paleoclimatic records from this region. Therefore, we first assess at high resolution the compositional variability, potential correlations and provenance for sediments of all cores of this study area. Subsequently, we focus on sediments from the Gallipoli Shelf, eastern Gulf of Taranto, which are thought to be related to more general, supra-regional climate variability. For sediments of the two most comprehensive and consistent cores, we give an in-depth paleoclimate reconstruction with emphasis on some important Holocene climate phases.

2. Regional setting

2.1 Oceanography

The Gulf of Taranto is situated in the north western Ionian Sea between Calabria and Apulia (Fig. 1). It can be divided into three distinct geological provinces, the Apulian Slope, the Taranto Valley and the eastern Calabrian Margin (Rossi et al., 1983). The main influence on transport along the southern Italian coast is the intensity of the Western Adriatic Current (WAC) which flows in a narrow coastal band from the northern Adriatic Sea into the Gulf of Taranto (Poulain, 2001; Bignami et al., 2007; Turchetto et al., 2007). The WAC has a significant interannual variability and its influence along the southern Italian coast and the Gulf of Taranto is higher in winter than in summer (Milligan and Cattaneo, 2007). In the Gulf of Taranto, the less saline waters from the WAC mix with the saline Ionian Surface Waters (ISW) from the central Ionian Sea.

The bottom layer of the water column in the southern Adriatic region is characterized by the Adriatic Deep Water (ADW) which is a dense water mass formed by two different processes (Turchetto et al., 2007); 1) during winter NE Bora wind events result in the formation of Northern Adriatic dense Deep Water (NAdDW) in the northern Adriatic Sea and 2) deep convection during late winter/early spring results in the for-

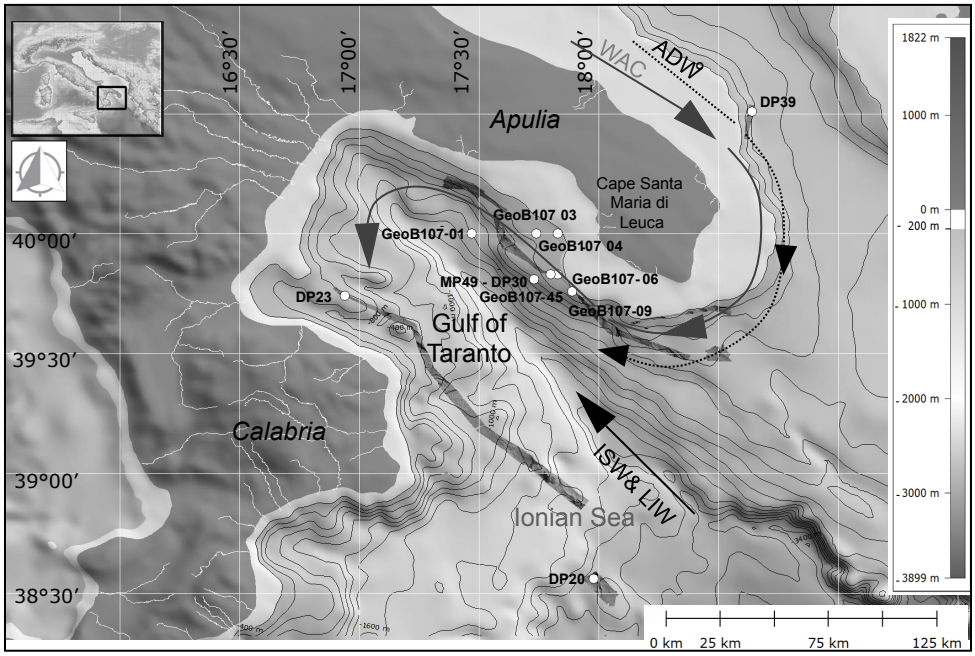

Fig. 1: Bathymetric map of the Gulf of Taranto area; core locations are indicated as well as the general circulation pattern (WAC=Western Adriatic Current, ADW= Adriatic Deep Water, ISW= Ionian Surface Water, LIW=Levantine Intermediate Water).

mation of Southern Adriatic dense Deep Water (SAdDW) in the southern Adriatic Sea (Artegiani et al., 1997; Vilibić and Orlića,2002). The NAdDW has an enhanced current and particle flux southward (Turchetto et al., 2007). Around the Cape Santa Maria di Leuca the bottom currents are more intense than the surface currents and have a strong influence on the sedimentation (Savini and Corselli, 2010).

2.2 Sediment accumulation and provenance

Primary sediment supply into the northern Adriatic Sea comes from the Po River in the north and additional contributions from smaller Alpine and Apennine Rivers (Turchetto et al., 2007). The mud wedge (also called Adriatic mud belt) formed by these sediments along the Italian shelf reaches up to 30 m thickness in the north and represents the modern high-stand system from ~5.5 ka BP onwards after early Holocene sea-level rise (Cattaneo et al., 2003; Vigliotti et al., 2008). Sediments can be transported by the WAC to the Gulf of Manfredonia (Weltje and Brommer, 2011), and as far south as the eastern Gulf of Taranto (**chapter 2**). Sediments from the western Gulf of Taranto have a more local provenance (**chapter 2**).

Cruise	Station	Latitude	Longi-tude	Bottom depth (m)	Gravity core length (m)	used methods
CAPPUCCINO	GeoB10701	40°00 N	17°47 E	1181	2.81	*XRF, line scan, Multicore grain size*
CAPPUCCINO	GeoB10703	40°00 N	17°74 E	277	3.78	*XRF, line scan, Multicore grain size*
CAPPUCCINO	GeoB10704	40°00 N	17°83 E	219	5.52	*XRF, line scan, Multicore grain size*
CAPPUCCINO	GeoB10706	39°83 N	17°83 E	218	4.87	*XRF, line scan, Multicore grain size*
CAPPUCCINO	GeoB10709	39°76 N	17°89 E	172	5.19	*XRF, line scan, Multicore grain size*
CAPPUCCINO	GeoB10745	39°81 N	17°73 E	689	3.99	*XRF, line scan*
DOPPIO	DP20	38°56 N	17°98 E	2446	5.56	*XRF, line scan*
DOPPIO	DP23	39°74 N	16°94 E	378	9.06	*XRF, line scan*
DOPPIO	DP30	39°83 N	17°80 E	270	8.28	*XRF, line scan, AMS ^{14}C dating, ICP-AES*
DOPPIO	DP39	40°51 N	18°64 E	527	7.96	*XRF, line scan*
MACCHIATO	MP49	39°83 N	17°80 E	267	9.61	*XRF, line scan*

Table 1: Geographic and bathymetric information of the core stations

3. Material and Methods

3.1 Core sites

All cores of this study, except core DP20PC, DP23PC and DP39PC, are from the Apulian Margin, a wide continental shelf with a slight depth gradient towards the deep Taranto Valley (Rossi et al., 1983). The slope is locally affected by slumping and active erosion processes (Rossi et al., 1983), thus pre-site survey Multibeam studies are essential. The bathymetric data are based on the integration of several Multibeam surveys which have been conducted during the RV Pelagia cruises DOPPIO (2008) and MACCHIATO (2009). The bathymetric data of the Gulf of Taranto area (grid size 15m) and for the shallower Adriatic Sea (grid size 10m) were combined with the GEBCO global grid data (grid size 100m) and integrated to construct a detailed bathymetric map (Fig. 1).

The gravity cores GeoB10701-5, -10703-5, -10704-5, -10706-4, -10709-6 and -10745-3 have been collected during the RV POSEIDON cruise "CAPPUCCINO" in June 2006 (Zonneveld et al., 2008; Fig. 1). The piston cores DP30PC, DP23PC and DP20PC have been collected during the RV PELAGIA cruise "DOPPIO" in October/November 2008, and the piston core MP49PC has been collected during RV PELAGIA cruise "MACCHIATO" in November/December 2009 (De Lange, 2009; Fig.1; Table 1). In

the following, these cores will be addressed by their station name only.

3.2. Grain size analyses

The grain size distributions were determined for 5 core top samples (0-2 cm) of multicores GeoB10701, -10703, -10704, -10706, and -10709 using a Malvern Laser Diffraction Grainsizer 2000 with the dispersing module Hydro 2000S (Table 2). For a better disaggregation of the sediment, the samples were suspended in $Na(PO_4)n$ (5g/l) overnight before measurements.

3.3. AMS 14C-dating

For dating purposes ^{210}Pb was determined for core NU04MC and for the top part of DP30 at the laboratories of CEAC, Cuba and NIOZ, The Netherlands (Fig. 2a and Table 1). In addition, nine samples of core DP30 were picked for planktonic foraminifera and analysed with a miniaturized radiocarbon dating system (MICADAS) (Ruff et al., 2007; Synal et al., 2007) at the AMS Radiocarbon Dating Laboratory at ETH Zurich (Table 3). Five samples were measured as solid graphite targets and four samples were measured directly as CO_2, where MICADAS was equipped with a gas ion source. The ^{14}C-ages were calibrated with the program OxCal v3.10 (Bronk Ramsey et al., 2009) with the references using the Marine04 calibration curve (Hughen et al., 2004) in combination with the region reservoir correction of 121±60 (ΔR) in addition to the standard reservoir correction of about 400 yr.

The age models for the other cores in the Gulf of Taranto were determined by correlation to core DP30 using the Ca/Ti curves (see 4.3. *Correlation of cores)* and the program AnalySeries 2.0 by Paillard et al. (1996).

3.4. ICP-AES

The topmost sections of DP30 (0-2.78 m) were sampled at 2.5 mm resolution. The major and minor elemental compositions of the freeze-dried samples were analysed at 1 cm resolution i.e. every 4th sample, using Inductively Coupled Plasma-Atomic Emission Spectroscopy (ICP-AES) with a Perkin Optima 3000 at Utrecht University. For this purpose 125 mg of sample was dissolved in a mixture of 2.5 ml HF (40%) and 2.5 mL pre-mixed acid (HNO_3 16.25% and $HClO_4$ 45.5 %) and heated at 90°C in a closed reaction vessel for at least 8 hours (Reitz and De Lange, 2006). Thereafter, they were dried by evaporating at 160°C until a gel formed. The gels were then dissolved in 25 ml 1M HNO_3. The relative precision (better than 5%) and accuracy was established by duplicates and in-house standards (ISE-921).

A Station	B Clay	C Silt	D Sand	e fine silt	f medium silt	g coarse silt	h very fine sand	i fine sand
size (µm)	0.01-2	2-63	63-2000	2-8	8-16	16-63	63-125	125-250
GeoB10701	20.7	72.8	6.5	36.5	15.1	21.3	5.8	0.6
GeoB10703	20.9	78.3	0.9	44.8	20.7	12.8	0.9	0.0
GeoB10704	17.9	76.5	5.6	36.6	17.0	22.9	5.1	0.5
GeoB10706	18.3	77.5	4.3	40.5	18.7	18.4	3.5	0.6

Table 2: Grain size distribution of surface sediments taken in the Gulf of Taranto. Columns e–g are sub-divisions of the silt fraction (column c),whereas columns h and i represent most of the sand (c)

3.5. Colour scanning and XRF analyses

To identify changes in colour, the sediments of core DP30 was scanned with a Minolata Colorscan Spectrophotometer CM-508i. Measurements were taken in a 1 cm resolution immediately after opening of the core.

For this study two different XRF core scanners, the AVAATECH core scanner (Richter et al., 2006) and the ITRAX XRF core scanner (COX Analytical Systems), were used (Croudace et al., 2006). The split core halves from the GeoB cores (10704, 10745, 10706, 10703, 10709) were scanned at 2 mm resolution with the ITRAX scanner at the Geography Institute (GEOPOLAR group), University of Bremen. The elements: Si, K, Ca, Ti, V, Cr, Mn, Fe, Rb, Sr, Zr, Br and Pb were measured using a Mo X-ray tube at 30kV. The cores GeoB10704 and GeoB10709 were additionally measured using a Cr X-ray tube at 30kV so as to include the lower atomic number elements; the measured elements were: Al, Si, S, K, Ca, Ti and Ba. The count time for each measurement was 30 seconds. Afterwards, five measurements were averaged so as to have the same 1-cm resolution as used for the cores measured with the AVAATECH core scanner.

The archive halves of the MP and DP cores (MP49, DP30, DP39, DP20, DP23) were scanned at 1 cm resolution with the AVAATECH scanner at the NIOZ in December 2008 (DP-cores: 20, 23, 30, 39) and January 2010 (MP49). The elements: Al, Si, P, S, Cl, K, Ca, Ti, Cr, Fe, Mn, Co, Rh, were measured at an X-ray voltage of 10kV, while the elements: Zn, Ga, Br, Rb, Sr, Y, Zr, Au, Pb, Bi and the elements: Sr, Zr, Nb, Mo, Ag, Sn, Te, I, Ba were measured with an X-ray voltage of 30kV and of 50kV, respectively. The count time of each measurement was 30 seconds. In September 2009 the detector in the core scanner was changed which resulted in higher counts in 2010 compared to 2008. In-house standards (SARM4, JB1 and JR1) measured daily during scanning indicate a standard deviation of less than 3% of the average for all elements presented in this study. All results are reported in counts per second.

As XRF core scanning data is considered to be semi-quantitative (Croudace et al., 2006; Richter et al., 2006; Weltje and Tjallingii, 2007), elemental ratios have been used rather

ETH Nº	Depth (mm)	Radiocarbon age (^{14}C age BP)	Calibrated age (year cal. BP)	Error (95%; ± yr)	Comment
38704	789	1290 ± 25	755	135	graphite target
38703	1792	2535 ± 30	2140	120	graphite target
40266	2794	3830 ± 40	3635	195	graphite target
37085	3286	4880 ± 40	5045	205	graphite target
37086	4285	6395 ± 45	6735	195	graphite target
42544	5280	8425 ± 118	8875	375	gas sample
42545	6276	10739 ± 191	11900	750	gas sample
42542	7276	11922 ± 147	13275	325	gas sample
42543	8266	13716 ± 171	15650	600	gas sample

Table 3: Age model and calculated sedimentation rates. The 14C-ages were calibrated with the program OxCal v3.10 (Bronk Ramsey et al., 2009), with the atmospheric calibration curve from Reimer et al. (2004) and the marine calibration curve Marine04 from Hughen et al. (2004) (additional reservoir age: ΔR=121±60 years).

than direct counts. The elements Al and Ti are amongst the most commonly used denominators (e.g., Croudace et al., 2006). Both elements are highly correlated and have a similar distribution, best illustrated by the quantitative ICP-AES data (Fig. 3a, b), concurring with results from other studies (e.g., Weltje and Tjallingii et al., 2008). Consequently, both of them would be suitable as a denominator, but preferably the one with the best reproducibility in XRF-scan data. Ti and Al counts from the XRF core scan indicate a positive trend but poor correlation (Fig. 3a). This is thought to be related to absorption due to water which is more severe for light elements such as Aluminium than for more heavy elements such as Titanium (Tjallingii et al., 2007; Hennekam and De Lange, 2013). Therefore, we will use Ti as a denominator in elemental ratios of XRF scan data. Furthermore, we will only compare trends, not absolute values of the elemental ratios, as small matrix effects may significantly influence instrumental performance within and between XRF-core scanners (Richter et al., 2006; Tjallingii et al., 2007).

4. Results

4.1. Core descriptions and Grain size analyses

The sediments from the Gulf of Taranto area and the Adriatic Sea are rather similar in colour, grain size and texture whereas deviating observations have been made for sediments from the western Ionian Sea (core DP20: heterogeneous sediments with large variations in colour, lamination and erosive horizons). The rather homogeneous sediments across the whole eastern Gallipoli Shelf consist of light grey-brown silty clays

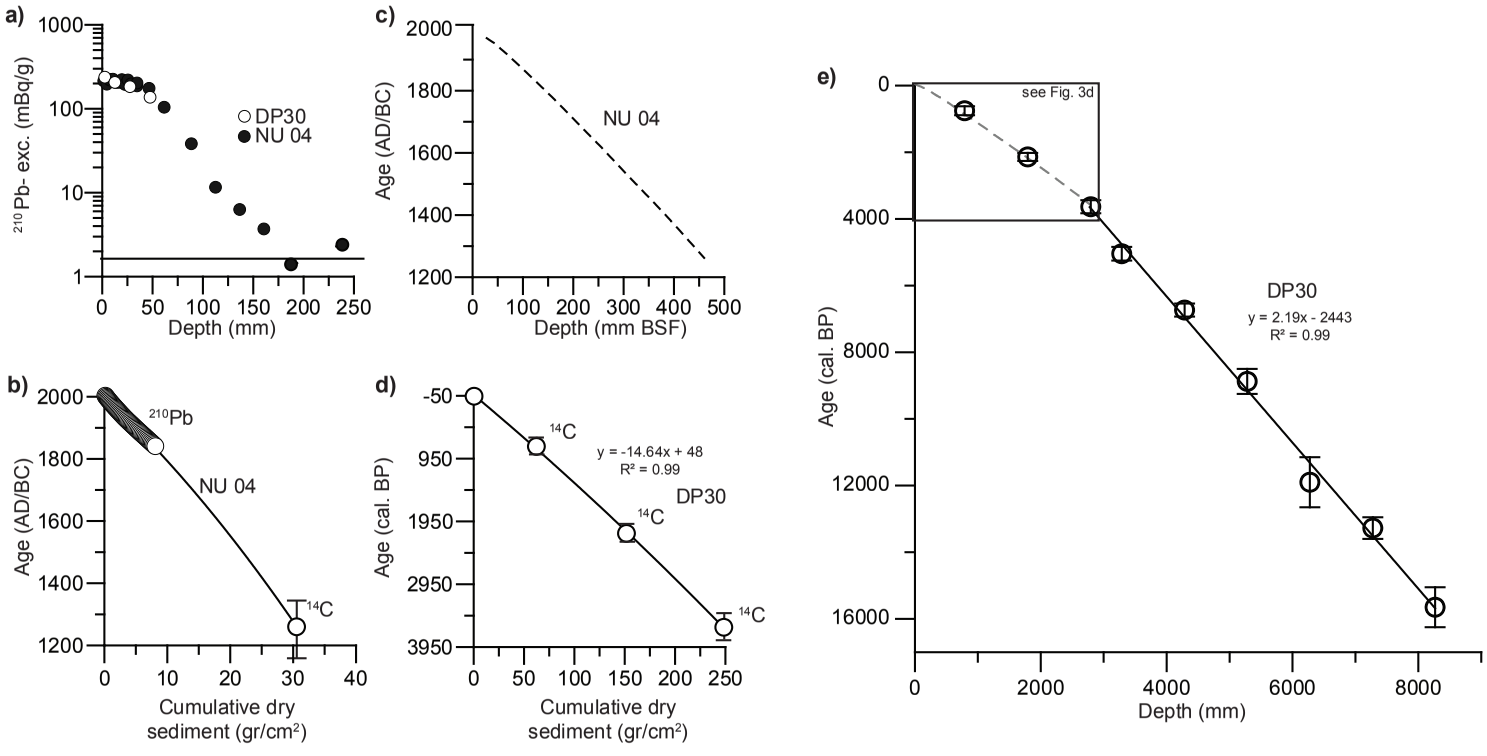

Fig. 2: (a) 210Pb depth profile of NU-04 (black circles) and DP-30 (white circles). Black line indicates the background values for the 210Pb model (b) age model of NU-04 using the cumulative dry sediment and the dating points from the 210Pb-model and radio-carbon dating (c) modeled age versus depth for NU-04 (d) age model of the first 2.5 m of DP30 using the cumulative dry sediment and the dating points from the 210Pb-model and radio-carbon dating (e) entire age model of DP30, the 14C-ages were calibrated with the program OxCal v3.10 (Bronk Ramsey et al., 2009), with atmospheric calibration curve from Reimer et al. (2004) and the marine calibration curve Marine04 from Hughen et al. (2004) (ΔR=121±60 years).

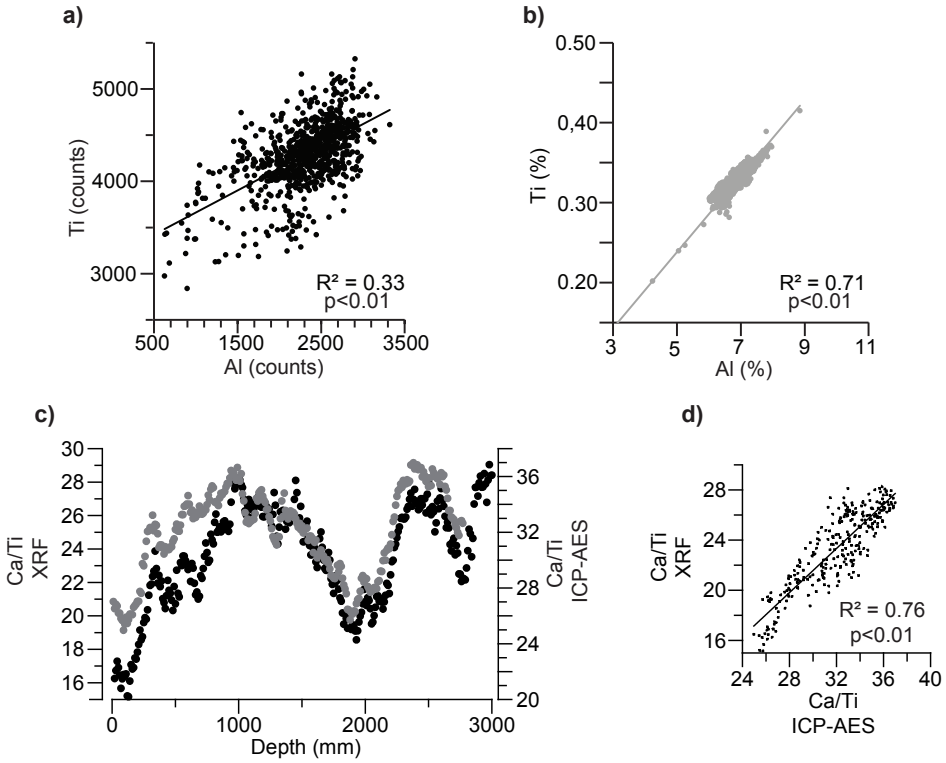

Fig. 3: Correlation between Ti and Al from XRF core scanning (a) and ICP-AES (b). (c) Comparison between Ca/Ti ratio by XRF core scanning (black dots) and by ICP-AES (grey) of the upper ~3 m of core DP30. (d) Correlation between the Ca/Ti ratios as found by both methods.

with isolated black, organic carbon-rich spots (for complete core descriptions contact authors and see Zonneveld et al. (2008). In the cores GeoB10703, GeoB10704, and GeoB10745, no distinctive sedimentological features were visible. In the lowermost meter of DP30 and MP49 shell fragments are present and the sediment is coarser. Moreover, the amount of organic carbon-rich spots is enhanced at the bottom of core MP49. In core GeoB10709 the interval 3.9-1.8 m contains much coarser material than below and above it. This core is located relatively close to the shelf edge, in an area potentially influenced by slump events (A. Savini, personal commun.), and is thus possibly affected by slumping and/or erosion (Fig. 1). Therefore, the sediments of this interval are attributed to a slump, and will not be discussed any further.

The grain size distribution for core-top sediments (0-2 cm) in the eastern part of the Gulf of Taranto is slightly bimodal, with elevated percentages in grain size in 2-8 μm (fine silt) and 30-40 μm (coarse silt) size fraction for all cores except GeoB10703 and GeoB10706 (Table 2). The latter lack the elevated percentages in the coarse silt fraction and are uni-modal (Table 2).

4.2. Age model of core DP30

The standard deviation for ^{14}C data in the four samples measured as CO_2 is slightly larger than that for the five samples measured as graphite (Fig. 2b,d,e, Table 3) because of the smaller amount of sample available (~200μg). Using a model (Boer et al., 2006) with a background of 15 Bq/kg, a sedimentation rate of 0.85 mm/yr with a bioturbation layer of 4.4 cm was determined on the basis of ^{210}Pb data for the upper part of the nearby NU-04 multicore (Fig. 2a, see Grauel et al., 2013a for more detailed description). This model for the upper-most part of the sediment was combined with a ^{14}C date and compared to the cumulative sediment accumulation taking the effects of increasing water content in the upper part into account (Fig 2b,c). A 1st order polynomial was used to combine ^{210}Pb and ^{14}C ages. During the recovery of DP30, the upper few mm were lost. Comparison between the 210Pb profile of DP30 and NU-04 revealed that this was equivalent to a loss of ~10 years (Fig. 2a). For the age model of DP30 we assumed a linear relationship between cumulative sediment accumulation and ^{14}C dates for the first 2500 mm (Fig. 2d). From this point (2500 mm) onwards, water content and thus compaction is thought to remain stable. Therefore, a linear relationship is assumed between ^{14}C dates and depth (mm) in this part of the core (Fig. 2e). The calibrated age for the bottom of core DP30 at 8270 mm is 15650 ± 600 cal. yr BP (±95% confidence) and thus includes the Older Dryas (Fig. 2e, Table 3). The latter suggest that the average sedimentation rate in DP30 is around 0.52 mm/yr.

4.3. Correlation of cores

The Ca/Ti ratio provides a distinct and consistent down-core pattern. This is not only related to the relatively good analytical reliability for these two elements using XRF core scanning (see also Tjallingii et al., 2007; Hennekam and De Lange, 2013), but also to the different provenances (from predominantly marine to terrestrial) represented by these elements (see 5.2). High-resolution ICP-AES data are available for the top 2.8 m of core DP30 (Fig. 3b, c and d). The Ca/Ti data for the two methods have a similar trend and show a high positive correlation (slope=0.86, R^2=0.76, $p<0.01$; Fig. 2d). However, some smaller scale oscillations in the Ca/Ti ratio which cannot be recognized in the XRF scan data are observed in the ICP-AES analyses (Fig. 3c).

Therefore, this ratio was used to correlate all cores to the dated core DP30. Based on a few tie- points, age models of all other cores are reconstructed (Fig. 4 and Supplem. Material). All cores from the Gallipoli shelf show a similar pattern in the upper part but with different sedimentation rates. Below 6.6 m, variations in the Ca/Ti ratio are small and thus correlation is more ambiguous (see Supplem. Material). Core GeoB10701 has a very different Ca/Ti profile and could not be correlated to the other cores (Supplem. Material). Sedimentation rates generally decrease with depth in each core, although not to the same extent in all cores (see Supplem. Material). No systematic difference in sedimentation rates is observed between the two different coring systems used (see Supplem. Material).

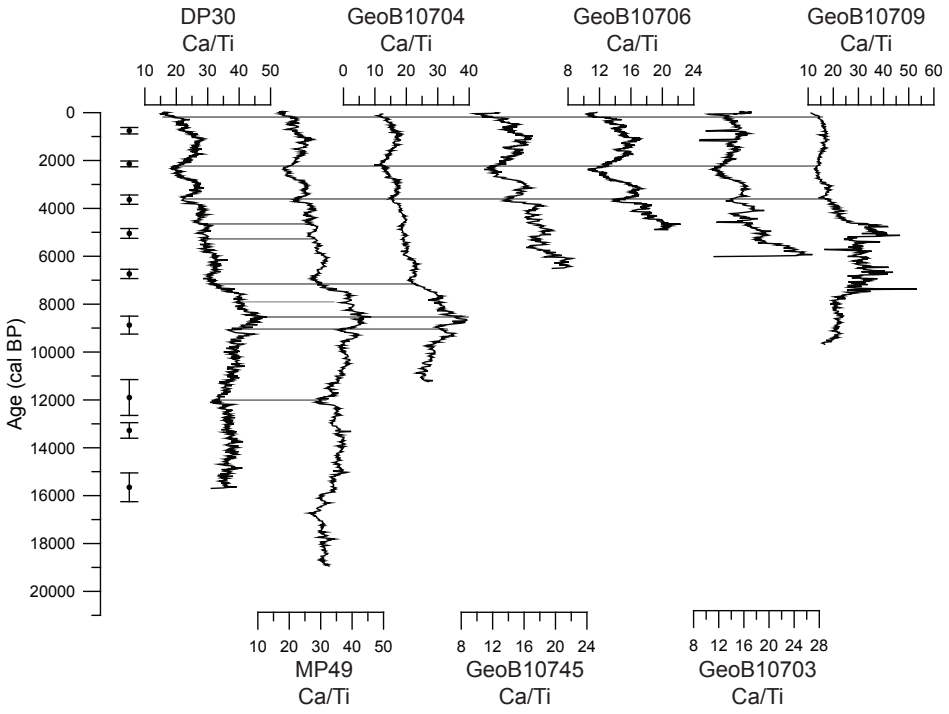

Fig. 4: Age models of the cores from the Gallipolli shelf calculated from the 14C-dated DP30 core (black dots with corresponding error bars) by correlation of the Ca/Ti curves (see Supplem. Material), and using the program AnalySeries 2.0, by D. Paillard (1996). The continuous lines mark the calibration tie points.

No correspondence is observed between Ionian Sea sediments (DP20) and sediments from the eastern Gulf of Taranto as observed in DP30 (Fig. 5). A clear correspondence is found between DP30 and DP39 (southern Adriatic Sea) from 4000 mm onwards, while DP23 (western Gulf of Taranto) resembles DP 30 from 1500 mm onwards (Fig. 5).

4.4 Element distributions in cores DP30 and GeoB10704

To study the overall changes in geochemical composition for sediments from the Gallipoli Shelf over the last 15000 years, Ca/Ti, Fe/Ti, K/Ti, Zr/Ti, Si/Ti, Ba/Ti, Br/Ti and Sr/Ca ratios derived by XRF core scanning are compared for cores DP30 and GeoB10704 (Fig. 6). These two cores have been selected as DP30 is well dated and GeoB10704 is located higher on the shelf at shallower water depth but from the same region and with a similar pattern in sedimentation rate and Ca/Ti ratio (Fig. 6a). Ba/Ti values are lacking for most of GeoB10704, as during these intervals the abundance of barium is below the detection limit for the equipment and setting used for XRF core-scanning of the GeoB cores (Fig. 6f).

During the Glacial-Interglacial transition (16-15 ka BP) Zr/Ti and Ba/Ti values decrease, while Si/Ti increases (Fig. 6d, e, f). The other elements (Ca/Ti, Fe/Ti, K/Ti and Br/Ti) show a relatively stable pattern in both cores (Fig. 6a, b, c, g) from 16 to 10.8 cal. ka BP. A small interruption is found around 12 cal. ka BP when low values of Ca/Ti and Si/Ti and high values of Ba/Ti and Fe/Ti are observed (Fig. 6a, b, e, f).

Sr/Ca values in both cores start to increase from 13 cal. ka BP (GeoB10704) and 11.5 cal. ka BP (DP30), respectively (Fig. 6h). Between ~11 and 7.5 cal. ka BP Br/Ti values are high in GeoB10704, while they are elevated from 9-7.5 cal. ka BP onward in DP30 (Fig. 6g), which concords with the occurrence of black spots and thus a darker colour of the sediments (Fig. 6i). Both cores show a step-wise increase in Fe/Ti around 9 cal. ka BP (Fig. 6b). This increase is coherent with a peak of K/Ti (Fig. 6c) and Zr/Ti (Fig 6d) and relatively low Ca/Ti values (Fig. 6a) in both cores (~8.7 cal. ka BP). The highest Ca/Ti values are found around 8.3 ka cal. BP. From ~8.3 to 0.5 cal. ka BP Ca/Ti, K/Ti, Zr/Ti, Si/Ti and Ba/Ti show a decreasing trend, while the Fe/Ti ratio increases (Fig. 6).

On top of these general trends, millennial-scale oscillations are observed for the Ca/Ti and Si/Ti ratios (Fig. 6a, e), and to some extent in the Fe/Ti, K/Ti , Zr/Ti (GeoB10704), Ba/Ti (DP30) and Sr/Ca ratios (GeoB10704; Fig. 6b, c, d, f, h).

5. Discussion

Potential variations in the detrital input will not only affect the terrestrial solid-phase fluxes but indirectly – via variations in dissolved riverine nutrient fluxes – also the marine primary productivity related fluxes. The terrigenous solid-phase fluxes can potentially originate from re-sedimentation of shelf sediments, and from input by local and by more remote (Adriatic) riverine systems, all of which are influenced by prevailing current directions and strengths (see 2: *Regional setting*). In addition, a minor eolian (Saharan) contribution is possible: For the present-day, 2/3 of the terrigenous fluxes to the central Ionian Sea sediments have been reported to result from eolian dust (e.g., Correggiari et al., 1989; Rutten et al., 2000). This eolian dust flux is equivalent to a sedimentation rate of ~10 mm/ka (Rutten et al., 2000) which is negligible compared to the total sedimentation rate of ~600 mm/ka in our study area, the Gulf of Taranto (Fig. 2). Therefore, we will not further discuss this option.

For the Holocene period, sea level change as well as partly related changes in current regimes may influence the sediment composition and deposition. Transport and accumulation of sediment in the Gulf of Taranto is thought to be highly dependent on bottom currents, which vary seasonally and interannually along the western Adriatic coast (Milligan and Cattaneo, 2007) and in the Gulf of Taranto. We will first outline the general sedimentation features for the region. Subsequently, we will discuss the constraints of the geochemical data from XRF core scanning as proxies for environmental variability. Subsequently, we zoom in on two cores from the Gulf of Taranto and discuss differences and changes in circulation using geochemical proxies.

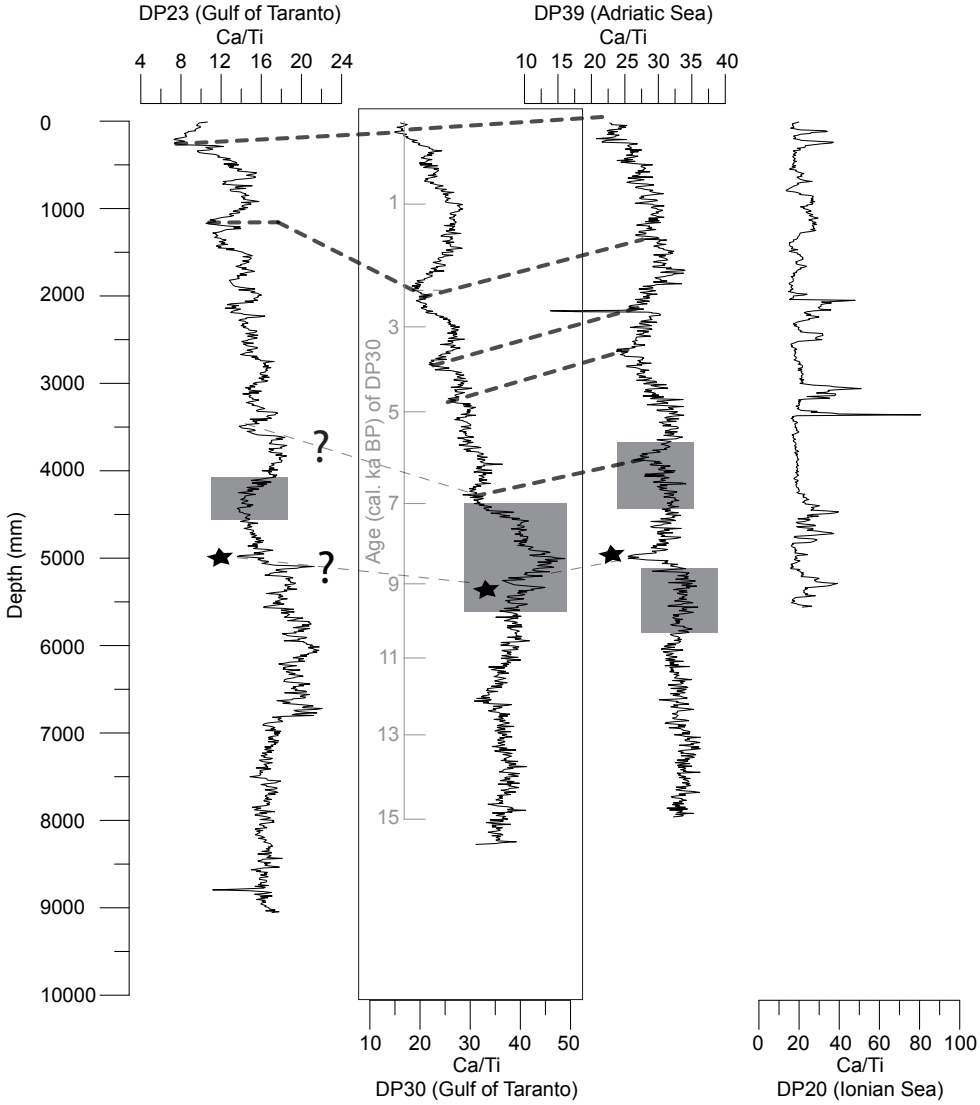

Fig. 5: Ca/Ti ratios of the cores DP23 (western part of the Gulf of Taranto), DP30 (eastern part of the Gulf of Taranto), DP39 (Adriatic Sea), and DP20 (Ionian Sea). Note that all Ca/Ti values are plotted against depth (mm) and that the grey vertical axes represents the age (cal. ka BP) of core DP30. The dashed lines indicate possible correlations. Grey boxes indicate intervals with more black particles, most likely corresponding to sapropel S1 formation. Stars indicate the possible tephra layer of the Mercato eruption.

5.1 Sedimentation in the Gulf of Taranto region

The Ca/Ti trends across the shelf are similar for data from XRF-core scanners and ICP-AES (Fig. 3c). This confirms the robustness of the Ca/Ti ratio for assessing a stratigraphic framework for the Gallipoli shelf sediments (Fig. 4, Supplem. Material). Sedimentation rates generally decrease with depth in each core, partly due to compaction, although not to the same extent for all cores. The average sedimentation rate varies between 0.49 mm/year (GeoB10704) and 0.92 mm/year (GeoB10706). This indicates that the seafloor structure and the sediment accumulation in the Gulf of Taranto may be rather heterogeneous (Rossi et al., 1983; Fig. 1). This may relate to areas with enhanced non-steady-state deposition as indicated by MultiBeam acoustic studies (A. Savini person. commun.) and shows that the sedimentation is not as uniform as initially anticipated and as suggested by previous studies (Cini Castagnoli et al., 1990). The latter study also identified several tephra layers from volcanic eruptions as thin horizons in the sediments from the Gulf of Taranto over the past 2000 years. These authors used the number of pyroxene grains in the sediment to identify volcanic eruptions in the area. These volcanic events are restricted to thin layers of < 0.5 cm i.e. below the resolution of our XRF data, and represent at most a minor fraction of the total sediment for regular 0.25 cm interval samples or for a 1 cm XRF scan interval. Therefore, it is concluded that with the methods used in this study it is not possible to identify such tephra layers. An exception to this is possibly an event around 9 cal. ka BP (cf. Section 5.3.2).

Although the sediments of DP23, located in the western Gulf of Taranto, are influenced by the same anticlockwise circulation within the Gulf, direct river discharge into the central and western Gulf of Taranto leads to a different chemical composition (Buccolieri et al., 2006; **chapter 2**) and sediment accumulation rate compared to the eastern part (Fig. 1,5). Such dominant local sources are virtually absent in the eastern Gulf (Fig. 1) and material may thus predominantly originate from more distal terrestrial and marine sources. The sediments in core DP20, located in the central Ionian Sea, also have a very different composition compared to those in the eastern Gulf (Fig. 5). This indicates that the major sediment supply to the eastern Gulf of Taranto originates from the Adriatic Sea (**chapter 2**). The sediment composition in the southern Adriatic Sea (DP39) is very similar to that in the eastern Gulf of Taranto, which is another indication for a common source of the sediments in these two areas (Fig. 5). In addition, surface samples in the Gulf of Taranto consist of relatively fine-grained sediments which concords with a distal source (e.g., Weltje and Brommer, 2011). Hence, the transport and deposition of sediments are influenced by a combination of regional and more remote terrestrial and marine environmental parameters. The good correspondence between sediments from the Adriatic Sea and the Gulf of Taranto, in combination with the fine grained sediments, all indicate that only small contributions of sediment may come from local sources (**chapter 2**). This is in agreement with minor local runoff in the eastern Gulf of Taranto. Therefore, we now focus the discussion on sediments from the eastern Gulf of Taranto, potentially reflecting supra-regional variability and being influenced by more remote and more general, prevailing paleoclimatic and hydrological conditions. Furthermore, the nearly identical patterns in geochemical composi-

tion across the Gallipoli Shelf (Fig. 4, 6) validate the use of one core to reconstruct Holocene environmental variability for the central Mediterranean area.

5.2 Elemental ratios as a proxy for environmental variability

The geochemical composition of surface sediments in the southern Adriatic Sea and Gulf of Taranto reflect changes in grain size, productivity, and provenance (Spagnoli et al., 2008; Weltje and Brommer, 2011; **chapter 2**). Geochemical data from XRF core scanning has been used successfully to reconstruct environmental variability (e.g., Haug et al., 2001; Richter et al., 2006; Hennekam and De Lange, 2013). However, proxies are usually not affected by a single parameter, and the dominating parameter may differ per region and time interval, especially in a complex area such as the Gulf of Taranto.

5.2.1 Detrital fluxes vs. marine biogenic fluxes

The stratigraphic framework of this study is based on patterns of Ca/Ti ratios, wich have been used as an indicator of marine biogenic carbonate versus terrestrial input (Richter et al., 2006; Rothwell and Rack, 2006). Although sediments from the Apulian margin contain carbonate (Pigorini, et al., 1968), their contribution to sediments of the Gallipoli shelf is considered to be minor at most. The values of Al (%), from detrital aluminosilicates (i.e., clay minerals), and Ca (%) mainly from marine carbonate in surface sediments from the study area fit to a Ca-Al mixing line (**chapter 2**). Thus, when sediments are enriched in clay minerals they are depleted in carbonates and vice versa. Samples from the western Gulf of Taranto deviate from this simple Ca-Al mixing line due to differing local terrestrial provenance (**chapter 2**). Hence, the Ca/Ti ratio is a valuable proxy for the variations in marine biogenic carbonate and terrestrial input into the eastern Gulf of Taranto.

5.2.3 Productivity

The Br/Ti, Si/Ti and Ba/Ti ratios are amongst the reported proxies for paleoproductivity (e.g., Rothwell and Rack, 2006; Ziegler, et al., 2008). Furthermore, enhanced Sr/Ca values indicate the presence of high-Sr aragonite, and therefore, usually are linked

next page **Fig. 6:** Comparison of selected elemental ratios from XRF core scanning a) Ca/Ti ; b) Fe/Ti; c) K/Ti; d) Zr/Ti; e) Si/Ti; f) Ba/Ti ; g) Br/Ti; h) Sr/Ca and i) Black-White scale (L*) of cores DP30 (AVAATECH core scanner, black lines, scale on the left) and GeoB10704 (ITRAX core scanner, grey line, scale on the right). Grey shaded intervals indicate periods with high detrital input (low Ca/Ti); dark-grey shaded box corresponds to the interval which contains an increased amount of black particles. B-A (B-A (a/Ti); dar), YD (Younger Dryas), S1 (sapropel S1 as defined by de Lange et al., 2008). Star indicates the possible tephra layer of the Mercato eruption.

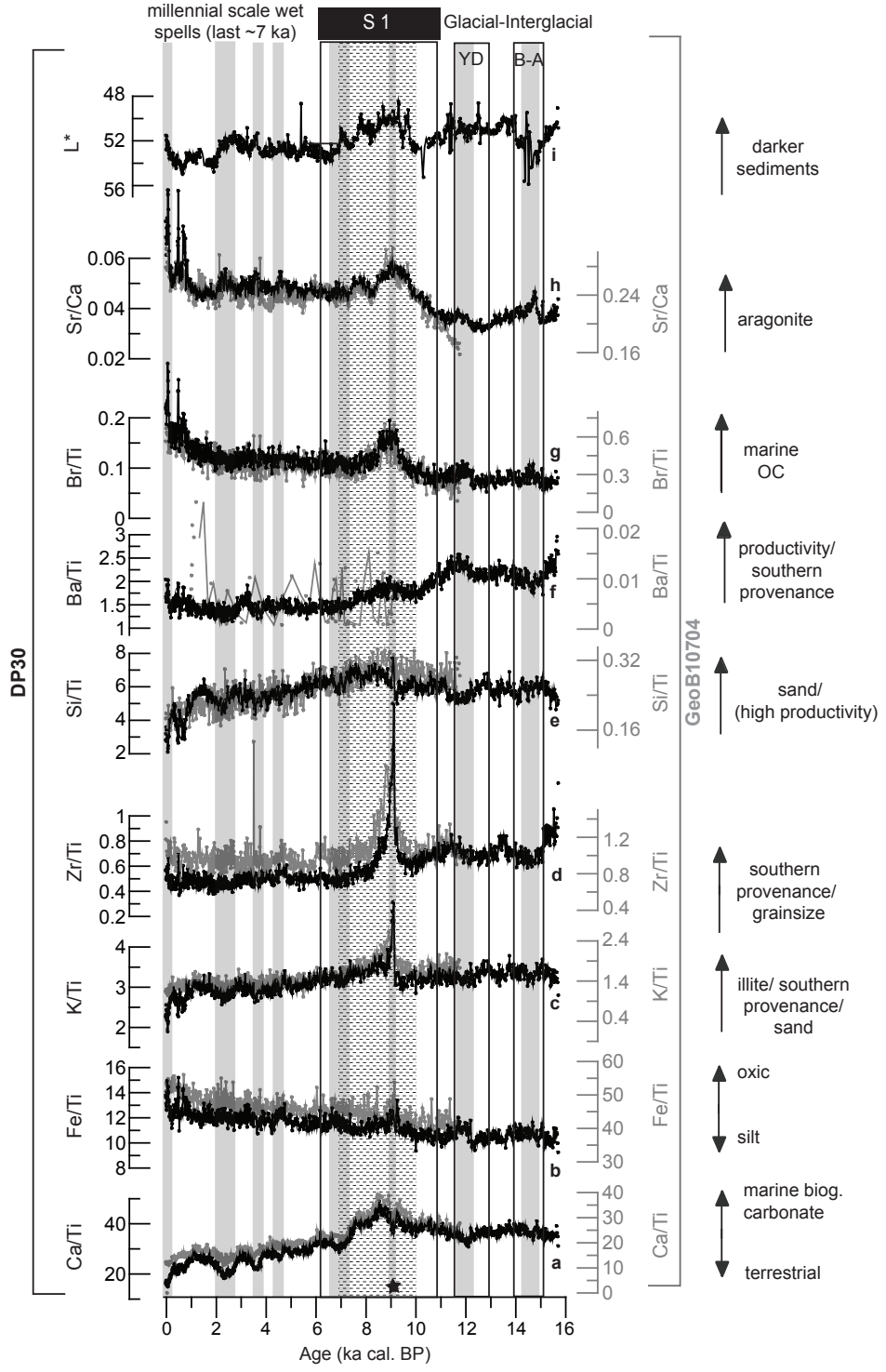
millennial scale wet spells (last ~7 ka)
S 1
Glacial-Interglacial
YD
B-A
DP30
GeoB10704
L*
Sr/Ca
Br/Ti
Ba/Ti
Si/Ti
Zr/Ti
K/Ti
Fe/Ti
Ca/Ti
Age (ka cal. BP)
darker sediments
aragonite
marine OC
productivity/ southern provenance
sand/ (high productivity)
southern provenance/ grainsize
illite/ southern provenance/ sand
oxic
silt
marine biog. carbonate
terrestrial

to shallow water biogenic carbonate, thus to carbonate productivity. Increased paleoproductivity and decreased oxygen exposure time of the organic matter, lead to higher preservation of marine organic matter which is highly associated with the Br/Ti ratio (Ziegler et al., 2008). High levels of Si/Ti may indicate the presence of quartz, but can also indicate increased opal concentrations, and thus diatom accumulation. The abundance of diatoms is associated with increased paleoproductivity, as has been reported for deep Mediterranean sediments during sapropel times (Kemp et al., 1999). As silica is highly undersaturated in the oligotrophic Mediterranean waters the preservation of opal seems unlikely at the core site at the present. However, some opal may remain, when productivity and sedimentation rates are high. Therefore, we assume the Si/Ti to be mainly related to changes in grain size, i.e. quartz content, but with some potential influence of diatom productivity.

The Ba/Ti ratio is like the Ba/Al ratio, a potential indicator for paleoproductivity (Reitz et al., 2004; Thomson et al., 2006). This ratio is influenced by two major components: 'detrital' and 'biogenic' (e.g., Klump et al., 2000; Reitz et al., 2004). The detrital component is strongly influenced by river source/provenance, whereas the biogenic component is related to marine primary productivity, i.e. to C_{org} (%). In our study area, barium is likely to vary with changing sediment provenance as the sites are strongly influenced by a variety of terrestrial sources. Furthermore, the accumulation rate of biogenic barite increases with water depth, as part of on-going diagenetic formation processes (e.g., Dymond et al., 1992; Von Breymann et al., 1992), and thus may be low- or even absent at shallow sites like the Gulf of Taranto. Hence, we consider the Ba/Ti ratio in these sediments to be predominantly related to provenance (see 5.2.2).

5.2.2 Provenance and grain size

Sediments from southern Italy are elevated in K, Zr, and to a lesser extent in Ba and Fe compared to sediments from northern Italy (Cocco, 1976; Spagnoli et al., 2008; **chapter 2**). Variability in the K/Ti, Zr/Ti, Ba/Ti and Fe/Ti, therefore, at least partly reflects variance in provenance of the sediments, the higher values being associated to a more southern source. However, in the study area K/Ti and Ba/Ti are also positively correlated with grain size. Elevated Fe/Ti, K/Ti and Zr/Ti have been associated with coarser grain size as well as with changes in provenance (e.g., Rothwell and Rack, 2006). For the surface sediments in the Gulf of Taranto and southern Adriatic Sea, the Fe/Al and thus the Fe/Ti ratio are correlated to the clay and sand fractions, while K/Al (K/Ti) and Zr/Al (Zr/Ti) are positively correlated to the sand fraction only (**chapter 2**). Some of these proxies are not only affected by grain size and provenance, but also by other parameters: Fe/Ti partly reflects changes in the redox state as in more sub-oxic environments Fe is mobilized in the sediments (Rothwell and Rack, 2006). In addition, climate may be reflected in the K/Ti ratio. K/Ti values are usually high in sediments that have a relatively high illite content. In general, more illite is eroded in cold environments. Here physical weathering is more dominant compared to tropical humid environments where chemical weathering dominates (Bonatti and Gartner, 1973, Yarincik et al., 2000).

Therefore, we consider the Fe/Ti, Ba/Ti, Zr/Ti, and K/Ti as proxies for provenance but with a potential impact of grain size. In addition, Fe/Ti may reflect redox conditions, while K/Ti may relate to illite content.

5.3 Reconstruction of environmental variability during the last 16 ka

During the Glacial-Interglacial transition and the subsequent Holocene, distinctly different climates occurred. In addition, considerable variability has taken place on millennial to decadal time-scales. To highlight related transitions and variability in our cores, we will focus the discussion on three periods: firstly the Glacial-Interglacial transition (16-10.8 cal. ka BP), secondly the most-recent Sapropel: S1 / Saharan humid period (10.8-7 cal. ka BP), and thirdly the Late Holocene (7 – 0 cal. ka BP) period.

5.3.1 Glacial-Interglacial transition (16-10.8 cal. ka BP)

5.3.1.1 Transition from the Last glacial to the Bølling-Allerød

The transition from the Last Glacial to the Bølling-Allerød (B-A, ~16-14 cal. ka BP) is generally characterized by a rapid change to warmer and wetter conditions in the Mediterranean region (Rossignol-Strick, 1999; Frisia et al., 2005; Bar-Matthews and Ayalon, 2011; Giraudi et al., 2011). The Ca/Ti ratio, an indicator of biogenic carbonate versus terrestrial input (see 5.2.1 above), remains constant until ~10.8 cal. ka BP (Fig. 6a), similar to other proxies of terrestrial provenance and marine productivity such as the K/Ti, Fe/Ti, Br/Ti and the Sr/Ca ratios (Fig. 6a-h). All these elemental ratios indicate that the influence of marine and terrestrial sources remained stable during this period. Remarkably, the Ba/Ti and Zr/Ti ratios show a sharp decrease in DP30 from 16 to 14.5 cal. ka BP (Fig. 6d, f) indicating an enhanced contribution from low-Ba/Ti northern river sources, but could also be a result of a decrease in grainsize. The latter may be related to a more distal provenance or to reduced winnowing at the coring site. Higher current velocities would have increase the relatively amount of coarse sediment and heavy minerals such as barite during periods of decreased water depth at the DP30 core site caused by low sea level stands. Taking the low sea level into account (Grant et al., 2012), the estimated water depth at 15 cal. ka BP at our core location was 160 m. However, if we consider the Si/Ti ratio to be an indicator for quartz content or coarseness of the sediment, then the slightly increasing Si/Ti values over the same time interval between 16 and 15 cal. ka. BP are inconsistent with a decrease in winnowing (Fig. 6e). In addition, if winnowing would play a role, we would expect K/Ti and Fe/Ti to also co-vary, which they do not. (Fig. 6b, c). Therefore, we conclude that the values for Ba/Ti and Zr/Ti, decreasing from 16 to 14.5 cal. ka. BP, are related to an increased contribution from northern relative to southern Adriatic Rivers (**chapter 2**). The lack of decreasing K/Ti values, can be explained by a relation of the K/Ti values and change in relative illite content (e.g., Yarincik et al., 2000). Illite is higher in sediments from northern riv-

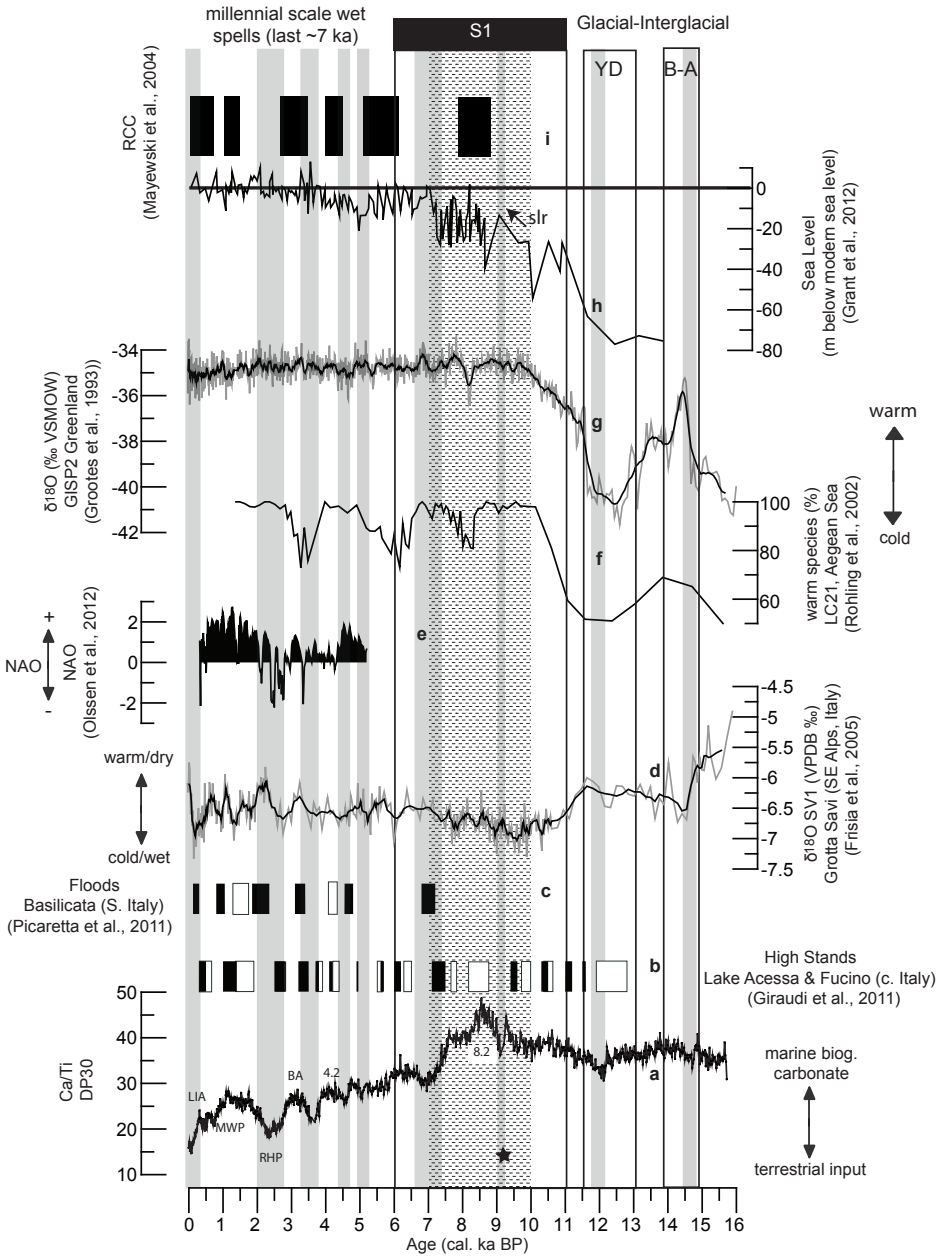
millennial scale wet spells (last ~7 ka)
S1
Glacial-Interglacial
YD
B-A
RCC (Mayewski et al., 2004)
i
slr
h
Sea Level (m below modern sea level) (Grant et al., 2012)
0
-20
-40
-60
-80
δ18O (‰ VSMOW) GISP2 Greenland (Grootes et al., 1993))
-34
-36
-38
-40
-42
g
warm
cold
f
warm species (%) LC21, Aegean Sea (Rohling et al., 2002)
100
80
60
NAO
NAO (Olssen et al., 2012)
+
-
2
0
-2
e
δ18O SV1 (VPDB ‰) Grotta Savi (SE Alps, Italy) (Frisia et al., 2005)
-4.5
-5
-5.5
-6
-6.5
-7
-7.5
d
warm/dry
cold/wet
Floods Basilicata (S. Italy) (Picaretta et al., 2011)
c
b
High Stands Lake Acessa & Fucino (c. Italy) (Giraudi et al., 2011)
Ca/Ti DP30
50
40
30
20
10
LIA
MWP
RHP
BA
4.2
8.2
a
marine biog. carbonate
terrestrial input
0 1 2 3 4 5 6 7 8 9 10 11 12 13 14 15 16
Age (cal. ka BP)

Previous page **Fig 7**: a) Ca/Ti ratio of DP30 compared to: b) Lake level high (black blocks) and low (grey blocks) stands of Lake Accesa and Lake Fucino, Central Italy (Giraudi et al., 2011); c) Periods of increased flood frequency in the Basillicata region, South Italy (Picaretta et al., 2011); grey blocks indicate potential summer flood events; d) Speleothem oxygen isotope record from Grotta Savi, SE Alps, Italy (Frisia et al., 2005); e) Reconstruction of the NAO from a lake in Greenland (Olssen et al., 2012); f) Percentage of warm water foraminifera in the Aegean Sea (Rohling et al., 2002); g) The GISP2 oxygen isotope record by Grootes et al. (1993); h) Reconstruction of sea level variability (Grant et al., 2012) and i) Rapid climate change events (Mayewski et al., 2004). Grey shaded boxes indicate periods of high detrital input (low Ca/Ti); grey shaded box marks the interval with an increased amount of black particles (see Fig. 6i). B-A (Bølling-Allerød), YD (Younger Dryas), S1 (sapropel S1 as defined by de Lange et al., 2008), 8.2 (8.2 ka event), 4.2 (4.2 ka event), BA (Bronze Age), RHP (Roman Humid Period), MWP (Medieval Warm Period), LIA (Little Ice Age), Star indicates the possible tephra layer of the Mercato eruption, slr indicates the sea level rise, related to flooding of the Northern Adriatic Sea shelf.

ers, but it is suggested that more illite is eroded under cold and arid conditions (cf. 5.2). The increasing influence from northern rivers as reflected by the decreasing Ba/Ti and Zr/Ti values is coherent with a more humid climate for northern Italy (e.g., Frisia et al., 2005; Giraudi et al., 2011).

5.3.1.2 The Bølling-Allerød and Younger Dryas

The stable Ca/Ti values are interrupted by two short intervals (around 14.5 and 12.3 cal. ka BP) with higher river-fluxes (low Ca/Ti and high Fe/Ti), and increased productivity and C_{org}-fluxes (enhanced Br/Ti ratios; Fig. 6g). These intervals correspond to the Bølling-Allerød (B-A; ~14.67 cal. ka cal. BP) and the Younger Dryas (YD; 12.9 to 11.5 cal. ka BP). During the B-A, Ba/Ti and Zr/Ti values are low compared to the YD (Fig. 6d, f). This indicates that during the YD sediments had a more southern provenance. The short period when Ca/Ti is low in our record (12.4-12.1 cal. ka BP) is coeval with a cold spell in the GISP2 oxygen isotope ice core-record (Fig 7a, g; Grootes et al., 1997). In contrast to the B-A, which is characterized as warm and wet, the YD has been described as cold and dry in Italy (e.g., Bottema et al., 1995; Zonneveld et al., 1996; Frisia et al., 2005). Other records from southern Italy recording the YD are scarce and lack high resolution to confirm our observation (e.g., Combourieu-Nebout et al., 1998; Allen et al. 2002). However, high resolution pollen records from the southern Balkan and the Aegean Sea suggest that the YD can be divided into three intervals (Bordon et al., 2009; Dormoy et al., 2009). The authors show that the cold and dry YD period is interrupted by a period where warmer and more humid conditions prevailed. They observed that winter precipitation remained low and that summer precipitation could have been similar or even higher than today. In our data we observe a drop in Ca/Ti. This is consistent with the warmer and wetter period observed by Bordon et al. (2009) and Dormoy et al. (2009). The latter relate these changing conditions to the southern emplacement of the high pressure cell of the Intertropical Convergence Zone during the YD. Today, the more northern emplacement of this zone during summer, blocks the moisture-rich

westerlies, which results in the characteristic dry summer conditions (Alpert et al., 2006; Piervitali et al., 1997).

Elevated sediment erosion and therefore increased terrestrial supply to the Gulf of Taranto due to short, but intensive rainfall after long arid periods is known from the southern rivers (Picaretta et al., 2011). Hence, it is plausible that during this warmer interval of the YD terrestrial runoff from southern Italian rivers was higher, whereas riverine input in northern and central Italy was lower.

5.3.2 Sapropel S1 –Saharan humid period (10.8-7 ka BP)

The formation of the most recent sapropel S1 occurred synchronously in the deeper parts of the eastern Mediterranean between 10.8 and 6.1 cal. ka BP (De Lange et al., 2008). The higher amount of black organic particles (L*), the higher Br/Ti ratio (10-8 cal. ka BP) and Sr/Ca ratio (10.5-7.5 cal. ka BP) all mainly coincide with the older part of sapropel formation time (Fig. 6g, h, i). At these shallow and high sedimentation rate sites, Ba/Ti cannot be used as a proxy for productivity but rather for provenance. The step-wise decrease of Ba/Ti during this period therefore reflects an increase in northern provenance of the sediments rather than a decrease in productivity. The increase in organic matter content as deduced from the enhanced Br/Ti, can thus be related to an increase in preservation and productivity. In general, the period corresponding to sapropel formation is considered wet in the northern borderlands (Kotthoff et al., 2008; Giraudi et al., 2011 and references within). The high Ca/Ti ratio seems to contradict these observations (Fig. 6a). However, a high Sr/Ca ratio and a relatively enhanced $CaCO_3$ (high Ca/Ti) content in near-coastal deposits of sapropel S1 have been reported in a variety of cores from the eastern Mediterranean, and have been attributed to an increased aragonite content from a shallow-water biogenic source or to diagenetic processes for deep-basin deposits (Reitz and De Lange, 2006; Thomson et al., 2004). In view of the elevated Br/Ti, Si/Ti and Sr/Ca ratios, an enhanced organic matter-, opal-, and carbonate- productivity seems likely for this period (Fig. 6e, g, h).

The pronounced shifts observed at ~ 9 cal. ka BP for Fe/Ti, K/Ti, and Zr/Ti may be related to tephra from a volcanic event, and to a shift or rerouting of sediment provenance (Fig. 6b, c, d). As the sediment interval of enhanced elemental ratios is much thicker than usually found for a tephra (cf. section 5.1) both options are possible. The tephra may be related to a series of eruptions known as the Mercato eruption (Mele et al., 2010), that resulted in distinctive, relatively thick tephras in the northern Ionian Sea (Caron et al., 2012). In addition, a potential provenance rerouting is, however, also possible as during this time sea-level rise, and flooding of the northern Adriatic occurred (Fig. 7c, h).

Often it is found that sapropel S1 is interrupted by the so-called 8.2 ka cooling event (Rohling et al. 1997; De Rijk et al., 1999). This cold event is expressed in our record by enhanced marine influence and/or dry conditions (high Ca/Ti), and enhanced marine organic matter (high Br/Ti) (Figs. 6b, g and 7a).

Gallipoli Shelf sediments from the upper sapropel S1 formation period, i.e. 7.5-6.1 cal. ka BP do not show any evidence for environmental changes in the records of Br/Ti or black organic particles (Fig. 6g, i). This could be due to post-depositional oxidation of organic matter or to diminished 'sapropelic conditions' for shallow sediments during that period (e.g., van Santvoort et al., 1997). Various authors have claimed that sapropel formation at shallower sites in the Adriatic Sea stopped earlier than at deeper sites (resp. ~ 7.5 ka and ~6.1 ka BP; Piva et al., 2008; De Lange et al., 2008). This is thought to be related to postglacial sea-level rise, the consequent flooding of the northern Adriatic, and the related onset of NAdDW, ventilating shallower bottom waters (Piva et al., 2008). The enhanced ventilation and concomitantly reduced primary productivity and preservation, are thought to have resulted in the suppression of detectable sapropel indicators in our shallow sediments of the eastern Gulf of Taranto.

5.3.3. Late Holocene (7 – 0 cal. ka BP)

The decrease in the Ca/Ti, Ba/Ti and Si/Ti ratio and the increase in the Fe/Ti ratio for both cores indicate a progressive increase in terrestrial input from a distal source during the mid-to-late Holocene (8.2 - 2.5 cal. ka BP; Figs. 6a, b, e, f and 7a). The most rapid increase in terrestrial input occurs at ~ 7 cal. ka BP and coincides with sea level rise (Fig. 7h; Grant et al., 2012) and the onset of NAdDW-formation, enhancing the southward transport of sediment, and presumably inducing the end of sapropel S1 formation in the southern Adriatic (De Rijk et al., 1999, Piva et al., 2008). Although there is no age model for core DP39, we observe a similar pattern in Ca/Ti in DP39 and DP30 from around 4.2 m depths onward, corresponding to ~ 7 cal. ka BP in DP30 (Fig. 4, 5). This correlation between Adriatic core DP39 and the Gulf of Taranto is consistent with a closer connection between these two areas during the period 0-7 cal. ka BP. Furthermore between 7 and 4 cal. ka BP, higher lake levels and increased flood frequency in Italy also indicate less aridity (e.g., Giraudi et al., 2011; Piccarreta et al., 2011), which is presumably related to the increased strength of the westerlies in the Mediterranean area (Fig. 7b, c). The observed increasing trend in terrestrial input thus corresponds to increased humidity that can be related to a reorganization of atmospheric circulation and hydrological patterns in the Northern Hemisphere (e.g., Mayewski et al., 2004; Haug et al., 2001; Knudsen et al., 2011). This has been attributed to changes in the orbital configuration and declining influence of continental ice sheets (e.g., Rossignol-Strick, 1985; Haug et al., 2001; Knudsen et al., 2011; Shuman and Plank, 2011). Moreover, deforestation, since 5500 years ago, possibly anthropogenic in origin, has resulted in higher sediment fluxes to the Adriatic Sea (Oldfield et al., 2003). This is in agreement with the high sedimentation rates and low Ca/Ti found in the upper part of DP30 which is thought to reflect enhanced deforestation especially during the last 700 years (Oldfield et al., 2003).

In addition to the long-term decreasing trend, Ca/Ti, K/Ti, Si/Ti and Sr/Ca ratios of the cores show oscillations with periods of ~1000-2000 years during the last 8 cal. ka BP (Fig. 6a, c, e, h a; 7a). Intervals of low Ca/Ti (high detrital input), low K/Ti (low illite content and therefore humid conditions), low Si/Ti (lower quartz content) and high Sr/

Ca (high aragonite content) ratios are observed at 7000-6500, 4900-4600, 3400-3600, 2500-2000 (RHP) and 250 cal. yr BP. These periods correspond to periods of high lake levels and increased flood frequency in central and southern Italy (Giraudi et al., 2011; Piccarreta et al., 2011; Fig. 7b, c). Some of the intervals with high lake levels and frequent floods during the MWP and around the 4.2 ka event seem to have no expression in the Ca/Ti ratios of this study (Fig. 7a). However, Picarreta et al. (2011) describe the observed floods during these particular periods as low-frequency, high-precipitation events, i.e. storms not related to mean annual rain fall (Fig. 7c). Furthermore, although lake levels are higher during these periods, they are not as pronounced as the other lake level high stands (Giraudi et al., 2011). In addition, Magny et al. (2003, 2009) have shown that the 4.2 ka event has a complex pattern of short wet and dry periods, which are not synchronous across the Mediterranean basin. A minor annual impact, low frequency, and complex nature of these wet spells can explain why they left no clear signal in the sediments of the Gulf of Taranto. Although, deforestation may play a role in the high sedimentation rates of the last 5500 years, this cannot explain the observed patterns of wet/dry spells in this study (Oldfield et al., 2003). In addition, human impact in the environment appears to be very restricted in southern Italy during the late Holocene (DiRita and Magri, 2009). Therefore, we assume that climatic variability must have been the major factor influencing the element composition,

With regard to large-scale climate events, the observed dry spells (high Ca/Ti) at ~6500-5000,4500-3600, 3400-2500 (Bronze Age (BA)) and 2000-1000 (MWP) cal. yr BP, correspond to globally recognized, so- called 'cool poles, dry tropics' rapid climate change (RCC) events (Mayewski et al., 2004, Fig. 7i). These events are also observed in the northern and central Adriatic Sea (Piva et al., 2008). The comparison of the Ca/Ti ratio to the Aegean cold spells (Fig. 7f; Rohling et al., 2002), demonstrates that increased runoff (low Ca/Ti ratio) can be found near the beginning and end of Aegean and Adriatic cold spells (De Rijk et al., 1999). Frisia et al., (2005) based on a stalagmite record, suggested relatively high temperatures in northern Italy during these 'wet' periods. Holocene cold spells as observed at 2.7 (BA), 6 and 8.2 cal. ka BP in the Aegean Sea and Adriatic Sea have been related to outbreaks of cold, dry winds from Siberia, known as the Bora in the Adriatic region, and fit to maximum alpine glacier extent and deep Icelandic Lows (Denton and Karlén, 1973; Rohling et al., 2002; Mayewski et al., 2004; Fig. 7f). Today deep Icelandic Lows are related to a more positive NAO, hence dryer and colder conditions in the Mediterranean region (Hurrell, 1995; Brandimarte et al., 2011, Fig. 7e). A persistent positive winter NAO is also inferred for the other RCC events (MWP and 4.2 ka event), in particular the MWP (Lamy et al., 2006; Trouet et al., 2009; Nieto-Moreno et al., 2011; Olssen et al., 2012, Fig. 7e). The positive state of the NAO today has been related to low sea surface temperatures in the North Atlantic and higher temperatures in Greenland (e.g., Hurell et al., 1995). This pattern is, however, neither evident in Icelandic Low reconstructions, nor in the Aegean cold spells (Rohling et al., 2002). Rohling et al. (2002) suggest that the absence of some RCC in the Aegean Sea record, is related to the attenuated forcing of ice-related feedback mechanisms since ~7 ka, affecting only sites directly influenced by the thermohaline circulation during relatively 'weak' and less widely recognised events as the MWP and the 4.2 ka event.

In summary, periods with high Ca/Ti ratio correspond to a positive NAO, hence dryer and colder conditions (Fig. 7a,e). We therefore suggest that periods of increased detrital input can be associated with a negative NAO, inducing humid and marginally warmer conditions in the Mediterranean region (e.g. Hurrell et al., 1995, Trigo et al., 2006). Although the increased detrital input during the LIA (~650-150 cal. yr BP) seems to contradict the patterns found during other periods between ~9000 and 600 cal. yr BP, it should be noted that most increased runoff is visible at the end of the LIA (~250 cal. yr BP- 150 cal. yr. BP), which is in agreement with reconstructions of western Mediterranean climate and NAO variability (e.g., Trouet, et al., 2009; Nieto-Moreno et al., 2011).

Besides the NAO, also local factors have an influence on river runoff in the Mediterranean (Lionello et al., 2006). First, during dry periods that lack cold Bora winds (i.e. the MWP and 4.2 ka event) it is relatively warm compared to the other RCC events (Frisia et al., 2005). This results in increased evaporation in the Italian hinterland and possibly contributes to reduced runoff. Secondly, less ADW is formed during warmer intervals (Turchetto et al., 2007). This leads to increased influence of the Levantine Intermediate Water (LIW) from the central Ionian Sea, and thus to a higher marine influence into the study area (higher Ca/Ti ratios). Thirdly, at transitions from cold to warm periods, melt-water from alpine glaciers may also contribute to the observed rising river runoff.

In summary, our data show that a positive state of NAO is related to a relatively dry climate in the Mediterranean. Such conditions may be modified by regional factors such as Mediterranean circulation patterns, increased evaporation, and dry Bora winds.

6. Conclusions

On the basis of multiple XRF core scans and precise AMS ^{14}C-dating, we show that sediment cores from the Gulf of Taranto can be accurately correlated using the Ca/Ti ratio. For the sites mostly affected by supra-regional influences, we have derived climate variability for the last 16 cal. ka. BP at high-resolution using a range of geochemical proxies.

In general, conditions were dry and stable during the Glacial/ Interglacial transition. Two short intervals of increased detrital input can be related to the Bølling-Allerød and late Younger Dryas (YD). During the late YD, this increased detrital input appears to originate from a Southern Italian source, suggesting an increased precipitation in Southern Italy, while run off from Northern Italy remained low.

On the shallow Gallipoli shelf, slightly increased concentrations of organic material and biogenic carbonate are observed during part of the sapropel S1 period (~10-7.5 cal. ka BP) indicating increased primary productivity and/or preservation. After 7 cal. ka BP, a constant increase in terrestrial input and increased sedimentation rates indicate a progressive change towards modern circulation for the Adriatic / NW Ionian Sea. In addition, wetter conditions and deforestation during this period have resulted in increased

terrestrial fluxes into the area.

Superimposed on this long-term trend, we observe millennial-scale variability in terrestrial input which corresponds to global climate variability and to the NAO in particular. Although regional factors such as increased evaporation also contribute, we suggest that a positive state of the NAO, i.e. dry conditions in the Mediterranean, dominated during RCC events such as the MWP and the Bronze Age.

Acknowledgements

This contribution is part of the MOCCHA project, supported by the European Science Foundation (ESF-EuroMarc) with associated financial support from the Netherlands Organization for Scientific Research (NWO-Project .817.01.002), the German Science Foundation (DFG grants to GV and KZ), and the Swiss National Science Foundation (SNF Projects 20MA21-115934 and 200020_134987). Alessandra Savini (Milan-Bicocca University) is thanked for access to Multibeam data and discussions of sedimentary dynamics of the area. We thank Helen de Waard for her help with ICP-AES analyses at Utrecht University and Rineke Gieles for core scanning assistance at the Royal Netherlands Institute for Sea Research. Prof. Dr. Bernd Zolischka, Sabine Stahl and Christian Ohlendorf are thanked for technical support and access to XRF-ITRAX scan equipment at the Geography Institute (GEOPOLAR group), University of Bremen. Sample material has been provided by the GeoB Core Repository at the MARUM- Center for Marine Environmental Sciences, University of Bremen, Germany. The data reported in this paper are achieved in Pangaea (www.pangea.de). Authors are grateful to Captain, Crew and Colleagues with RV Pelagia DOPPIO-cruise (October-November 2008) and MACCHIATO-cruise (November-December 2009), both coordinated by Gert J. De Lange, and with RV Poseidon CAPPUCCIONO-cruise (July 2006) coordinated by Karin Zonneveld. In addition, we acknowledge financial, technical, and logistic support given by NIOZ/NWO for DOPPIO and MACCHIATO cruises and the DFG for CAPPUCCINO cruise. We thank two anonymous reviewers for constructive and helpful comments.

Supplementary Information

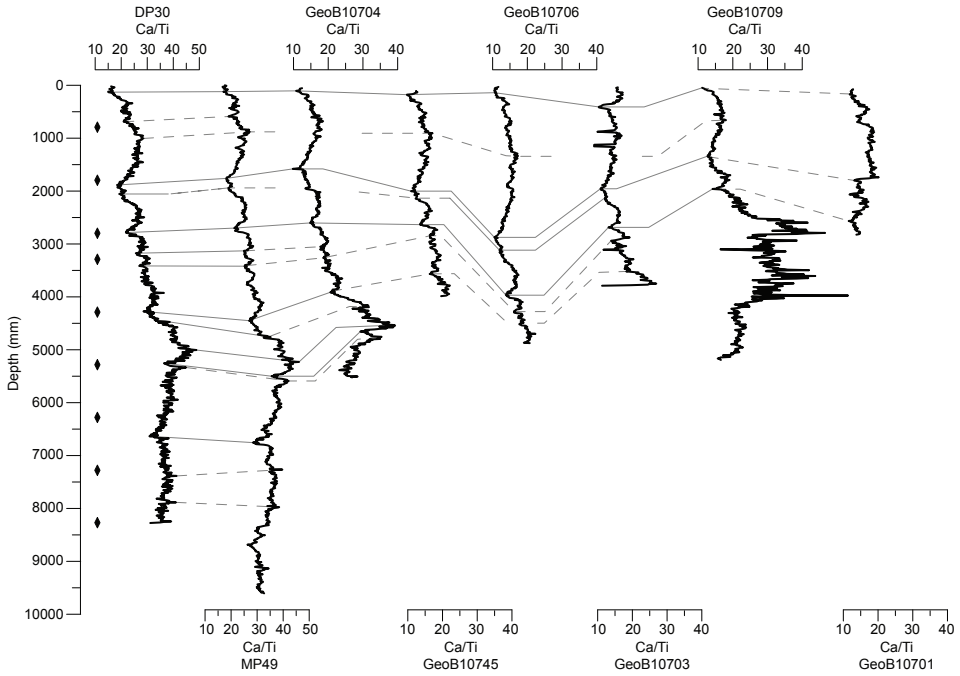

S.I.:Ca/Ti ratio versus depth (mm) for all cores in the eastern Gulf of Taranto. The continuous correlation lines have been used to build an age model for the cores without 14C-dating, while the dashed lines indicate potential correlations that have not been used for the age model calculation

Chapter 4: High and low latitude climate variability during the last 3500 years as observed in Central Mediterranean marine deposits

Marie-Louise S. Goudeau, L.J. de Nooijer, W, Boer, S. M. Bernasconi, A-L. Grauel, G-J. Reichart and G.J. de Lange

(In review for Palaeocenography)

Dating uncertainties prohibit comparison between independent records of high and low latitude paleoclimate. The Mediterranean climate is influenced by the mid-latitude westerlies in winter and the sub-tropical high pressure belt during summer. As it is sensitive to climate variability of both latitudes, its sedimentary records allow reconstructing changes of and the interplay between both. Here, we present a 3500 year long high-resolution, multi-proxy study from the Central Mediterranean. Sediment geochemistry is combined with carbonate test-chemistry of two foraminiferal species, the planktonic *Globigerinoides ruber* (white) and the benthic *Hyalinea balthica*. Carbon isotope chemistry of *G. ruber* (white) reflects summer conditions and, hence, can be used to reconstruct the influence of the subtropical high-pressure cell. Since bottom waters at the study site are ventilated during winter, Na/Ca values of *H. balthica* can be used to reconstruct variability of the mid-latitude westerlies. The test chemistry of both species reveal centennial scale variability in seawater salinity. Furthermore, results suggest alternating coupling of high and low latitude climate variability. During episodes with minor ENSO activity a relatively northern pathway of the westerlies is associated with a southward shift of the position of sub-tropical high pressure cell. In contrast, under strong ENSO conditions, both move north or southwards simultaneously. Moreover, under these conditions the westerlies show a 60-90 year periodicity, corresponding to the Atlantic Multi-decadal Oscillation (AMO). Since low latitude climate variability is inevitably affected by AMO, this implies that during strong ENSO conditions low as well as high latitude climate are enforced by AMO.

1. Introduction

The climate of the Holocene is characterized by major millennial to decadal time scale variability (e.g. Mayewski et al., 2004; Wanner et al., 2008). At high and low latitudes, atmospheric circulation patterns varied on short time scales, albeit with different frequencies (Wanner et al., 2008). At low latitudes, shifts in the average summer position of the Inter Tropical Convergence Zone (ITCZ) played a dominant role in climate variability on short time scales (e.g. Haug et al., 2003; Wang et al., 2005). At higher latitudes (i.e. Europe), precipitation patterns are strongly influenced by the North Atlantic Oscillation (NAO). The NAO is defined as the atmospheric pressure gradient between the Icelandic Low and the Azores High (Hurrell et al., 1995). Periods with a low NAO index (NAO-) are characterized by more humid conditions in the Mediterranean region. The strength of the NAO varies not only intra- and interannually, but also on decadal to centennial time scales. The exact mechanism responsible for NAO variability on these time scales is not fully understood (e.g. Hurrell and Deser, 2009). Instrumental records spanning the last 100 years, suggest a causal relation between winter NAO and Atlantic Sea Surface Temperature (SST). This connection appears to be non-stationary since it has only been observed during strong El Niño Southern Oscillation (ENSO) conditions or periods with relatively high North Atlantic SSTs (Hoerling et al., 2001; Sutton and Hodson, 2003; Knudsen et al., 2011). In contrast to the non-stationary connection of Atlantic SST and the winter NAO, decadal shifts of the position of the ITCZ in West Africa, causing Sahel drought, have been consistently linked to Atlantic SST variability (Knight et al., 2006; Shanahan et al., 2009).

Low and high latitude climate variability in the Atlantic region are connected by Atlantic SST and hence are affected by millennial-scale variations in strength of the North Atlantic Meridional Overturning Circulation (AMOC, e.g. Lamb et al., 1995; Tjallingii et al., 2008). If and how climate variability at high and low latitudes are linked on a centennial scale is, however, poorly constrained. Comparing paleoclimate-records of high latitudes with those of low latitudes on centennial time-scales is challenging due to uncertainties associated with dating techniques (often more than a century) when correlating independent records. This prevents identification of leads and lags in the signals of such records on centennial time scales. Hence high-resolution climate archives, recording both high and low latitude variability within the same record, are necessary to directly compare and interpret the interplay between high and low latitude climate, and variability therein.

Here we present a multi-proxy record spanning the last 3500 years from the Gulf of Taranto, southern Italy. This area is characterized by high sedimentation rates enabling high resolution palaeo-climate studies (e.g. Cini Castagnoli et al., 1992a,b). Variability in Italian winter precipitation is dominated by the NAO (e.g. Brandimarte et al., 2011; Caloiero et al., 2011). Summers are relatively dry as a result of the northward extension of the high pressure zone of the Hadley cell (Alpert et al., 2006 and references therein) which is linked to the summer position of the ITCZ. Hence both changes in winter NAO and the summer position of the ITCZ are potentially reflected in these sediments.

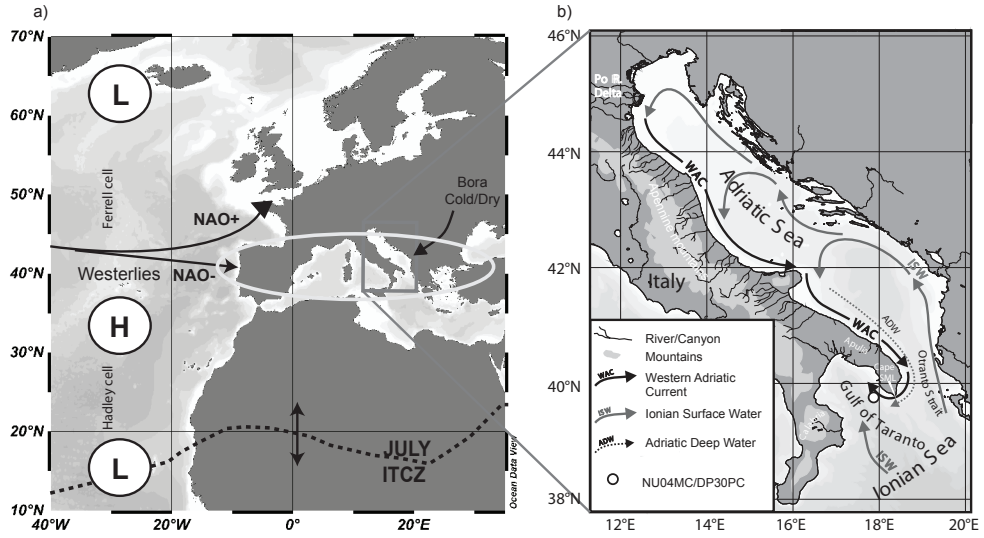

Fig. 1: (a) Map of Western Europe and Northern Africa showing precipitation patterns during a positive NAO mode(NAO+) and negative NAO mode (NAO-), the position of the ITCZ during summer and Bora winds. (b) Map of the study area showing the Adriatic Sea and Ionian Sea, general surface water circulation, water masses (WAC – Western Adriatic Current; North and South Adriatic deep water (nADW and sADW, ISW – Ionian Surface Water) and the core locations in the Gulf of Taranto (Adapted after Grauel et al., 2013a).

Here, we use benthic and planktonic foraminiferal test chemistry to independently reconstruct winter and summer seawater temperatures and salinities. Comparison of these results to bulk sediment geochemistry provides the continuous background environmental variability over the last millennia.

2. Study Area

The Gulf of Taranto is located between the heel (Apulia) and the toe (Calabria) of the Italian boot (Fig. 1). The Western Adriatic Current (WAC) transports large amount of sediments from the Adriatic Sea into the Gulf of Taranto (e.g., **chapter 2**). The WAC has a relatively low salinity due to discharge of the Po and several smaller Alpine and Apennine Rivers into the Adriatic Sea (Turchetto et al., 2007). Moisture transport from the Atlantic to the Italian peninsula increases during winter, and is enhanced in periods with a high NAO that pushes the westerlies southward (Brandimarte et al., 2011). Hence, intensity of the WAC and salinity of seawater transported into the Gulf of Taranto is controlled by winter conditions over the northern Mediterranean (Sellschopp and Álvarez, 2003). River discharge is reduced in summer months (e.g., Struglia et al., 2003; Sellschopp and Álvarez, 2003), resulting in a less intense WAC and higher salinities in the Gulf of Taranto (Poulain, 2001). High salinities in the Gulf of Taranto are thus directly related to the northern-most position of the high-pressure field of the

Hadley cell over the Mediterranean area during summer.

Besides the WAC, also surface waters from the Ionian Sea (ISW) enter the Gulf of Taranto from the south (Poulain, 2001; Fig. 1). Furthermore, highly saline Levantine Intermediate water can be traced in the basin at a water depth between 200-600 m (Savini and Corselli, 2010; Fig. 1). During winter (December to February) cold air temperatures cause mixing of the water column, whereas in summer it is highly stratified (Zonneveld et al., 2008; Grauel and Bernasconi, 2010). Consequently, the annual bottom water composition at the study site is thought to reflect winter surface water conditions.

3. Material and Methods

3.1 Core sites and age model

Multicore NU-04 (39.764°N / 17.892°E, water depth 160 m) was recovered during RV Universitatis cruise 'ESPRESSO' in 2005 (Fig. 1). Sampling of the core material for sediment and foraminifera was performed at a resolution of 3 mm. The nearby piston core DP30 was collected at 39.835°N / 17.801°E, water depth 270 m (Fig. 1) during RV Pelagia cruise 'DOPPIO' in 2008. This core was sampled at a resolution of 2.5 mm with the exception of the top 20 cm which was sampled every 5 mm. Each sample was split into a part for sediment geochemical analyses and a part for foraminiferal studies.

For dating purposes, ^{210}Pb was determined for the top part of NU-04 and DP 30 at the laboratories of CEAC, Cuba and the NIOZ, The Netherlands. In addition, 3 bulk planktonic foraminifera samples of core DP30 and one from the bottom of NU -04 were picked and analyzed for AMS ^{14}C (MICADAS, Ruff et al., 2007; Synal et al., 2007) at the AMS Radiocarbon Dating Laboratory at ETH Zurich. ^{14}C-ages were calibrated using the program OxCal v3.10 (Bronk Ramsey, 2009) with the Marine04 calibration curve (Hughen et al., 2004) with an additional regional reservoir correction of 121±60 (ΔR). The age model for these cores, based on AMS ^{14}C and ^{210}Pb dating is described in **chapter 3**.

3.2 Foraminifera

Samples for foraminiferal analysis were freeze-dried and wet sieved into size fractions of >355 μm, 355-250 μm, 250-200 μm and 200-125 μm.

3.2.1 *Hyalinea balthica*

Hyalinea balthica (Schroeter, 1783) is a primarily neritic to upper bathyal species (<600 m) and has a preference for shallow infaunal microhabitats in the topmost sediment (Van Morkhoven et al., 1986; Fontanier et al., 2002, 2008). Its distribution indicates that

this is a species with high tolerance to stressed conditions and can be abundant in, for example sediments with low oxygen contents (e.g. Hess and Jorissen, 2009).

For Mg/Ca and Na/Ca analysis of *H. balthica* between 7 and 10 specimens (125-250 μm size fraction) were selected from every 4th sample. For samples containing less than 7 specimens, foraminifera were combined with those from the sample directly below it, which was necessary for a number of samples from sections 8 and 9 of DP30, i.e. the topmost 1.5 m. Samples were cleaned using the method of Boyle and Keigwin (1985) as modified after Rosenthal et al. (1997). To avoid possible contamination with Na during cleaning we replaced the 2 x 10^{-5} M H_2O_2 in NaOH by 1% H_2O_2. Samples with low foraminiferal abundances (<8 specimens) were dissolved in 2 ml 0.1 M HNO_3, while samples with >8 specimens were dissolved in 3 ml 0.1 M HNO_3. Element composition of the foraminiferal calcium carbonate was analyzed by a high resolution ICP-MS using a Thermo Fischer Scientific Element 2 equipped with a double spray chamber and Teflon microflow nebulizer at the NIOZ, The Netherlands. Precision (<4 %) and accuracy were established using standards (BAS ECRM-752-1, GJR, Jct, and CMSI). Every analysis consumed 1.8 ml of solution, permitting a second analysis after dilution of the remainder to 10 ppm of calcium. To correct for a variable calcium matrix, a 3-D ratio calibration method was used (Rosenthal, et al., 1999). For this, 5 standards with known calcium concentration were measured for a range of dilutions (5, 10, 20, 30, 50 en 100 ppm calcium matrix).

From a selection of *H. balthica* samples from core NU-04, a part of the crushed material was used for isotope analysis. Samples were cleaned using the method described by Grauel and Bernasconi (2010) and measured on a MAT Finnegan 253 gas source mass spectrometer connected with an automated Kiel (III) type carbonate preparation line at Utrecht University. Results were calibrated to Vienna Pee Dee Belemnite standard (VPDB) using NBS-19 with an internal reproducibility of 0.1 ‰ for $\delta^{18}O$ and $\delta^{13}C$.

3.2.2 *Globigerinoides ruber* (white)

G. ruber (white) is a planktonic species calcifying in surface waters (0-50 meters, e.g. Numberger et al., 2009). For isotopic analyses, approximately 20 specimens of *G. ruber* (white) were selected from the size fraction 200-355 μm of every 4th sample between 2050 and 2800 mm, i.e. ~1450 -540 BC of core DP30. Results from the upper part were previously reported in Grauel et al. (2013b). To avoid variations in $\delta^{18}O$ and $\delta^{13}C$ caused by different morphotypes for *G. ruber* (white), we selected only the type *platys* according to the nomenclature of Numberger et al. (2009). Foraminiferal tests were thoroughly cleaned according to the protocol described by Grauel and Bernasconi (2010) to eliminate carbonate particles adhering to the shell surface. For isotope analyses 150-200 μg of cleaned shell material was dissolved in vacuum with two drops of ~103% phosphoric-acid at 70°C and cleaned cryogenically using a Thermo Fisher Kiel IV preparation device coupled to a Thermo Fisher MAT 253 mass spectrometer at ETH Zurich. Reproducibility of the $\delta^{13}C$ and $\delta^{18}O$ analysis based on repeated measurements of the *MS2*, a laboratory standard calibrated to the international standards NBS19 ($\delta^{13}C_{VPDB}$

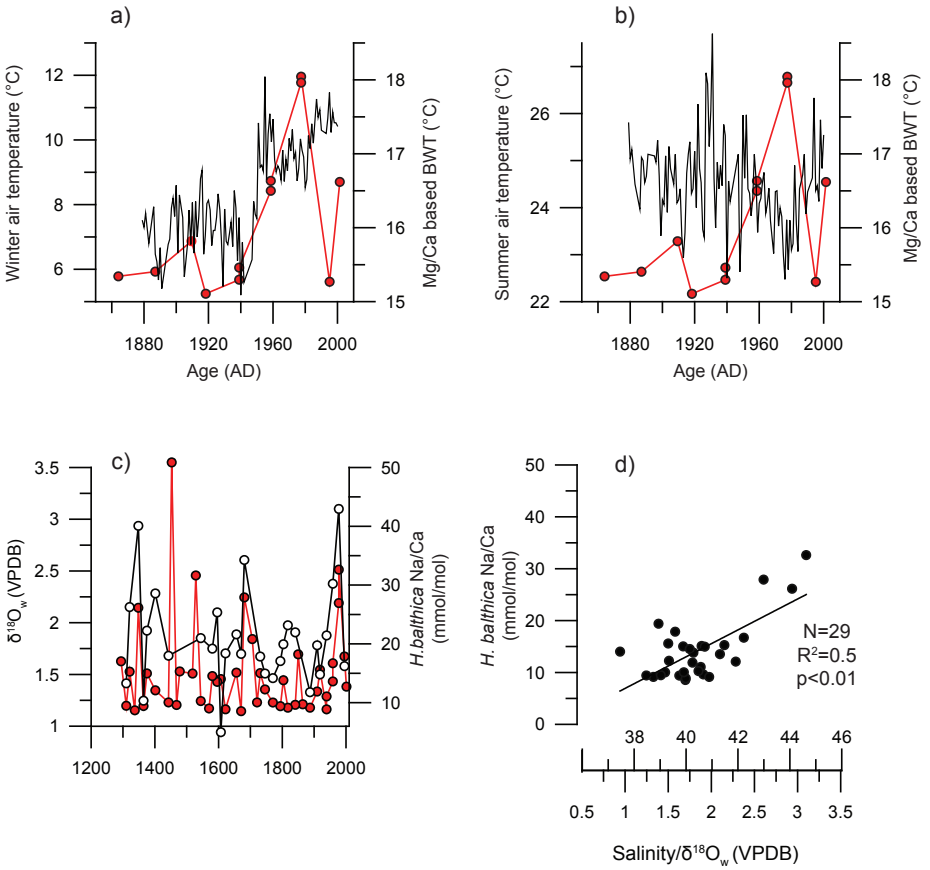

Fig. 2: (a and b) *H. balthica* Mg/Ca–based bottom water temperatures using the non- linear equation by Rosenthal et al. (2011) of core NU-04 (red line) compared to measured Italian winter (a) and summer (b) air temperatures (black lines; Versteegh et al., 2007) based on a combination of historical records from a variety of Italian cities as found in the National Climate Data Centre (http://www.ncdc.noaa.gov/oa/pub/data/ghcn/v2/ghcnftp.html). (c) Trends in the Na/Ca of *H. balthica* (red) and $\delta^{18}O_w$ (black) in NU-04 spanning the last ~800 years. (d) Relation between the results from (c) as well as the salinity based on $\delta^{18}O_w$.

+1.95‰, $\delta^{18}O_{VPDB}$ -2.2‰) and L-SVEC ($\delta^{13}C_{VPDB}$ -46.6‰, $\delta^{18}O_{VPDB}$ -26.41‰), was better than 0.1‰ (1σ). All $\delta^{13}C$ and $\delta^{18}O$ results are reported in the conventional delta notation with respect to VPDB.

3.3 Bulk geochemistry

Sediments samples were freeze-dried and powdered using an agate mortar. From every powdered sample, 125 mg was dissolved in 2.5 ml HF (40%) and 2.5 ml pre-mixed acid (HNO_3 16.25% and $HClO_4$ 45.5%) and placed at 90 °C in a closed vessel for at least 8 hours. Subsequently, the lid was removed and the samples were evaporated at

next page **Fig. 3**: (a) *H. balthica* Na/Ca and (b) the adapted H. balthica Na/Ca, mirrored for the interval with low Zr/Cr (see Fig. 4 of DP-30 to consistently reflect NAO variability(see text for more details) compared with the NAO-index from Olsen et al. (2012) and Trouet et al. (2009, red lines). Black box indicates the period when Zr/Cr ratio are lower than 0.775 (see text, Fig. 4d). (c) *H. balthica* Na/Ca (DP-30) compared with the AMO (Gray et al., 2009, red line).(d) *G. ruber* (white) $\delta^{13}C$ of DP-30 and two ITCZ records the $\delta^{18}O$ stalagmite record from China (d, red line, Wang et al., 2005) and (e) the PCA-1 from a lake in West Africa (red line, Shanahan et al.,2009) and (f) compared with the AMO (Gray et al., 2009, red line). ISW stands for Ionian Surface water and WAC is West Adriatic Current. Dark rectangles correspond to various periods mentioned in the text: Bronze Age (BA), Roman Humid Period (RHP) a.k.a. Roman Warm Period (RWP), Roman Classical period (RCP), Dark Ages (DA), Medieval warm period (MWP) and Little Ice Age (LIA) as defined by Grauel et al. (2013b).

160°C until a gel formed. The gels were then dissolved in 25 ml 1 M HNO_3. Dissolved samples were analyzed for their major and minor elemental composition using Inductively Coupled Plasma-Atomic Emission Spectroscopy (ICP-AES) with a Perkin Optima 3000 at Utrecht University. Relative precision (<5%) and accuracy were established by duplicate samples, and by in house and international standards (ISE-921).

The total organic carbon (TOC) content and organic carbon isotope ratios ($\delta^{13}C_{org}$) were determined for a selection of samples taken at a resolution of 2.5 mm between 800 mm and 1800 mm and every 4th sample for the upper 800 mm and the 1800-2800 mm interval. For these samples, 300 mg of sediment was decalcified using 1 M HCl to remove inorganic carbon (Reitz et al., 2006). Decalcified samples were dried at 60°C and finely ground using an agate mortar. For the decalcified sediments the TOC contents was determined on Fisons Instruments NCS NA 1500 analyzer using dry combustion at 1030°C. In addition, $\delta^{13}C_{org}$ was determined using Fisons Instruments NCS NA 1500 analyzer coupled to a Finnigan deltaplus isotope mass spectrometer. The isotope data are reported in the conventional delta notation with respect to VPDB. Precision (≤0.1‰) and accuracy were established using international and in-house standards (GQ, ASS, Acetanilide and Atropine).

4. Results

4.1 Foraminiferal test chemistry

Mg/Ca ratios of *H. balthica* test carbonate from multicore NU-04 vary between 7.48 and 12.2 mmol/mol. Variability between samples is, thus higher than the analytical error for measuring Mg/Ca (<4‰). Na/Ca values for *H. balthica* vary between 10 and 60 mmol/mol (Fig 2 c-d, Fig. 3 a, b). Maximal values are found between 1250- 1100 BC and 400 BC and 200 BC. For all specimens, Fe/Ca and Mn/Ca was monitored to check for contamination. For all samples, these values were below 40 and 0.6 cps/cps respectively and, therefore, the impact of contamination on determined Mg/Ca and Na/Ca was considered negligible.

Hadley cell / ITCZ
North
South
Dongge Cave δ18O (‰, VPDB)
-8
-7.6
-7.2
-6.8
d)
G. ruber δ 13C (‰)
1.2
0.8
0.4
0
ISW/Dry
ASW/ Wet
e)
PCA-1
2
0
-2
BA
RHP
RCP
DA
MWP
LIA
1500
1000
500
0
BC
AD
Age
NAO
+
-
NAO Index
a)
H.baltica Na/Ca (mmol/mol)
60
40
20
0
Dry
Wet
b)
H.baltica -Na/Ca adp.
Low Zr/Cr (see Fig. 4)
AMO
c)
50
40
30
20
10
0
f)
1.2
0.8
0.4
0
-0.4
1500 1600 1700 1800 1900 2000
Age (AD)

Stable carbon isotope ratios of *G. ruber* (white) from this study vary between -0.4‰ and 1.2‰ (average = 0.79‰, Fig. 3 d, e). Maximal values are found between 1200 and 900 BC after which a decreasing trend to more depleted values can be found until 100 AD. To check for consistency between our data and previously reported stable isotope analyses of *G. ruber* (white) for the same core we compared averages and standard deviations. The standard deviation (stdev), taking the lower resolution of our samples into account (Standard error, SE), indicates that our series (stdev =0.41, SE= stdev* (1/√4) = 0.20) and the data previously reported for the upper part of the core (stdev=0.26; SE= 0.26; Grauel et al., 2013b) have a similar variability. Although, the average values for the samples reported here are somewhat higher than those for the previously reported samples, this difference is consistent with the observed trend.

4.2 Sediment chemistry

The sedimentary Ca/Fe (%/%) ratio varies between 2 and 3.5 (Fig. 4a). Minimal values are found for 700 BC - 100 AD and 1800 - 1880 AD. The carbon isotopic composition of TOC ($\delta^{13}C_{org}$) varies between -23 and -22.4‰ (1700 – 700 BC), -23 and -24‰ (700-200 BC) and -23 and 22‰ (200 BC – 1994 AD; Fig. 4b). TOC (%) varies between 0.3-0.4 (1700 – 700 BC), 0.4-0.6 (700-200 BC) and 0.4-0.5 (200 BC – 1994 AD; Fig. 4c). Changes in Zr/Cr, $\delta^{13}C_{org}$ and TOC are modest but clear, the amplitude being several times higher than the analytical precision. Zr/Cr varies between 0.7 and 0.9 ppm/ppm (Fig. 4d). A general decreasing trend in Zr/Cr is observed from 1700 BC until 900 AD whereas values abruptly increase around 1600 AD (Fig. 4d).

5. Discussion

5.1 Geochemistry of *G. ruber* (white) and *H. balthica*: proxies for different seasons?

5.1.1. Geochemistry of *H. balthica*

Rosenthal et al. (2011) showed that Mg incorporation in *H. balthica* tests is highly sensitive to seawater temperature (eq. 1). Because this calibration shows a much stronger increase in Mg/Ca with temperature than that found for other species, the reconstructed temperatures based on this species will be less susceptible to effects of parameters such as salinity and carbonate chemistry (e.g. Dissard et al., 2010a; Dueñas-Bohórquez et al., 2009). The derived bottom water temperatures (BWT), using eq. 1 from Rosenthal et al. (2011) varied between 14.5 and 17.5 °C over the studied interval (Fig. 2a, b).

(1) Mg/Ca=1.327exp (0.123) BWT

These values are close to present-day values (~15°C), implying that the calibration from Rosenthal et al. (2011) is applicable to specimens from the Mediterranean.

The oxygen isotope composition is known to be related to temperature and to the isotope composition of seawater. Therefore, combining the bottom water temperature reconstruction derived from Mg/Ca with oxygen isotope analysis of the same specimens allows deconvolving seawater stable isotope composition ($\delta^{18}O_w$). The $\delta^{18}O_w$ is calculated using the equation by Epstein et al. (1953; eq. 2), ignoring the squared term.

(2) $BWT = 16.0 - 4.14 * (\delta^{18}O_{\textit{H. balthica}} - \delta^{18}O_w)$

Calculated values vary between 0.5‰ and 3.5‰. The topmost sample has a reconstructed $\delta^{18}O_w$ of 1.5‰, which is close to present-day average value of ~1.47‰ (Grauel and Bernasconi, 2010).

Seawater stable oxygen isotope composition is controlled by the same factors as salinity (evaporation, precipitation and river input) and hence the two are highly correlated in the ocean today (e.g. Pierre et al., 1999; Ganssen and Kroon, 2000). Therefore, we subsequently compared reconstructed $\delta^{18}O_w$ values to the Na/Ca value measured on the same specimen. Wit et al. (2013) showed that Na incorporation in benthic foraminifera depends on salinity. Na/Ca values found in *H. balthica* are higher than observed in other foraminiferal species (Wit et al., 2013). A higher Na/Ca value of the *H. balthica* tests compared to e.g. *Ammonia* sp. is possibly related to the relatively high concentrations of Mg in its test, resulting in a more open carbonate structure. Since Na is likely to be primarily incorporated interstitially (Kitano et al., 1975; Ishikawa and Ichikuni, 1984), a more open crystal structure would promote Na incorporation. The significant positive correlation (R^2=0.5, $p<0.01$) found between Na/Ca and the $\delta^{18}O_w$ (Fig. 2c, d) shows that also for *H. balthica* Na incorporation reflects, at least partly, seawater salinity.

5.1.2 *H. balthica* Na/Ca as a proxy for the winter NAO

The relation between the Mg/Ca of *H. balthica* and seawater temperature results in a sensitivity which is approximately 4 times higher than that observed for many other benthic foraminifera (compare Rosenthal et al., 2011 to e.g. Toyofuku et al., 2011; Wit et al., 2012). This makes it an ideal species for bottom water temperature reconstructions based on Mg/Ca. The upper water column in the Gulf of Taranto is stratified in summer. During winter, surface water cooling causes convective overturning which mixes the water column down to at least 270 m water depth (Fig. 1d; Grauel et al., 2013a). As during summer the water column stays stratified, bottom waters keep this winter signature during the rest of the year. Therefore, bottom water salinity and temperature for our shallow core site (270 m) reflect surface water winter conditions. This is confirmed by the high similarity between measured Italian winter air temperature over the last hundred years and the *H. balthica* Mg/Ca temperature reconstruction (Fig. 2a, b). Moreover, minima and maxima fit with $U^{k'}_{37}$ based SST records from the Gulf of Taranto, which are suggested to reflect SST variability in the winter/spring season (Versteegh et al., 2007; Grauel et al., 2013a). Thus, *H. balthica* test chemistry reflects variability in the

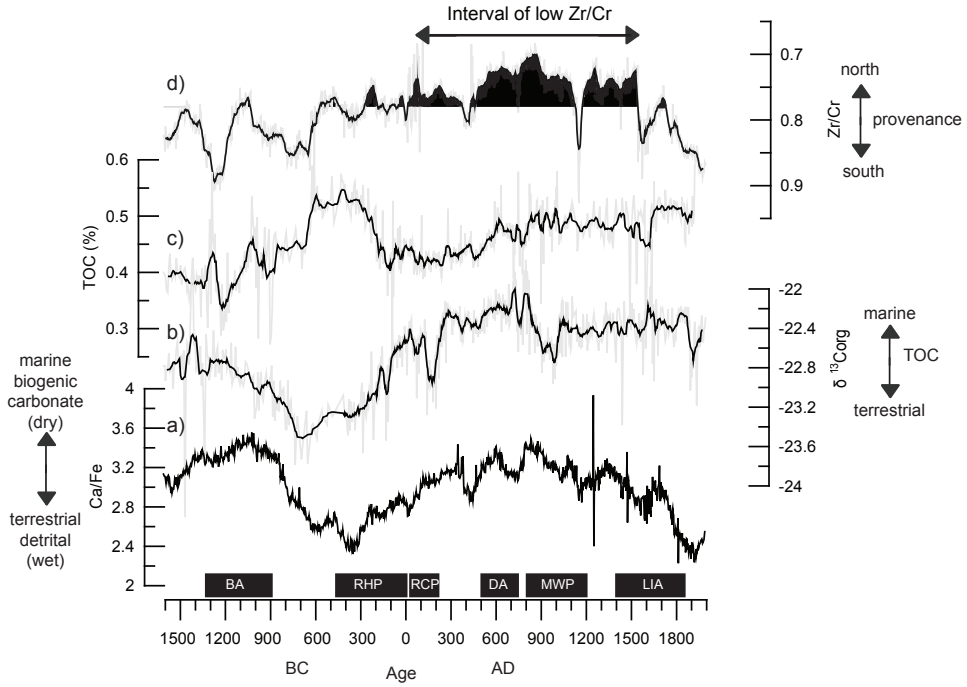

Fig 4 Overview of proxies measured in sediments from core DP 30 (a) Ca/Fe ratio (%/%) reflecting to marine biogenic Ca and riverine Fe. (b) The carbon isotopes of organic matter ($\delta^{13}C$), (c) Total organic carbon content (%) and (d) the Zr/Cr ratio and their 5–point moving average (black). Dark rectangles correspond to various periods mentioned in the text: Bronze Age (BA), Roman Humid Period (RHP) a.k.a. Roman Warm Period (RWP), Roman Classical period (RCP), Dark Ages (DA), Medieval warm period (MWP) and Little Ice Age (LIA) as defined by Grauel et al. (2013b).

winter season.

During winter, run off controls salinity in the study area and is thus expected to be the major factor influencing Na/Ca ratios of *H. balthica*. During this season, precipitation in southern Italy is dominated by the North Atlantic Oscillation (NAO), with a negative state causing more humid conditions (e.g. Brandimarte et al., 2011). Therefore, we expect our benthic foraminifera *H. balthica* downcore Na/Ca data to correspond to reconstructed NAO patterns (Trouet et al., 2009; Olsen et al., 2012). Indeed, a convincing correlation between the NAO index and Na/Ca of *H. balthica* is observed between 1800 and 100 BC (including the Bronze Age (BA; Fig. 3b)). Furthermore, low Na/Ca values correspond to high SST reconstructed by Grauel et al. (2013a) with $U^{k'}_{37}$. $U^{k'}_{37}$ is suggested not only to reflect SST of the winter/spring season, but also to be partly reflecting NAO variability in the Gulf of Taranto (Grauel et al. 2013a). A more negative NAO would prolong the PP season and therefore lead to high SST reconstructions based on $U^{k'}_{37}$. However, from 100 BC- 1500 AD (a combination of the Dark Ages (DA)/ Medieval Warm Period (MWP)) an opposite pattern exists between the NAO reconstruction and *H. balthica* Na/Ca. This suggests that either bottom water salinities

are also influenced by factors other than the NAO, or that sea surface salinity during winter is not reflecting local precipitation alone.

The Ca/Fe ratio of bulk material reflects mainly input of marine biogenic carbonate relative to that of riverine terrestrial material, similar to the Ca/Ti ratio (c**hapter 3**). Reduced riverine input during a dry climate period thus corresponds to a high Ca/Fe and vice versa. The Ca/Fe ratio record for the last 3500 years indicates the presence of two dry episodes. These are closely related to 1) the Bronze Age (BA) and 2) Dark Ages (DA) /Medieval Warm Period (MWP), lasting for approximately 500 and 1000 years, respectively (Fig. 4a). Furthermore, their pattern corresponds with the millennial trends in the NAO (Olsen et al., 2012) in winter, the dominant season for humidity. These dry episodes are also characterized by reduced input of terrestrial organic material, indicated by overall relatively low TOC concentrations (Fig 4c). The stable carbon isotopes for episodes with less total organic matter are characterized by relatively more marine organic matter as $\delta^{13}C_{org}$ values are less depleted during these intervals (Fig. 4 b, c). Nevertheless, considerable differences are observed between both dry periods. The Na/Ca of *H. balthica* indicates less saline (i.e. wetter) conditions during the DA/MWP compared to the BA. In contrast, relatively high $\delta^{13}C_{org}$ values indicate more marine organic matter during the last 2000 years (Fig. 4c). The Zr/Cr ratio, high in sediments originating from the more southern Apennine rivers (**chapter 2**), is relatively low during the DA/MWP period (<0.775, Fig 4d). These low values suggest that the proportion of material transported by northern rivers relative to material from southern Italian rivers was relatively large during this period.

During the MWP (1000-1300 AD), the winter NAO was characterized by the most positive phase of the last 3500 years (Olsen et al., 2012). Such a positive phase is known to be associated with a more northern trajectory for the westerlies increasing moisture transport to northern Europe (Hurell et al., 1999). During this positive NAO mode the region affected by the westerlies was probably extended and likely included the Alps, thus affecting the Po drainage area and increasing runoff by rivers located in Northern Italy (Fig.1). A similar contrast in humid/ arid conditions between northern and southern Italy during other rapid climate change (RCC) events, such as the 4.2 kyr event, was demonstrated on the basis of Italian lake deposits (e.g. Magny et al., 2003; Joannin et al., 2012). Increased runoff from more northern sources period during the DA/MWP period is also evident from the contrasting patterns found in cores taken in the Northern Adriatic (Piva et al., 2008) and the Southern Adriatic Sea (Siani et al., 2013) during the MWP/DA. Present-day Po and northern Adriatic river discharge account for 70% of the drainage into the WAC (Raicich, 1996). Therefore, increased northern runoff will result in reduced salinity for the WAC and, thus, for the water mass in the Gulf of Taranto. This is in line with the observed correlation between low sedimentary Zr/Cr ratios, thus enhanced northern provenance, and lower local salinity, indicated by the Na/Ca values of *H. balthica* (Fig. 3, 4). Despite decreased salinity of the WAC during these periods, overall terrestrial sediment input did not increase, as evidenced by high Ca/Fe and less negative $\delta^{13}C_{org}$ values during the DA/MWP period (Fig. 4). Previous studies showed that the amount of terrestrial material transported by the WAC de-

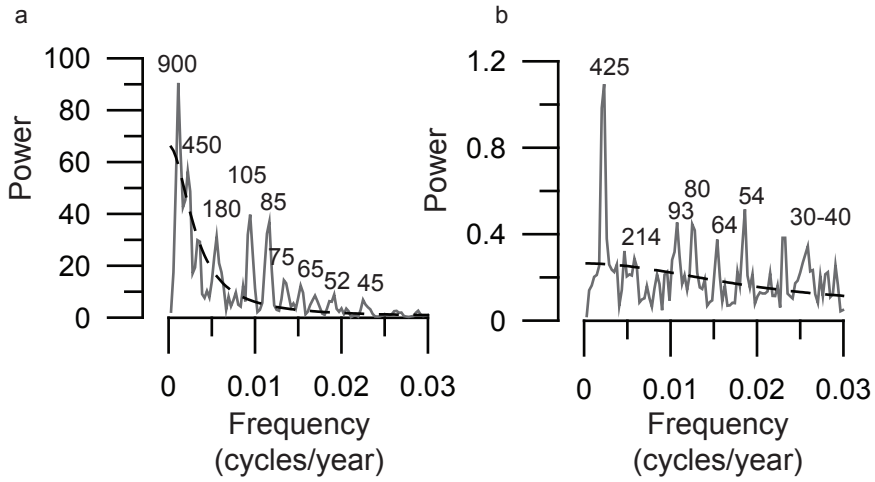

Fig. 5: a) REDFIT analysis of the (a) adapted *H. balthica* Na/Ca record and (b) *G. ruber* (white) $\delta^{13}C$. Numbers correspond to periods in years; dashed line is the 80% confidence interval.

creases as it travels southwards (e.g., **chapter 2**; Leider et al., 2013). Hence, although the terrestrial sediment input in the Gulf of Taranto is dominated by northern sources, the total amount deposited during this period is relatively low (high Ca/Fe values). This implies that local, i.e. terrestrial matter input from southern Italy must have ceased almost completely during the DA/MWP period. This concords with the enhanced humidity contrast between northern and southern Italy. Hence, these contrasting precipitation patterns in northern and southern Italy explain the opposite pattern of foraminiferal Na/Ca_{adp} and the NAO during the DA/MWP period.

To perform a spectral analysis of the complete record to derive the dominant frequencies from a continuous time series compared to global variability, the interval of regionally reversed signal expression needs to be converted ('adapted'). Therefore, the *H. balthica* Na/Ca record during this period is mirrored (see Fig. 4b). By doing so, high *H. balthica* Na/Ca (from now onwards *H. balthica* Na/Ca_{adp}) values should consistently reflect a positive NAO mode and vice versa. We consider this legitimate as the Zr/Cr ratio is used as an internal control for the duration of the change in provenance. Although our *H. balthica* Na/Ca_{adp} record does not reflect the millennial time scale variability in NAO as found by Olsen et al. (2012), a high correlation is observed on a centennial timescale (Fig. 3b). The lack of a clear millennial NAO+ mode, as found by Olsen et al. (2012) in our record is presumably related to the contrasting precipitation patterns in northern and southern Italy during this event, which might not have been a stable situation. However, this NAO reconstruction based on *H. balthica* Na/Ca_{adp} is consistent with other NAO reconstructions from North Morocco (Wassenberg et al., 2013) and the Black Sea (Lamy et al., 2006). Hence, we consider *H. balthica* a local proxy for winter NAO on at least a centennial timescale.

To unravel the dominant period in the data set, a spectral analysis was done using a

REDFIT analysis with the program PAST © (Hammer et al., 2001). A REDFIT spectral analysis takes red noise into account, and is therefore suitable for frequency analysis of paleoclimate records (Schulz and Mudelsee, 2002). The REDFIT-analysis of the adapted *H. balthica* Na/Ca record (Fig. 5a) shows significant (above 80% confidence interval) periodicities at 45, 65-105, 180 and 450-900 yr. These periodicities are consistent with those reported for NAO in the same time interval (Olsen et al., 2012).

5.1.3 Isotope chemistry of *G. ruber* (white) as a proxy for variability of the position of the subtropical high pressure cell

The stable oxygen isotope geochemistry of *G. ruber* in the Gulf of Taranto appears to reflect mainly summer conditions (Grauel and Bernasconi, 2010; Grauel et al., 2013a, b). More specifically, $\delta^{13}C$ reflects changes in nutrient conditions by variability in the dominant water masses, i.e. the influence of the nutrient-poor ISW versus the nutrient-rich WAC. Hence *G. ruber* $\delta^{13}C$ reflects changes in the WAC and therefore, Italian river runoff during summer (Grauel and Bernasconi, 2010). The high *G. ruber* $\delta^{13}C$ values around 1000 AD, for example, are coherent to summer aridity as observed in an Italian lake record (Peyron et al., 2011). A detailed description about the connections of the record with local summer records from the Mediterranean and Southern Alps are given in Grauel et al., (2013b).

Summer conditions in the Mediterranean area are influenced by shifts in the latitudinal position of the Hadley cell. The southern ascendant of the Hadley cell is the ITCZ, which itself is thought to be associated to changes in the African and Asian Monsoon (Alpert et al., 2006). With the northward movement of the ITCZ in summer, the high-pressure field associated with the northern boundary of the Hadley cell also moves northward, resulting in relatively warm and dry conditions over the Italian peninsula (Alpert et al., 2006). This stable high-pressure field reduces the impact of the westerlies in Southern Europe, hence decreasing summer precipitation.

The timing for environmental changes in the $\delta^{13}C$ of *G.ruber* (white) record is rather similar to that observed for ITCZ reconstructions from a West African lake (Shanahan et al., 2009) and an Asian cave (Wang et al., 2005). This indicates a possible connection between the climate of these regions. Shanahan et al. (2009) deviates from the *G. ruber* (white) $\delta^{13}C$ record (Fig 3d). A southward displacement of the ITCZ as suggested by Shanahan et al. (2009) is, however, not recognized in other reconstructions of the position of the southern ascendant of the Hadley cell in Africa (Weldeab et al., 2007), Asia (Wang et al., 2005; Fig. 3e) or Oman (Fleitmann et al., 2003). These records all show changes more similar to the data from the Gulf of Taranto. Hence, we conclude that *G. ruber* (white) $\delta^{13}C$ reflects variability in the position of the Hadley cell, and thus partly also the position of the ITCZ during summer. To unravel dominant frequencies in the combined data set, a REDFIT analysis was performed. This reveals several significant peaks (above the 80% confidence interval), with periodicities between 900 and 30 yrs. Highest peaks cluster around 30-40, 54, 64-93, 214 and 425yr (Fig. 5b). Similar frequencies are also observed in ITCZ reconstructions from West Africa (Shanahan et al.,

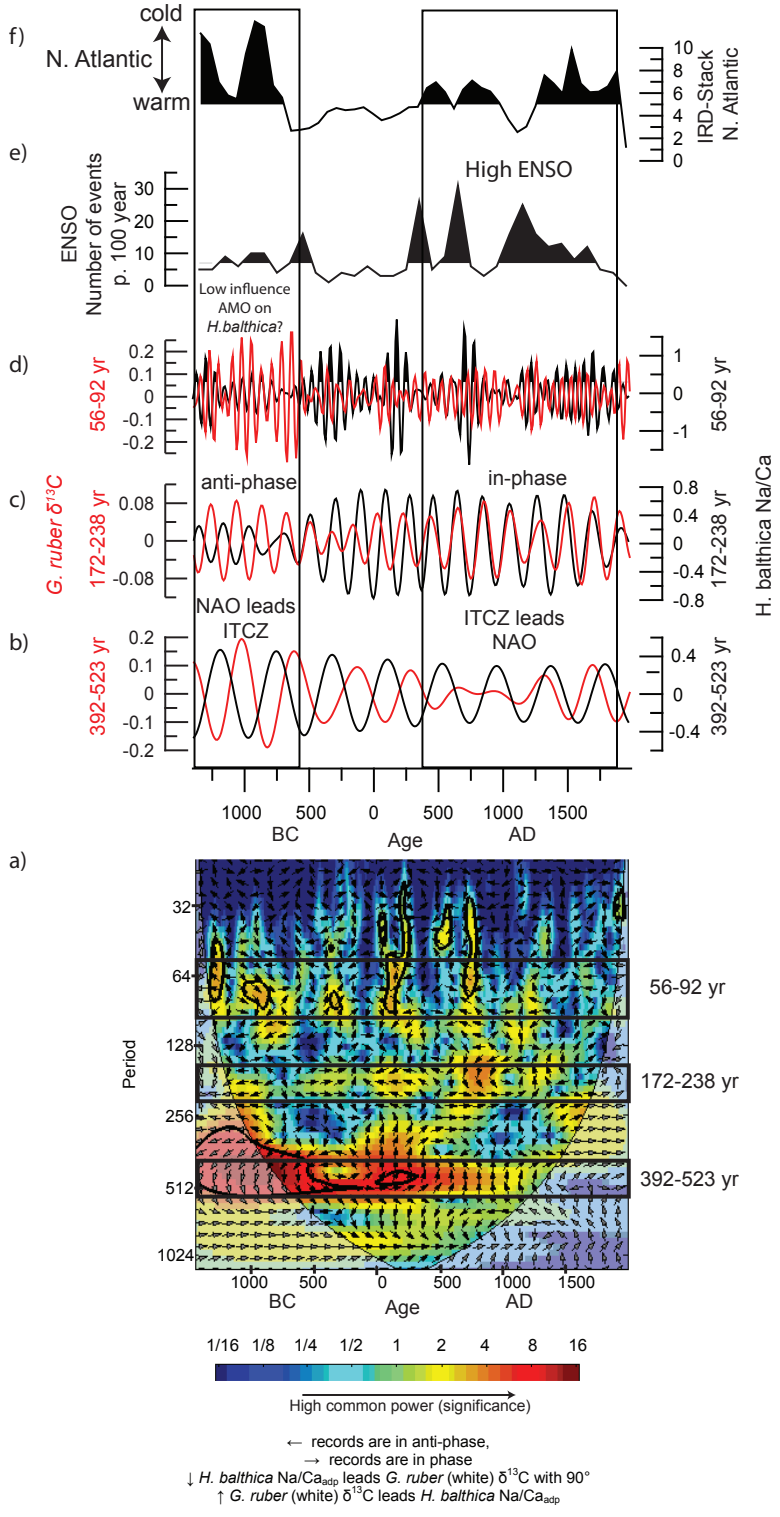
f)
cold
N. Atlantic
warm
10
8
6
4
2
0
IRD-Stack
N. Atlantic
e)
ENSO
Number of events
p. 100 year
30
20
10
0
High ENSO
Low influence
AMO on
H.balthica?
d)
56-92 yr
0.2
0.1
0
-0.1
-0.2
1
0
-1
56-92 yr
c)
G. ruber δ13C
172-238 yr
0.08
0
-0.08
anti-phase
in-phase
0.8
0.4
0
-0.4
-0.8
172-238 yr
H. balthica Na/Ca
NAO leads
ITCZ
ITCZ leads
NAO
b)
392-523 yr
0.2
0.1
0
-0.1
-0.2
0.4
0
-0.4
392-523 yr
1000
500
0
500
1000
1500
BC
Age
AD
a)
Period
32
64
128
256
512
1024
56-92 yr
172-238 yr
392-523 yr
1000
500
0
500
1000
1500
BC
Age
AD
1/16
1/8
1/4
1/2
1
2
4
8
16
High common power (significance)
← records are in anti-phase,
→ records are in phase
↓ H. balthica Na/Cadp leads G. ruber (white) δ13C with 90°
↑ G. ruber (white) δ13C leads H. balthica Na/Cadp

Previous page **Fig. 6:** (a) Cross wavelet analysis of the normalized *H. balthica* Na/Ca and *G. ruber* (white) $\delta^{13}C$ with ←= records are in anti-phase, → = records are in phase,↓= *H. balthica* Na/Ca leads *G. ruber* (white) $\delta^{13}C$ with 90°, ↑= *G. ruber* (white) $\delta^{13}C$ leads *H. balthica* Na/Ca , color code indicates high common power (significance) and the bandpassfilters of *G. ruber* (white) $\delta^{13}C$ (red lines) and *H. balthica* Na/Ca (black lines) of DP30 with a bandwidth of 392-523 yr (b), 172-228 yr (c) and 56-92 yr (d) compared to ENSO variability as recorded in a South American lake (Moy et al., 2002) (e) and the IRD stack from the north Atlantic (Bond et al., 2001) (f).

2009), Oman (Fleitmann et al., 2003) and China (Wang et al., 2005). (Fig. 3d, e).

5.2 Coherent centennial variability of NAO and ITCZ

To investigate the coherence of variability contained in our samples with that observed in NAO and ITCZ, a cross wavelet was calculated using *H. balthica* Na/Ca_{adp} and the *G. ruber* (white) $\delta^{13}C$ records (Fig. 6a). This analysis allows identification of regions in-time-frequency space where the time series show high common power, at the same time providing information on possible leads and lags (Grinsted et al., 2004). Both REDFIT and cross wavelet analysis show significant common periods around 56-92 yrs, 172-228 yrs and 392-523 yrs (Fig. 5a, b; Fig. 6a). The centennial frequencies correspond with known variability in solar irradiance (Wanner et al., 2008), which have been reported to influence the NAO and the position of the ITCZ. The 56-92 year periodicities correspond to the Atlantic Multi-decadal oscillation (AMO; Kerr et al., 2000).

5.2.1 Connection with Atlantic multi-decadal oscillation

On a decadal scale the AMO, expressed by Atlantic SST distribution pattern, affects movement of the ITCZ in Africa (e.g. Shanahan et al., 2009). At higher latitudes the impact of the AMO on short-term climate change is less well understood. Knudsen et al. (2011) suggested that impact of AMO on high latitude climates was restricted to periods characterized by high northern Atlantic SSTs. Alternatively, Hoerling et al. (2001) proposed that an AMO connection to the NAO is controlled by ENSO, with a stronger coupling during periods with strong ENSO activity. Thus, both AMO and ENSO are likely modulating NAO intensity (Sutton and Hodson, 2003).

A good correlation exists between the AMO reconstruction by Gray et al. (2004) for the last 400 years and our *G. ruber* (white) carbon isotope record a proxy for the relative latitudinal position of the Hadley cell, thus ITCZ. This implies that, in line with previous studies, an increased AMO mode (i.e. warm North Atlantic) is related to a northward shift of the ITCZ and hence a reduced WAC during summer in the Gulf of Taranto (Fig. 4f). No convincing correlation is observed between Na/Ca of *H. balthica* and the reconstructed AMO during the last 400 years, in contrast to the carbon isotope record of *G. ruber* (Fig 4c). This suggests that there is no direct link between NAO and AMO during this interval.

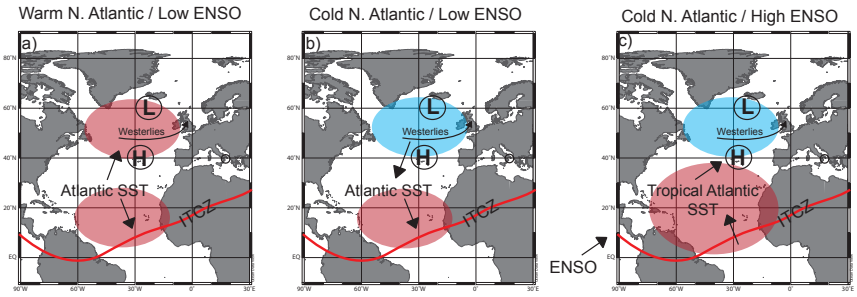

Fig. 7: Simplified, scheme on how Atlantic SSTs, ENSO, NAO and the ITCZ may be connected under a) low ENSO variability and high North Atlantic SSTs, Atlantic SST force variability of the mode of the NAO (westerlies) as well as variations in the extent of the ITCZ b) low ENSO variability and low North Atlantic SSTs, Atlantic SST force variance in the position of the ITCZ, while variance in extent of the westerlies may force Atlantic SST and c) high ENSO variability and low North Atlantic SSTs. ENSO variance forces tropical Atlantic SST, which forces variability in the ITCZ and the mode of the NAO. Black circle indicates the study area.

5.3 Coherent variability of ITCZ and NAO: impact of AMO?

Unfortunately, no direct AMO reconstruction covering the past 3500 years is available yet. However, the robust correspondence over the last 400 years between our *G. ruber* (white) $\delta^{13}C$ and the position of the Hadley cell on one hand, and the reconstructed AMO on the other hand, suggests that the *G. ruber* (white) $\delta^{13}C$ record and the AMO are related throughout the record. This implicitly means that the position of the Hadley cell (and thus the ITCZ) and AMO remain coupled over this time interval. This seems reasonable as the time interval studied is limited compared to that of major reorganizations in global climate, such as glaciations. Moreover, typical AMO cyclicity of 56-92 year is visible throughout the *G. ruber* (white) $\delta^{13}C$ record, except between ±500 AD and ±500 BC (Fig. 5b, 6).

To distinguish those parts of the *H. balthica* Na/Ca_{adp} record that have a clear AMO periodicity the record was filtered at the 56-92 yrs frequency band. This shows that AMO periodicity is reduced from 1250-400 BC in the Na/Ca_{adp} record (Fig. 6d). During this episode, weak ENSO and low Atlantic SST prevailed (Bond et al., 2001; Moy et al., 2002; Seyrup et al., 2011). In contrast, during periods of a strong 56-92 yrs periodicity (500 BC -1998 AD) in the *H. balthica* Na/Ca_{adp} record the Atlantic was characterized by high SSTs or a strong ENSO. This implies that during these intervals the NAO was impacted by changes in the AMO. This is coherent with previous studies suggesting a connection between high Atlantic SST and ENSO variability and the influence of AMO on NAO (Hoerling et al. 2001; Sutton and Hudson, 2003; Knudsen et al., 2011; Fig. 6e, f). The interval during which the *G. ruber* $\delta^{13}C$ and hence ITCZ variability has only little variability in the AMO frequency band, i.e. 1250-400 BC there is a high variability in *H. balthica* Na/Ca_{adp} and thus in the winter NAO. This implies that although the AMO remained active during this interval with reduced AMO cyclicity, it did not affect the

position of the summer ITCZ. During this interval the overall warm Northern Atlantic (Fig 6; Bond et al., 2001; Sejrup et al., 2011) might have forced the summer ITCZ northwards in which it no longer influenced the Gulf of Taranto. Alternatively, impact of the AMO on the ITCZ short time scale variability was weaker because of the already elevated Atlantic sea surface temperatures at that time. The latter seems more plausible, as there is no indication of a general, more northward position of the ITCZ during this interval in Asia, Oman or the Western Mediterranean (Wang et al., 2005, Fleitmann et al., 2003; Nieto-Moreno et al., 2011).

Bandpass filtering of the centennial time scale periodicities (172-228 yrs and 392-523 yrs), evident in both the *H. balthica* Na/Ca and *G. ruber* (white) $\delta^{13}C$, shows opposite patterns during different time intervals (Fig. 6). During the interval from 1250 to 400 BC, the records are in anti-phase in the 172-228 yrs frequency band. However, in the 392-523 yrs frequency band, *H. balthica* Na/Ca_{adp} leads the reconstructed position of the ITCZ. This suggests that the NAO might have forced changes in ITCZ during this time of low North Atlantic SSTs and low ENSO variability on centennial time scales (Fig. 7b). Although changes in North Atlantic SST affect the NAO, the NAO can also alter Atlantic SSTs itself (example:. stronger winds affect evaporation and thus reduce SST; Bjerkness, 1964; Daly, 1978; Cayan, 1992; Fig 7). Altered Atlantic SSTs, subsequently influence the position of the ITCZ and subsequently summer climate in our study area (Fig. 7).

The interval from 500 BC -1750 AD, characterized by a stronger influence of AMO variability on the *H. balthica* Na/Ca_{adp} record, consists of two periods related to different AMO forcings (Fig. 6). From 300 AD -1750 AD the Northern Atlantic is relatively cold, but in contrast to the 1250 BC- 400 BC interval there are strong ENSO conditions. Hoerling et al. (2001) suggested that during episodes with strong ENSO events the ITCZ is affected directly by AMO, which in turn also determines tropical North Atlantic SSTs. A strong ENSO thus affects tropical North Atlantic SSTs, which also impacts the winter NAO (Fig. 7). This implies that under such conditions, changes in summer ITCZ should be in phase, or even lead, NAO variability. This is exactly what is observed during this interval. The *G. ruber* (white) $\delta^{13}C$ and *H. balthica* Na/Ca_{adp} are in phase in de 172-238 yrs band, and the summer ITCZ leads the winter NAO in the 392-523 yrs band (Fig. 6).

From 500 BC – 300 AD high North Atlantic SSTs, i.e. strong AMO variability, result in a distinct AMO signal in the otherwise NAO dominated *H. balthica* Na/Ca_{adp} record (e.g. Sutton and Hudson, 2003; Fig. 6). During the same interval, part of the centennial time scale variability filtered from the ITCZ record (for the 172-238 yrs frequency band) leads the NAO, whereas for another part of the centennial time scale variability the position of the ITCZ and NAO are in anti-phase (for the 392-523 yrs frequency band, Fig. 6). The lead of the ITCZ compared to NAO seems to be robust for the 172-238 frequency band, whereas a statistical artefact cannot be fully excluded for the 392-523 yr frequency band which only covers two full cycles during this interval. This delay suggests that the NAO response to changes in Atlantic SST is slow compared to

changes in the position of the ITCZ. A reduced AMO variability, as indicated by the *G. ruber* (white) $\delta^{13}C$, during this period (500 BC- 300 AD), might be related to this slower response.

6. Conclusions

H. balthica Na/Ca has been shown to reflect variability in winter salinity of the Gulf of Taranto and thus in the winter NAO. In contrast, the carbon isotope chemistry of *G. ruber* (white) is related to the latitudinal position of the Hadley cell and thus the ITCZ in summer. In line with this, patterns found in the carbon isotopes of *G. ruber* (white) are coherent with a reported AMO reconstruction of the last 400 years. During warm north Atlantic SST or high ENSO variability, the characteristic ~50-90 yr period of the AMO is found in the *H. balthica* Na/Ca (i.e. NAO). Similar centennial scale variability is found in the *H. balthica* Na/Ca and in the carbon isotope composition of *G. ruber* (white). It is shown that variability of the NAO and the movement of the Hadley cell are more coherent during periods of a warm north Atlantic SST and in particular during high ENSO variability, when prominent AMO variability is found in the *H. balthica* record. We conclude that this coherency is related to the influence of the AMO on both the NAO and position of the ITCZ during these intervals. Our results emphasize the relevance of both ENSO and Atlantic SST anomalies on northern hemisphere climate variability.

Acknowledgments

At Utrecht University we thank Arnold van Dijk, Helen de Waard and Dineke van de Meent for lab assistance with ICP-AES, TOC and isotopes analysis. At ETH Zurich we thank S.E. Bishop and M. Coray-Strasser for technical assistance. We are grateful for sample collection by all participants onboard the DOPPIO and ESPRESSO cruises (coordinated by Gert J. de Lange and E. Malinverno respectively) and for help during sub sampling of DP30 by A. Leider and C.E. Casalino. This work was supported by the Nederlandse Organisatie voor Wetenschappelijk Onderzoek (NWO) as part of the MOCCHA- project funded by the European Science Foundation (ESF) Eurocores Programme EuroMARC.

5

Chapter 5: Seasonality variations during Late Holocene Rapid Climate Change Events in the Central Mediterranean

Marie-Louise S. Goudeau, G-J. Reichart, J.C. Wit, L.J. de Nooijer, A-L. Grauel, S. M. Bernasconi and G.J. De Lange

(In review for Palaeogeography, Palaeoclimatology, Palaeoecology)

Holocene rapid climate change (RCC) events, such as the Bronze Age (BA) and Little Ice Age (LIA), are thought to have influenced average annual temperatures only marginally, but to have affected winter temperatures relatively strongly. With summer temperatures relatively unaffected, reconstructing climate change with a seasonal resolution is crucial to fully capture Holocene climate variability. Mediterranean climate is highly seasonal, being influenced by both the subtropical high-pressure belt in summer and the mid-latitude westerlies and the outbreaks of polar winds in winter. We identified events of high- and low- detrital input to the Gulf of Taranto (Central Mediterranean Sea), anticipated to be linked to wet and dry conditions respectively. These events represent the BA, Roman Humid Period (RHP), Medieval Warm Period (MWP), LIA, and present-day. Because of their potentially contrasting seasonality, these events were selected for the analysis of single specimen *Globigerinoides ruber* (white) carbonate test chemistry (Mg/Ca, $\delta^{18}O$ and $\delta^{13}C$). The dynamic range found for these parameters for the measured single individuals in the most recent interval, reflects seasonal contrasts in present-day temperature and precipitation, albeit with a bias towards the summer season. These results are compared with high-resolution (<15yr/sample) SST and BWT reconstructions. Since BWT reflects winter sea surface temperature (SSTw) minima (i.e. convective turnover events), the temperature derived from Mg/Ca of benthic foraminifer *H. balthica* represents SSTw. As planktonic foraminifer *G. ruber* (white) thrives during the summer season, its $\delta^{18}O$ can be taken to represent summer SST (SSTs). Our reconstruction indicates that during the BA and LIA the contrast between winter and summer precipitation is significantly smaller than during the other intervals. Although the seasonal temperature contrast remains relatively stable, significant winter cooling is observed during the BA and LIA. Connections between high-latitude climate (winter conditions) and low-latitude climate (summer conditions) appear not straightforward during RCC events. This results in changes in the moisture balance, and in shifts in seasonal dominance between RCCs. During the LIA, winter-like conditions (cold and wet) can be found throughout the year. In contrast, during the BA winters are cold and dry, and are accompanied by warm and dry summers, suggesting year-round aridity and a high seasonal temperature contrast.

1. Introduction

Holocene climate is often considered more or less stable. However, for specific time intervals and regions, distinct centennial to millennial climate variability has been reconstructed (Mayewski et al., 2004; Wanner et al., 2008). This variability is thought to have been instrumental for the rise and fall of past civilizations (e.g. Haug et al., 2003; Büntgen et al., 2011). Such changes have affected specific parts of the climate system rather than impacting the average state of climate. For example, cold spells in the Northern Hemisphere, such as the Little Ice Age (LIA) and Bronze Age (BA), have been suggested to be primarily a winter phenomenon, implying an enhanced seasonal contrast during these periods (Denton et al., 2005). Changes in seasonality, therefore, may have played a crucial role in shaping Holocene climate variability.

High-frequency climate change has been different between regions, resulting in a complex spatial pattern, presumably reflecting interactions between low and high latitude climate change (Mayewski et al., 2004; Wanner et al., 2008, 2011; Mann et al., 2009). The Mediterranean lies on the boundary between the subtropical high-pressure belt and the mid-latitude westerlies (Fig. 1a). During summer Mediterranean climate is under the influence of the subtropics, which are closely linked to the position of the Inter-Tropical Convergence Zone (ITCZ; Alpert et al., 2006). In contrast, during winter climate is connected to the higher latitudes and primarily influenced by the westerlies (Trigo et al., 2006). Together, this results in relatively mild, wet winters and warm, dry summers. The Mediterranean thus provides an ideal area for investigating the interactions between high- and low- latitude climate change (Alpert et al., 2006; Trigo et al., 2006), but at the same time requires reconstructions at the seasonal scale. The observed millennial scale climate variability in this area during the Holocene has been explained by changes in extend of high northern latitude climate during winter (Rohling and Pälike, 2005; Peyron et al., 2011). Precipitation records indicate both increased droughts and floods during the LIA, suggesting an enhanced contrast between dry summer conditions and winter precipitation (e.g. Grove, 2001; Mann et al., 2009). Relatively wet conditions during the reign of the romans, the Roman Humid Period (RHP), are generally associated with stronger impact of the westerlies, increasing winter precipitation (Dermody et al., 2012).

Understanding seasonality is, however, not only vital for understanding the physical processes underlying short-term climate change, but is also important for unravelling proxy records, which may have a seasonal bias. Most proxies for sea surface temperature (SST) or sea surface salinity (SSS) are influenced by a variety of environmental parameters, of which seasonality is one. Distinguishing between shifts in seasonality and the other parameters is, therefore, often difficult (Grauel et al., 2013a). Still, novel techniques combined with multi-proxy studies can resolve seasonality in climate archives from sensitive areas, such as the Mediterranean.

Recently Wit et al. (2010) showed that Mg/Ca values measured on single specimens of the planktonic foraminifer *Globigerinoides ruber* (white) reflect the seasonal sea surface

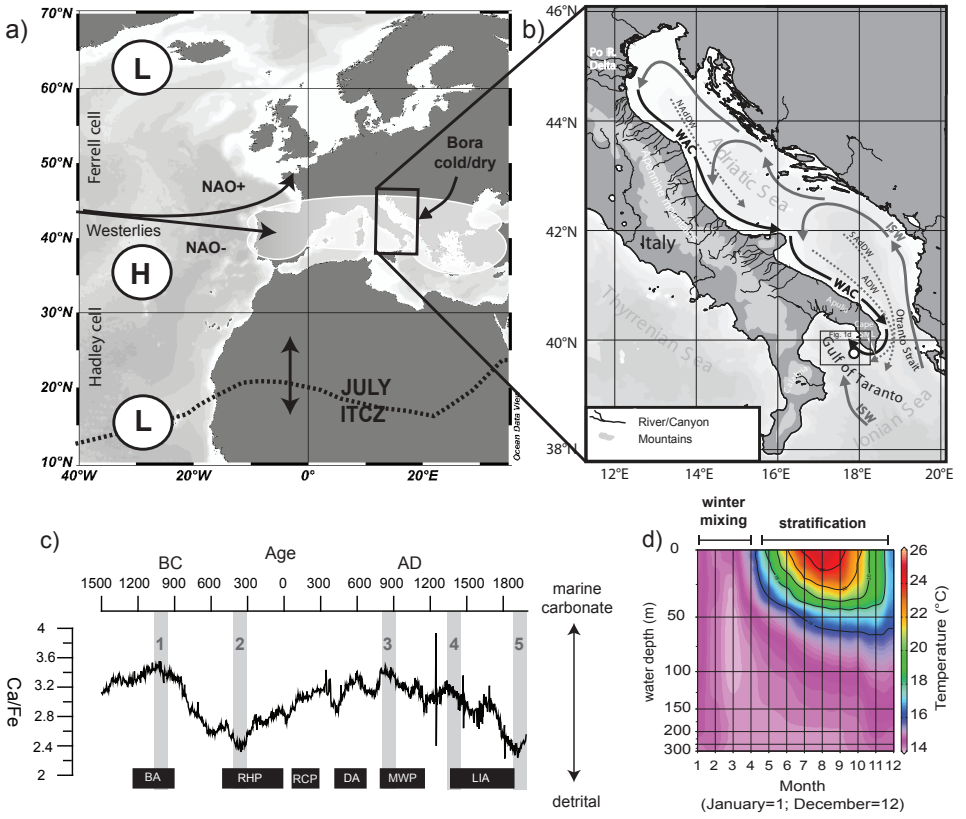

Fig. 1: (a) Map of Western Europe and Northern Africa showing winter precipitation patterns during a positive NAO , the position of the ITCZ during summer and Bora (b) Map of the study area showing the Adriatic Sea and Ionian Sea, general water circulation and water masses (WAC – Western Adriatic Current; nADW, sADW, and ADW - North-, South-, and - Adriatic deep water, ISW – Ionian Surface Water), and the core locations in the Gulf of Taranto (adapted after Grauel et al.,2013a) and (c) the Ca/Fe ratio of the sediments of core DP30 (Chapter 4), and the intervals selected for individual *G. ruber* (white) test chemistry (see table 1) Dark rectangles correspond to various periods mentioned in the text: Bronze Age (BA), Roman humid Period (RHP), Roman classical period (RCP), Dark Ages (DA), Medieval warm period (MWP) and Little Ice age (LIA) as defined by Grauel et al. (2013b) and (d) the monthly distribution of water column temperatures in the Gulf of Taranto (Locarini et al., 2010; data retrieved from world ocean atlas, 2009 (http://www.nodc.noaa.gov), averaged for 38.875°N/ 17.125 °E- 40.375°N/18.375°E (adapted after Grauel et al., 2013a).

temperature contrast in the Mediterranean Sea. Here, we apply this technique to a number of time slices such as the BA, RHP, Medieval Warm period (MWP) and the LIA from a core in the Gulf of Taranto (Central Mediterranean). The relatively high sedimentation rates in this area create an ideal setting for high-resolution studies (e.g. Cini Castagnoli et al., 1990). Results from the Mg/Ca, $\delta^{18}O$ and $\delta^{13}C$ analyses on single specimens of *G. ruber* (white) are evaluated in comparison to several more established proxy records: Mg/Ca of *Hyalinea balthica* (this study), $U^{k'}_{37}$ (Versteegh et al., 2010; Grauel et al., 2013a) and pooled $\delta^{18}O$ and $\delta^{13}C$ from *G. ruber* (white) (both extended from Grauel et al., 2013b). Results provide a high-resolution multi-proxy record of seasonality for both precipitation and temperature of the last ±3500 years in the Gulf of Taranto.

2. Study Area

The Gulf of Taranto is located between the two southern Italian regions Apulia and Calabria, the heel and forefeet of the Italian boot (Fig. 1b). Large amount of sediments are transported to the Gulf of Taranto from the Adriatic Sea by the West Adriatic Current (WAC; **chapter 2**). This WAC has a relatively low salinity as it is fed by freshwater runoff from the Po River and several smaller Alpine and Apennine Rivers (Turchetto et al., 2007). In the Gulf of Taranto the surface water from the low-salinity and nutrient rich WAC mixes with the more saline, nutrient poor Ionian surface waters (ISW) from the south (Poulain, 2001; Morovic et al., 2006).

During summer an anti-cyclonic atmospheric circulation prevails over the Mediterranean, which is related to the northward displacement of the North African Hadley cell, i.e. the ITCZ (Piervitali et al., 1997; Alpert et al., 2006). Hence summer climate is characterized by warm and dry conditions. Subsequently, river discharge is reduced during this season (Alpert et al., 2006) and thus also the influence of the WAC in the Gulf of Taranto (Poulain, 2001). Highest discharge and cooling and hence the largest extend of the WAC is associated with the winter season (Sellschopp and Álvarez, 2003). During winter, westerlies penetrate more southward, enhancing transport of moist air from the Atlantic Ocean to the Mediterranean (Brandimarte et al., 2011). This corresponds to a more positive mode of the North Atlantic Oscillation (NAO) during winter (Hurrell, 1995). In addition, during winter a positive Siberian high potentially stimulates outbreaks of cold polar air from the north, also known as the Bora. Cooling increases the formation of deep water in the Northern Adriatic, the northern Adriatic Deep water (nADW) and in the Southern Adriatic, Southern Adriatic Deep water (sADW). More intense deep-water formation increases ventilation of bottom waters in the Adriatic and the Gulf of Taranto. In addition, the sea surface temperature drop during winter results in the convective overturning of the water column in the Gulf of Taranto that subsequently remains stratified throughout the summer (Zonneveld et al., 2008; Grauel and Bernasconi, 2010). Consequently, bottom water conditions as recorded by benthic foraminifera reflect the winter SST composition.

# (Fig. 1c)	Period Total Age Interval(yr AD/BC)*	Sampled Interval (yr AD/BC)	Sampled Interval Depth (cm) (bottom-top)	N	$\delta^{18}O$ (down core) average	$\delta^{18}O$ (individuals) average
1	Bronze Age (BA)	1032-982 BC	234-237	29	0.67	0.60
2	Roman Humid Period (RHP) a.k.a. Roman Warm Period (RWP) (450-0 BC)	366-319 BC	190-186	30	0.66	*0.26*
3	Medieval Warm Period (MWP) (800-1200 AD)	883-835 AD	990-953	31	0.67	0.62
4	Little Ice Age (LIA) (1400-1850 AD)	1378-1428 AD	574-536	30	0.98	0.78
5	Present	1904-1958 AD	111-44	32	0.83	0.60

Table 1: Overview of samples (name, age, and depth in the core, and number of individuals (N)) used for individual single spec *G. ruber* test chemistry (Mg/Ca) and the average $\delta^{18}O$ of *G. ruber* in the interval based on the pooled specimens and the individual specimens. (*): total age interval for Rapid Climate Change periods as reported in Grauel et al., 2013b)

3. Material and Methods

3.1 Core site and age model

Piston core DP30 was collected at 39.835°N / 17.801°E , at a water depth of 270 m (Fig. 1b) during RV Pelagia cruise 'DOPPIO' in 2008. This core was sampled with a 2.5 mm resolution except for the top 20 cm, which was sampled at 5 mm resolution. All samples were split for geochemical analyses and foraminiferal studies. The age model, based on AMS ^{14}C and ^{210}Pb dating is described in **chapter 3**.

3.2 Foraminifera

Samples for foraminiferal studies were sieved into size fractions of 125-200 μm, 200-250 μm, 250-355 μm and >355 μm. From these fractions foraminiferal tests were selected for stable isotope and trace metal analyses as listed below.

For Mg/Ca analysis of *Hyalinea balthica* between 7 and 10 individuals from the 125- 250 μm size fraction were picked from every 4th sample. When a sample contained less than 7 foraminifera it was combined with the sample directly below. This was primarily

needed for the upper 1.5 m of core DP30. Samples were cleaned using the protocol by Boyle and Keigwin (1985) and modified after Rosenthal et al., (1997) involving 4 cleaning steps (see **chapter 4**). First samples are cleaned by ultrasonic agitation, followed by a treatment in a hot basic reducing solution (0.25 M cirtic acid in 16 M ammonia made up to 1 M in hydrazine) and a hot basic oxidizing solution (1% H_2O_2). The cleaning process is completed with multiple weak acid (0.001 M HNO_3) leaches.

To obtain an optimal dilution factor, samples with low amount of specimens (<8) were dissolved in 2 ml 0.1 M HNO_3, while samples with >8 individual foraminifera were dissolved in 3 ml 0.1 M HNO_3. Elemental composition of the samples was analysed by a high resolution ICP-MS (Element 2, Thermo Fischer Scientific) equipped with a double spray chamber and Teflon micro-flow nebulizer. Relative precision (<4 %) was determined by multiple measurements on international (ECRM-752-1) and in-house standards (GJR and CMSI). Every measurement consumed 1.8 ml of solution, permitting duplicate analyses. For duplicate analyses the samples were diluted to 10 ppm of calcium by adding 0.1 M HNO_3. To correct for a variable calcium matrix a 3-D ratio calibration method was used (Rosenthal et al., 1999). For this 5 standards (with fixed calcium concentration) were measured for a variety of dilutions (5, 10, 20, 30, 50 en 100 ppm calcium matrix).

Twenty specimens of *G. ruber* (white) were picked under the microscope from the fraction 200-355 μm of every 4th sample between 2050 and 2800 mm for down core isotopic analyses. Results from the upper part of the core (0 – 2050 mm) were previously reported in Grauel et al. (2013b). To avoid variations in $\delta^{18}O$ and $\delta^{13}C$ caused by different morphotypes for *G. ruber* (white), we selected only the morphotype *platys* following to the nomenclature of Nümberger et al. (2009). After picking, foraminiferal tests were cleaned according to the protocol described by Grauel and Bernasconi (2010) to eliminate carbonate particles adhering to the shell surface. For isotope analyses, 150-200 μg of cleaned shell material was dissolved under vacuum with two drops of ~103% H_3PO_4 at 70°C and the formed CO_2 cleaned cryogenically using a Thermo Fisher Kiel IV preparation device coupled online to a Thermo Fisher MAT 253 mass spectrometer. The reproducibility of the $\delta^{13}C$ and $\delta^{18}O$ analysis is based on repeated measurements of the *MS2* in-house standard and calibrated to the international standards NBS19 ($\delta^{13}C_{VPDB}$ +1.95‰, $\delta^{18}O_{VPDB}$ -2.2‰) and L-SVEC ($\delta^{13}C_{VPDB}$ -46.6‰, $\delta^{18}O_{VPDB}$ -26.41‰), was better than 0.1‰ (1σ). All $\delta^{13}C$ and $\delta^{18}O$ results are reported in the conventional delta notation with respect to VPDB.

Intervals were selected for reconstructing seasonality based on the down core Ca/Fe record, covering both maximum and minimum values (see Fig 1c, table 1, **chapter 4**). The Ca/Fe ratio reflects variability between marine biogenic carbonate (Ca) and terrestrial (Fe) inputs, and therefore likely changes in runoff and precipitation (**chapter 2, 3 and 4**). As precipitation in the Mediterranean region is highly seasonal, we expect that seasonal differences are maximal between samples with contrasting high and low runoff and precipitation. Therefore two samples with high Ca/Fe values (low terrestrial

input), and two with low Ca/Fe (high terrestrial input) as well as one with intermediate Ca/Fe values (intermediate terrestrial input; Fig 1c) were selected. These intervals, furthermore, correspond to recognised climate change events: the Bronze Age (BA), the Roman Humid Period (RHP), the Medieval Warm period (MWP) and the Little Ice age (LIA). From these intervals up to 30 single *G. ruber* (white) tests were picked for single specimen Mg/Ca analysis using laser ablation-ICP-MS. The limited number of available specimens in the 200-355 μm size fraction, also larger individuals (355-500 μm) are included in the single specimen analysis for the RHP and MWP interval. Samples were pre- cleaned in a similar way as for the isotope analysis, but without crushing the foraminiferal tests. Limited test size of individual specimen did not permit multiple measurements on one single chamber. Therefore, the 3 latest formed chambers per specimen were ablated with a deep-ultraviolet wavelength laser (193 nm) using a Lambda Physik excimer laser system with GeoLas 200Q optics. The carbonate test was ablated with an 80 μm spot diameter and a pulse repetition rate of 5 Hz for approximately 30–60 s with an energy density of 1 J/cm^2. Ablated material was transported on a He gas flow and mixed with Argon before being introduced into the ICP-MS plasma. Element to calcium ratios were quantified using ^{24}Mg, ^{26}Mg, ^{27}Al, ^{42}Ca, ^{43}Ca, ^{44}Ca, ^{55}Mn, ^{88}Sr isotopes and their relative natural abundances on SF-ICP-MS (Thermo Finnigan Element II). Elemental ratios were based on averaging counts for each ablation crater. Calibration is performed against U.S. National Institute of Standards and Technology SRM N610 glass (5 J/cm^2) using values from Jochum et al. (2011) and checked with an in-house matrix matched calcite standard GJR (1 J/cm^2) using ^{43}Ca as an internal standard (Reichart et al., 2003). Using different ablation energies between glass standard and calcite samples was shown to not affect accuracy (Dueñas-Bohórquez et al., 2011). Measurements were checked for possible remaining traces of surface contamination by evaluating Al and Mn profiles acquired during ablation. Any remaining clay particles or post-depositional Mn-rich inorganic coatings that are usually also enriched in Mg potentially influence the detected Mg/Ca value, thus biasing foraminiferal Mg/Ca values. Therefore, samples with elevated Al/Ca (> 2.0 cps/cps) and Mn/Ca (> 0.6 cps/cps) counts were excluded.

After Mg/Ca analysis with LA-ICP-MS, the same single specimens were analysed for stable carbon and oxygen isotopes, using the method described earlier for the bulk *G. ruber* (white) samples. Because of smaller sample size, the reproducibility of these measurements was ±0.15‰.

As not all data sets were of a similar size (n) a Kruskal-Wallis test (a non-parametric ANOVA) was performed, using the program PAST to identify whether differences between sample populations medians were significant (Hammer et al., 2001). To test whether the individual samples in each time slice come from populations with different variance, i.e. the homogeneity of variances, a Bartlett's test was performed (Snedecor and Cochran, 1989). With a Bartlett's test the null hypothesis 'all tested population variances are equal' is tested. Both the Kruskal- Wallis and Bartlett's test demand normal distributed data sets. To test for normality we performed a Shapiro-Wilk test (Shapiro and Wilk, 1965).

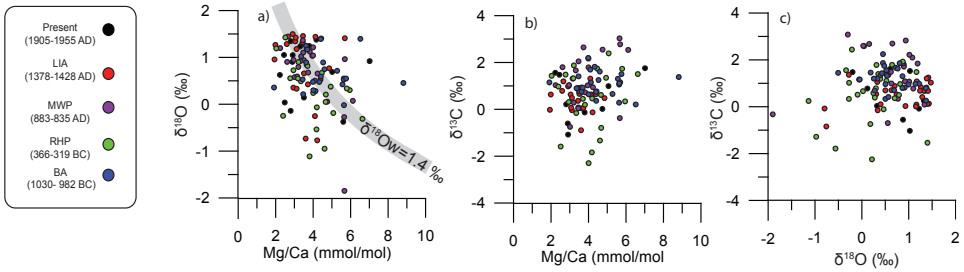

Fig 2: (a) The individual measured *G. ruber* (white) Mg/Ca versus $\delta^{18}O$ and (b) $\delta^{13}C$ and $\delta^{13}C$ versus $\delta^{18}O$. (c)The grey line in (a) represents the correspondence between temperature and $\delta^{18}O$ and Mg/Ca when the $\delta^{18}O_w$ equals 1.4‰.

4. Results

4.1 Stable isotopes of pooled *G. ruber* (white) specimens

The oxygen isotopes of *G.ruber* (white) (about 20 species pooled for a single analysis) from this study vary between 1.2 ‰ and 0.4 ‰ and have an average of 0.8 ‰ V-PDB (not shown). To transfer the oxygen isotope value to SST we used the paleotemperature equation of O'Neil et al., (1969) as refitted by Shackleton, (1974):

(1) $T=16.9-4.38*(\delta^{18}O_c-\delta^{18}O_w)+0.1*(\delta^{18}O_c-\delta^{18}O_w)$,

with T representing temperature in °C, $\delta^{18}O_c$ the $\delta^{18}O$ of the carbonate shells, and $\delta^{18}O_w$ the $\delta^{18}O$ of ambient seawater. Initially we take a constant $\delta^{18}O_w$ of 1.4‰ (the modern water value in the Gulf of Taranto (Grauel and Bernasconi, 2010), however, later in the discussion we also evaluate changes of $\delta^{18}O_w$ over time. The pooled down core oxygen isotope data represents temperatures between ~18 and 22 °C, using eq. 1. (Fig. 4b)

To check for consistency between the new data presented here (samples between 2050-2800 mm) and previously reported stable isotope analyses of *G. ruber* (white) for the same core (samples between 0 and 2050 mm; Grauel et al., 2013b) we compared averages and standard deviations. To do so we need to take into account the lower resolution of the new data set (the standard error of the mean (SE)), thus we correct the standard deviation (σ) by eq. 2.

(2) $SE = (\sigma/\sqrt{n})$

with n representing the difference in resolution (n=4).

Taking the lower sample resolution of our present data relative to previously reported data for the upper part of the core (Grauel et al., 2013b) into account, then the new series and previous data have similar standard errors (SE = 0.15 and 0.25 resp.). The

Proxy	Period	RHP	MWP	LIA	Present
Temp. Mg/Ca	BA	0.32	**0.05**	**0.001**	**0.04**
	RHP		0.59	**0.04**	0.35
	MWP			0.28	0.53
	LIA				0.66
Temp. $\delta^{18}O$	BA	**0.02**	x	x	x
	RHP		x	x	x
	MWP			x	x
	LIA				x
$\delta^{13}C$	BA	0.22	0.21	**0**	0.1
	RHP		**0.04**	0.1	0.75
	MWP			**0**	**0.02**
	LIA				0.26

Table 2: Kruskal Wallis for the different proxies of the individual measured *G.ruber*. If $p<0.05$ (in bold) than the nul hypothesis $\mu x=\mu y$ is false (with μ being the median of the sample) these are the significant results. If one of the data sets did not have a normal distribution and thus no Kruskal Wallis could be performed this is indicated with an x.

carbon isotopes of *G .ruber* (white) from this study vary between -0.4 ‰ and 1.2 ‰ (average = 0.79, Fig. 4c). The standard deviation, taking the lower resolution of our samples into account, indicates that also new and previous carbon isotope data have similar standard errors (SE =0.20 and 0.26 resp.). The oxygen and carbon isotope record do not display significantly different values between the lower and higher resolution series (Fig. 4b,c).

4.2 Single specimen *G. ruber* (white) test chemistry

G. ruber (white) stable isotopes of single specimens vary between -1.8 ‰ and 3.0 ‰ for carbon and from -4 to 1.6 for oxygen isotopes (Fig. 2 and 3). The latter corresponds to SSTs varying between 16 and 32°C (eq. 1; Fig. 3c). Mg/Ca values of the entire data set vary between 1.28 to 6.10 mmol/mol, based on averaging 3 single chamber measurements per single specimen (Fig. 2). Mg/Ca values for *G. ruber* (white) were converted to temperature (T) using the calibration of Elderfield and Ganssen (2000):

$$(3)\quad Mg/Ca = 0.52 \exp(0.10T)$$

Calculated sea surface temperatures indicate a range from ~13 to 28.3°C (Fig. 3b). Using the calibration of Anand et al. (2003) values would shift to somewhat higher temperatures, especially at the higher end of the observed range in Mg/Ca. Although these values are not unrealistic (see also discussion in Wit et al., 2010), the Elderfield and Ganssen (2000) calibration results in average temperature more closely to the oxygen isotope based averages.

Using the average Mg/Ca temperature (eq. 1) and $\delta^{18}O_c$ as measured on the same individuals $\delta^{18}O_w$ was calculated, taking advantage of the truly paired data set (resulting from analyses of the same specimen). We do realize that combining stable oxygen isotope analyses with Mg/Ca based temperatures may cause a major propagation of errors (Schmidt, 1999; Rohling, 2000). Therefore, we consider the values obtained as semi-quantitative only.

The $\delta^{18}O_w$ was correlated to sea surface salinity (SSS) for the region using the equation (3) of Wit et al. (2010), which is based on the data from Pierre, (1999) and Schmidt et al. (1999):

(4) $\delta^{18}O_w = 0.285 * SSS - 9.47$

Converting $\delta^{18}O_w$ values from VSMOW values to VPDB values was corrected for by addition of 0.27 ‰ (Hut, 1987).

The Shapiro- Wilk test identifies all individually measured $\delta^{18}O$, $\delta^{13}C$ and Mg/Ca as normally distributed, except the $\delta^{18}O$ of the samples from the MWP, LIA and the most recent sample. Therefore, a Kruskal-Wallis and Bartlets test was performed only on the RHP and BA intervals of the $\delta^{18}O$ datasets. The Kruskal-Wallis test of *G. ruber* (white) Mg/Ca indicates that the median of the BA samples is significantly higher than all other samples (Table 2). Furthermore, the LIA is significantly colder than the RHP. Bartlett's test has a p-value larger than 0.05 indicating that the ranges of all the sampled intervals are similar. The Kruskal-Wallis test of the oxygen isotopes BA and RHP interval indicate that their medians are significantly different (Table 2). Testing with Bartlett's test reveals that there are no significant changes in the range between the BA and RHP interval ($p > 0.05$). The *G. ruber* (white) carbon isotope median during the MWP is significantly higher than that from the RHP, LIA, and present (Table 2). Furthermore, the *G. ruber* (white) carbon isotope median during the BA is significantly higher than that during the LIA. Bartlett's test reveals a significant difference between the range of the different intervals at $p<0.01$ (with a $Chi^2 = 23.87$). Only the average calculated SSS during the BA is significantly higher than during the RHP (Table 2).

No correlation is found between individual *G. ruber* (white) Mg/Ca, $\delta^{18}O$ and $\delta^{13}C$ (Fig. 2). Averages values based on individuals, however, are in line with the down core record based on pooled specimens. Mg/Ca-based SSTs correspond to stable oxygen isotope-based temperatures for all intervals, except during the BA (Fig. 4b). For all intervals,

Next page **Fig. 3**: Histogram of the different time slices of (a) the individual *G. ruber* (white) $\delta^{13}C$ compared to the *G. ruber* (white) $\delta^{13}C$ as found in core top samples in the Gulf of Taranto and south-western Adriatic coast (Grauel et al., 2010) as well as SST based on Mg/Ca (b) and (c) $\delta^{18}O$ of individual *G. ruber* (white) compared to measured present-day monthly SST in the Gulf of Taranto (see Fig. 1d). Black triangles represent the average, white triangles the median. Please note that the indicated time interval represents that for our samples and *not* the full climate period.

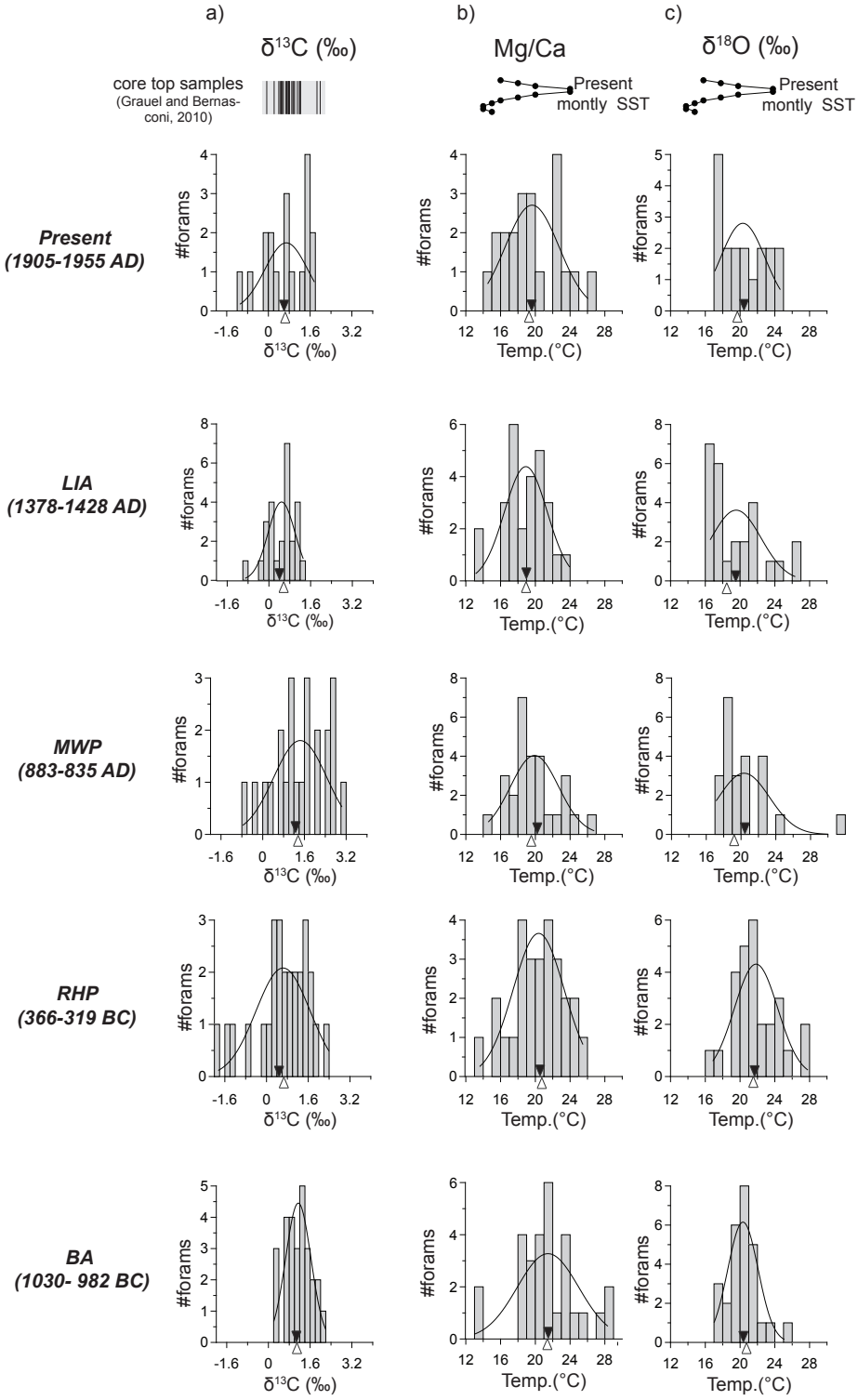
a)
δ13C (‰)
core top samples
(Grauel and Bernas-
coni, 2010)
b)
Mg/Ca
Present
montly SST
c)
δ18O (‰)
Present
montly SST
Present
(1905-1955 AD)
LIA
(1378-1428 AD)
MWP
(883-835 AD)
RHP
(366-319 BC)
BA
(1030- 982 BC)
#forams
δ13C (‰)
Temp.(°C)

.average carbon isotope values of the individuals correspond to the average down core values, except during the RHP and the MWP. During these specific intervals, however, the limited number of available specimens resulted in larger individuals (355-500 μm) being included for single specimen analysis. The observed offset (±0.5 ‰) is in line with previous studies showing ontogenetic impact on carbon isotopic fractionation (Erez and Honjo, 1981; Elderfield et al., 2002; Diz et al., 2012). The impact on oxygen isotopes over the same size range is negligible (e.g. Diz et al., 2012). Comparing oxygen isotope values based on averaging the down core record with the averages based on the individual specimen analysis show a major offset during the RHP, and minor offsets during the LIA and Present intervals (Table 1). Because the pooled samples are based on measuring 20 individuals, values integrate intra annual variability. The standard error observed during the RHP interval in the down core record (0.33) is high compared to the standard error based on the individual specimens (0.5). This suggests that interannual variability played a major role during this interval. Since the down core record integrates both intra- and interannual variability best, averages based on the down core isotope records are used for the selected intervals. Also statistically these averages are more robust as they generally include over 200 specimens per interval.

4.3 *H. balthica* Mg/Ca

The Mg/Ca values for *H. balthica* vary between 7.5 and 12 mmol/mol, corresponding to sea water temperatures ranging from ~14.5 to 17 °C (Fig. 4b) using the exponential equation of Rosenthal et al. (2011):

(5) $Mg/Ca=1.327\exp(0.123)\,BWT$

Low BWT (~15°C and below) are found between 600 to 750 BC, 900 to 1600 AD and 1800 to 1900 AD (Fig. 4b).

5. Discussion

5. 1 Reconstructing Seasonality

Changes in winter temperature and precipitation in the Mediterranean have previously been related to high-latitude climate change (e.g. Rohling et al., 2002; Giraudi et al., 2011). A stronger Siberian High enhances cold Bora winds from the north, affecting Adriatic Sea surface temperatures (Rohling et al., 2002). Winter precipitation in Italy is modulated by the North Atlantic Oscillation (NAO), which changes the route of the westerlies over Europe. During a positive phase of the NAO, the westerlies follow a more northward track and less winter precipitation reaches Italy (Fig. 1a ;Hurrell, 1995; Brandimarte et al., 2011). In contrast, Mediterranean summers are influenced by low latitude climate patterns (Piervitali et al., 1997; Alpert et al., 2006). An important feature

of low latitude climate is the so-called Inter Tropical Convergence Zone (ITCZ), where the northern and southern Hadley cells collide. During summer the ITCZ moves north and the high-pressure field of the associated northern Hadley cell shifts over the Mediterranean, resulting in dry and warm conditions (Alpert et al., 2006). Hence, the Mediterranean is characterized by high seasonality, both in temperature and precipitation.

5.1.1 Individual *G. ruber* (white) test chemistry as a proxy for seasonality

G. ruber (white) is a planktonic species inhabiting the upper part of the water column (Waelbroeck et al., 2005). Wit et al. (2010) showed that test chemistry (Mg/Ca and $\delta^{18}O$) of individual *G. ruber* (white) specimens from surface sediments in the Mediterranean Sea reflect present-day seasonality. In the Gulf of Taranto *G. ruber* (white) is thought to thrive mainly during the warm summer season (Grauel and Bernasconi, 2010). Nevertheless, it is also known to reproduce throughout the year (Pujol and Grazzini, 1995; Bárcena et al., 2004) and hence its test chemistry should reflect the full annual cycle, albeit biased towards summer conditions.

Present-day sea surface temperatures in the Gulf of Taranto range from 14°C in winter to 24°C during summer (Fig. 1d). The Mg/Ca temperature estimates, based on single specimens of *G. ruber* (white) for the most recent time slice (1905-1955 AD) show a similar range (15- 26 °C, Fig. 3b, 4b). The median of the reconstructed temperatures (~20°C) reflects a bias towards summer season SSTs, in line with *G. ruber* (white) productivity. In view of sedimentation rate and interval taken, each sample represents at least 50 years; consequently, interannual variability will also affect the reconstructed temperature range. However, the good fit with the present-day seasonal range indicates that primarily seasonality is recorded.

The range of SSTs based on oxygen isotopes (16 to 26°C; Fig. 3c) measured on the same *G ruber* (white) individuals that have been analysed for Mg/Ca is similar to today as well. Hence, both Mg/Ca and the oxygen isotopes of individually measured *G. ruber* (white) are in line with the present-day seasonal range. Plotting the oxygen-isotope-based temperatures for individual specimens against the Mg/Ca values of the same individuals, however, shows only a weak correlation (Fig. 2a). This implies that other factors than temperature also affected one or both proxies on the level of individuals. In addition to temperature, Mg/Ca and oxygen isotopic values of foraminifera tests are also, influenced by salinity and sea water carbonate chemistry (e.g. Dueñas-Bohórquez et al., 2009; Dissard et al.,2010 a,b; Wit et al., 2010; Hönisch et al., 2013). In the study area, salinity potentially plays an appreciable role, as it is located at the end of the relatively low-salinity plume of the west Adriatic current (WAC) (Sellschopp and Álvarez, 2003). Changes in salinity and the related offset in de oxygen isotope values of the surface waters impact the oxygen isotope values of the carbonates recorded in foraminifera, whereas the effect on the Mg/Ca values of foraminiferal tests is limited (Wit et al., 2010, 2013; Hönisch et al., 2013). Hence, when appreciable changes in salinity occur, temperature reconstructions based on oxygen isotopes do not exclusively reflect the seasonal SST range (Wit et al., 2010). Such combined temperature and salinity influence

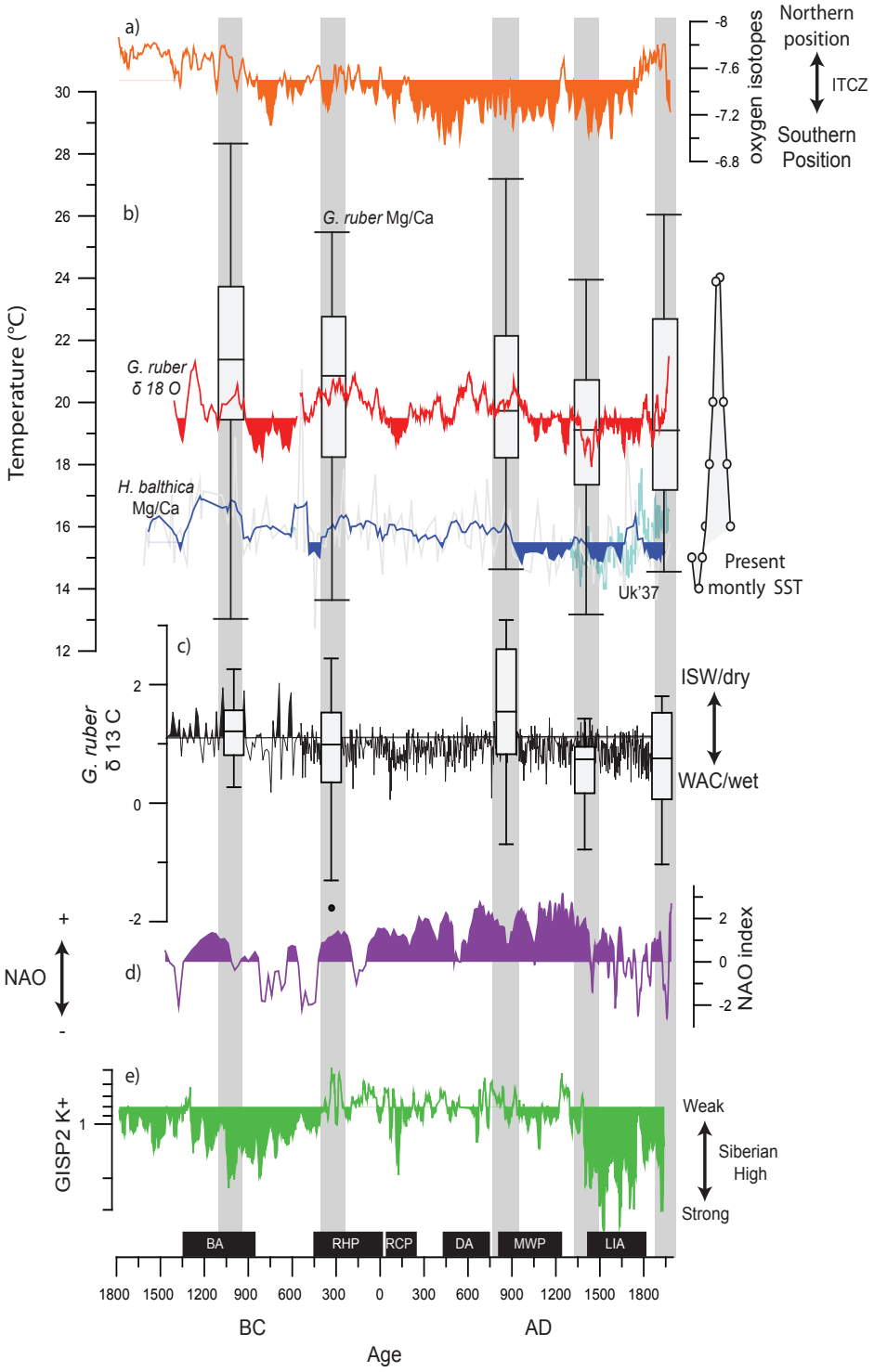
a)
-8
-7.6
-7.2
-6.8
oxygen isotopes
Northern position
ITCZ
Southern Position
b)
G. ruber Mg/Ca
G. ruber δ 18 O
H. balthica Mg/Ca
Uk'37
Present monthly SST
Temperature (°C)
30
28
26
24
22
20
18
16
14
12
c)
G. ruber δ 13 C
2
0
-2
ISW/dry
WAC/wet
NAO
+
-
d)
2
0
-2
NAO index
e)
GISP2 K+
1
Weak
Siberian High
Strong
BA
RHP
RCP
DA
MWP
LIA
1800 1500 1200 900 600 300 0 300 600 900 1200 1500 1800
BC
AD
Age

Previous page **Fig. 4**: (a) Proxy for the strength of the ITCZ the oxygen isotope record from a stalagmite from the Dongge Cave, southern China (Wang et al., 2005) compared with (b) SST based on individual *G. ruber* (white) Mg/Ca (box-whisker plots, this study), *G. ruber* (white) $\delta^{18}O$ (red line, Grauel et al. 2013 and this study), $U^{k'}_{37}$ (light blue line, Versteegh et al., 2007) and BWT based on *H. balthica* Mg/Ca (dark blue line this study); compared with (c) *G. ruber* (white) $\delta^{13}C$ of individual specimens from the selected time intervals (box-whisker plots, this study) and *G. ruber* (white) $\delta^{13}C$ of bulk samples (Grauel et al. 2013 and this study), (d) reconstructions of the NAO based on geochemical data from a lake in Greenland (Olsen et al., 2012) and the difference between records from Scotland and Morocco (Trouet et al., 2009) as well as e) potassium content of the GISP2 ice core, a proxy for the Siberian high (Mayeweski et al.,1997). Box-whisker plots display statistical data. The caps at the end of each box indicate the extreme values (minimum and maximum), the box is defined by the lower and upper quartiles, and the line in the center of the box is the median. Outliers beyond the extreme values are indicated with black dots. Dark rectangles correspond to various periods mentioned in text: Bronze Age (BA), Roman Humid Period (RHP), Roman Classical Period (RCP), Dark Ages (DA), Medieval Warm Period (MWP) and Little Ice Age (LIA) as defined by Grauel et al. (2013b).

on the $\delta^{18}O$ recorded may be reflected in the observed multiple maxima in the distribution of values at some intervals studied here (Fig. 3c).

Changes in salinity can theoretically be calculated by combining oxygen isotope and Mg/Ca values. However, the range in SSS's calculated this way is much broader than is observed today. When calculating sea surface salinity from Mg/Ca value and oxygen isotopes uncertainties of both proxies and effects related to additional variables contribute to the range in values (Schmidt et al., 1999; Rohling, 2000). In addition, the relationship between $\delta^{18}O_w$ and salinity is not straightforward and might vary over time, space, and region (Schmidt et al., 1999, Rohling, 2000). Amongst others, oxygen isotopes of Italian winter precipitation are more depleted (<-6‰) than summer precipitation (>-6‰) (Longinelli and Selmo, 2003). Hence, variance of reconstructed SSS reflects both actual SSS variance and combined analytical and calibration uncertainties. This implies that it is probably not possible to accurately calculate salinities for individual specimens in this way. Nevertheless, as these errors should act upon each individual specimen in a random direction, averaged $\delta^{18}O_w$ values should still provide a robust estimate of past (summer) SSS. This is confirmed by the good correspondence between the average of the calculated present SSS (39.2) based on $\delta^{18}O_w$ and measured present-day SSS in the Gulf of Taranto in summer (38.9; Zonneveld et al., 2009).

The average carbon isotope values of single *G. ruber* (white) specimen are similar to those found for the bulk *G. ruber* (white) samples during the last 3500 years for most of the selected time intervals (Fig. 3, 4). A Bartlets and a Kruskal-Wallis test indicate that variance and average carbon isotopes vary significantly between the different time slices. Grauel and Bernasconi (2010) observed strong variability in surface sediments samples from the south-western Adriatic and Gulf of Taranto. They related the high

variance to the strong nutrient gradient between the eutrophic waters from the WAC and the more oligotrophic ISW. When the WAC dominates, the nutrient regime in the Gulf of Taranto promotes abundance of *G. ruber* (white) in the upper 5 m, while it lives deeper (~30-50 m) when the influence of the WAC is reduced. Such a shift affects the carbon isotope chemistry of the shell of *G. ruber* (white) severely as it induces a change in symbiont activity, one of the main controlling factors of foraminiferal test carbon isotope values (Spero and Williams, 1989; Spero, 1992). Therefore, the range observed in $\delta^{13}C$ of individual specimens of *G. ruber* (white) in each sample is a potential representation of variance in the influence of the WAC in the study area. It should be taken into account, that differences in the depth habitat of *G. ruber* (white) also affect SST reconstructions, as deeper waters are colder. This could also potentially affect the temperature reconstructions made. However, although SSTs of the upper 30 m vary greatly over the year (Δ=12°C), temperature variability is much lower (max Δ=4°C) within the upper 30 m of the water column during a single month (Fig. 1d). Furthermore, no significant correlation is observed between individual specimen Mg/Ca ratios and $\delta^{13}C$ values (Fig. 2). This suggests that changes in reconstructed temperatures due to differences in calcification depth of *G. ruber* (white) are minimal.

The carbon isotopes of tests of *G. ruber* (white) from core tops in the Gulf of Taranto and South Adriatic range from 0 to 2 ‰ (Grauel and Bernasconi, 2010), closely corresponding to the observed range for the individual *G. ruber* (white) $\delta^{13}C$ from the Present-day interval of core DP30 (Fig. 3a). The other intervals show a somewhat larger range in *G. ruber* (white) $\delta^{13}C$ values. Because average values of *G. ruber* (white) test geochemistry are biased towards summer conditions and the WAC is reduced during summer, average $\delta^{13}C$ of *G. ruber (*white) should be enriched as well. Therefore, we suggest that the lower values (-1 – 0 ‰) in the most recent sample represent individuals from the winter / spring season, when WAC impact is higher than today.

Since the variance of *G. ruber* (white) Mg/Ca based SSTs seems to represent seasonality in the Gulf of Taranto, differences in the observed range should reflect changes in seasonality. Trends in variance, thus seasonality, are observed. However, the performed Bartlett's test shows no significant changes in the temperature range between the different intervals. Trends can be verified by comparing the ranges with those of other down core temperature reconstructions.

5.1.2 Reconstructing summer and winter conditions

5.1.2.1. Winter conditions reflected by *H. balthica* Mg/Ca values

H. balthica (Schroeter, 1783*)* is a primarily neritic to upper bathyal benthic foraminiferal species (<600 m), with a preference for shallow infaunal microhabitats in the topmost sediment (Van Morkhoven et al., 1986; Fontanier et al., 2002, 2008). *H. balthica* exhibits an unusual high temperature sensitivity, which is ~4 times higher than observed for other benthic foraminiferal species (Rosenthal et al., 2011), making this species ideal for

bottom water temperature reconstructions (Wit et al., 2012). Although the temperature calibration for *H. balthica* was derived elsewhere, temperatures based on the Mg/Ca values measured on *H. balthica* over the last decades (~16°C) resemble present-day bottom water temperature (14 to 15°C; Fig. 1d, 4).

Bottom water temperatures (BWT) in the Gulf of Taranto are set during late winter/early spring when surface waters cool, resulting in convective turnover (Fig. 1d). This mixing thereby sets temperature and composition of this deep water, which is maintained until the subsequent deep, winter mixing event. Coherently, the record of reconstructed BWTs shows similar changes as historical records of Italian winter and spring air temperatures of the last hundred years (**chapter 4**). Furthermore, observed maxima in winter temperature based on *H. balthica* Mg/Ca values during the last 800 years correspond to SST maxima based on the $U^{k'}_{37}$ from nearby cores (Versteegh et al., 2007; Grauel et al., 2013a; Fig. 4). This is in line with our inferences on the *H. balthica* Mg/Ca record as several studies suggested that $U^{k'}_{37}$ in this region is strongly influenced by changes in surface water temperature during winter and early spring (Sangiorgi et al., 2003; Versteegh et al., 2007; Leider et al., 2010; Grauel et al., 2013a).

5.1.2.2 Reconstructing summer conditions: bulk *G. ruber* (white) test chemistry

Because the bulk oxygen and carbon isotopes of *G. ruber* (white) are skewed towards the warm and more oligotrophic summer season in the Gulf of Taranto, bulk oxygen isotope values of *G. ruber* (white) can potentially be used to reconstruct variability in average summer temperature. However, oxygen isotope based temperatures are also impacted by changes in $\delta^{18}O_w$. Still, average Mg/Ca of single specimens of *G. ruber* (white) based temperature reconstructions and the bulk *G. ruber* (white) $\delta^{18}O$ match for largest part of the record, except during the BA (Fig. 4b). This suggests that in general, bulk *G. ruber* (white) $\delta^{18}O$ reflects primarily summer temperatures for this region.

For the intervals in which Mg/Ca of *G. ruber* (white) have been measured, it is possible to compare average Mg-Ca/based temperatures with the average oxygen isotope values for the down core foraminiferal record of the interval (Fig. 5a). Plotting iso-isotope lines in the same plot, makes it possible to unravel the effect of temperature and surface water stable isotope composition ($\delta^{18}O_w$). This shows that during all intervals, except the BA, the oxygen isotopic value of the surface waters has been very close to the present-day value of 1.4 ‰. During the BA surface stable oxygen isotope values must have been higher, at about 1.65 ‰ (Fig. 5a). The higher isotopic value for the surface water during the BA is probably connected to higher surface water salinity at that time. This is confirmed when comparing this data to the down core $\delta^{13}C$ record for *G. ruber* (white). During the BA $\delta^{13}C$ values are higher, reflecting a reduced influence of the WAC, hence dryer overall conditions (Fig. 5b). All other intervals appear more or less similar to the present-day interval (Fig. 5b).

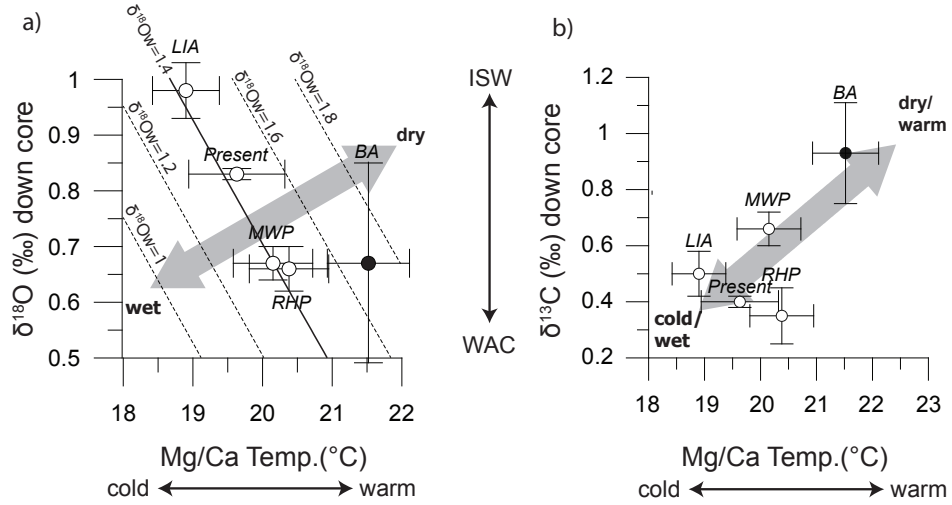

Fig. 5: Average of the SSTs based on the individual measured *G. ruber* (white) Mg/Ca versus average (a) $\delta^{18}O$ and (b) $\delta^{13}C$ of *G. ruber* (white) from the pooled down core data set down core. Dashed lines in (a) represent the correlation between $\delta^{18}O$ and temperature under variations of $\delta^{18}O_w$ based on eq. 1 (see text). Abbreviations stand for the events matching with the studied intervals (see figure 1c and table 1): Bronze Age (BA), Roman humid Period (RHP) , Roman classical period (RCP), Dark Ages (DA), Medieval warm period (MWP) and Little Ice age (LIA) as defined by Grauel et al. (2013b).

5.2 Temperature, precipitation and seasonality

5.2.1 The MWP, RHP and Present interval

The reconstructed similarity in humidity for Present, MWP and RHP as reflected in the inferred $\delta^{18}O_w$ of 1.4 ‰ (Fig. 5a) is confirmed by similar variance in the individual $\delta^{13}C$ of *G. ruber* (white) during these intervals (Fig. 4c). In contrast, variance during LIA and BA is smaller, albeit with averages that are not similar. The high variance during present-day, MWP and RHP suggests a high seasonal contrast in precipitation, which is also typical for the present-day Mediterranean climate (Fig. 3a, 4). Down core $\delta^{18}O$ combined with Mg/Ca_{ruber}, suggests similar $\delta^{18}O_w$ values as today (1.4 ‰, Fig.5a), which suggests that summers were as dry as today. This in combination with a similar variance in individual $\delta^{13}C$ of *G. ruber* (white) implies that winter precipitation has remained the main source for moisture during the RHP and MWP. However, the average $\delta^{13}C$ of the pooled *G. ruber* (white) suggest that summer conditions were slightly wetter during the RHP and drier during the MWP.

General consensus on the relatively wet nature of the RHP is that these conditions are related to a negative state of the NAO (e.g. Giraudi et al., 2011; Nieto-Moreno et al., 2011; Dermody et al., 2012) mainly impacting winter precipitation. However, during

this interval also a centennial scale southward placement of the subtropical high-pressure cell is found (Fig 4a, Fleitmann et al., 2003; Wang et al., 2005; Shanahan et al., 2009) which would allow the westerlies to enter the study area also in summer. The observed range in $\delta^{13}C$ is similar to the recent range suggesting a similar range in precipitation as today. This indicates that either winter precipitation was also increased, or that summer was the wettest season during this humid period. The latter seems reasonable as the interval studied here is coherent with a centennial shift to a relatively positive NAO (Olsen et al., 2012), and with enhanced *H. balthica* Na/Ca values indicating increased winter salinity (**chapter 4**). In contrast, the calculated $\delta^{18}O_w$ (~1.4‰) is not in line with wetter summer conditions during the RHP. However, this may be due to the less depleted $\delta^{18}O_w$ of summer precipitation (>-6‰) compared to winter precipitation (<-6‰). In addition, during the sampled interval interannual variability appeared to be large (see 4.2), which could have biased our calculated $\delta^{18}O_w$.

Apart from a centennial scale event, the interval corresponding to the MWP is predominantly characterized by a relatively positive mode of NAO (Olsen et al., 2012; Fig. 4d). Under persistent positive NAO conditions a more southern area may be reached by the westerlies as compared to today (e.g. Magny et al., 2003; **chapter 4**). Under such conditions the associated excess rain would enhance Po River outflow. As the Po River contributes up to ~70% of all river input to the Adriatic Sea (Raicich, 1996), this would severely increase the WAC, reducing salinity in the Gulf of Taranto. Such an increased WAC in winter is in line with the observed depleted $\delta^{13}C$ values during the MWP (Fig. 3a, 4c), while the enriched $\delta^{13}C$ values can be related to a dry summer season.

A similar range in temperatures (ΔT= ~10°C) is observed for present-day conditions, MWP and RHP. For the RHP the median of the Mg/Ca-based temperatures as well as the bulk *G. ruber* (white) oxygen isotopes indicate relatively warmer summers compared to present-day (Fig. 3, 5), whereas winters conditions were probably slightly colder based on of *H. balthica* Mg/Ca (Fig. 3, 5). Although the higher summer SST may be partly related to a shallower and thus warmer habitat of *G. ruber* (white) during the wet summer season, somewhat higher summer SSTs are in line with a reconstruction based on dinoflagellate cysts from the same core during the latest part of the RHP (60 BC-90 AC; Chen et al., 2011). Several other studies also inferred overall warm conditions across southern Europe during the RHP (e.g. Desprat et al., 2003; Holzhauser et al., 2005; Martín-Chivelet et al., 2011). Nonetheless, overall seasonal contrast during the RHP was similar to the present-day. During the early MWP (~850 AD) mild winters and warm summers, similar as today, are reconstructed based on the *H. balthica* Mg/Ca and individual measured *G. ruber* Mg/Ca respectively. Mild winter conditions are coherent with a variety of other reconstructions from the area (e.g. Rohling, et al., 2002; Frisia et al., 2005) and might be linked to a weak Siberian high (Mayewski et al., 1997; Fig. 4). However, for the latest part of the MWP (1000-1200 AD) SSTs based on *H. balthica* Mg/Ca and on *G. ruber* $\delta^{18}O$ indicate a swift transition to colder conditions during both winter and summer. Also the dinoflagellate cyst-based SST reconstruction from the same core suggests lower SSTs during this interval (Chen et al., 2013). High primary productivity (PP) in the study area is reconstructed for the early MWP (**chapter 4**),

which could result in shallower and thus warmer habitat of *G. ruber* (white). However, a warm early MWP (~900 AD) and colder conditions during the late MWP (1000-1200 AD) are found across the Mediterranean (Pla and Catalan, 2005; Frisia et al., 2006) and in the Southern Alps (Frisia et al., 2005; Holzhauser et al., 2005; Giraudi, 2009). Colder summer conditions agree with a more southward position of the ITCZ inferred from a speleothem $\delta^{18}O$ record (Wang et al., 2005; Fig. 4a). The colder winter temperatures are, however, more difficult to explain as the Siberian high appears relative weak (Fig. 4e). A recent study on ice-rafted debris, however,has suggested that a negative Arctic Oscillation (AO) persisted between 800 and 1800 AD (Darby et al., 2012). The latter could enhance the potential of outbreaks of cold polar air across the study area during winter (Rohling et al. 2002).

5.3.2 The LIA

Cool winter conditions are reconstructed for the early LIA, inferred from the BWT based on *H. balthica* Mg/Ca (Fig.4). The GISP2 K^+ indicates that during the LIA, Bora winds might have increased, as they are closely linked to the Siberian high (Mayewski et al., 1997). This is in line with Rohling et al. (2002) suggesting that cold Bora winds are responsible for winter cooling in the Mediterranean area during other cold events. In addition to the colder winters, summer temperatures are also lower (~19-24°C) for the LIA (Fig. 4b). This indicates that cool conditions persisted year-round, which is consistent with results of previous studies from the same area (Grauel et al. 2013a). These year-round cool conditions are accompanied by a similar seasonality as today (ΔT = ~10°C). During the late LIA (1645-1715 AD), however, a higher seasonal contrast may have existed (e.g. Grove, 2001; Nicault et al., 2008; Grauel et al. 2013a). Low BWTs based on *H. balthica* Mg/Ca, and high SSTs based on *G. ruber* (white) $\delta^{18}O$, confirm a relatively high seasonal contrast for the later LIA (Fig. 4b).

The individually measured *G. ruber* (white) $\delta^{13}C$ values show a relatively small range during the LIA, also when compared to present-day core top data. The range in $\delta^{13}C$ is primarily controlled by changes in WAC inflow during the year. The observed limited range and overall depleted values, therefore, suggests prolonged inflow of the relatively low-saline WAC over the year. Hence, summers would be relatively humid in addition to the already typically wet winters. Because the oxygen isotopes for summer precipitation are less depleted than those for winter precipitation, this may not be reflected in the average oxygen isotope value of the surface water (Fig. 5a). Relatively wet winters and summers are coherent with patterns found in cores from the north Adriatic Sea and Italian lakes (Piva et al., 2008; Giraudi et al., 2011). Furthermore, during the LIA, the more southern position of the Hadley cell (Wang et al., 2005) would allow the westerlies to enter the Mediterranean area also during summer. Thus the overall relatively wet and cool LIA period in the central Mediterranean, as reflected in our results, is consistent with observations made in records elsewhere (Piva et al., 2008; Grauel et al., 2013a). It should be noted that under influence of the increased influence of WAC in summer, *G. ruber* (white) may live shallower and warmer waters, and therefore, actual summer SSTs could have been slightly lower than those recorded by our proxies.

5.2.3 The Bronze Age

The BA is the only episode in our record during which both temperature and salinity deviate considerably from the other intervals of climate variation. Summer temperatures were high, apparent from both $\delta^{18}O$ and Mg/Ca values of *G. ruber* (white). Dry summer conditions, allows *G ruber* (white) to live in a deeper and colder habitat which could affect our summer SST reconstruction. Actual summer SST thus may have been somewhat higher than the reconstructed SST. Although *G. ruber* (white) habitat changes under influence of the WAC, it is also known to have a preference for relatively low-salinity waters (Rohling et al., 2004). Therefore, we assume that the deepening of its habitat, resulting in lower reconstructed summer SSTs, was relatively restricted during this extremely dry interval compared to present-day migration of *G. ruber* (white). Warm and dry summers are consistent with a relatively northward summer position of the ITCZ at that time (Fleitmann et al., 2003; Wang et al., 2005; Weldeab et al., 2007; Table 1; Fig. 4a). Increased summer temperatures are in line with pollen records from Greek and Italian lakes (e.g. Peyron et al., 2011). The high range of inferred temperatures (13 -28°C) based on Mg/Ca measured in individual *G. ruber* (white) tests suggest that warm summers were accompanied by cool winters.

The GISP2 K^+ indicates a relatively strong Siberian high and possibly related increased strong Bora winds (Mayewski et al., 1997; Rohling et al., 2002). This period is coherent with the timing of one of the RCC-events as indicated by Mayweski et al. (2004). Cold outbreaks associated with this RCC event would explain the inferred low winter temperatures (reduced by 2°C compared to the most recent time slice). In general, these RCC-events are mostly related to changes in northern hemisphere high-latitude winter conditions (Denton et al., 2005; Wanner et al., 2011). Decreased winter/early spring temperatures are also suggested by $U^{k'}_{37}$ from a core in the southern Adriatic Sea (Sangiorgi et al., 2003). In contrast, our *H. balthica* Mg/Ca record indicates higher BWT, thus suggesting increased winter temperatures. However, as discussed above in section 5.1.2.2 the surface waters were much more saline during this period (Fig. 5a). Such enhanced salinity water mass would require less cooling to descend to the same depth. In addition, the outbreaks of polar air over the Adriatic Sea would enhance the formation of nADW and sADW, contributing to a more ventilated and less stratified water column for a longer period during the year. This adequately explains the observed apparent discrepancy between the *H. balthica* Mg/Ca and the other winter temperature records.

Dry conditions, responsible for enriched $\delta^{18}O_w$, is also reflected in a lower impact of the WAC in the Gulf of Taranto, evidenced by relatively high $\delta^{13}C$ of *G.ruber* (bulk) values (Fig. 3, 4, 5b). Furthermore, the lowest range in the individually measured *G. ruber* (white) $\delta^{13}C$ values is observed during the BA (Fig. 3a, 4c). Such a narrow range implies that both summer and winter precipitation was modest. A relatively positive mode of the NAO during this period (Olsen et al., 2012), in combination with cold, dry Bora winds (Rohling et al. 2002) would reduce winter precipitation (Fig. 5d, e). Similar year-round low precipitation during the BA in central Italy was suggested by Peyron et al. (2011), in coherence with other records across the Mediterranean (Bar-Matthews et

al., 2003; Di Rita and Magri, 2009; Kaniewski et al., 2010; Giraudi et al., 2011, Nieto-Moreno et al., 2011; **chapters 3, 4**). Reconstructed SSTs based on $U^{k'}_{37}$ (Sangiorgi et al., 2003) and the test chemistry of *G. ruber* (white) both suggest that these conditions may have persisted from 1200 to 900 BC (Fig. 5b). During the Late Bronze Age several cities and states in the Eastern Mediterranean region were distorted, such as amongst others the Mycenean civilization (e.g. Carpenter, 1966; Weiss, 1982). This has been related to severe drought (Carpenter, 1966; Weiss, 1982). The reconstruction presented here illustrates that during the BA summers were warm and winters cold, but aridity lasted year-round. This must have had a profound impact on early agriculture, also in Southern Italy.

5.3. Overall patterns

Although seasonality remained more or less constant throughout the intervals studied here, comparison with other proxies reveals that during the BA and the LIA winter conditions were relatively cold. This is in coherence with earlier work by Denton et al. (2005) and Rohling et al. (2002), who suggested that millennial scale cold events in the northern hemisphere were mainly related to winter climate. These changes in northern hemisphere winter climate were suggested to also affect the position of the ITCZ during summer (Denton et al., 2005). Mediterranean summer climate is closely coupled to the ITCZ position as the descending limb of the northern Hadley cell is responsible for the strong high pressure cell over the Mediterranean during summer. This high pressure cell effectively blocks the Mediterranean from the influence of the westerlies. The contrasting seasonality between the BA (high variance) and the LIA (low variance) suggest that the connection between high- and low- latitude climate variability did not remain stable through time.

Comparing the $\delta^{13}C$ values of individual *G. ruber* (white) tests indicates that the seasonal contrast in precipitation in the Central Mediterranean did not remain constant over the last 3500 years. Differences in the ITCZ position during summer and the NAO state during winter together control changes in the seasonal contrast in Mediterranean precipitation. The high intra-annual variability inferred for the RHP and MWP, contrasts with the low intra-annual variability during LIA and BA. Decoupled changes in winter and summer precipitation imply that ITCZ and NAO variability are not necessarily linked in a direct and coherent way.

Nonetheless, a relation between temperature/precipitation and seasonality is apparent from the trend between average *G ruber* (white) $\delta^{13}C$ and the SSTs based on Mg/Ca (Fig. 5b). The trend observed between the different episodes studied here suggests that when warmer conditions prevail, it is also dryer, while it is moister during colder conditions. These observations conform in general with the sub-tropical, Mediterranean setting. Warm and dry conditions are known for summer, while wet and cold conditions prevail during winter. Although the seasonal temperature contrast remained constant for these intervals, the precipitation balance was dramatically different. During the LIA wet and cold, winter–like conditions dominated. In contrast during the BA dry conditions pre-

vailed throughout the year.

6. Conclusions

Variance of the individual *G. ruber* (white) Mg /Ca and $\delta^{13}C$ values reflect the present-day range of Gulf of Taranto temperatures and precipitation respectively, albeit with their averages biased towards summer conditions. Reconstructions based on the measured individual test chemistry indicate that temperature contrast did not change significantly during the last 3500 years. However, comparing overall patterns with other proxies for winter and summer SST in the Gulf of Taranto, there are appreciable differences. Present-day bottom water temperature (BWT) in the Gulf of Taranto is set in winter. Reconstructed BWT based on *H. balthica* Mg/Ca reflect patterns of southern Italian air temperatures in winter/spring and concord with previously reconstructed SST based on $U^{k'}_{37}$ (a winter/spring proxy). Therefore, the BWT based on *H. balthica Mg/Ca* is considered as a proxy for winter/spring SST. Summer SSTs can be reconstructed using pooled *G. ruber* (white) test chemistry as a proxy. Our data suggest, that winters are cool during Rapid Climate Change events as the BA and LIA compared to other intervals. However, the results from our proxies also suggest that during the early LIA summers are cold and wet, whereas during the BA interval summer conditions are indicated to be warm and dry. Furthermore, reconstructed humidity suggests year-round aridity during the BA interval, while the LIA interval is characterised by relatively humid conditions throughout the year. The trend observed between average carbon isotopes and SST based on Mg/Ca *G. ruber* (white), reflecting respectively precipitation and temperature, indicates that the LIA is characterized by more 'winter'-like conditions (cold and wet), while the BA is more skewed to 'summer'-like conditions (warm and dry). The other RCC-periods (MWP and RHP) are characterized by intermediate seasonal conditions similar to today. Summer conditions are controlled by low-latitude climate forcing (e.g. ITCZ) and winter climate by high-latitude climate variability (NAO, Siberian High). The contrasting patterns during the LIA and BA suggest that connections between high and low latitude climate variability are not necessarily continuous during RCC events.

Acknowledgments

We thank Helen de Waard, at Utrecht University, for lab assistance with LA-ICP-MS; Wim Boer, at the NIOZ for lab assistance with ICP-MS and S.E. Bishop and M Coray-Strasser at ETH for lab assistance. We are grateful to captain and crew, and all participants for sample collection on board the DOPPIO cruise with R.V. Pelagia (coordinated by Gert J. De Lange) and for help during sub-sampling of DP30 by A. Leider and C.E. Casalino. This work was supported by the Nederlandse Organisatie voor Wetenschappelijk Onderzoek (NWO) as part of the MOCCHA- project initiated by the European Science Foundation (ESF) Eurocores Programme EuroMARC.

Chapter 6: Decadal modulations of bottom water oxygen depletionduring deposition of Sapropel S1 in the Southern Adriatic

Marie-Louise S. Goudeau, Tom Jilbert, Christian Zeeden, Stefano M. Bernasconi, Shauna Ni Fhlaithearta, Gert-Jan Reichart and Gert J de Lange

(In preparation)

Abstract

The Eastern Mediterranean Sea sedimentary record contains regularly recurring organic rich black layers, so-called sapropels. These are thought to be related to high export productivity and low ventilation rates, causing anoxia, which resulted in enhanced preservation of organic matter. During the formation of these sapropels intensity of oxygen depletion probably varied on multi-decadal to centennial time scales. Here we present a laminated sapropel from the Adriatic shelf, close to the critical upper-depth for sapropel formation during deposition of the last sapropel (S1, at 565 mbss). The age model indicates each laminae cycle (from dark to light) covers 8-10 year. Besides laminations, also centennial to multi-decadal scale changes are observed in sediment darkness. Based on Ba/Al analyses darker sediments correspond to increased export productivity, whereas redox sensitive elements (V) suggest simultaneous enhanced oxygen depletion. Throughout the record relatively constant Ca/Al ratios indicates variability in detrital fluxes were modest. Detailed analyses of individual laminae reveal that pyrite within in the dark laminations are framboidal shaped. This indicates that anoxic to suboxic conditions prevailed within the water column during deposition of the darker parts of the laminations. Comparison with other high-resolution paleoclimate records and historical records of Siberian High and monsoon intensity, suggest that outbreaks of cold northerly winds resulted in enhanced convective turnover in the southern Adriatic on both centennial and decadal time scales. The well-known 8.2 kyr sapropel interruption event has previously been related to increased cold northerly winds as well. Hence northerly winds played a major role in enhancing convective turnover, and thus Eastern Mediterranean ventilation, on various time scales and with differing magnitude.

1. Introduction

1.1 Sapropel formation

Organic rich, black layers found in sediments of the Eastern Mediterranean Sea , so-called sapropels, have been studied intensively since their discovery (e.g. Olausson, 1961; Rohling and Hilgen,1991; Emeis et al., 2000). The dominant forcing resulting in low-oxygen conditions required for sapropel formation are subject of an on-going debate in sapropel research: increased primary productivity (PP) versus stratification of the water column, or a combination of both (e.g. Olausson, 1961; Calvert, 1983; De Lange and Ten Haven, 1983; Rohling and Hilgen, 1991; Emeis et al., 2000; Thomson et al., 2004; De Lange et al., 2008; Gallego-Torres et al., 2010). Sapropels formed close to insolation minima of the orbital precession index (Rossignol-Strick, 1985, Hilgen, 1991; Lourens et al., 1996). Prior to the onset of the most recent sapropel, S1 (10.8-6.1 kyr cal BP, De Lange et al., 2008) precipitation and concomitant discharge of the Nile (and possibly other north-eastern Mediterranean rivers) increased, in line with an intensification of the African/ Indian monsoon (AM/IM) and enhanced moisture transport by the westerlies (Rossignol-Strick, 1985; Rohling and Hilgen, 1991; Kotthoff et al., 2008 and references within). Increased river runoff not only supplies nutrients to the system, enhancing PP (e.g. Rossignol-Strick, 1985; Kemp et al., 1998), but also reduces thermohaline deep-water formation, causing suboxia and anoxia in the deeper waters of the eastern Mediterranean (e.g. Rohling and Hilgen, 1991; Sachs and Repeta, 1999; Pinardi and Masetti, 2000). Enhanced PP and associated improved preservation under anoxia both lead to the observed higher levels of organic carbon, characteristic of sapropel sediments.

1.1 Interruptions of S1

Sediments across the Eastern Mediterranean located down to ~1500 m water depth show a centennial scale (7.9-8.4 cal. ka BP) interruption of Sapropel S1 simultaneously with a cold event centred on 8.2 ka BP (Rohling, et al. 1997; Rohling, 1999; Casford et al., 2003; De Lange et al., 2008; De Rijk et al., 2009; Marino et al., 2009). The interruption has been attributed to increased bottom water ventilation by deep waters formed in the Aegean and Adriatic Seas, a result of increased outbreaks of cold air from the Polar region to these basins, which enhance deep water formation (De Rijk, et al., 1999; Marino et al., 2009).

Recent high resolution studies have indicated that besides the well-documented interruption centred on 8.2 ka BP, export productivity and ventilation varied on multi-centennial to multi-decadal time scales throughout S1 (Kotthoff et al., 2008; Gennari et al., 2009; Jilbert, et al., 2010b). Indeed, the occurrence of benthic foraminifera throughout sapropel S1 in cores from the Aegean Sea and the Libyan shelf suggest that bottom waters were not completely anoxic for longer than 50 years at any time (Casford et al., 2003). Two distinct centennial scale re-oxygenation events (from ~7.5 to7.2 ka BP and

~8.8-8.6 ka BP) appear as interruptions of sapropel formation in a high resolution core in the Aegean Sea (Kotthoff et al., 2008). Furthermore, millimetre scale laminations consisting of alternating dense diatom mats and darker more clastic layers indicate changes in nutrient availability on short time scales during older sapropels (Kemp et al., 1998; Kemp et al., 1999; Moller et al., 2012). Based on the observed variability on such short time scales, Casford et al. (2003) proposed that bottom water conditions during sapropel formation are characterized by only a thin 'blanket' of anoxia/suboxia at the sediment water interface, which is highly sensitive to changing environmental conditions.

Jilbert et al. (2010b) observed coherent centennial to multi-decadal patterns in ventilation and export productivity during S1, and high resolution proxy records of both the Indian Monsoon (IM, (Fleitmann et al., 2003) and the Siberian High (SH, Mayewski et al., 1997), confirming that climate variability forced rapid oscillations in water column conditions during sapropel deposition. If changes in the strength of the Siberian High (SH) and connected outbreaks of cold air to the eastern Mediterranean indeed triggered the observed centennial to multi-decadal variability in S1 intensity, their influence should be most apparent in sapropels from the key regions of deep water formation, such as the Adriatic shelf (Robinson et al., 1992; Roether et al., 1996).

1.3 This study

Here, we present a high resolution record from a finely laminated (~1 mm) Sapropel S1 from the Southern Adriatic Sea, to investigate re-oxygenation events during S1 at high temporal resolution. The core was retrieved from a water depth of 565 m below the sea surface (mbss). This was likely close to the critical upper depth for sapropel formation during S1 (Bianchi et al., 2006, Ni Fhlaithearta et al., 2010). In the Aegean Sea benthic foraminifera can be found throughout S1 in cores taken from above 420 m water depth (Abu-Zied et al. 2008; Ni Fhlaithearta et al., 2010) whereas below ~700 m water depth no benthic foraminifera are observed in sediments of S1 age (Geraga et al., 2000; Kuhnt et al., 2007). At the core location a combination of high sedimentation rates, likely proximity to the redoxcline, and the generally laminated sediment fabric allow investigation of very-short timescale variability in sediment geochemistry. Presence or absence of laminations in different sections of S1 may be used to reconstruct longer-timescale changes in bottom water oxygenation.

Using high-resolution geochemical techniques such as Laser Ablation-Inductively Coupled Plasma Mass Spectrometry (LA-ICP-MS), micro X-ray Fluorescence (μXRF) and Scanning Electron microscopy (SEM) we characterized the composition of the laminations and infer environmental conditions during their deposition. We employed a novel sediment colour analysis technique (Zeeden et al., 2014) to construct a continuous high-resolution record of pixel intensity in images of epoxy-embedded sediment blocks. Correlating colour and geochemical proxies, this record is used to unravel impact of high frequency changes in regional and global climate on local water column conditions and sapropel formation.

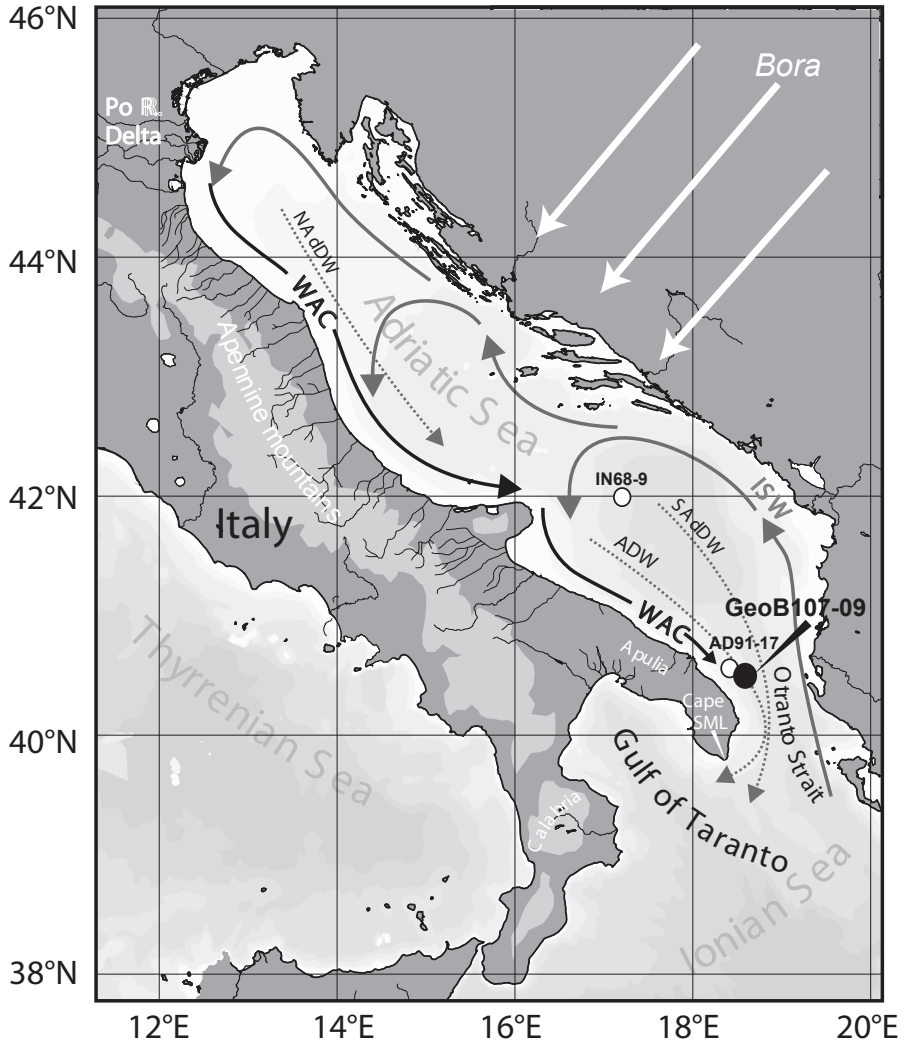

Fig. 1: Map of the study area showing the Adriatic Sea and Ionian Sea, general surface water circulation, water masses (WAC – Western Adriatic Current; north and south Adriatic deep water (nADW and sADW, ISW – Ionian Surface Water) and the core location of the studied core GeoB107-09, as well as core AD91-7 (Sangiorgi et al., 2003) and IN68-9 (Rohling et al., 1997; De Rijk et al., 1999)

2. Material and Methods

2.1 Core site

Multicore GeoB107-39 (40°50 N; 18°64 E, 565 m water depth) was collected from the south-western Adriatic Sea shelf during POSEIDON cruise 'CAPPUCCINO' in 2006 (Zonneveld et al., 2008; Fig. 1). The core site is located in the pathway of the

low-salinity, nutrient rich West Adriatic current (WAC), albeit close to the boundary with the more saline, oligotrophic Ionian surface waters (ISW; Fig. 1; Poulain, 2001; Bignami et al., 2007; Turchetto et al., 2007). The WAC forms a narrow belt along the eastern coast of the Italian peninsula, where its high sediment loads originating from mostly rivers north of the Gargano Peninsula (Po and Apennine) form the Adriatic mud belt (e.g. Trincardi, et al., 1994, Cattaneo et al., 2003; Syvitski and Kettner, 2007). The WAC is extended in winter and spring when precipitation and snow melting in the Alps respectively peak. During winter moisture transportation by the westerlies to the region increases (e.g. Hurrell and Deser, 2009; Brandimarte et al., 2011). Levantine Intermediate Water (LIW, nutrient rich, and highly saline), a water mass formed in the more eastern Levantine basin (Pinardi et al., 2000 and references therein) enters the southern Adriatic Sea during winter at the western Adriatic shelf (at a depth of ~200 m; Turchetto et al., 2007). Here it mixes with Adriatic Surface Water (ASW, Caroppo, et al., 2001). Bottom waters (consisting of Adriatic deep Water (ADW) in the Adriatic are formed in the northern Adriatic and southern Adriatic by surface water cooling due to cold outbreaks from the north (Bora winds) in winter as part of the thermohaline circulation in the Adriatic (e.g. Vilibić and Supić, 2005). Primary productivity is highest in winter/spring concomitant with an extended WAC, following intensive mixing of the water column by cold winds from the north (e.g. Socal et al., 1999; Boldrin et al., 2002; Sellschopp and Álvarez, 2003).

2.2 Core sampling and dating

The top layer (0-4 cm below sea floor (bsf)) of the core GeoB107-39 consists of light brownish green and bioturbated mud (Fig. 2a). From 4-30 cm bsf, fine laminations are observed in more greyish green mud. Within the laminated section still one distinct burrow is observed (23.5-25.5 cm bsf).

After recovery the multicore was stored at 4°C. Upon splitting of the core, one half was sampled at 3mm resolution. Samples were freeze-dried, homogenized in preparation for ICP-AES and determination of total organic carbon (TOC (%)). From the other half, overlapping aluminium trays of sediment were taken for resin embedding (Jilbert et al., 2008). The remaining sediment was then sampled at 5 mm resolution. These 5 mm resolution samples were freeze-dried and homogenized in preparation for ICP-AES analysis. From two samples from the second half (average depth of 7.25 and 16.25 cm bsf) a mixture of planktonic foraminifera were picked for accelerator mass spectrometry (AMS) ^{14}C dating at the AMS Radiocarbon Dating Laboratory at ETH Zurich. The ^{14}C-ages were calibrated with the program OxCal v3.10 (Bronk Ramsey, 2009) using the Marine04 calibration curve (Hughen et al., 2004) and application of a regional reservoir correction of 121 ± 60 yr (ΔR) in addition to the standard reservoir correction of 400 yr.

2.3 Elemental concentrations and isotope analysis

Discrete samples were freeze dried and powdered using an agate mortar. Major-minor elemental concentrations of the discrete samples were determined by Inductively Coupled Plasma-Atomic Emission Spectroscopy (ICP-AES, Perkin Optima 3000) at Utrecht University. For this purpose 125 mg of each sample was dissolved in 2.5 ml HF (40 %) and 2.5 mL pre-mixed acid of HNO_3 and $HClO_4$ (HNO_3 : $HClO_4$ = 2:3) and heated at 90˚C in a closed vessel for at least 8 hours. Next, they were evaporated at 160˚C until a gel formed. The gels were then dissolved in 25 ml 1 M HNO_3. Relative precision (<5 %) and accuracy were established by duplicates and in house standards (ISE-921).

To determine organic carbon content, 300 mg of each sample was first decalcified using 1 M HCl to remove inorganic carbon. The decalcified sample was dried at 60˚C and finely ground using an agate mortar. For the decalcified sediments the TOC content was determined on an elemental analyser (Fisons Instruments NCS NA 1500), using dry combustion at 1030˚C at Utrecht University. Calibration was achieved using, an ammonium sulphate standard (ASS), Acetanilide and Atropine, whereas precision and accuracy (≤0.1 ‰) were established using international and in house standards (Graphite quartzite NAXOS, GQ, and Rheenen).

2.4 Embedding and Microanalysis

The two sediment blocks recovered using aluminium trays were embedded in resin inside a nitrogen-filled glove box using the method described by Jilbert, et al., (2008). Each embedded block was cut into ±2 cm pieces and polished for further analysis. All embedded blocks were scanned by image scanner. Colour data (RGB) of these images were calculated with the 'DeCrack' routine in Matlab© developed by Zeeden et al. (2014). One block was selected (see Fig. 2a, b) for further analysis using μXRF analyser (EDAX Orbis) to map elements at a spatial resolution of 30 μm (Rh tube at 30 kV, 500 μA, no filter, 300 ms dwell time, 30 μm capillary beam) at Utrecht University. From the same blocks features of interest were further investigated (SEM) using back scatter.

Two laser traces (LA-ICP-MS) were acquired from all blocks using a Lambda Physik excimer laser system with Geolas 200 Q (λ193nm) and a Thermo Element 2 Sector Field at Utrecht University. Samples were mounted in a sealed ablation chamber, which was moved at a constant speed of while targeted with a laser beam (25 μm/s, Ø120 μm, repetition rate 20 Hz). Material was ablated under a He atmosphere, before being mixed with Argon and transported to the ICP-MS. Measuring SRM NIST 610 standard before and after each trace, raw counts of 27Al, 44Ca, 51V, 55Mn, 97Mo and 138Ba were converted to approximate elemental concentrations using the concentration data of Jochum et al. (2011). By comparing the measured isotopes and the known isotope composition of the standard ionisation factors (IF) are determined. Raw isotope data of the sediments are subsequently corrected for IF factor and background values. The corrected isotope data were converted to elemental concentrations using natural relative

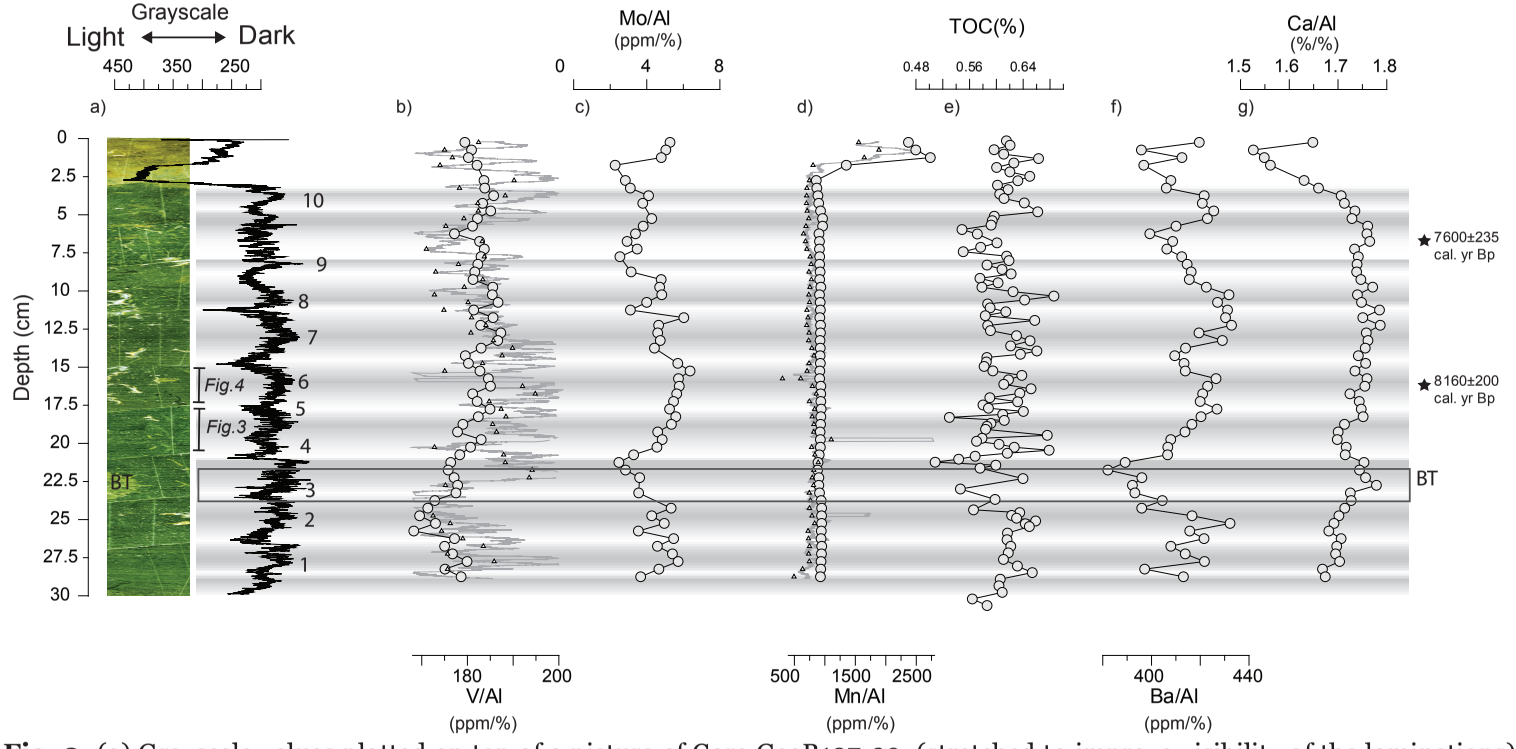

Fig. 2: (a) Grayscale values plotted on top of a picture of Core GeoB107-39 (stretched to improve visibility of the laminations) and (b) V/Al (c), Mo/Al, (d) Mn/Al, (e) TOC % (f) Ba/Al (ppm/ppm) and (g) Ca/Al. Grey circles are results from discrete samples , light grey line is the 200 point moving average of values retrieved from LA-ICP MS (when available), binned means of LA-ICP-MS are indicates with triangles. Grey background indicate intervals with darker sediments, black bordered box indicates bioturbated layer (BT), stars indicate the depth of the samples used for radiocarbon dating, black lines are the blocks used for further studying (see Fig. 3, 4), numbers indicated next to the grayscale are the darker interval regonised in both V/Al and the grayscale record.

isotopic abundance. Still, as relative changes in ablation efficiency affects concentrations between sections, runs and laminae, elements are as elemental ratios only. To avoid artefacts related to constant-sum constraints on concentrations (Weltje and Tjallingii et al., 2008) detailed LA-ICP-MS traces are presented as Log (element/ Al) ratios. For a better comparison with the elemental composition of the discrete samples, LA-ICP-MS data were binned for intervals equivalent to the interval sampled for the discrete samples using a Geometric mean (Fig. 2).

Not all isotopes analysed could be reliably transformed in elemental ratios. The low sedimentary Mo concentration, in combination with its many natural occurring isotopes did not allow quantification. The Ba concentrations calculated using ^{138}Ba counts from the LA-ICP-MS trace were significantly offset from the analyses based on discrete samples. This is in contrast with earlier studies using the exact same analytical setup and settings (Jilbert et al., 2010). We therefore suspect that this is somehow related to the sedimentary matrix and with no further constraints available for now refrained from including the Ba LA-ICP-MS data from further discussion.

3. Results and Discussion

3.1. Sedimentary history and sediment colour variability

The ^{14}C dating at 7.25 cm bsf (7600 ±235 cal. yr BP) and 16.25 cm bsf (8160±200 cal. yr BP) shows that the sediments from 7.25 cm bsf downwards correspond to Sapropel S1 and imply a sedimentation rate of 16 cm/kyr. Such high sedimentation rates are in line with other previously dated records from the south-western Adriatic Shelf (Zonneveld et al., 2009 and references therein). An abrupt transition from the darker, greenish laminated sapropel sediments to the overlying lighter sediments, without laminations is observed around 4 cm bsf (Fig. 2). This suggests a hiatus in the sedimentary record through either a stop in deposition between S1 and present, or the top of the sedimentary sequence has been removed. Several authors have suggested increased precipitation at the Northern borderlands during sapropel times (e.g. Zanchetta et al., 2007; Kotthoff, et al., 2008; Spötl et al., 2010). Hence, it seems plausible that the WAC was broader and transported more sediments southwards during sapropel times, causing the observed high sedimentation rates. During the period after sapropel formation erosion may have occurred due to strong bottom currents (e.g. Vigliotti et al., 2008; **chapter 3**). Irrespective of the process(es) involved the clear Mn peak at the top of the sapropel, with associated high Ba/Al and Mo/Al and the upper ^{14}C date indicate that the top of sapropel S1 was recovered (Reitz et al., 2006).

Within the sediments dated to be of sapropel S1 age, low grayscale values correspond to visibly darker layers in the impregnated blocks, while high values correspond to the lighter layers (Fig. 2,3), confirming the reliability of the routine developed by Zeeden et al. (2014). Over the 30 centimetre of the interval covered ~11 oscillations between

darker and lighter sediments (i.e. each interval being equivalent to ~200-300 yr) can be recognised (Fig. 2). Within these oscillations, fine laminae couplets each covering 1-5 mm can be observed (Fig. 3a, b). A sedimentation rate of 16.1 cm/kyr hence implies that the observed laminae couplets (dark to light) are equivalent to time intervals of 8 to 30 years.

3.2 Sediment geochemistry during S1: evidence for variable ventilation and productivity

The observed centennial, cm-scale variability between lighter and darker sediments broadly corresponds to variability seen in the discrete sample profiles of the redox sensitive elements V/Al and Mo/Al, although being at the limit of the resolution (Fig. 2). The V/Al record shows the same ~11 oscillations observed in the grayscale record. Elevated values of V/Al and Mo/Al point to more anoxic bottom-water conditions during the formation of the darker sediments (Tribovillard et al., 2006). Although some variability is observed in the TOC record changes are minor (less than 10% relatively) and do not show a clear correlation to the trace metal records. Concentration of the organic carbon stays high even after the sapropel, suggesting that other processes than local productivity controlled accumulation. In general, the patterns of sediment darkness, V/Al and Ba/Al show a good correspondence. Elevated Ba/Al values in sapropel S1 are related to an increase in export productivity due to the precipitation of barite in decaying organic matter (e.g. van Santvoort et al., 1997). In contrast, to the V/Al, Mo/Al, Ba/Al ratio and TOC (%), we observe no direct correspondence between the grayscale record and the Ca/Al ratio (Fig. 2). The ratio between calcium (related to biogenic formed carbonate from marine origin) and aluminium (related to clay input from terrestrial origin) has previously been used successfully as a proxy for runoff versus marine productivity in the study area (**chapter 3, 4**). The observed low variability in Ca/Al ratio suggests that high frequency variability in river runoff was minimal over the interval studied (Fig. 2). Overall the Ca/Al ratio shows a marked drop at the end of sapropel times, in contrast with the higher terrestrial sediment input inferred previously to explain the observed high sedimentation rates during sapropel times. This implies that the carbonate production during sapropel deposition played an important role in determining Ca/Al ratios. A simple model for the observed variability links deposition of the dark intervals with more intense bottom-water oxygen depletion related to enhanced export productivity, whereas the lighter layers represent more oxygenated, low export productivity conditions.

Millimetre scale variations in redox sensitive elements V and Mn can be studied by analysis of sediments with LA-ICP-MS (e.g. Jilbert et al., 2010b). Similar values and trends are observed for V/Al and Mn/Al found by traditional ICP-OES of discrete samples and the semi-continuous scanning using LA-ICP-MS of embedded blocks (Fig. 2). The binned geometric means of the LA-ICP-MS data show more scatter than the discrete samples. Although not as heterogeneous as in the vertical direction between light and dark intervals, we observe high lateral heterogeneity within the laminations on

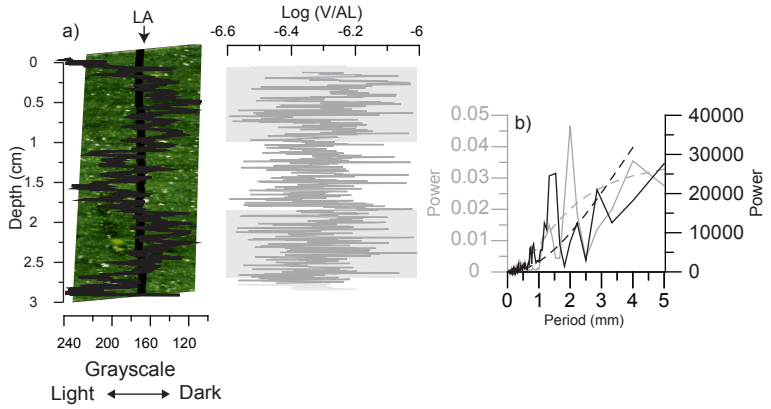

Fig 3: (a) Grayscale record of section of core GeoB107-39 (see Fig 2), and a 50 point moving average of V/Al as found with LA-ICP-MS from the same section. LA indicates the track analysed with LA-ICP-MS, grey bars indicate distinctive darker sediments (b) REDFIT analysis of the grayscale (black line) and V/Al (grey line) record as presented in (a) dotted lines indicate the 90% confidence interval.

the μXRF maps (Fig. 3c) as well. This implies that the LA-ICP-MS line scan, even when binned in the vertical direction, will contain more scatter than the discrete samples, which average both in the vertical and horizontal direction. Hence, we consider the LA-ICP-MS line scan to provide a realistic measure of down core variability with a much higher resolution, albeit including additional scatter from horizontal heterogeneity. Down core interpretation of these records, therefore, requires adequate statistical filtering.

To investigate whether also on millimetre scale (individual laminations) V/Al and the grayscale of the sediments are coupled we performed a REDFIT analysis (Schulz and Mudelsee, 2002). REDFIT analysis employs an advanced version of the simple Lomb periodogram, which accounts for red noise and, therefore, is particularly suited for the spectral analysis of climate records **(**Schulz and Mudelsee, 2002). The REDFIT analysis of the grayscale record as well as a 50 point moving average (combining 0.7mm) of the LA-ICP-MS V/Al record from a selected block (Fig. 3), reveals that both contain millimetre (and thus decadal scale) periodicities of ~1.25 mm and ~2.25 mm (Fig. 3b).

Enhanced oxygen depletion during deposition of the dark laminations is supported by μXRF mapping. Although iron and sulphur distributions are fairly homogeneous in the μXRF maps, the two darkest laminae in the interval analysed are notably enriched in both elements, with "hot spots" of the two elements overlapping. This strongly suggests the enhanced presence of Fe-sulphides within the dark layers, most likely pyrite (FeS_2; Fig. 3c). Under anoxic conditions, OM is degraded by bacterial sulphate reduction, producing bisulphite (HS^-) which reacts with dissolved iron to form pyrite (Berner, 1984).

Pyrite micro-texture in sapropels has been linked to conditions at the sediment-water

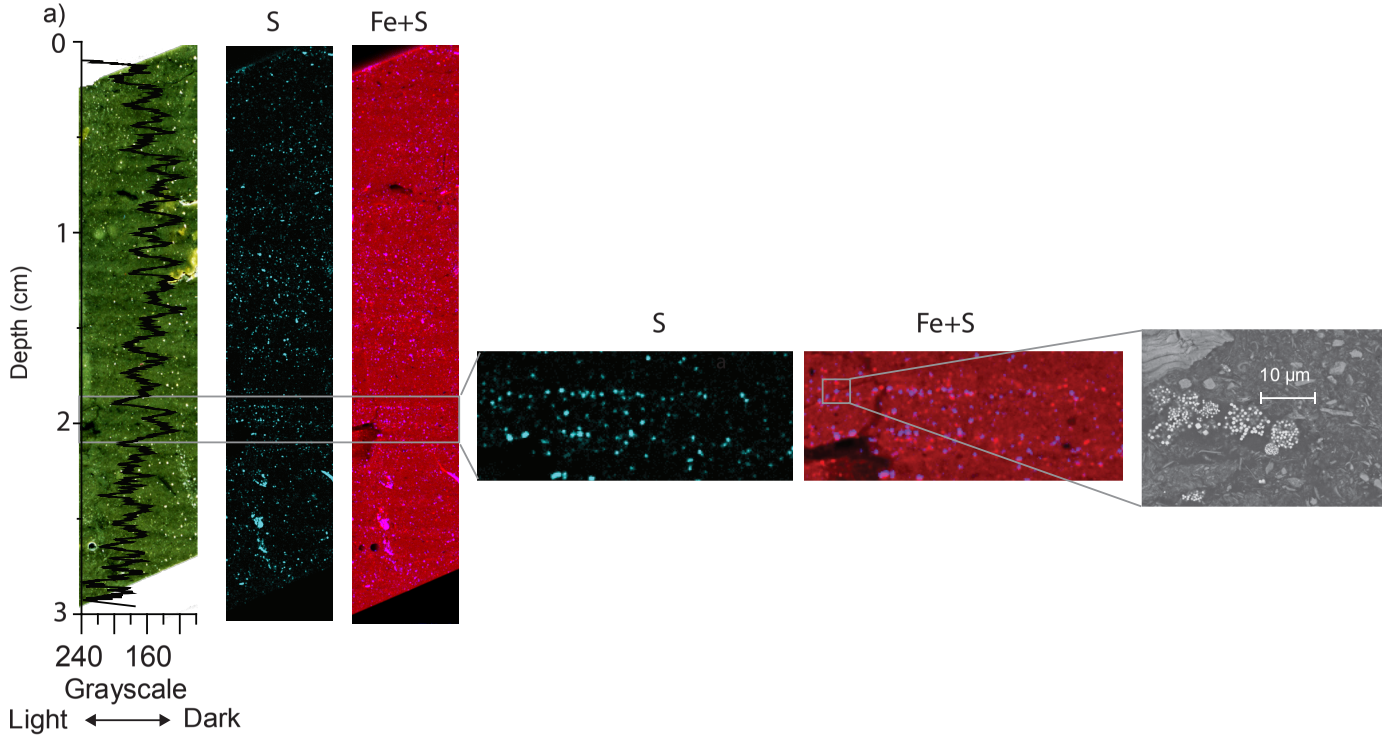

Fig. 4:(a) Grayscale record of a section from core GeoB107-39 (see Fig 2), and the results of µXRF from the same section for the elements S (Blue) and a combination of Fe and S (Pink= both Fe and S, only Fe= red) and (b) SEM (with backscatter) picture of framboidal pyrites as found in the dark layer with high Fe and S.

interface during sapropel formation (e.g. Passier et al., 1997, 1999). Passier et al. (1999) described two modes of pyrite formation in sapropels, which each lead to distinct crystal morphologies. Of these, framboidal pyrites derive from fast formation in the presence of plentiful sulphate, when sulphide production is similar to or higher than iron supply and liberation. A SEM image of the pyrites found in the dark laminae shows that these are small and have distinct framboidal shapes (Fig. 3d), indicating that they formed under anoxic bottom water conditions (Passier et al., 1997). The size distribution of the framboids has also been suggested to be indicative of the redox state of the overlying water column (Wilkin et al., 1996). The framboidal pyrites we observed appear to be smaller or around 5 μm in diameter (Fig. 3d), implying that the water column was at least partially anoxic and possibly euxinic during deposition of the dark laminae.

Our dark laminae, characterized by framboidal pyrite, resemble those found in older sapropels (e.g. sapropel S5) near Crete, which contain mat-forming diatoms (Kemp et al., 1998; Moller et al., 2012). Enhanced productivity, with diatoms being the dominant primary producers, has more often been suggested as an important factor during sapropel formation (Kemp et al., 1998; Kemp et al., 1999). However, high opal dissolution in the Mediterranean Sea presumably left most sapropels barren of diatom remains (Kemp et al., 1998; Kemp et al., 1999). Accordingly, the dark laminae in our sediments could be the remnants of such mat-forming diatom events, from which the opal frustules have since dissolved.

The coring site lies close to the critical water depth for sapropel formation during S1(Bianchi et al., 2006; Ni Fhlaithearta et al., 2010) and in a key area for deep water formation (Robinson et al., 1992; Roether et al., 1996), where sapropel formation is easily interrupted (Rohling et al.,1997). Vertical migration of the redoxcline related to variable ventilation rates could, therefore, have played an important role in the observed decadal interruptions of sapropel formation. The absence of local changes in detrital input, which would have accompanied variable freshwater inputs, and the relatively small-sized framboidal pyrites are in agreement with ventilation rather than productivity controlling the laminae. Consequently, the alternations between dark and light layers of 2-5 mm thickness indicate that the intensity of the redox conditions varied greatly on decadal time scales.

3.3 Climatic controls on ventilation and productivity variability during S1

Henceforth, the sediment grayscale profile is preferred over the geochemical data as a record of past ventilation and productivity conditions for two reasons. First, it is of higher resolution than the discrete-sample geochemical data. Second, in comparison to the LA-ICP-MS line-scan data, it integrates a higher number of laterally equivalent data points, increasing the signal to noise ratio of the vertical profile. Multi-decadal variability of water column anoxia during sapropel S1 has been shown to be similar to that observed in records of monsoon intensity and the strength of the Siberian high,

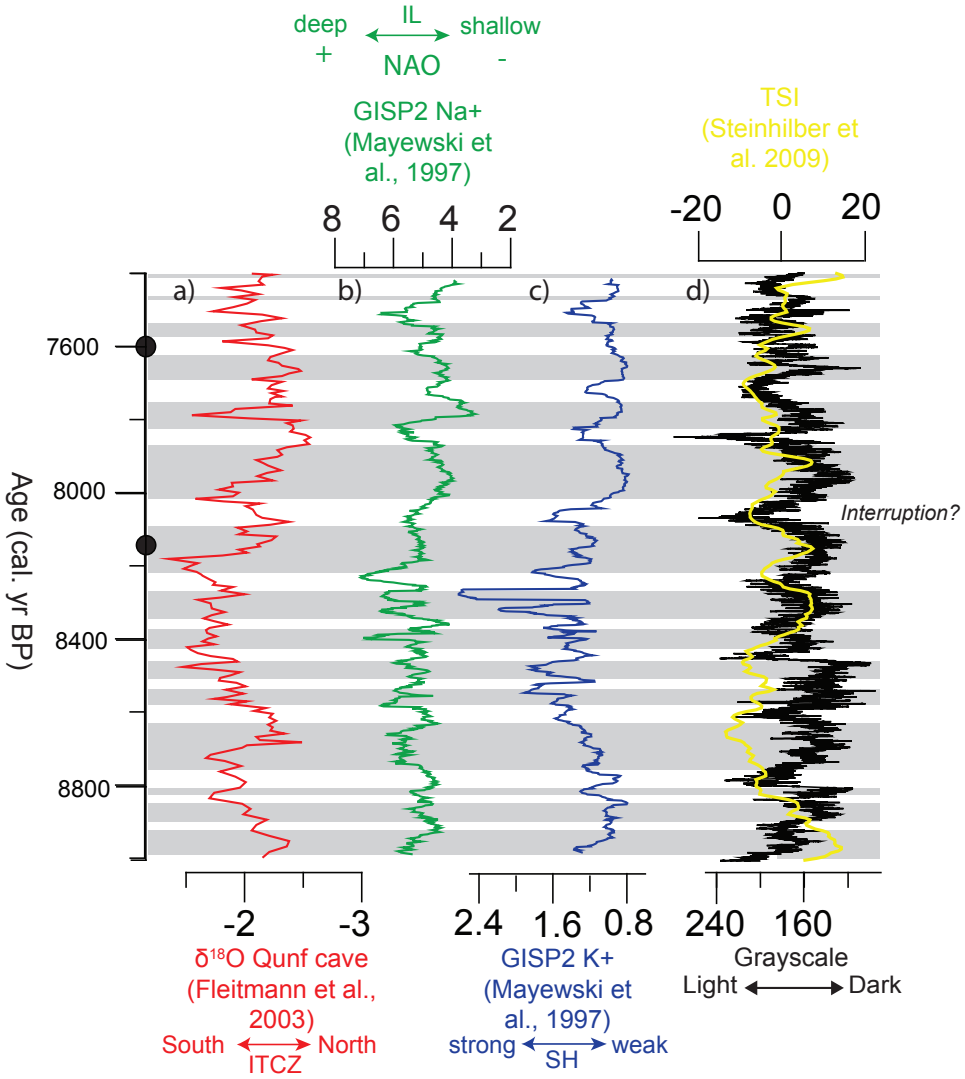

Fig. 5: (a) the $\delta^{18}O$ from the Qunf cave (Fleitmann et al., 2003), (b) GISP2 K+ and GISP2 Na+ ; (Mayewski et al., 1997), and (d) grayscale (this study) and (e) Total Solar Irradiance (TSI) based on Be isotopes (Steinhilber et al., 2009) , during the interval 7400-9000 cal. yr BP. Grey bars indicated periods with darker sediments, black circles indicate radio carbon dates. ITCZ is Inter Tropical Convergence Zone, IL = Icelandic Low, SH= Siberian high and NAO=North Atlantic Oscillation.

indicating that both high and low-latitude climate variability may force sapropel intensity (Jilbert et al., 2010b). In the following, we compare our data with contemporaneous climate records from the early Holocene of a comparably resolution (Mayewski et al., 1997, Fleitmann et al., 2003, section 3.3.1) using normal spectral analysis (REDFIT, section 3.3.2). Furthermore, to understand sub-decadal climate variability we compare our date with modern instrumental records of climatic indices with relevance to the Medi-

terranean region: the Siberian high Index SHI (D'Arrigo et al., 2005), the winter NAO Index (Hurell et al., 1995) and a Tropical Rainfall Index (Therrell et al., 2006), using an evolutionary power spectrum (EPS) approach (section 3.3.2).

3.3.1 Multi-centennial scale ventilation/productivity patterns

During the well–known interruption of sapropel S1, around 8 ka BP, linked to major winter cooling by increased Bora winds, one of the lightest sediments and lowest Ba/Al values are found (Fig. 2, 4). In line with this, two lighter coloured sediment intervals centred around 8550-8800 yr BP and 7700-7800 yr BP concord with small interruption events observed in sediments from the Aegean Sea (Kotthoff et al., 2008). However, the continued formation of laminations during the interruption event around 8 ka BP suggests that, although ventilation increased considerably, redox conditions still varied on decadal time scales during the interval. Low sediment rates and possibly a less sensitive position to decadal changes in the redox cline might have prevented such variance to be recorded in deeper cores in the Adriatic such as IN68-9 (Rohling et al., 1997; De Rijk et al., 1999) and AD91-7 (Giunta et al., 2003; Sangiorgi et al., 2003).

The 8.2 kyr event is linked to increased convective turnover by outbreaks of cold air from the north, the Bora. The GISP2-K^+ is proposed to reflect variability in the Siberian high (Mayewski et al. 1997). A strong Siberian high increases the chance for outbreaks of cold Bora winds. Between 7400 and 8300 yr BP lighter sediments are concomitant with increased K^+ in the GISP2 ice core, which is in line with observations for the interruption at 8.2 kyr. Furthermore, the grayscale record also reflects some of the variability observed in the Na+ in the GISP2 ice core (Fig. 4). The GISP2 Na+ reflects variability of the Icelandic low and, therefore, partly reflects changes in NAO. Both intensity of the Siberian high and NAO are heavily correlated phenomena, making it is difficult to distinguish between both (Thompson and Wallace, 2001; Rimbu et al., 2003). Cold outbreaks to the Mediterranean are consistent with a more positive NAO mode and thus dry conditions in the Mediterranean. Darker sediments are coherent with a weak Icelandic low, as reflected by the GISP2 Na+ record. Increased moisture transport, resulting in increased discharge and thus nutrient input could have increased PP, enhancing oxygen depletion in the water column. However, as changes in Ca/Al do not vary much on these time scales, we consider the effect of changes in river discharge as minor. In contrast, no obvious correlation is found with the isotope record from Qunf cave (Fleitmann et al., 2003), which mainly reflects variability of the Indian Monsoon/ITCZ (Fig. 4).

The good correspondence between the GISP2 K^+ record and our grayscale record between 7300 and 8300 yr BP is remarkable considering the possible error associated with the age models of both records. However, the coherence observed between the GISP2 K+ record and the grayscale record breaks down between 8300 and 9000 yr BP (Fig. 4). First of all, the GISP2 K+, as well as the GISP2 Na+ records, suggest a multi-centennial interval characterized by a strong SH and deep IL from 8100-8700 yr BP, which is not reflected by the grayscale record. Export productivity and water column

oxygenation possibly became less sensitive to climate variability during fully developed sapropel conditions (Jilbert et al., 2010b). Furthermore, in the older part of our record, the age model is less constraint, which could also obscure a potential link. Because the Ca/Al values in this part of the record are relatively low (Fig. 2 slightly higher detrital fluxes may have offset the age model. Nonetheless, the GISP2 K^+ record, as well as the grayscale record, continue to display shorter time scale variability during the interval. The observed variance in both records, in contrast to the absence of similar variability in the Qunf cave record, suggests that also during this interval, SH and redox cline in the Adriatic Sea were coupled.

The correspondence between the GISP2 K^+ and sediment grayscale records suggests that variability in winter mixing by surface water-cooling controlled water column redox conditions on a centennial scale. This is in line with previous studies, which linked interruptions of bottom water anoxia during sapropel S1 formation to cold outbreaks (e.g. Rohling, et al., 1997; De Rijk, et al., 1999; Marino et al., 2009). Episodes characterized by low concentrations of redox sensitive elements in a core from the central Ionian Sea are coherent with the record shown here (Jilbert et al., 2010b). Hence centennial scale cold events probably affected water column conditions beyond the Adriatic Sea. In theory, similar processes might also affect water column conditions on (multi)decadal time scales (Myers and Rohling, 2000) and be responsible for the observed laminations themselves. 3.3.2 (Multi-decadal) scale ventilation/productivity forcing

REDFIT analysis of the grayscale record from S1 reveals dominant periods of ~200, 70, 50, 14, 11 and 8-10 years (Fig. 5a). Periods of 200, 70 and 50 yr are also found in high resolution records of Sapropel S1 near the Cretan Ridge and the central Ionian Sea (Gennari et al., 2009; Jilbert et al., 2010b) and variability within these sediments may therefore relate to similar processes. Because the non-sea salt K^+ GISP 2 record shows similar periodicities (200, 50, 14, 12, 10 and 8 years), outbreaks of cold air from the north are most likely responsible for changes in deep water formation on these time scales (Fig. 5b).

The strong 70 yr cycle appearing in the grayscale record is, however, missing from the non-sea salt K^+ GISP2 record as well from in the non-sea salt Na^+ record (Fig. 5a-e). Although a 67 year cycle found in the Qunf Cave $\delta^{18}O$ (Fig. 5e) suggests a possible tropical monsoonal origin for this cycle in the Adriatic, other multi-decadal cycles found at Qunf cave (100 and 33 yr) are absent from the grayscale record (Fig. 5a-e). The 70 yr cycle is known as a typical periodicity of the Atlantic multi-decadal oscillation (AMO; e.g. Knight, et al., 2006). The AMO affects Sahel drought, but is also linked to climate

Next page **Fig. 6:** REDFIT analysis of (a) grayscale and (b) the grayscale (red) in comparison with GISP2 K+ and (c) Na+(Mayewski et al., 1997) , (d) $\delta^{18}O$ from the Qunf cave (Fleitmann et al., 2003) and (e) Total Solar Irradiance (Steinhilber et al., 2009) for the interval 7400- 9000 cal. yr BP, dotted line represents the 80% confidence interval. Evolutionary power spectrum of the (f) grayscale record;(g) Siberian high Index (SHI) (D'Arrigo et al., 2005); (h) NAO (Hurrell, 1995); (i) Tropical African rainfall (TAR) in Zimbabwe (Therrell et al., 2006) and (j) the sunspot cycle (Van der Linden et al, 2000).

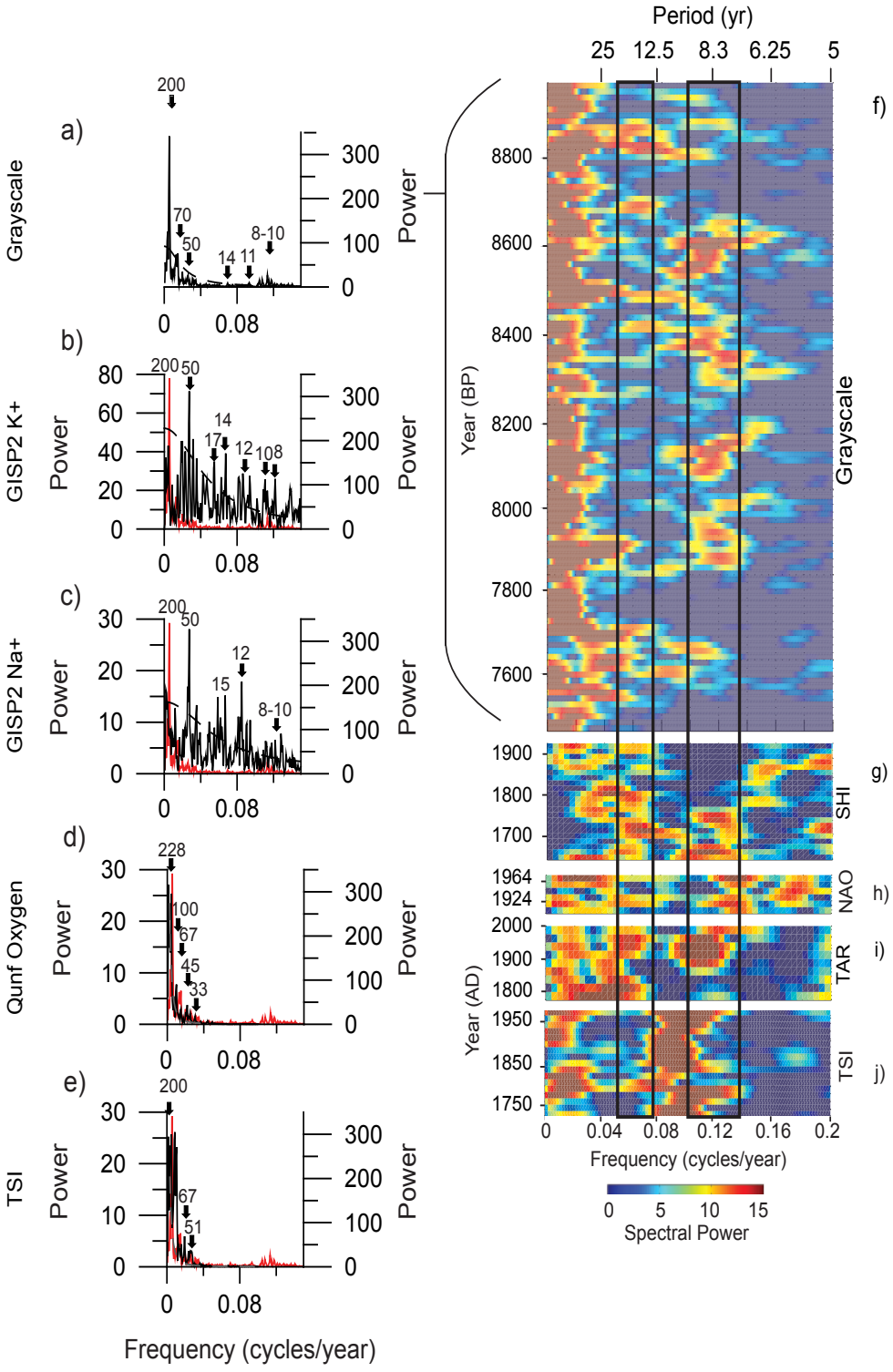
a)
Grayscale
200
70
50
14
11
8-10
Power
b)
GISP2 K+
200
50
14
17
12
10
8
c)
GISP2 Na+
200
50
12
15
8-10
d)
Qunf Oxygen
228
100
67
45
33
e)
TSI
200
67
51
Frequency (cycles/year)
Period (yr)
25
12.5
8.3
6.25
5
f)
Year (BP)
Grayscale
g)
SHI
h)
NAO
i)
TAR
Year (AD)
j)
TSI
Frequency (cycles/year)
Spectral Power

phenomena at higher latitudes (e.g. Knight, et al., 2006; Shanahan et al., 2009). Knudsen et al. (2011) suggested that during the Holocene thermal maximum, when sapropel S1 was deposited, the AMO was more pronounced in climate records from higher latitudes (such as the GISP2 oxygen isotope record) than in records from lower latitudes. Hence, the observed 70 yr cyclicity could also be linked to higher latitude climate, although not observed in the GISP 2 Ion (K^+ and Na^+) records.

The resolution of the Qunf Cave $\delta^{18}O$ record is too low to resolve the highest frequency cycles (8-10 yr; Fleitmann et al., 2003). Therefore we compare the patterns of the highest frequency cycles with reconstructions of the SH, NAO and ITCZ based on instrumental data. Frequencies vary over time, and patterns show shifts between dominant frequencies, which are characteristic for certain climate phenomena. For example, the sunspot cycle shows a stationary periodicity of 11 years, whereas periodicities of the NAO range from ~~5-10 years, showing non-stationarity. This different behaviour in cyclicity over time is clearly visible when applying an EPS.

The EPS of the grayscale record indicates dominant periodicities of 8-10 years and less dominant periodicities between 12.5 and 25 yr (Fig. 5f). Similar periodicities are found in the EPS of reconstructions of the SHI (D'Arrigo et al., 2005), the NAOm (Hurrell, 1995) and TAR (Therrell et al., 2006; Fig. 5f-j). The EPS of the TAR record suggests that the decadal variability of the ITCZ is stationary and constant. Such a clear periodicity was also observed in a historical record of river Nile outflow before construction of the Aswan dam (Cobb, 1978). This record was, however, of an insufficient length (<100 yrs.) for an EPS analysis. In contrast to the ITCZ records, our grayscale record, SHI, and the NAOm show far less stable and continuous periodicities. Moreover similar shifts in dominant cycles are observed in the SHI and the grayscale records EPSs: when the 8-10 yr cycle is absent, a more pronounced 12.5-25 yr periodicity appears. Hence, our grayscale record and SH variability are similar on decadal to centennial time scales. Therefore, we suggest that ventilation events on decadal time scales are caused by outbreaks of cold air, enhancing deep convective turnover.

3.3.3 The impact of variance of Total solar irradiance

TSI has been suggested as a possible forcing mechanism for centennial time scale variability in ventilation and export productivity during sapropel formation (Jilbert, et al., 2010b). Furthermore, a $CaCO_3$ record from the nearby Gulf of Taranto suggests that climate and related oceanographic changes in the study area are controlled by TSI on decadal time scales (Cini Castagnoli et al., 1992a, b). Changes in TSI have also been invoked to explain changes in river Nile outflow (Hennekam et al., 2014) on centennial time scales. Intervals of strong solar activity supposedly correspond to periods of high tropical precipitation, enhancing Nile discharge (Hennekam et al., 2014). Also a weakened NAO/AO, which in turn may be correlated to the SH, and a weakened SH itself, have been related to high TSI (e.g. Bond et al., 2001; Meeker and Mayewski, 2002; Mann et al., 2009; Trouet et al., 2009). Therefore, we compared the grayscale record with a TSI reconstruction during sapropel S1 times and recent sunspot cycle observations (Van der

Linden et al., 2000; Steinhilber et al., 2009).

Patterns in the TSI reconstructions are concordant with patterns in the grayscale record between 8600-7600 (Fig. 4): relatively dark sediments correspond to high TSI. Furthermore, multi-decadal to centennial scale perturbations (200, 67 and 50 yr) found in the grayscale record are also observed in the TSI reconstruction from the same interval (Fig. 5). In contrast, variations on a decadal scale show a less stationary pattern compared to the Sunspot cycle record from the last 300 years (Fig. 3b, e). In addition, the sunspot cycle exhibits slightly lower frequencies, with a mean periodicity of 11 year, in addition to longer term periodicities (>25 years, Fig 5). On these time scales the SH may be linked to other climate phenomena, such as ENSO (D'arrigo et al, 2005). Hence decadal variability is probably not directly related to solar variability, but variability in ventilation during sapropel formation is similar to solar variability on multi-decadal to a centennial time scales.

Conclusions

A laminated sapropel of S1 age has been studied, showing framboidal shaped pyrites within the dark layers. These dark layers are also characterized by increased concentrations of redox sensitive elements (V and Mo). Hence, during the formation of these dark layers more oxygen depleted conditions prevailed compared to the lighter layers. Based on the age model it appears that each set of laminae (from dark to light) covers 8-10 years. Hence, ventilation in the Adriatic Sea varied on decadal time scales. Besides this decadal variability, centennial and multi-decadal scale variability is reconstructed. Coherency in frequencies and patterns between the sapropel record and a reconstruction of the Siberian high suggests that these ventilation events are related to convective surface water turnover by cold northerly winds.

Acknowledgments

At Utrecht University we thank Arnold van Dijk, Tilly Bouten, Helen de Waard and Dineke van der Meent for lab assistance with ICP-AES, TOC, LA-ICP-MS, SEM and μXRF analysis. Sample material has been provided by the GeoB Core Repository at the MARUM- Center for Marine Environmental Sciences, University of Bremen, Germany. Authors are grateful to Captain, Crew and Colleagues with RV Poseidon CAPPUCCIONO-cruise (July, 2006) coordinated by Karin Zonneveld. We thank Karin Zonneveld for providing us with the studied core. This contribution is part of the MOCCHA project, supported by the European Science Foundation (ESF-EuroMarc) with associated financial support from the Netherlands Organization for Scientific Research (NWO-Project .817.01.002). In addition, we acknowledge financial, technical, and logistic support given by NIOZ/NWO for DOPPIO and MACCHIATO cruises

and the DFG for CAPPUCCINO cruise.

References

Abu-Zied, R. H., Rohling, E. J., Jorissen, F. J., Fontanier, C., Casford, J. S., and Cooke, S., 2008. Benthic foraminiferal response to changes in bottom-water oxygenation and organic carbon flux in the eastern Mediterranean during LGM to Recent times. *Marine Micropaleontology 67*(1), 46-68.

Allen, J. R. M., Watts, W. A., McGee, E., and Huntley, B., 2002. Holocene environmental variability-the record from Lago Grande di Monticchio, Italy. *Quaternary International* 88(1), 69-80.

Alley, R.B., 2007. Wally was right: Predictive ability of the North Atlantic "conveyor belt" hypothesis for abrupt climate change. *Annual Review of Earth Planetery Science 35*, 241-272.

Alpert, P., Baldi, M., Ilani, R., Krichak, S., Price, C., Rodó, X., Saaroni, H., Ziv, B., Kishcha, P., Barkan, J., Mariotti, A., and Xoplaki, E., 2006. Chapter 2: Relations between climate variability in the Mediterranean region and the tropics: ENSO, South Asian and African monsoons, hurricanes and Saharan dust, in: P. Lionello, P.M.-R., Boscolo, R. (Eds.), Developments in Earth and Environmental Sciences. Elsevier, 149-177.

Amorosi, A., Centineo, M. C., Dinelli, E., Lucchini, F., and Tateo, F., 2002. Geochemical and mineralogical variations as indicators of provenance changes in Late Quaternary deposits of SE Po Plain. *Sedimentary Geology* 151 (3–4), 273-292.

Anand, P., Elderfield, H., and Conte, M. H., 2003. Calibration of Mg/Ca thermometry in planktonic foraminifera from a sediment trap time series. *Paleoceanography 18*(2).

Artegiani, A., Paschini, E., Russo, A., Bregant, D., Raicich, F., and Pinardi, N., 1997. The Adriatic Sea general circulation. Part I: Atmospheric Sea Interactions and Water Mass Structure. *Journal of Physical Oceanography* 27 (8), 1492-1514.

Bárcena, M.A., Flores, J.A., Sierro, F.J., Pérez-Folgado, M., Fabres, J., Calafat, A. and Canals, M.., 2004. Planktonic response to main oceanographic changes in the Alboran sea (western Mediterranean) as documented in sediment traps and surface sediments. *Marine Micropaleontology* 53 (3) 423-45.

Bard, E., and Frank, M., 2006. Climate change and solar variability: What's new under the sun? *Earth and Planetary Science Letters 248*(1), 1-14.

Bard, E., Hamelin, B., and Delanghe-Sabatier, D., 2010. Deglacial meltwater pulse 1B and Younger Dryas sea levels revisited with boreholes at Tahiti. *Science*, *327*(5970), 1235-1237.

Bar-Matthews and M., Ayalon, A., 2011. Mid-Holocene climate variations revealed by high-resolution speleothem records from Soreq Cave, Israel and their correlation with cultural changes. *The Holocene* 21, 163-171.

Berner, R.A., 1989. Biogeochemical cycles of carbon and sulfur and their effect on atmospheric oxygen over phanerozoic time. *Palaeogeography, Palaeoclimatology, Palaeoecology* 75, 97-122.

Bianchi, D., Zavatarelli, M., Pinardi, N., Capozzi, R., Capotondi, L., Corselli, C., and Masina, S. 2006. Simulations of ecosystem response during the sapropel S1 deposition event. *Palaeogeography, Palaeoclimatology, Palaeoecology* 235(1), 265-287.

Bignami, F., Sciarra, R., Carniel, S., and Santoleri, R., 2007. Variability of Adriatic Sea coastal turbid waters from SeaWiFS imagery. *Journal of Geophysical Research* 112, C03S10.

Bjerknes, Jf., 1964.. Atlantic air-sea interaction. *Advances in Geophysics* 10 (1), 1-82.

Boer, W., Van den Bergh, G. D., De Haas, H., De Stigter, H. C., Gieles, R., and Van Weering, T. C., 2006. Validation of accumulation rates in Teluk Banten (Indonesia) from commonly applied ^{210}Pb models, using the 1883 Krakatau tephra as time marker. *Marine Geology*, *227*(3), 263-277.

Boldrin, A., Miserocchi, S., Rabitti, S., Turchetto, M. M. , Balboni, V. and Socal, G. , 2002. Particulate matter in the Southern Adriatic and Ionian Sea: Characterisation and Downward Fluxes. *Journal of Marine Systems* 33-34, 89-410.

Bonatti, E., and Gartner, S., 1973. Caribbean climate during Pleistocene ice ages. *Nature* 244, 563-565.

Bond, G., Kromer, B., Beer, J., Muscheler, R., Evans, M.N., Showers, W., Hoffmann, S., Lotti-Bond, R., R., Hajdas I. and Bonani, G., 2001. Persistent Solar Influence on North Atlantic Climate during the Holocene, *Science* 294 (5549), 2130-2136.

Bordon, A., Peyron, O., Lézine, A. M., Brewer, S., and Fouache, E., 2009. Pollen-inferred Late-Glacial and Holocene climate in southern Balkans (lake Maliq). *Quaternary International*, 200(1), 19-30.

Bosmans, J. H. C., Drijfhout, S. S., Tuenter, E., Lourens, L. J., Hilgen, F. J., and Weber, S. L., 2011. Monsoonal response to Mid-Holocene orbital forcing in a high resolution GCM. *Climate of the Past Discussions*, *7*(5), 3609-3652.

Bottema, S., 1995. The Younger Dryas in the Eastern Mediterranean. *Quaternary Science Reviews*, *14*(9), 883-891.

Boyle, E.A. and Keigwin, L.D., 1985. Comparison of Atlantic and Pacific paleochemical records for the last 215,000 years: changes in deep ocean circulation and chemical inventories, *Earth and Planetary Science Letters,* 76 (1-2), 135-150.

Brandimarte, L., Di Baldassarre, G., Bruni, G., D'Odorico, P. and Montanari. A., 2011. Relation between the North-Atlantic Oscillation and hydroclimatic conditions in Mediterranean areas. *Water Resources Management* 25 (5), 1269-79.

Broecker, W. S., Andree, M., Wolfli, W., Oeschger, H., Bonani, G., Kennett, J., and Peteet, D., 1988. The chronology of the Last Deglaciation: Implications to the cause of the Younger Dryas event. *Paleoceanography*, *3*(1), 1-19.

Broecker, W. S., Denton, G. H., Edwards, R. L., Cheng, H., Alley, R. B., and Putnam, A.E., 2010. Putting the Younger Dryas cold event into context. *Quaternary Science Reviews*, *29*(9), 1078-1081.

Bronk Ramsey, C., Higham, T.F.G., Brock, F., Baker, D., and Ditchfield, P., 2009. Radiocarbon dates from the Oxford AMS System: Archaeometry Datelist 33. *Archaeometry* 51, 323-349.

Buccolieri, A., Buccolieri, G., Cardellicchio, N., Dell'Atti, A., Di Leo, A. And Maci, A., 2005. Distribution and speciation of metals in surface sediments of Taranto Gulf (Ionian Sea, Southern Italy). *Annali Di Chimica* 95 (1-2), 115-115.

Buccolieri, A., Buccolieri, G., Cardellicchio, N., Dell'Atti, A. , Di Leo, A. and Maci, A., 2006. Heavy metals in marine sediments of Taranto Gulf (Ionian Sea, Southern Italy). *Marine Chemistry* 99 (1-4), 227-235.

Büntgen, U., Tegel, W., Nicolussi, K., McCormick, M., Frank, D., Trouet, V., Kaplan, J.O,. Herzig, K.U. Heussner, F. and Wanner, H., 2011. 2500 years of European climate variability and human susceptibility, *Science* 331 (6017), 578-582.

Caloiero, T., Coscarelli, R., Ferrari, E., and Mancini, M., 2011. Trend detection of annual and seasonal rainfall in Calabria (Southern Italy), *International Journal of Climatology* 31(1), 44-56.

Calvert, S., 1983. Geochemistry of Pleistocene sapropels and associated sediments from the EasternMediterranean. *Oceanologica Acta* 6(3), 255-267.

Calvert, S.E. and Pedersen, T. F., 1993. Geochemistry of recent oxic and anoxic marine sediments: implications for the geological record. *Marine Geology* 113(1), 67-88.

Caron, B., Siani, G., Sulpizio, R., Zanchetta, G., Paterne, M., Santacroce, R., Tema, E., and Zanella, E., 2012. Late Pleistocene to Holocene tephrostratigraphic record from the Northern Ionian Sea. *Marine Geology 311*, 41-51.

Caroppo, C., R. Congestri and M. Bruno, 2001. Dynamics of dinophysis sensu lato species (Dinophyceae) in a coastal Mediterranean environment (Adriatic Sea*). Continental Shelf Research* 21(16), 1839-1854.

Carpenter, R. 1966, Discontinuity in Greek Civilization, Cambridge, Cambridge University Press

Casford, J., E. Rohling, R. Abu-Zied, C Fontanier, F.J Jorissen, M.J Leng, G Schmiedl, and J Thomson, 2003.A dynamic concept for eastern Mediterranean circulation and oxygenation during sapropel formation. *Palaeogeography, Palaeoclimatology, Palaeoecology* 190, 103-119.

Cattaneo, A, Correggiari, A., Langone, L., Trincardi, F., 2003. The Late-Holocene Gargano subaqueous delta, Adriatic Shelf: sediment pathways and supply fluctuations. *Marine Geology* 193 (1-2), 61-91.

Cayan, D. R., 1992. Latent and sensible heat flux anomalies over the northern oceans: Driving the sea surface temperature. *Journal of Physical Oceanography*, *22*(8), 859-881.

Chen, L., Zonneveld, K.A.F. and Versteegh, G.J.M., 2011. Short term climate variability during "Roman classical period" in the eastern Mediterranean. *Quaternary Science Reviews* 30, 3880-91.

Chen, L. Zonneveld, K. A. F. and Versteegh, G. J. M., 2013. Paleoclimate of the Southern Adriatic Sea region during the 'Medieval Climate Anomaly' reflected by organic walled dinoflagellate cysts. *The Holocene* 23 (5), 645-655.

Cini Castagnoli, G., Bonino, G., Caprioglio, F., Provenzale, A., Serio, M. Guang, and Zhu Mei, 1990. The carbonate profile of two recent Ionian sea cores: Evidence that the sedimentation rate is constant over the last millennia. *Geophysical Research Letters* 17(11), 1937-1940.

Cini Castagnoli, G., Bonino, G., Serio, M., and Callegari, E., 1992a. The $CaCO_3$ profiles of deep and shallow Mediterrenean Sea cores as indicators of past Solar- Terrestrial relationships. *Nuovo Cimento Soc.Ital.Fis.C.* 15 (5), 547-16.

Cini Castagnoli, G., Bonino, G., and Serio, M., 1992b. Common Spectral Features in the 5500-Year record of total carbonate in sea sediments and radiocarbon in tree rings. *Radiocarbon* 34, 798-805.

Cini Castagnoli, G., Bernasconi, S.M., Bonino, G., Della Monica, P. and Taricco, C., 1999. 700 year record of the 11 year solar cycle by planktonic foraminifera of a shallow water Mediterranean core. *Helioseismology and Solar Variability* 24, 233-236.

Civitarese, G., Gačić, M., Vetrano, A., Boldrin, A., Bregant, D., Rabitti, S., and Souvermezoglou, E., 1998. Biogeochemical fluxes through the Strait of Otranto (Eastern Mediterranean). *Continental Shelf Research* 18 (7), 773-789.

Cobb, G. W., 1978. The problem of the Nile: conditional solution to a changepoint problem. B*iometrika*, *65*(2), 243-251.

Cocco, E., 1976. Italian North Ionian Coast - Tendency Towards Erosion. *Marine Geology* 21, 49-57.

Collins, R. P. and Jones, M. B., 1985. The influence of climatic factors on the distribution of C4 species in Europe. *Plant Ecology* 64, 121-129

Correggiari, A., Guerzoni, S., Lenaz, R., Quarantotto, G., and Rampazzo, G., 1989. Dust deposition in the central Mediterranean (Tyrrhenian and Adriatic Seas): Relationships with marine sediments and riverine input. *Terra Nova* 1, 549-558.

Correggiari, A., Field, M. E., and Trincardi, F., 1996. Late Quaternary transgressive large dunes on the sediment-starved Adriatic Shelf. Geological Society, London, Special Publications 117 (1), 155-169.

Combourieu-Nebout, N., Paterne, M., Turon, J. L., and Siani, G., 1998. A high-resolution record of the last deglaciation in the central Mediterranean Sea: Palaeovegetation and palaeohydrological evolution. *Quaternary Science Reviews* 17(4-5), 303-317.

Croudace, I.W., Rindby, A., Rothwell, R.G., 2006. ITRAX: description and evaluation of a new multi-function X-ray core scanner. Geological Society, London, Special Publications 267, 51-63.

Crusius, J., and J. Thomson, 2003. Mobility of authigenic rhenium, silver, and selenium during postdepositional oxidation in marine sediments. *Geochimica et Cosmochimica Acta* 67 (2), 265-273.

Daly, A. W., 1978. The response of North Atlantic sea surface temperature to atmospheric forcing processes. *Quarterly Journal of the Royal Meteorological Society 104*(440), 363-382.

Darby, D. A., Ortiz, J. D., Grosch, C. E. and Lund, S.P., 2012. 1,500-year cycle in the arctic oscillation identified in Holocene arctic sea-ice drift. *Nature Geoscience* 5(12), 897-900

D'Arrigo, R., Jacoby, G., Wilson, R., and Panagiotopoulos, F., 2005. A reconstructed Siberian high index since AD 1599 from Eurasian and north American tree rings. *Geophysical Research Letters* 32(5)

De Lange G.J., 1992. Distribution of exchangeable, fixed, organic and total Nitrogen in interbedded turbiditic/pelagic sediments of the Madeira Abyssal Plain, eastern North Atlantic. *Marine. Geology* 109, 95-114

De Lange, G. J., Van Santvoort, P. J. M. , Langereis, C., Thomson, C. J., Corselli, C., Michard, A., Rossignol-Strick, M., Paterne, M., and Anastasakis, G., 1999. Palaeo-Environmental variations in Eastern Mediterranean Sediments: A Multidisciplinary Approach in a Prehistoric Setting. *Progress in Oceanography* 44 (1-3), 369-386.

De Lange, G.J., Thomson, J., Reitz, A., Slomp, C.P., Speranza Principato, M., Erba, E. and Corselli, C., 2008. Synchronous basin-wide formation and redox-controlled preservation of a Mediterranean sapropel. *Nature Geoscience* 1, 606-610.

De Lange, G.J.a.c.p., 2009. MACCHIATO cruise with R.V. PELAGIA to the Eastern Mediterranean.

De Lazzari, A., Rampazzo, G., Pavoni, B., 2004. Geochemistry of sediments in the Northern and Central Adriatic Sea. *Estuarine, Coastal and Shelf Science* 59 (3), 429-440.

De Rijk, S., Hayes, A. and Rohling, E.J., 1999. Eastern Mediterranean sapropel S1 interruption: An expression of the onset of climatic deterioration around 7 ka BP. *Marine Geology* 153(1–4), 337-343.

DeMenocal, P., Ortiz, J., Guilderson, T., Adkins, J., Sarnthein, M., Baker, L., and Yarusinsky, M., 2000. Abrupt onset and termination of the African Humid Period: rapid climate responses to gradual insolation forcing. *Quaternary Science Reviews* 19(1), 347-361.

DeMenocal, P., Ortiz, J., Guilderson, T., and Sarnthein, M., 2000. Coherent High- and Low-Latitude Climate Variability During the Holocene Warm Period. *Science* 288, 2198-2202.

Denton, G. H., Alley, R.B., Comer, G.C. and Broecker, W.S., 2005. The role of seasonality in abrupt climate change. *Quaternary Science Reviews* 24 (10), 1159-82.

Denton, G. H., Karlén, W., 1973. Holocene climatic variations-their pattern and possible cause. *Quaternary Research*, *3*(2), 155-205.

Dermody, BJ, de Boer, H.J., Bierkens, M.F.P., Weber, S.L.,Wassen, M.J. And Dekker, S.C., 2012. A seesaw in Mediterranean precipitation during the roman period linked to millennial-scale changes in the north atlantic. *Climate of the Past* 8 (2), 637-51.

Desprat, S., Sánchez Goñi, M.F. and Loutre, M.F., 2003. Revealing climatic variability of the last three millennia in northwestern Iberia using pollen influx data. *Earth and Planetary Science Letters* 213 (1), 63-78.

Deuser, W. G., 1987. Seasonal variations in isotopic composition and deep-water fluxes of the tests of perennially abundant planktonic foraminifera of the Sargasso Sea; results from sediment-trap collections and their paleoceanographic significance. *The Journal of Foraminiferal Research 17*(1), 14-27.

Di Rita, F., and Magri, D., 2009. Holocene drought, deforestation and evergreen vegetation development in the Central Mediterranean: A 5500 year record from Lago Alimini Piccolo, Apulia, southeast Italy. *The Holocene* 19 (2), 295-306.

Diaz, H. F., Hoerling, M. P., and Eischeid, J. K., 2001. ENSO variability, teleconnections and climate change. *International Journal of Climatology 21*(15), 1845-1862.

Dinelli, E., Tateo, F., and Summa, V., 2007. Geochemical and mineralogical proxies for grain size in mudstones and siltstones from the Pleistocene and Holocene of the Po River Alluvial Plain, Italy. Geological Society of America Special Papers 420, 25-36.

Dissard, D., Nehrke, G., Reichart G.J.and Bijma, J., 2010a. Impact of seawater pCO_2 on calcification and Mg/Ca and Sr/Ca ratios in benthic foraminifera calcite: results from culturing experiments with *Ammonia tepida*. *Biogeosciences* 7, 81-93.

Dissard, D., Nehrke, G., Reichart, G. J., and Bijma, J., 2010b. The impact of salinity on the Mg/Ca and Sr/Ca ratio in the benthic foraminifera *Ammonia tepida*: Results from culture experiments. *Geochimica et Cosmochimica Acta 74*(3), 928-940.

Diz, P., Barras, C., Geslin, E., Reichart, G. J., Metzger, E., Jorissen, F., and Bijma, J., 2012. Incorporation of Mg and Sr and oxygen and carbon stable isotope fractionation in cultured *Ammonia tepida*. *Marine Micropaleontology* 92, 16-28.

Dolenec, T., Faganeli, J., and Pirc, S., 1998. Major, minor and trace elements in surficial sediments from the open Adriatic Sea: A regional geochemical study. *Geol. Craotia* 51(1), 59–73

Dormoy, I., Peyron, O., Combourieu Nebout, N., Goring, S., Kotthoff, U., Magny, M., and Pross, J., 2009. Terrestrial climate variability and seasonality changes in the Mediterranean region between 15000 and 4000 years BP deduced from marine pollen records. *Climate of the Past* 5(4), 615-632.

Dudley, W.C., Blackwelder, P., Brand, L., and Duplessy, J.C., 1986. Stable isotopic composition of coccoliths. *Marine Micropaleontology* 10(1), 1-8.

Dueñas-Bohórquez, A., da Rocha, R.E., Kuroyanagi, A., Bijma, J. and Reichart, G.J., 2009. Effect of salinity and seawater calcite saturation state on Mg and Sr incorporation in cultured planktonic foraminifera. *Marine Micropaleontology* 73 (3), 178-89.

Dymond, J., Suess, E., and Lyle, M., 1992. Barium in Deep-Sea Sediment: a geochemical proxy for paleoproductivity. *Paleoceanography* 7, 163-181.

Elderfield, H., and Ganssen, G., 2000. Past temperature and $\delta^{18}O$ of surface ocean waters inferred from foraminiferal Mg/Ca ratios. *Nature* 405 (6785), 442-5.

Emeis, K. C., Struck, U., Schulz, H. M., Rosenberg, R., Bernasconi, S., Erlenkeuser, H., Sakamoto, T. and Martinez-Ruiz, F., 2000. Temperature and salinity variations of Mediterranean sea surface waters over the last 16,000 years from records of planktonic stable oxygen isotopes and alkenone unsaturation ratios. *Palaeogeography, Palaeoclimatology, Palaeoecology* 158(3), 259-280.

Emiliani, C., 1954. Depth habitats of some species of pelagic foraminifera as indicated by oxygen isotope ratios. *American Journal of Science 252*(3), 149-158.

Erez, J., and Honjo, S., 1981. Comparison of isotopic composition of planktonic foraminifera in plankton tows, sediment traps and sediments. *Palaeogeography, Palaeoclimatology, Palaeoecology 33*(1), 129-156.

Faganeli, J., Pezdic, J., Ogorelec, B., Misic, M., and Najdek, M., 1994. The Origin of sedimentary organic matter in the Adriatic. *Continental Shelf Research* 14 (4),365-384

Fain, A.M.V., Ogston, A.S., and Sternberg, R.W., 2007. Sediment transport event analysis on the western Adriatic continental shelf. *Continental Shelf Research* 27, 431-451.

Fairbanks, R. G., 1989. A 17,000-year glacio-eustatic sea level record: influence of glacial melting rates on the Younger Dryas event and deep-ocean circulation. *Nature* 342(6250), 637-642.

Fleitmann, D., Burns, S. J., Mudelsee, M., Neff, U., Kramers, J., Mangini, A., and Matter, A., 2003. Holocene forcing of the Indian monsoon recorded in a stalagmite from southern Oman. *Science* 300 (5626), 1737-1739.

Fontanier, C., Jorissen, F., Licari, L., Alexandre, A., Anschutz, P., and Carbonel, P., 2002. Live benthic foraminiferal faunas from the Bay of Biscay: faunal density, composition, and microhabitats, *Deep Sea Research Part I: Oceanographic Research Papers* 49 (4), 751-785.

Fontanier, C., Jorissen, F., Geslin, E., Zaragosi, S., Duchemin, G., Laversin, M. and Gaultier, M., 2008. Live and dead foraminiferal faunas from Saint-Tropez Canyon (Bay of Frejus): Observations based on in situ and incubated cores, *The Journal of Foraminiferal Research* 38 (2), 137-156.

François, R, 1988. A study on the regulation of the concentrations of some trace metals (Rb, Sr, Zn, Pb, Cu, V, Cr, Ni, Mn and Mo) in Saanich Inlet sediments, British Columbia, Canada. *Marine Geology* 83, 285–308.

Frignani, M., Langone, L., Ravaioli, M., Sorgente, D., Alvisi, F., and Albertazzi, S., 2005. Fine-Sediment mass balance in the Western Adriatic Continental Shelf over a century time scale. *Marine Geology* 222-223, 113-133.

Frisia, S., Borsato, A., Spötl, C., Villa, I.M. and Cucchi, F., 2005. Climate variability in the SE alps of Italy over the past 17 000 years reconstructed from a stalagmite record. *Boreas* 34 (4), 445-55.

Frisia, S., Borsato, A., Mangini, A., Spötl, C., Madonia, G., and Sauro, U., 2006. Holocene climate variability in Sicily from a discontinuous stalagmite record and the mesolithic to neolithic transition. *Quaternary Research* 66 (3), 388-400.

Fry, B., and Sherr, E.B., 1984. $\delta^{13}C$ measurements as indicators of carbon flow in marine and freshwater ecosystems. *Marine Science* 27, 13-47.

Gallego-Torres, D., Martinez-Ruiz, F., De Lange, G. J., Jimenez-Espejo, F. J., and Ortega-Huertas, M., 2010. Trace-elemental derived paleoceanographic and paleoclimatic conditions for Pleistocene eastern Mediterranean sapropels. *Palaeogeography, Palaeoclimatology, Palaeoecology* 293(1), 76-89.

Ganssen, G. M., and Kroon, D., 2000. The isotopic signature of planktonic foraminifera from NE Atlantic surface sediments: Implications for the reconstruction of past oceanic conditions. *Journal of the Geological Society 157*(3), 693-699.

Garcia, D., Ravenne, C., Maréchal, B., and Moutte, J., 2004. Geochemical variability induced by entrainment sorting: quantified signals for provenance analysis. *Sedimentary Geology* 171 (1–4), 113-128.

Gennari, G., Tamburini, F., Ariztegui, D., Hajdas, I., and Spezzaferri, S., 2009. Geochemical evidence for high-resolution variations during deposition of the Holocene S1 sapropel on the Cretan ridge, eastern Mediterranean. *Palaeogeography, Palaeoclimatology, Palaeoecology* 273(3-4), 239-248.

Geraga, M., Tsaila-Monopolis, S., Ioakim, C., Papatheodorou, G., and Ferentinos, G., 2000. Evaluation of palaeoenvironmental changes during the last 18,000 years in the Myrtoon basin, SW Aegean Sea. *Palaeogeography, Palaeoclimatology, Palaeoecology*, *156*(1), 1-17.

Giraudi, C., Magny, M., Zanchetta, G. and Drysdale. R. N., 2011. The Holocene climatic evolution of Mediterranean Italy: A review of the continental geological data. *The Holocene* 21 (1), 105-15.

Giunta, S., Negri, A., Morigi, C., Capotondi, L., Combourieu-Nebout, N., Emeis, K. C., Sangiorgi, F. and Vigliotti, L, 2003. Coccolithophorid ecostratigraphy and multi-proxy paleoceanographic reconstruction in the southern adriatic sea during the last deglacial time (core AD91-17). *Palaeogeography, Palaeoclimatology, Palaeoecology* 190, 39-59.

Goldsmith, S. L., Krom, M. D., Sandler, A., and Herut, B., 2001. Spatial trends in the chemical composition of sediments on the continental shelf and slope off the Mediterranean coast of Israel. *Continental Shelf Research* 21(16), 1879-1900.

Graham, N.E., Ammann, C.M., Fleitmann, D., Cobb, K.M. and Luterbacher, J., 2011. Support for global climate reorganization during the "Medieval climate anomaly". *Climate Dynamics* 37 (5-6), 1217-45.

Grant, K. M., Rohling, E. J., Bar-Matthews, M., Ayalon, A., Medina-Elizalde, M., Bronk Ramsey, C., Satow, C., Roberts, A. P., 2012. Rapid coupling between ice volume and polar temperature over the past 150,000 years. *Nature* 491 (7426), 744-747.

Grauel, A. L., and Bernasconi, S. M., 2010. Core-top calibration of $\delta^{18}O$ and $\delta^{13}C$ of *G. ruber* (white) and *U. mediterranea* along the southern Adriatic coast of Italy. *Marine Micropaleontology* 77 (3-4) (12), 175-86.

Grauel, A.L., Leider, A., Goudeau, M-L.S., Müller, I., Versteegh, G.J.M., Hinrichs, K-U., de Lange, G.J. and Bernasconi, S.M., 2013a. What do SST really tell us? A high-resolution multiproxy (UK'37, TEXH86 and foraminfera δ18O) study in the Gulf of Taranto, central Mediterranean Sea. *Quaternary Science Reviews* 73, 115-131.

Grauel, A-L., Goudeau, M-L., de Lange, G.J., and Bernasconi, S.M., 2013b. Climate of the past 2500 years in the Gulf of Taranto, central Mediterranean Sea: A high-resolution climate reconstruction based on δ18O and δ13C of *Globigerinoides ruber* (white). *The Holocene* 23(10), 1440-1446.

Gray, L. J., Beer, J., Geller, M., Haigh, J. D., Lockwood, M,. Matthes, K., Cubasch, U., Fleitmann, D., Harrison, G., Hood, L., Luterbacher, J., Meehl, G. A., Shindell, D., van Geel, B. and White, W., 2010. Solar influences on climate. *Reviews of Geophysics*, *48*(4)

Gray, S.T.,. Graumlich, L.J, Betancourt, J.L. and Pederson, G.T., 2004. A tree-ring based reconstruction of the Atlantic Multidecadal Oscillation since 1567 AD, *Geophysical Research Letters* 31 (12), 1944-8007, L12205.

Grinsted, A., Moore, J. and Jevrejeva, S., 2004. Application of the cross wavelet transform and wavelet coherence to geophysical time series, *Nonlinear processes in geophysics* 11 (5/6), 561-566.

Grootes, P.M., and Stuiver, M., 1997. Oxygen 18/16 variability in Greenland snow and ice with 10^3 to 10^5-year time resolution. *Journal of Geophysical Research* 102, 26455-26470.

Grove, A.T.. 2001. The "Little ice age" and its geomorphological consequences in Mediterranean Europe. In *The iceberg in the mist: Northern research in pursuit of a "Little ice age"*. 121-136 Springer.

Hammer, Ø., Harper, D.A.T. and Ryan. P.D., 2001. PAST-palaeontological statistics. www. Uv.Es/~ pardomv/pe/2001_1/past/pastprog/past.Pdf, Acessado Em 25 (07): 2009.

Haug, G. H., Hughen, K. A., Sigman, D. M., Peterson, L. C., and Röhl, U., 2001. Southward migration of the Intertropical Convergence Zone through the Holocene. *Science 293*(5533), 1304-1308.

Haug, G. H., Günther, D., Peterson, L. C., Sigman, D. M., Hughen, K. A., and Aeschlimann, B., 2003. Climate and the collapse of Maya civilization. *Science 299*(5613), 1731-1735.

Hedges, J.I., Clark, W.A.; Quay; P.D., Richey, J.E.; Devol, A.H., and Santos, U.M, 1986. Compositions and fluxes of particulate organic material in the Amazon River. *Limnology and Oceanography* 31 (4), 717-738

Hedges, J.I., and Keil, R.G., 1995. Sedimentary organic matter preservation: an assessment and speculative synthesis. *Marine Chemistry* 49, 81-115.

Hennekam, R., and De Lange, G.J., 2012. X-ray fluorescence core scanning of wet marine sediments: methods to improve quality and reproducibility of high-resolution paleoenvironmental records. *Limnology and Oceanography: Methods* 10, 991-1003.

Hennekam, R., Jilbert, T. and De Lange, G.J., 2014. Solar forcing of early- to mid Holocene Nile discharge into the eastern Mediterranean.Submitted to *Paleoceanography*.

Hess, S. and Jorissen, F.J., 2009. Distribution patterns of living benthic foraminifera from Cap Breton canyon, Bay of Biscay: Faunal response to sediment instability. *Deep Sea Research Part I: Oceanographic Research Papers* 56 (9), 1555-1578.

Hilgen, F.J., 1991. Astronomical calibration of gauss to Matuyama sapropels in the Mediterranean and implication for the geomagnetic polarity time scale. *Earth and Planetary Science Letters* 104 (2-4), 226-244.

Hoerling, M.P., Hurrell, J.W. and Xu, T., 2001. Tropical origins for recent North Atlantic climate change. *Science* 292 (5514), 90-92.

Holzhauser, H., Magny, M. and Zumbuühl. H.J, 2005. Glacier and lake-level variations in West-Central Europe over the last 3500 years. *The Holocene* 15 (6), 789-801.

Hönisch, B., Allen, K.A., Lea, D.W., Spero, H.J., Eggins, S.M., Arbuszewski, J., deMenocal, P., Rosenthal, Y., Russell, A.D. and Elderfield, H., 2013. The influence of salinity on Mg/Ca in planktic foraminifers-evidence from cultures, core-top sediments and complementary $\delta^{18}O$. *Geochimica Et Cosmochimica Acta.*

Horikawa, K., Murayama, M., Minagawa, M., Kato, Y., and Sagawa, T., 2010. Latitudinal and downcore (0-750 ka) changes in n-alkane chain lengths in the eastern equatorial Pacific. *Quatanary Research* 73, 573-582.

Hughen, K.A., Baillie, M.G.L., Bard, E., Beck, J.W. Bertrand, C.J.H., Blackwell, P.G., Buck, C.E. Burr, G.S., Cutler, K.B., Damon, P.E., Edwards, R.L., Fairbanks, R.G., Friedrich, M., Guilderson, T.P., Kromer, B., McCormac, G., Manning, S., Ramsey, C.B., Reimer, P.J., Reimer, R.W., Remmele, S., Southon, J.R., Stuiver, M., Talamo, S., Taylor, F.W., van der Plicht, J. and Weyhenmeyer, C.E., 2004. Marine04 marine radiocarbon age calibration, 0-26 cal kyr BP. *Radiocarbon* 46 (3), 1059-1086.

Hurrell, J. W., 1995. Decadal trends in the north Atlantic oscillation: Regional temperatures and precipitation. *Science* 269 (5224), 676-679.

Hurrell, J.W. and Deser, C., 2009. North Atlantic climate variability: The role of the North Atlantic Oscillation. *Journal of Marine Systems* 78(1), 28-41.

Hut, G. 1987. *Consultants' group meeting on stable isotope reference samples for geochemical and hydrological investigations: IAEA, vienna 16-18 september 1985: Report to the director general*International Atomic Energy Agency.

Ishikawa, M. and Ichikuni, M., 1984. Uptake of sodium and potassium by calcite, *Chemical Geology* 42, 137–146.

Jilbert, T., G. de Lange and Reichart, G.J., 2008. Fluid displacive resin embedding of laminated sediments: Preserving trace metals for high-resolution paleoclimate investigations. *Limnol.Oceanogr.: Methods* 6, pp.16-22.

Jilbert, T., Reichart, G-J., Aeschlimann, B., Gunther, D.W., and de Lange, G. J., 2010a. Climate-controlled multidecadal variability in North African dust transport to the Mediterranean. *Geology* 38 (1), 19-22.

Jilbert, T., Reichart, G. J., Mason, P., and de Lange, G. J., 2010b. Short-time-scale variability in ventilation and export productivity during the formation of Mediterranean sapropel S1. *Paleoceanography* 25(4), PA4232.

Joannin, S., Brugiapaglia, E., de Beaulieu, J., Bernardo, L., Magny, M., Peyron, O., Goring, S., and Vannière, B., 2012. Pollen-based reconstruction of Holocene vegetation and climate in southern Italy: the case of Lago Trifoglietti. *Climate of the Past* 8, 1973-1996.

Jochum, K. P., Weis, U., Stoll, B., Kuzmin, D., Yang, Q., Raczek, I., Jacob, D.E., Stracke, A., Birbaum, K., Frick, D.A., Günther, D. and Enzweiler, J., 2011. Determination of reference values for NIST SRM 610–617 glasses following ISO guidelines. *Geostandards and Geoanalytical Research 35*(4), 397-429.

Jones, B., and Manning, D.A.C., 1994. Comparison of geochemical indices used for the interpretation of paleoredox conditions in ancient mudstones. *Chemical Geology* 114, 111–129

Kaniewski, D., Paulissen, E., Van Campo, E., Weiss, H., Otto, T., Bretschneider, J. and Van Lerberghe, K., 2010. Late second–early first millennium BC abrupt climate changes in coastal Syria and their possible significance for the history of the Eastern Mediterranean. *Quaternary Research* 74 (2), 207-15.

Kemp, A. E., Pearce, R. B., Pike, J., and Marshall, J. E., 1998. Microfabric and microcompositional studies of Pliocene and Quaternary sapropels from the eastern Mediterranean. In *Proceedings of the Ocean Drilling Program. Scientific results* 160, 333-348.

Kemp, A. E., Pearce, R. B., Koizumi, I., Pike, J., and Rance, S. J., 1999. The role of mat-forming diatoms in the formation of Mediterranean sapropels. *Nature*, 398(6722), 57-61.

Kerr, R.A., 2000. A North Atlantic climate pacemaker for the centuries. *Science* 288 (5473), 1984-1985.

Kidd, R.B., Cita, M.B. and Ryan, W.B., 1978. Stratigraphy of eastern Mediterranean sapropel sequences recovered during DSDP leg 42A and their paleoenvironmental significance. Initial Reports of the Deep Sea Drilling Project 42(Part 1), 421-443.

Kim, J.-H., Schouten, S., Buscail, R., Ludwig, W., Bonnin, J., Sinninghe Damsté, J.S., and Bourrin, F., 2006. Origin and distribution of terrestrial organic matter in the NW Mediterranean (Gulf of Lions): exploring the newly developed BIT index. *Geochemistry, Geophysics, Geosystems* 7(11), 1525-2027 Q11017.

Kitano, Y., Okumura, M., and Idogaki, M., 1975. Incorporation of sodium, chloride and sulfate with calcium carbonate. *Geochemical Journal* 9, 75–84.

Klump, J., Hebbeln, D., and Wefer, G., 2000. The impact of sediment provenance on Barium-based productivity estimates. *Marine Geology* 169, 259-271.

Knight, J. R., Folland, C.K. and Scaife, A.A., 2006. Climate impacts of the Atlantic Multidecadal Oscillation. *Geophysical Research Letters 33*(17), 1994-8007.

Knudsen, M. F., Seidenkrantz, M. S., Jacobsen, B. H., and Kuijpers, A., 2011. Tracking the Atlantic Multidecadal Oscillation through the last 8,000 years. *Nature Communications* 2, 178.

Kotthoff, U., Pross, J., Müller, U. C., Peyron, O., Schmiedl, G., Schulz, H., and Bordon, A., 2008. Climate dynamics in the borderlands of the Aegean Sea during formation of sapropel S1 deduced from a marine pollen record. *Quaternary Science Reviews* 27(7), 832-845.

Kuhnt, T., Schmiedl, G., Ehrmann, W., Hamann, Y., and Hemleben, C., 2007. Deep-sea ecosystem variability of the Aegean Sea during the past 22 kyr as revealed by benthic foraminifera. *Marine Micropaleontology 64*(3), 141-162.

Lamb, H., Gasse, F., Benkaddour, A., El Hamouti, N., Van der Kaars, S., Perkins, W., Pearce, N. and Roberts, C., 1995. Relation between century-scale Holocene arid intervals in tropical and temperate zones. *Nature* 373 (6510), 134-137.

Lamy, F., Arz, H.W., Bond, G.C., Bahr, A., Pätzold, J., 2006. Multicentennial-scale hydrological changes in the Black Sea and northern Red Sea during the Holocene and the Arctic/North Atlantic Oscillation. *Paleoceanography* 21, PA 1008.

Leider, A., Hinrichs, K-U., Mollenhauer, G., Versteegh, G. J. M., 2010. Core-Top Calibration of the Lipid-Based and TEX^{86} temperature proxies on the Southern Italian Shelf (SW Adriatic Sea, Gulf of Taranto). *Earth and Planetary Science Letters* 300 (1-2), 112-124.

Leider, A., Hinrichs, K.-U., Schefuß, E., and Versteegh, G. J. M., 2013. Distribution and stable isotopes of plant wax-derived *n*-alkanes in marine surface sediments along a SE Italian transect and their potential to reconstruct the water balance. *Geochimica et Cosmochimica Acta* 117, 16-32.

Lionello, P., Malanotte-Rizzoli, P., Boscolo, R., Alpert, P., Artale, V., Li, L., Luterbacher, J., May, W., Trigo, R., Tsimplis, M., Ulbrich, U., and Xoplaki, E., 2006. The Mediterranean climate: An overview of the main characteristics and issues, in: P. Lionello, P.M.-R., Boscolo, R. (Eds.), Developments in Earth and Environmental Sciences. Elsevier, 1-26.

Longinelli, A., and Selmo, E., 2003. Isotopic composition of precipitation in Italy: a first overall map. *Journal of Hydrology*, *270*(1-2), 75-88.

Lourens, L. J., Antonarakou, A., Hilgen, F. J., Van Hoof, A. A. M., Vergnaud-Grazzini, C., and Zachariasse, W. J., 1996. Evaluation of the Plio-Pleistocene astronomical timescale. *Paleoceanography* 11(4), 391-413.

Magny, M., Bégeot, C., Guiot, J. and Peyron, O., 2003. Contrasting patterns of hydrological changes in Europe in response to Holocene climate cooling phases. *Quaternary Science Reviews* 22 (15), 1589-1596.

Magny, M., Vannière,B., Zanchetta,G.. Fouache,E., Touchais, G., Petrika, L.,Coussot, C., Walter-Simonnet, A-V., and Arnaud, F., 2009. Possible complexity of the climatic event around 4300—3800 cal. BP in the central and western Mediterranean. *The Holocene* 19, 823-833.

Malinverno, E., Taviani, M. , Rosso, A. , Violanti, D. , Villa, I. , Savini, A. , Vertino, A., Remia, A., and Corselli, C., 2010. Stratigraphic framework of the Apulian Deep-Water Coral Province, Ionian Sea. *Deep Sea Research Part II*: *Topical Studies in Oceanography* 57 (5-6), 345-359.

Mann, M. E., Zhang, Z., Rutherford, S., Bradley, R.S., Hughes, M.K., Shindell, D., Ammann, C. Faluvegi, G. and Ni, F. 2009. Global signatures and dynamical origins of the little ice age and medieval climate anomaly. *Science* 326 (5957), 1256-60.

Marino, G., Rohling, E.J., Sangiorgi, F., Hayes, A., Casford, J. L., Lotter, A. F., Kucera, M. and Brinkhuis, H., 2009. Early and middle Holocene in the Aegean sea: Interplay between high and low latitude climate variability. *Quaternary Science Reviews* 28(27), 3246-3262.

Martín-Puertas, C., Valero-Garcés, B.L., Brauer, A., Mata, M.P., Delgado-Huertas, A. and Dulski, P., 2009. The Iberian–Roman Humid Period (2600–1600 cal yr BP) in the Zoñar Lake varve record (Andalucía, southern Spain). *Quaternary Research* 71 (2), 108-120.

Mayewski, P. A., Meeker, L. D., Twickler, M. S., Whitlow, S., Yang, Q., Lyons, W. B., and Prentice, M., 1997. Major features and forcing of high-latitude northern hemisphere atmospheric circulation using a 110,000-year-long glaciochemical series. *Journal of Geophysical Research* 102(C12), 26345-26,366.

Mayewski, P.A., Rohling, E.E., Curt Stager, J., Karlén, W., Maasch., K.A., Meeker, L.D., Meyerson, E.A., Gasse, F., van Kreveld, S., Holmgren, K., Lee-Thorp, J., Rosqvist, G., Rack, F., Staubwasser, M., Schneider, R.R., and Steig, E.J., 2004. Holocene climate variability. *Quaternary Research* 62 (3), 243-255.

Medici, L., Bellanova, J., Belviso, C., Cavalcante, F., Lettino, A., Ragone, P. P., and Fiore, S., 2011. Trace metals speciation in sediments of the Basento River (Italy). *Applied Clay Science* 53 (3), 414-442.

Meeker, L.D. and P.A. Mayewski, 2002. A 1400-year high-resolution record of atmospheric circulation over the North Atlantic and Asia. *The Holocene* 12(3), 257-266.

Mele,D., Sulpizio, R., Dellino, P., La Volpe, L., 2010. Stratigraphy and eruptive dynamics of a long-lasting Plinian eruption of Somma-Vesuvius: the Pomici di Mercato (8900 years BP). *Bulletin of Volcanology* 73, 257-278.

Milankovitch, M., 1941. *Kanon der Erdebestrahlung und seine anwendung auf das eiszeitenproblem*. Königlich Serbische Akademie.

Milligan, T.G., and Cattaneo, A., 2007. Sediment dynamics in the western Adriatic Sea: From transport to stratigraphy. *Continental Shelf Research* 27, 287-295.

Moller, T., Schulz, H., Hamann, Y., Dellwig, O., and Kucera, M., 2012. Sedimentology and geochemistry of an exceptionally preserved last interglacial sapropel S5 in the Levantine basin (Mediterranean sea). *Marine Geology* 291, 34-48.

Morford, J. L., Russell, A. D., and Emerson, S., 2001. Trace metal evidence for changes in the redox environment associated with the transition from terrigenous clay to diatomaceous sediment, Saanich Inlet, BC. *Marine Geology* 174 (1), 355-369.

Morovic, M., Mati, F., Grbec, B., Dadi, V., Ivankovi, D., 2006. South Adriatic Phenomena observable through VOS XBT and Other ADRICOSM Data. *Acta Adriatica* 47, 33-49.

Moy, C.M., Seltzer, G.O., Rodbell, D.T. and Anderson, D.M., 2002. Variability of El Nino/Southern Oscillation activity at millennial timescales during the Holocene epoch. *Nature* 420 (6912), 162-165.

Mueller, P.J., 1977. C/N ratios in Pacific deep-sea sediments: Effect of inorganic ammonium and organic nitrogen compounds absorbed by clays. *Geochemica Cosmochemica Acta* 41, 765-776.

Myers, P.G. and Rohling, E.J., 2000. Modeling a 200-yr interruption of the holocene sapropel S1. *Quaternary Research* 53(1), 98-104.

Nicault, A., S. Alleaume, S. Brewer, M. Carrer, P. N., and Guiot, J., 2008. Mediterranean drought fluctuation during the last 500 years based on tree-ring data. *Climate Dynamics* 31 (2-3), 227-45.

Nieto-Moreno, V., Martínez-Ruiz, F., Giralt, S., Jiménez-Espejo, F., Gallego-Torres, D., Rodrigo-Gámiz, M., García-Orellana, J., Ortega-Huertas, M., and De Lange, G.J., 2011. Tracking climate variability in the western Mediterranean during the Late Holocene: a multiproxy approach. *Climate of the Past* 7 (4), 1395-1414.

Nittrouer, C., S. Miserocchi, Trincardi, F., 2004. The PASTA Project: Investigation of Po and Apennine sediment transport and accumulation. *Oceanography* 17 (4), 46-57.

Numberger, L., Hemleben, C., Hoffmann, R., Mackensen, A., Schulz, H., Wunderlich, J.M. and Kucera, M., 2009. Habitats, abundance patterns and isotopic signals of morphotypes of the planktonic foraminifer *Globigerinoides ruber* (d'Orbigny) in the eastern Mediterranean Sea since the Marine Isotopic Stage 12. *Marine Micropaleontology* 73 (1), 90-104.

Oeltzschner, H., Sigl, W., 1970. Sedimentologische untersuchungen im Golf Von Manfredonia (Südadria). *Geologische Rundschau* 60 (1), 131-140.

Olausson, E., 1961. Studies of deep sea core. *Reports of of the swedish deep sea expedition* 1947-1948, 353-391

Oldfield, F., Asioli, A., Accorsi, C. A., Mercuri, A. M., Juggins, S., Langone, L., Rolph, T., Trincardi, F., Woff, G., Gibbsa, Z., Vigliotti, L. Frignani, M., van der Post, K., and Branch, N., 2003. A high resolution late Holocene palaeo environmental record from the central Adriatic Sea. *Quaternary Science Reviews 22*(2), 319-342.

Olsen, J., Anderson, N. J., and Knudsen, M. F., 2012. Variability of the North Atlantic Oscillation over the past 5,200 years. *Nature Geoscience* 5, 808–812.

O'Neil, J. R., Clayton, R.N. and Mayeda, T.K., 1969. Oxygen isotope fractionation in divalent metal carbonates. *The Journal of Chemical Physics* 51, 5547.

Paillard, D., Labeyrie, L., and Yiou, P., 1996. Macintosh program performs time-series analysis. *Eos*, Transactions, American Geophysical Union 77, 379.

Passier, H. F., Middelburg, J.J., de Lange, G.J., and Böttcher, M. E., 1997. Pyrite contents, microtextures, and sulfur isotopes in relation to formation of the youngest Eastern Mediterranean sapropel. *Geology* 25(6), 519-522.

Passier, H. F., Middelburg, J.J., de Lange, G.J., and Böttcher, M.E., 1999. Modes of sapropel formation in the Eastern Mediterranean: Some constraints based on pyrite properties. *Marine Geology* 153(1), 199-219.

Perri, F., Critelli, S., Dominici, R., Muto, F., Tripodi, V., and Ceramicola, S., 2012. Provenance and accommodation pathways of Late Quaternary sediments in the Deep-Water Northern Ionian Basin, Southern Italy. *Sedimentary Geology* 280, 244-259

Peyron, O., Goring, S., Dormoy, I., Kotthoff, U., Pross, J., de Beaulieu, J-L, Drescher-Schneider, R., Vannière, B. and Magny, M., 2011. Holocene seasonality changes in the Central Mediterranean region reconstructed from the pollen sequences of Lake Accesa (Italy) and Tenaghi Philippon (Greece). *The Holocene* 21 (1), 131-146.

Piccarreta, M., Caldara, M., Capolongo, D., Boenzi, F., 2011. Holocene Geomorphic activity related to climatic change and human impact in Basilicata, Southern Italy. *Geomorphology* 128 (3-4), 137-147.

Pierre, C., 1999. The oxygen and carbon isotope distribution in the Mediterranean water masses. *Marine Geology* 153 (1), 41-55.

Piervitali, E., Colacino, M. and Conte. M., 1997. Signals of climatic change in the Central-Western Mediterranean basin. *Theoretical and Applied Climatology* 58 (3-4), 211-9.

Pigorini, B., 1968. Sources and dispersion of recent sediments of the Adriatic Sea. *Marine Geology* 6 (3), 187-229.

Pinardi, N. and Masetti, E., 2000. Variability of the large scale general circulation of the Mediterranean sea from observations and modelling: A review. *Palaeogeography, Palaeoclimatology, Palaeoecology* 158(3), 153-173.

Piper, D. Z., Ludington, S., Duval, J. S., and Taylor, H. E., 2006. Geochemistry of bed and suspended sediment in the Mississippi river system: Provenance versus weathering and winnowing. *Science of the total environment* 362(1), 179-204.

Piva, A., Asioli, A., Trincardi, F., Schneide, R.R. and Vigliotti, L., 2008. Late-Holocene climate variability in the Adriatic sea (Central Mediterranean). *The Holocene*, *18*(1), 153-167.

Pla, S. and Catalan. J., 2005. Chrysophyte cysts from lake sediments reveal the submillennial winter/spring climate variability in the northwestern Mediterranean region throughout the Holocene. *Climate Dynamics* 24 (2-3), 263-78.

Poulain, P-M., 2001. Adriatic Sea surface circulation as derived from drifter data between 1990 and 1999. *Journal of Marine Systems* 29 (1-4) (5), 3-32.

Poulos S.E, Drakopoulos P.G, and Collins M.B., 1997. Seasonal variability in sea surface oceanographic conditions in the Aegean Sea (eastern Mediterranean): an overview. *Journal of Marine Systems* 13, 225-244

Prahl, F.G. and Wakeham, S.G., 1987. *Nature* 330, 367-369.

Pujol, C., and Vergnaud-Grazzini, C., 1995. Distribution patterns of live planktic foraminifers as related to regional hydrography and productive systems of the Mediterranean Sea. *Marine Micropaleontology* 25 (2), 187-.217.

Qi, S., Leipe, T., Rueckert, P., Di, Z., and Harff, J., 2010. Geochemical sources, deposition and enrichment of heavy metals in short sediment cores from the Pearl River Estuary, Southern China. *Journal of Marine Systems* 82, S28-S42.

Raicich, F., 1996. On the fresh balance of the Adriatic Sea. *Journal of Marine Systems* 9 (3–4), 305-319.

Reale, O., and Dirmeyer, P., 2000. Modeling the effects of vegetation on Mediterranean climate during the Roman Classical Period: Part I: Climate history and model sensitivity. *Global and Planetary Change* 25 (3), 163-84.

Reichart, G.J., Lourens, L.J., and Zachariasse, W.J., 1998. Temporal variability in the northern Arabian Sea Oxygen Minimum Zone (OMZ) during the last 225,000 years. *Paleoceanography 13*(6), 607-621.

Reichart, G-J, Jorissen, F., Anschutz, P. and Mason P.R.D., 2003. Single foraminiferal test chemistry records the marine environment. *Geology* 31 (4), 355-8.

Reimer, P.J., Baillie, M.G.L., Bard, E., Bayliss, A., Beck, J.W., Bertrand, C.J.H., Blackwell, P.G., Buck, C.E., Burr, G.S., Cutler, K.B., Damon, P.E., Edwards, R.L., Fairbanks, R.G., Friedrich, M., Guilderson, T.P., Hogg, A.G., Hughen, K.A., Kromer, B., McCormac, G., Manning, S., Ramsey, C.B., Reimer, R.W., Remmele, S., Southon, J.R., Stuiver, M., Talamo, S., Taylor, F.W., van der Plicht, J., and Weyhenmeyer, C.E., 2004. IntCal04 terrestrial radiocarbon age calibration, 0-26 cal kyr BP. *Radiocarbon* 46, 1029-1058.

Reitz, A., Pfeifer, K., De Lange, G. J., Klump, J., 2004. Biogenic barium and the detrital Ba/Al ratio: a comparison of their direct and indirect determination. *Marine Geology* 204(3), 289-300.

Reitz, A., and De Lange, G.J., 2006. Abundant Sr-rich aragonite in Eastern Mediterranean sapropel S1: Diagenetic vs. detrital/biogenic origin. *Palaeogeography, Palaeoclimatology, Paleoecology* 235, 135-148.

Reitz, A., Thomson, J., De Lange, G.J., and Hensen, C., 2006. Source and development of large manganese enrichments above eastern Mediterranean sapropel S1. *Paleoceanography*, 21, PA3007.

Richter, T.O., van der Gaast, S., Koster, B., Vaars, A., Gieles, R., de Stigter, H.C., de Haas, H., and van Weering, T.C.E., 2006. The Avaatech XRF Core Scanner: technical description and applications to NE Atlantic sediments, in: Rothwell, G. (Eds.), New Techniques in Sediment Core Analysis. Geological Society London Special Publication, London, 39-11.

Ridente, D., Foglini, F., Minisini, D., Trincardi, F., and Verdicchio, G., 2007. Shelf-Edge erosion, sediment failure and inception of Bari Canyon on the Southwestern Adriatic Margin (Central Mediterranean). *Marine Geology* 246 (2–4), 193-207.

Rimbu, N., Lohmann, G., Kim, J. H., Arz, H. W., and Schneider, R., 2003. Arctic/North Atlantic Oscillation signature in Holocene sea surface temperature trends as obtained from alkenone data. *Geophysical Research Letters* 30(6)

Robinson, A. R., Malanotte-Rizzoli, P., Hecht, A., Michelato, A., Roether, W., Theocharis, A., U. Unliiata, N.Pinardi, A. Artegiani, A. Bergamasco ,J. Bishop, S. Brenner, S. Christianidis M. Gacic , D. Georgopoulos, M. Golnaraghi, M. Hausmann, H.-G. Junghaus, A. Lascaratos M.A. Latif, W.G. Leslie, C.J. Lozano, T. Oguz, E. Özsoy, E. Papageorgiou, E. Paschini Z. Rozentroub, E. Sansone, P.Scarazzato, R. Schlitzer, G.-C. Spezie, E. Tziperman G. Zodiatis, L. Athanassiadou, M. Gerges and Osman, M., 1992. General circulation of the Eastern Mediterranean. *Earth-Science Reviews* 32(4), 285-309.

Roether, W., Manca, B.B., and Klein, B., 1996. Recent changes in Eastern Mediterranean deep waters. *Science* 271 (5247), 333-335.

Rohling, E.J. and Gieskes, W.W., 1989. Late Quaternary changes in Mediterranean intermediate water density and formation rate. *Paleoceanography* 4(5), 531-545.

Rohling, E. and Hilgen, F., 1991. The Eastern Mediterranean climate at times of sapropel formation: A review. *Geologie en Mijnbouw* 70, 253-264.

Rohling, E.J., Jorissen, F.J. and De Stigter, H.C., 1997. 200 year interruption of Holocene sapropel formation in the Adriatic sea. *Journal of Micropalaeontology* 16(2), 97-108.

Rohling, E. J., 2000. Paleosalinity: confidence limits and future applications. *Marine Geology* 163 (1), 1-11

Rohling, E. J., Mayewski, P. A., Abu-Zied, R. H., Casford, J. S. L. and Hayes, A., 2002. Holocene atmosphere-ocean interactions: Records from Greenland and the Aegean sea. *Climate Dynamics* 18 (7), 587-593.

Rohling, E.J., Sprovieri, M., Cane, T., Casford, J.S.L., Cooke, S., Bouloubassi, I., Emeis, K.C., Schiebel, R., Rogerson, M., Hayes, A., Jorissen, F.J. and Kroon, D., 2004. Reconstructing past planktic foraminiferal habitats using stable isotope data: a case history for Mediterranean sapropel S5. *Marine Micropaleontology 50*(1), 89-123.

Rohling, E. J., and Pälike, H., 2005. Centennial-scale climate cooling with a sudden cold event around 8,200 years ago. *Nature* 434 (7036), 975-979.

Rommerskirchen, F., Eglinton, G., Dupont, L., and Rullkőtter, J., 2006.Glacial/ interglacial changes in southern Africa: Compound-specific $\delta^{13}C$ land plant biomarker and pollen recods from southeast Atlantic continental margin sediments. *Geochemistry, Geophysics, Geosystems* 7 (8), 1525-2027

Rosenthal, Y., Boyle, E. A. and Labeyrie, L., 1997. Last glacial maximum paleochemistry and deepwater circulation in the Southern ocean: Evidence from foraminiferal cadmium. *Paleoceanography* 12 (6), 787-96.

Rosenthal, Y., Field, M.P. and Sherrell, R.M., 1999. Precise determination of element/calcium ratios in calcareous samples using sector field inductively coupled plasma mass spectrometry. *Analytical Chemistry 71*(15), 3248-3253.

Rosenthal, Y., Morley, A., Barras, C., Katz, M.E., Jorissen, F., Reichart, G.J., Oppo, D.W. and Linsley, B.K., 2011. Temperature calibration of Mg/Ca ratios in the intermediate water benthic foraminifer *Hyalinea balthica*. *Geochemistry Geophysics Geosystems* 12 (4), Q04003.

Rossi, S., Auroux, C., and Mascle, J., 1983. The Gulf of Taranto (Southern Italy): Seismic stratigraphy and shallow structure. *Marine Geology* 51, 327-346.

Rossignol-Strick, M., 1985. Mediterranean Quaternary sapropels, an immediate response of the African monsoon to variation of insolation. *Palaeogeography, Palaeoclimatology, Palaeoecology* 49(3-4), 237-263.

Rossignol-Strick, M., 1999. The Holocene climatic optimum and pollen records of sapropel 1 in the eastern Mediterranean, 9000-6000 BP. *Quaternary Science Reviews* 18, 515-530.

Rothwell, R.G., and Rack, F.R., 2006. New techniques in sediment core analysis: an introduction. Geological Society, London, Special Publications 267, 1-29.

Ruff, M., Wacker, L., Gäggeler, H. W., Suter, M., Synal, H. A. and Szidat, S., 2007. A gas ion source for radiocarbon measurments at 200 kV. *Radiocarbon* 49 (2), 7-307.

Rutten, A., De Lange, G.J., Ziveri P., Thomson J., Van Sanvoort P.J.M., Colley S., and Corselli C., 2000.Recent terrestrial and carbonate fluxes in the pelagic eastern Mediterranean ; a comparison between sediment trap and surface sediment. *Palaeogeography, Palaeoclimatology, Palaeoecology* 158, 197-213.

Sachs, J.P. and Repeta, D.J., 1999. Oligotrophy and nitrogen fixation during eastern Mediterranean sapropel events. *Science* 286 (5449), 2485-2488.

Sachse, D., Billault, I., Bowen, G. J., Chikaraishi, Y., Dawson, T. E., Feakins, S. J., and Kahmen, A., 2012. Molecular paleohydrology: interpreting the hydrogen-isotopic composition of lipid biomarkers from photosynthesizing organisms. *Annual Review of Earth and Planetary Sciences 40*, 221-249.

Sangiorgi, F., Capotondi, L., Combourieu Nebout, N., Vigliotti, L., Brinkhuis, H., Giunta, S., Lotter, A.F., Morigi, C., Negri, A. and Reichart, G-J., 2003. Holocene seasonal sea-surface temperature variations in the southern Adriatic sea inferred from a multiproxy approach. *Journal of Quaternary Science* 18 (8), 723-32.

Santvoort, P. J. M., Lange, G. J., Langereis, C. G., Dekkers, M. J., Paterne, M., 1997. Geochemical and paleomagnetic evidence for the occurrence of "missing" sapropels in Eastern Mediterranean sediments. *Paleoceanography 12*(6), 773-786.

Savini, A., and Corselli, C., 2010. High-Resolution bathymetry and acoustic geophysical data from Santa Maria Di Leuca cold water coral province (Northern Ionian Sea-Apulian continental slope). *Deep Sea Research Part II: Topical Studies in Oceanography* 57 (5-6), 326-344.

Schilman, B., Bar-Matthews, M., Almogi-Labin, A., and Luz, B., 2001. Global climate instability reflected by Eastern Mediterranean marine records during the late Holocene. *Palaeogeography, Palaeoclimatology, Palaeoecology* 176, 157-176.

Schimmelmann, A., Sessions, A. L., Mastalerz, M., 2006. Hydrogen isotopic (D/H) composition of organic matter during diagenesis and thermal maturation. *Annual Review of Earth Planetery Science* 34, 501-533.

Schmidt, G. A., Biggs, G.A., and Rohling, E.J., 1999, Global Seawater Oxygen-18 database. http://data.giss.nasa..gov/o18data/

Schmidt, G. A., 1999. Error analysis of paleosalinity calculations. *Paleoceanography*, *14*(3), 422-429.

Schroeter, J. S., 1783. Einleitung in die conchylienkenntniss. *Nach Linne* 1: 860.

Schulz, M. and Mudelsee, M., 2002. REDFIT: estimating red-noise spectra directly from unevenly spaced paleoclimatic time series. *Computers and Geosciences* 28, 421-426.

Sejrup, H. P., Haflidason, H. and Andrews, J.T., 2011. A Holocene North Atlantic SST record and regional climate variability. *Quaternary Science Reviews* 30(21), 3181-3195.

Sellschopp, J. and Álvarez, A., 2003. Dense low-salinity outflow from the Adriatic sea under mild (2001) and strong (1999) winter conditions. *Journal of Geophysical Research* 108(C9), 8104.

Shackleton, N. J., 1967. Oxygen isotope analyses and Pleistocene temperatures re-assessed. *Nature*, *215*(5096).

Shackleton, N.J., 1974. Attainment of isotopic equilibrium between ocean water and the benthonic foraminifera genus uvigerina: Isotopic changes in the ocean during the Last Glacial.

Shanahan, TM, Overpeck, J.T., Anchukaitis, K.J., Beck, J.W., Cole, J.E., Dettman, D.L., Peck,J.A., Scholz, C.A., and King, J.W., 2009. Atlantic forcing of persistent drought in West Africa. *Science* 324 (5925), 377-80.

Shapiro, S. S., and Wilk, M. B., 1965. An analysis of variance test for normality (complete samples). *Biometrika*, *52*(3/4), 591-611.

Shuman, B., Plank, C., 2011. Orbital, ice sheet, and possible solar controls on Holocene moisture trends in the North Atlantic drainage basin. *Geology* 39, 151-154.

Siani, G., Magny, M., Paterne, M., Debret, M., and Fontugne, M., 2013. Paleohydrology reconstruction and Holocene climate variability in the South Adriatic Sea. *Climate of the Past 9*(1), 499-515.

Simeoni, U., 1992. I Litorali Tra Manfredonia E Barletta (Basso Adriatico): Dissesti, Sedimenti, Problematiche Ambientali. Bollettino Della Societa. *Geologica Italiana* 111, 67-398.

Snedecor, G. W., and Cochran, W.G., 1989. Statistical methods, eight edition. *Iowa State University Press, Ames, Iowa.*

Socal, G., Boldrin, A., Bianchi, F., Civitarese, G., De Lazzari, A., Rabitti, S., and Turchetto, M. M., 1999. Nutrient, particulate matter and phytoplankton variability in the photic layer of the Otranto strait. *Journal of Marine Systems* 20(1-4), 381-398.

Spagnoli, F., Bartholini, G., Dinelli, E., and Giordano, P., 2008. Geochemistry and particle size of surface sediments of Gulf of Manfredonia (Southern Adriatic Sea). *Estuarine, Coastal and Shelf Science* 80 (1), 21-30.

Spagnoli, F., Dell'Anno, A., De Marco, A., Dinelli, E., Fabiano, M., Gadaleta, M. V., Ianni, C., Loiacono, F., Manini, E., Marini, M., Mongelli, G., Rampazzo, G., Rivaro, P., and Vezzulli, L., 2010. Biogeochemistry, grain size and mineralogy of the Central and Southern Adriatic Sea sediments: A Review. *Chemistry and Ecology* 26, 19-44.

Spero, H.J., 1992. Do planktic foraminifera accurately record shifts in the carbon isotopic composition of seawater ΣCO_2. *Marine Micropaleontology* 19 (4), 275-85.

Spero, H.J., and Williams, D.F., 1989. Opening the carbon isotope "vital effect" black box 1. seasonal temperatures in the euphotic zone. *Paleoceanography* 4 (6), 593-601.

Spötl, C., Nicolussi, K., Patzelt, G., and Boch, R., 2010. Humid climate during deposition of sapropel 1 in the Mediterranean Sea: Assessing the influence on the Alps. *Global and Planetary Change*, *71*(3), 242-248.

Steinhilber, F., Beer, J. and Fröhlich,C., 2009. Total solar irradiance during the Holocene. *Geophysical Research Letters* 36(19), L19704.

Stocker, T. F., Qin, D., and Platner, G. K., 2013. Climate Change 2013: The Physical Science Basis. *Working Group I Contribution to the Fifth Assessment Report of the Intergovernmental Panel on Climate Change. Summary for Policymakers (IPCC, 2013).*

Sutton, R. and Hodson, D., 2003. Influence of the ocean on North Atlantic climate variability 1871-1999. *Journal of Climate* 16(20), 3296-3313.

Synal, H-A., Stocker, M. and Suter, M., 2007. MICADAS: A new compact radiocarbon AMS system. *Nuclear Instruments and Methods in Physics Research Section B: Beam Interactions with Materials and Atoms* 259 (1) (6), 7-13.

Syvitski, J. P. M., and Kettner, A.J., 2007. On the flux of water and sediment into the Northern Adriatic Sea. *Continental Shelf Research* 27 (3-4), 296-308.

Tesi, T., Langone, L., Goni, M. A., Miserocchi, S., Bertasi, F., 2007. Organic matter origin and distribution in suspended particulate materials and surficial sediments from the Western Adriatic Sea (Italy). *Estuarine, Coastal and Shelf Science* 73 (3-4), 431-446.

Tesi, T., Langone, L., Goni, M. A., Miserocchi, S., Bertasi, F., 2008. Changes in the composition of organic matter from Prodeltaic sediments after a Large Flood Event (Po River, Italy). *Geochimica Et Cosmochimica Acta* 72 (8), 2100-2114.

Theocharis A., and Georgopoulos D.,1993 Dense water formation over the Samothraki and Limnos Plateaux in the north Aegean Sea (eastern Mediterranean Sea). *Continental Shelf Research* 13, 919–939

Therrell, M. D., Stahle, D. W., Ries, L. P., and Shugart, H. H., 2006. Tree-ring reconstructed rainfall variability in Zimbabwe. *Climate Dynamics* 26(7-8), 677-685.

Thompson, D. W. J., and Wallace, J. M., 1998. The Arctic Oscillation signature in the wintertime geopotential height and temperature fields. *Geophysical Research Letters* 25**,** 1297–1300

Thompson, D. W., and Wallace, J. M., 2001. Regional climate impacts of the Northern Hemisphere annular mode. *Science 293*(5527), 85-89.

Thomson, J., Crudeli, D., De Lange, G. J., Slomp, C. P., Erba, E., Corselli, C., and Calvert, S. E, 2004. *Florisphaera profunda* and the origin and diagenesis of carbonate phases in eastern Mediterranean sapropel units. *Paleoceanography* 19(3), PA3003

Thomson, J., Croudace, I.W., Rothwell, R.G., 2006. A geochemical application of the ITRAX scanner to a sediment core containing eastern Mediterranean sapropel units. Geological Society, London, Special Publications 267, 65-77.

Tjallingii, R., Röhl, U., Kölling, M., Bickert, T., 2007. Influence of the water content on X-ray fluorescence core-scanning measurements in soft marine sediments. *Geochemistry, Geophysics, Geosystems* 8, Q02004.

Tjallingii, R., Claussen, M., Stuut, J.B.W., Fohlmeister, J., Jahn, A., Bickert, T., Lamy, F. and Röhl, U., 2008. Coherent high-and low-latitude control of the northwest African hydrological balance, *Nature Geoscience* 1 (10), 670-675.

Tomadin, L., 2000. Sedimentary fluxes and different dispersion mechanisms of the clay sediments in the Adriatic Basin. *Rendiconti Lincei* 9 (11): 161-174.

Toyofuku, T., Suzuki, M., Suga, H., Sakai, S., Suzuki, A., Ishikawa, T., de Nooijer, L.J., Schiebel, R., Kawahata, H., and Kitazato, H., 2011. Mg/Ca and $\delta^{18}O$ in the brackish shallow-water benthic foraminifer *Ammonia 'beccarii'*. *Marine Micropaleontology*, 78, 113-120.

Tribovillard, N., Algeo, T. J., Lyons, T., Riboulleau, A., 2006. Trace Metals as paleoredox and paleoproductivity proxies: an update. *Chemical Geology* 232 (1–2), 12-32.

Trigo, R., Xoplaki, E., Zorita, E., Luterbacher, J., Krichak, S.O., Alpert, P., Jacobeit, J., Sáenz, J., Fernández, J., González-Rouco, F., Garcia-Herrera, R., Rodo, X., Brunetti, M., Nanni, T., Maugeri, M., Türke, M., Gimeno, L., Ribera, P., Brunet, M., Trigo, I.F., Crepon, M., Mariotti, A., 2006. Chapter 3: Relations between variability in the Mediterranean region and mid-latitude variability, in: P. Lionello, P.M.-R., Boscolo, R. (Eds.), Developments in Earth and Environmental Sciences. Elsevier, 179-226.

Trincardi, F, Cattaneo, A., Correggiari, A., 2004. Mediterranean Prodelta Systems. *Oceanography* 17, 4-34.

Trincardi, F., Correggiari, A., and Roveri, M., 1994. Late Quaternary transgressive erosion and deposition in a modern epicontinental shelf: the Adriatic Semi-enclosed Basin. *Geo-Marine Letters* 14 (1), 41-51

Trouet, V., Esper, J., Graham, N. E., Baker, A., Scourse, J. D., and Frank, D. C., 2009. Persistent positive north Atlantic oscillation mode dominated the medieval climate anomaly. *Science* 324(5923), 78-80.

Turchetto, M., Boldrin, A., Langone, L., Miserocchi, S., Tesi, T. and Foglini, F., 2007. Particle transport in the Bari Canyon (southern Adriatic Sea). *Marine Geology* 246 (2-4), 231-247.

Van der Linden. R.A.M. and the SIDC team, online catalogue of the sunspot index, http://sidc.oma.be/html/sunspot.html

Van Morkhoven, F.P.C.M., Berggren, W.A., Edwards, A.S. and Oertli, H.J., 1986. Cenozoic cosmopolitan deep-water benthic foraminifera. *Elf Aquitaine* 11.

van Santvoort, P.J.M., de Lange, G.J., Langereis, C.G., Dekkers, G., and Paterne, M., 1997. Geochemical and paleomagnetic evidence for the occurrence of 'missing' sapropels in eastern Mediterranean sediments. *Paleoceanography* 12(6), 773-786.

Versteegh, G. J. M., de Leeuw, J. W., Taricco, C. and Romero, A., 2007. Temperature and productivity influences on U37K' and their possible relation to solar forcing of the Mediterranean winter. *Geochemistry, Geophysics, Geosystems* 8 (9), Q09005.

Vigliotti, L., Verosub, K. L., Cattaneo, A., Trincardi, F., Asioli, A., and Piva, A., 2008. Palaeomagnetic and rock magnetic analysis of Holocene deposits from the Adriatic sea: Detecting and dating short-term fluctuations in sediment supply. *The Holocene* 18(1), 141-152.

Vilibić, I. and Orlić, M., 2002. Adriatic water masses, their rates of formation and transport through the Otranto Strait. *Deep-Sea Research I* 49, 1321-1340.

Vilibić, I. and N. Supić, 2005. Dense water generation on a shelf: The case of the Adriatic sea. *Ocean Dynamics* 55(5-6), 403-415.

Vital, H., and Stattegger, K., 2000. Major and trace elements of stream sediments from the lowermost Amazon River. *Chemical Geology*, *168*(1), 151-168.

Vogts, A., Moossen, H., Rommerskirchen, F., and Rullkőtter, J., 2009. Distrubution patterns and stable carbon isotopic composistion of alkanes and alkan-1-ols from plant waxes of African rain forest and savannah C_3 species. *Organic Geochemistry* 40, 1037-1054

Von Breymann, M.T., Emeis, K.-C., and Suess, E., 1992. Water depth and diagenetic constraints on the use of barium as a palaeoproductivity indicator. Geological Society, London, Special Publications 64, 273-284.

Waelbroeck, C., Mulitza, S., Spero, H., Dokken, T., Kiefer, T. and Cortijo, E., 2005. A global compilation of late Holocene planktonic foraminiferal $\delta^{18}O$: Relationship between surface water temperature and δ^{18} O. *Quaternary Science Reviews* 24 (7), 853-68.

Wang, Y., Cheng, H., Edwards, R.L., He, Y., Kong, X., An, Z., Wu, J., Kelly, M.J., Dykoski, C.A. and Li, X., 2005. The Holocene Asian Monsoon: Links to Solar Changes and North Atlantic Climate. *Science* 308 (5723), 854-857.

Wanner, H., Beer, J., Bütikofer, J., Crowley, T.J., Cubasch, U., Flückiger, J., Goosse, H., Grosjean, M., Joos, J.O. Kaplan, M. Küttel, S.A. Müller, I.C. Prentice, O. Solomina, T.F. Stocker, P. Tarasov, M. Wagner, F. and Widmann, M., 2008. Mid- to Late Holocene climate change: an overview. *Quaternary Science Reviews* 27 (19–20), 1791-1828.

Wanner, H., Solomina, O., Grosjean, M., Ritz, S.P. and Jetel. M., 2011. Structure and origin of holocene cold events. *Quaternary Science Reviews* 30 (21), 3109-23.

Wassenburg, J.A., Immenhauser, A., Richter, D.K., Niedermayr, A., Riechelmann, S., Fietzke, J., Scholz, D., Jochum, K.P., Fohlmeister, J., Schröder-Ritzrau, A., Sabaoui, A., Riechelmann, D.F.C., Schneider, L. and Esper, J. 2013. Moroccan speleothem and tree ring records suggest a variable positive state of the North Atlantic Oscillation during the Medieval Warm Period. *Earth and Planetary Science Letters 375*, 291-302.

Wehausen, R., and Brumsack, H. J., 2000. Chemical cycles in Pliocene sapropel-bearing and sapropel-barren eastern Mediterranean sediments. *Palaeogeography, Palaeoclimatology, Palaeoecology 158*(3), 325-352.

Weijers, J.W.H., Schouten, S., Hopmans, E.C., Geenevasen, J.A.J., David, O.R.P., Coleman, J.M., Pancost, R.D., Sinninghe Damsté, J.S., 2006a. Membrane lipids of mesophilic anaerobic bacteria thriving in peats have typical archaeal traits. *Environmental Microbiology* 8, 648–657.

Weijers, J.W.H., Schouten, S., Spaargaren, O.C., Sinninghe Damsté, J.S., 2006b.Occurrence and distribution of tetraether membrane lipids in soils: implications for the use of the TEX^{86} proxy and the BIT index. *Organic Geochemistry* 37, 1680–1693.

Weiss, B., 1982. The decline of late bronze age civilization as a possible response to climatic change. *Climatic Change* 4 (2), 173-98.

Weldeab, S., Lea, D.W., Schneider, R.R. and Andersen, N., 2007. 155,000 years of West African monsoon and ocean thermal evolution. *Science* 316 (5829), 1303-7.

Weltje, G. J., and Tjallingii, R., 2008. Calibration of XRF core scanners for quantitative geochemical logging of sediment cores: Theory and application. *Earth and Planetary Science Letters*, *274*(3), 423-438.

Weltje, G.J., and Brommer, M. B., 2011. Sediment-Budget modelling of multi-sourced basin fills: Application to recent deposits of the Western Adriatic Mud Wedge (Italy). *Basin Research* 23 (3), 291-308.

Wilkin, R., Barnes, H., and Brantley, S., 1996. The size distribution of framboidal pyrite in modern sediments: An indicator of redox conditions. *Geochimica et Cosmochimica Acta* 60(20), 3897-3912.

Wit, J.C., de Nooijer, L.J., Barras, C., Jorissen, F.J., and Reichart, G.J., 2012. A reappraisal of the vital effect in cultured benthic foraminifer *Bulimina marginata* on Mg/Ca values: assessing temperature uncertainty relationships. *Biogeosciences* 9, 3693-3704.

Wit, J.C., de Nooijer, L.J., de Lange, G.J. and Reichart, G.J., 2013. A novel salinity proxy based on Na incorporation into foraminiferal calcite. *Biogeosciences* 10, 6375-6387.

Woodward, F. I., Lomas, M. R., and Kelly, C. K., 2004. Global climate and the distribution of plant biomes. Philos. Trans. R. Soc. Lond. *B* 359, 1465-1476.

Wu, P. and Haines, K., 1996. Modeling the dispersal of levantine intermediate water and its role in mediterranean deep water formation. *Journal of Geophysical Research* 101(C3), 591-6607.

Yang, S., Youn, J. S., 2007. Geochemical compositions and provenance discrimination of the central south Yellow Sea sediments. *Marine Geology*, 243(1), 229-241.

Yarincik, K. M., Murray, R. W., and Peterson, L. C., 2000. Climatically sensitive eolian and hemipelagic deposition in the Cariaco Basin, Venezuela, over the past 578,000 years: Results from Al/Ti and K/Al. *Paleoceanography*, *15*(2), 210-228.

Zanchetta, G., Drysdale, R. N., Hellstrom, J. C., Fallick, A. E., Isola, I., Gagan, M. K., and Pareschi, M. T., 2007. Enhanced rainfall in the Western Mediterranean during deposition of sapropel S1: stalagmite evidence from Corchia cave (Central Italy). *Quaternary Science Reviews*, *26*(3), 279-286.

Zeeden, C., Hilgen, F., Rohl, U., Seelos, K. and Lourens, L., 2014. An application to correct for cracks in core images. Submitted

Zhang, D. D., Lee, H. F., Wang, C., Li, B., Pei, Q., Zhang, J., and An, Y., 2011. The causality analysis of climate change and large-scale human crisis. *Proceedings of the National Academy of Sciences*, *108*(42), 17296-17301.

Ziegler, M., Jilbert, T., de Lange, G.J., Lourens, L.J., and Reichart, G.J., 2008. Bromine counts from XRF scanning as an estimate of the marine organic carbon content of sediment cores. *Geochemistry, Geophysics, Geosystems* 9 (5), Q05009.

Ziv, B., Saaroni, H., and Alpert, P., 2004. The factors governing the summer regime of the eastern Mediterranean. *International Journal of Climatology 24*(14), 1859-1871.

Ziveri, P., Stoll, H., Probert, I., Klaas, C., Geisen, M., Ganssen, G., and Young, J., 2003. Stable isotope 'vital effects' in coccolith calcite. *Earth and Planetary Science Letters* 210(1), 137-149.

Zonneveld, K.A.F., 1996. Palaeoclimatic reconstruction of the last deglaciation (18 ka. BP. - 8 ka. BP.) In the Adriatic Sea region: a land-sea correlation based on palynological evidence. *Palaeogeography Palaeoclimatology Palaeoecology* 122, 89-106.

Zonneveld, K. A. F. and cruise participants, 2008. Report and preliminary results of R/V POSEIDON cruise P339, piräus - messina, 16 june - 2 july 2006. CAPPUCCINO - calabrian and Adriatic palaeoproductivity and climatic variability in the last two millenia. *Berichte, Fachbereich Geowissenschaften* 268, 61-1.

Zonneveld, K. A. F., Chen, L., Möbius, J. and Mahmoud, M. S., 2009. Environmental significance of Dinoflagellate cysts from the proximal part of the Po-River discharge plume (Off Southern Italy, Eastern Mediterranean). *Journal of Sea Research* 62 (4), 189-213

Zonneveld, K.A.F., Chen, L., Elshanawany, R., Fischer, H.W., Hoins, M., Ibrahim, M.I., Pittauerova, D., and Versteegh, G.J.M., 2012. The use of dinoflagellate cysts to separate human-induced from natural variability in the trophic state of the Po River discharge plume over the last two centuries. *Marine pollution bulletin* 64, 114-132.

.

Samenvatting

Het klimaat in de toekomst

Door het gebruik van fossiele brandstoffen door de mens is de uitstoot van broeikasgassen sterk toegenomen. Naast een algehele opwarming van de aarde verwacht men dat dit ook zal leiden tot lokale veranderingen in neerslag en temperatuur. Sommige gebieden zullen mogelijk worden, terwijl anderen juist natter worden. Echter, tot noch toe geven verschillende klimaatmodellen uiteenlopende voorspellingen voor veranderingen in het toekomstige lokale klimaat. Een belangrijke oorzaak hiervan is dat veranderingen in het klimaat als gevolg van menselijk handelen en veranderingen met een natuurlijke oorzaak moeilijk van elkaar te onderscheiden zijn. Een beter begrip van de natuurlijke schommelingen in het klimaat zou dan ook de voorspellende waarde van de modellen kunnen verbeteren.

Solide datasets van instrumentale metingen gaan echter vaak niet verder terug dan enkele tientallen jaren, wat gelet op de duur van natuurlijke cycli te kort is om een betrouwbare voorspelling te kunnen doen. Zo word er door sommige deskundige geopperd dat er een periode van lagere zonneactiviteit en een daarmee samenhangend koeler klimaat op handen is. De laatste keer dat er zo een lage zonneactiviteit was, was tijdens de Kleine IJstijd (~1400-1850 na Chr.). De winterse taferelen tijdens deze koude periode werden vastgelegd op beroemde schilderijen van Hollandse meesters, zoals 'Winterlandschap met schaatsers' van Hendrick Avercamp (Fig. 1). Om de ontwikkeling van het klimaat beter te kunnen bestuderen zijn archieven nodig die verder teruggaan in de tijd dan ten minste 500 jaar en die dus onder andere ook het klimaat gedurende koude periodes zoals de Kleine IJstijd vastleggen.

Wie met behulp van een boor een sedimentkern uit de bodem van de zee haalt, heeft zo'n archief. Met elke meter dieper in de bodem ga je verder terug in de tijd. Maar ook koralen, boomringen, stalagmieten en ijskernen zijn zulke klimaatarchieven. Voor het aflezen van het archief gebruikt men zogenaamde 'proxies'. Proxies zijn meetbare chemische of fysische eigenschappen van bijvoorbeeld het sediment of de daarin aanwezige fossielen die klimaatsvariabelen zoals temperatuur of de hoeveelheid regenval reflecteren. Eerdere onderzoeken van deze archieven hebben al laten zien dat het klimaat in het verleden alles behalve stabiel was.

Holocene klimaatveranderingen

Onderzoek met behulp van proxies heeft aangetoond dat er wereldwijd zeer koude periodes zijn geweest waarin de poolkappen zich verder naar het zuiden strekten, de zogenaamde IJstijden, waarvan de laatste zo'n 11,500 jaar geleden eindigde. Ook tijdens het Holoceen, de periode vanaf de laatste IJstijd tot het heden, is het klimaat alles behalve stabiel gebleven. Dit is bijzonder omdat tijdens deze periode de randvoorwaarden voor klimaatsverandering, zoals het de afwezigheid van grote ijskappen, hetzelfde zijn als nu. Met andere woorden: het Holocene klimaat vormt de natuurlijke

achtergrond waartegen de menselijke invloed op het klimaat kan worden bepaald.

De Holocene klimaat geschiedenis word gekenmerkt door abrupte klimaatveranderingen (AKV's), waaronder de Kleine IJstijd (~1400-1850 na Chr.), maar bijvoorbeeld ook een warme periode tijdens de middeleeuwen, het middeleeuwse klimaat optimum (MKO, ~1200 na Chr.). Deze veranderingen zijn weliswaar van een kleinere omvang dan die van de IJstijd naar Holoceen, maar lijken een grote impact gehad te hebben op lokale klimaat fluctuaties wereldwijd. De verschillen in de expressie van klimaatsverandering op een lokaal niveau en dus een gebrek aan een wereldwijd synchroon patroon is zeer waarschijnlijk te wijden aan veranderingen in de atmosferische circulatie tijdens AKV's (zie Fig. 1, **hoofdstuk 1**).

Fig. 1: Winterlandschap met schaatsers, Hendrick Avercamp, ca. 1608 na Chr.

Op lagere breedtegraden, dicht bij de evenaar, worden de verschillen in neerslag grotendeels bepaald door de intensiteit en positie van de zogenaamde Intertropische convergentiezone (ITCZ), waar tropische luchtstromen van het noordelijk en zuidelijk halfrond samenkomen. Hier ontstaat een gebied met een lage luchtdruk, waar opstijgende lucht zorgt voor veel neerslag en het vrijkomen van opgeslagen warmte Gedurende het jaar verandert de positie van de ITCZ; in de zomer ligt hij noordelijker dan in de winter. Dit proces ligt ten grondslag aan de moesson, de regens in onder andere de Sahel en India. In het noordelijker gelegen Europa daarentegen wordt de hoeveelheid neerslag voornamelijk beïnvloed door de westenwind, die vocht van de Atlantische Oceaan naar het vasteland brengt. Variaties in de richting van de westenwind worden gelinkt aan de Noordelijke Atlantische Oscillatie (NAO). Dit is een index die het verschil in atmosferische druk tussen het subpolaire lagedrukgebied boven IJsland en het subtropische hogedrukgebied boven de Azoren weergeeft. Als dit verschil groot is, een positieve NAO (NAO+), worden de westenwinden geblok-

keerd en verplaatsen zij zich noordwaarts waardoor het natter is in het noorden van Europa. Nabij de polen, tenslotte, is de AO-index van belang, die het drukverschil weergeeft tussen de polen en het gebied op 37-45°noorderbreedte. Bij een negatieve AO (AO-)zijn de poolgebieden relatief koud en is er een grote kans dat koude lucht ontsnapt naar Noord-Amerika, Azië en Europa.

Aangezien de meeste AKV's gepaard gaan met relatief koude poolgebieden en weinig neerslag nabij de evenaar, is het aannemelijk dat variaties in de genoemde patronen van de ITCZ en de AO hierbij betrokken zijn. Ook in het gebied tussen de polen en de tropen speelt de verandering in atmosferische circulatie patronen een grote rol. De geobserveerde omslag in noordwest Europa van het warme en natte klimaatoptimum in de Middeleeuwen naar de koudere en drogere Kleine IJstijd kan bijvoorbeeld verklaard worden door een verandering in de NAO. Het lijkt het erop dat tijdens AKV's, zoals de bovengenoemde omslag, voornamelijk het klimaat van het winterseizoen veranderde. Hierdoor lijken de gemiddelde verschillen tussen jaren minder groot, maar kunnen er wel grote verschillen tussen de seizoenen gedurende het jaar voorkomen. De regionale veranderingen en veranderingen in het contrast tussen de seizoenen lijken een grote invloed te hebben gehad op de menselijke beschaving. Zo valt de val van de Maya-beschaving samen met een korte droge periode van ongeveer honderd jaar. Maar ook de val van het Romeinse Rijk en de onrust van de 'grote volksverhuizing' die daarop volgde lijken samen te vallen met korte periodes van klimaatsverandering. Het is echter nog steeds onduidelijk welke processen klimaatsveranderingen op deze korte tijdschalen kunnen veroorzaken.

Veranderingen in zonneactiviteit is één van de mogelijke oorzaken van de AKV's tijdens het Holoceen. Zonneactiviteit hangt af van het aantal zonnevlekken, dat toe- en afneemt volgens bepaalde cycli die tientallen, soms wel honderden jaren kunnen duren. Zo viel een deel van de Kleine IJstijd samen met een periode van zeer lage zonneactiviteit, het zogenaamde Maunder Minimum. De directe invloed van zonneactiviteit op het klimaat is echter gering; slechts één procent van veranderingen in het warmtebudget op aarde kan worden verklaard door een verandering van het aantal zonnevlekken. Wel hebben schommelingen in de ultraviolette straling (~10% verschil tussen minima en maxima) een groot effect op wolkenvorming in de hoger gelegen stratosfeer, wat indirect van invloed kan zijn op de circulatiepatronen in de atmosfeer. Naast de zonneactiviteit spelen de oceanen en hun warmtebudget mogelijk ook een belangrijke rol tijdens AKV's. Een goed voorbeeld hiervan is het verschijnsel El Niño, waarbij een relatief hoge temperatuur van het oppervlaktewater van de Grote Oceaan zorgt voor meer neerslag in de Andes, maar in Australië juist leidt tot veel droogte. Het effect van variaties in El Nino activiteit (ENSO), beperkt zich niet alleen tot de regio's rondom de Grote Oceaan, maar heeft via verschillende schakelingen in het klimaatsysteem ook een invloed op het weer in de rest van de wereld. Ook in de Atlantische oceaan zijn er patronen waargenomen in de temperatuurveranderingen van het oppervlaktewater. Een typische periode van dit patroon, van relatief koud naar relatief warm oppervlaktewater, neemt ongeveer 70 jaar in beslag. Er blijkt een duidelijke connectie te zijn tussen droogte in de Sahel, en dus in zekere mate de ITCZ,

en de oppervlaktetemperaturen van de Atlantische Oceaan. Het effect van deze temperatuurschommelingen op het klimaat van noordelijker gelegen gebieden is echter nog niet eenduidig.

Het Middellandse zeegebied als klimaatarchief

Een geschikte plaats voor het onderzoek naar de mogelijke veranderingen in atmosferische circulatie tijdens AKV's is het Middellandse Zeegebied, waar het klimaat niet alleen wordt bepaald door veranderingen in de ITCZ en NAO, maar ook de AO. In de zomer, als de ITCZ naar het noorden beweegt, ontstaat er een hogedrukgebied boven het Middellandse Zeegebied. Dit hogedrukgebied blokkeert de westenwinden, die normaal veel regen brengen, en zorgt voor de karakteristieke droge, mediterrane zomer. In de winter, als de ITCZ en het hogedrukgebied weer naar het zuiden zijn teruggekeerd, bereiken deze westenwinden wel het gebied en valt er doorgaans meer regen. Hoeveel regen er precies valt hangt dan af van de NAO; als deze in een negatieve modus is volgen de westenwinden een meer zuidelijkere route en zal er meer neerslag zijn dan wanneer hij in een positieve modus is. Verder zorgen tijdens het winterseizoen koude winden afkomstig van de polen, bekend als de Bora in Italië en de Mistral in Zuid-Frankrijk voor relatief lage temperaturen, want samenhangt met de AO.

De invloed van de verschillende klimaatsystemen op het Middellandse Zeegebied is misschien wel het meest duidelijk tijdens de vorming van zogenaamde sapropelen die gevonden worden in sedimenten van de Middellandse Zee. Deze sapropelen zijn veel donkerder van kleur doordat ze rijker in organisch materiaal zijn dan de sedimenten er omheen (zie Fig. 2, **hoofdstuk 1**). De laatste sapropel werd circa 10.000 tot 6000 jaar geleden gevormd toen het klimaat in noordelijk Afrika veel natter was door toedoen van een noordelijker gelegen ITCZ. De grotere hoeveelheid regen zorgde voor een grote uitstroom van zoet water van de Nijl in de Middellandse Zee. Meer rivierwater betekent ook meer nutriënten en dus ook meer productie van organisch materiaal. Bovendien heeft zoet water een lagere dichtheid dan zeewater, waardoor het minder makkelijk mengt met het diepere zeewater en er minder zuurstof naar de bodem van de Middellandse Zee gebracht kan worden. Onder zuurstofarme condities is het veel moeilijker om organisch materiaal aftebreken, en blijft er dus ook meer organisch materiaal bewaard. Tijdens het vormen van de laatste sapropel zo'n achtduizend jaar geleden werd deze zuurstofarme omgeving echter verstoord. Er wordt aangenomen dat koude lucht van de polen het oppervlaktewater van de Adriatische en Egeïsche zeeën dermate afkoelde, tijdens deze relatief koude periode, dat het begon te zinken. Dit proces zorgde vervolgens voor meer zuurstofrijke condities op de bodem van de oostelijke Middellandse Zee, wat de vorming van de karateristieke organischrijke sapropel tegenging.

Door zijn unieke positie is het Middellandse Zeegebied uitermate geschikt om korte klimaatsveranderingen in het Holoceen te onderzoeken. De snelheid van sediment afzetting (sedimentatiesnelheid) in de Middellandse Zee is doorgaans echter erg laag. Hierdoor ontbreekt dus vaak de benodigde resolutie voor Holoceen klimaatonder-

zoek. Een uitzondering hierop wordt gevormd door een kustgebied in het oosten van Italië. Hier brengen de Po en enkele anderen rivieren grote hoeveelheden sediment van het vasteland naar de Adriatische Zee, waar het onder invloed van de zeestroming wordt verspreid van de oostelijke Italiaanse kust tot aan de Golf van Tarante in het zuiden (zie Fig. 3, **hoofdstuk 1**). De grote hoeveelheid sediment zorgt voor hoge sedimentatiesnelheden, en dus de benodigde resolutie voor Holocene klimaatstudies. Bovendien bevatten sedimenten genomen in het zuidelijkste deel van dit gebied signalen van zowel noordelijke als zuidelijk Italiaans rivieren, en geven ze dus informatie over een groter gebied dan kernen in de meer noordelijke delen van de Adriatische zee. Om het klimaat in dit gebied te reconstrueren is het echter van belang dat we eerst begrijpen waar het sediment nu precies vandaan komt en hoe het zich tegenwoordig verspreidt (zie **hoofdstuk 2 en 3**).

Proxies voor het lezen van het klimaatarchief

Zoals eerder genoemd zijn proxies van belang voor het aflezen van het archief. In dit proefschrift gebruiken we hiervoor eigenschappen van het sediment, maar ook eigenschappen van bepaalde fossielen die er in bewaard zijn.

Het sediment

Eigenschappen van het sediment die gebruikt kunnen worden, zijn de chemische eigenschappen van het sediment, maar ook de korrelgrootte en de kleur van het sediment. Voordat het sediment wordt afgezet op de bodem van de zee legt het een lange weg af. Sediment ontstaat door erosie van een gesteente met een bepaalde chemische samenstelling. Op basis van de verschillen in de gesteentes waaruit het sediment is ontstaan kunnen we dus in principe ook herkennen waar het materiaal oorspronkelijk vandaan komt. Sediment kan geërodeerd worden onder verschillende omstandigheden. Droge omstandigheden zorgen voor andere chemische eigenschappen van het sediment dan natte omstandigheden. Op deze manier worden dus ook veranderingen in het klimaat opgeslagen in het sediment. Omstandigheden tijdens het transport van land naar zee beïnvloeden ook de korrelgrootte van het sediment. Sedimenttransport via wind of via rivieren leidt tot verschillende korrelgroottes maar ook tot andere chemische eigenschappen. Een deel van het sediment wordt ook in de zee zelf gevormd. Primaire productie in het oppervlaktewater zorgt voor grote hoeveelheden organische koolstof, carbonaat en opaal die op de zeebodem bewaard kunnen blijven. Lagen rijk aan organisch materiaal zijn vaak donkerder van kleur dan andere lagen. Als condities op de zeebodem relatief zuurstofarm zijn, neemt de kans dat organisch materiaal bewaard blijft toe. Onder de zuurstofarme condities worden er andere chemische reacties in gang gezet dan in zuurstofrijke condities. Sporenelementen zoals vanadium en molybdeen spelen een belangrijke rol in deze reacties onder zuurstofarme condities en kunnen gebruikt worden als indicatoren voor zuurstoffloosheid.

De elementsamenstelling van het sediment kan op verschillende manieren bepaald worden. Zo kan men het sediment oplossen in een sterk zuur en vervolgens meten met behulp van bijvoorbeeld inductief gekoppeld plasma (ICP) en een daaraan

gekoppelde massaspectrometer (MS). Voor hoge resolutie studies (een resolutie fijner dan een millimeter) kan een laser gebruikt worden om een kleine hoeveelheid intact sediment te analyseren met ICP-MS. Ook met behulp van röntgenstraling kan tot op zekere hoogte de samenstelling van het sediment worden bepaald. Met deze zogenaamde XRF techniek hoeft geen sediment te worden opgelost en kan een genomen kern in principe geheel bewaard blijven. Voor studies op hoge resoluties, zoals in dit proefschrift, kan ook een micro-XRF-scanner worden gebruikt die een veel hogere resolutie heeft dan de reguliere XRF kern scanner. Bovendien kan met deze methode, in tegenstelling tot de laser-ICP-MS methode, de chemische samenstelling over het gehele oppervlak van de kern in kaart gebracht worden. Op deze manier kunnen ook meer heterogene patronen in de chemische samenstelling worden herkend.

Foraminiferen

In het sediment blijven allerlei fossielen bewaard. Een groot gedeelte hiervan bestaat uit de overblijfselen van foraminiferen, eencellige organismen die van in de zeebodem (benthische foraminiferen) tot en met het wateroppervlak (planktonische foraminiferen) van de zee voorkomen. Sommige foraminiferen maken een kalkskelet aan, waarvan de chemische samenstelling mede bepaald wordt door de temperatuur en het zout- en nutriëntgehalte van het water. Verandering van deze drie variabelen leidt tot een andere soorten zuurstof- en koolstofisotoop samenstelling van het water, die zijn terug te vinden in het kalkskelet. Met behulp hiervan kunnen we dus de omstandigheden waarin de foraminiferen hebben geleefd reconstrueren.

In het onderzoeksgebied in de Adriatische Zee is de uitstroom van zoetwaterrivieren, en daarmee verlaging van het zoutgehalte, goed af te lezen aan de zuurstofisotopen van de planktonische foraminifeer *Globigerinoides ruber*. Meer uitstroom zorgt bovendien voor een toename van voedingsstoffen die hogere productie van organisch materiaal in gang zetten. Door deze hoge productiviteit dringt er veel minder licht door de waterkolom heen. Omdat *G. ruber* in symbiose leeft met organismen die afhankelijk zijn van fotosynthese, is hij gedwongen om dichter bij het wateroppervlak te gaan leven. Hier zorgt de verandering in symbiontenactiviteit voor een andere koolstofisotopensamenstelling van het kalkschaaltje gevormd door de foraminifeer.

Naast zuurstof en koolstof bestaat het het kalkskelet ook uit magnesium en calcium, waarvan de onderlinge verhouding onder andere bepaald wordt door de temperatuur van het water op het moment van ontstaan. Dit effect komt het sterkst tot uitdrukking bij de soort *Hyalinea balthica*, waar een lichte stijging van de temperatuur al kan leiden tot een relatief grote toename van het magnesiumgehalte. Omdat veranderingen in temperatuur tijdens het Holoceen marginaal zijn, lijkt het gebruik van deze soort dus ideaal voor het bestuderen van het veranderingen in het klimaat tijdens deze periode.

Met behulp van een laser kan de chemische samenstelling van verschillende kamers van een enkele foraminifeer worden vastgesteld. Als een foraminiferensoort gedurende het hele jaar voorkomt, kan door het bepalen van de Mg/Ca van meerdere individuen de spreiding in temperatuur, en dus de contrasten tussen de seizoenen,

worden bepaald. Bovendien kan na het bepalen van de Mg/Ca waarde, de zuurstofisotopensamenstelling van hetzelfde individu worden bepaald. Door deze twee waardes te combineren kan dan in principe de oorspronkelijke zuurstofisotopenwaarde van het zeewater, en dus tot op zekere hoogte de saliniteit van het water, worden bepaald. Beide methodes kennen echter een grote onzekerheidsfactor, die toeneemt wanneer ze gezamenlijk worden toegepast. Het is daarom beter om het zoutgehalte van het water afzonderlijk te bepalen aan de hand van een andere eigenschap, de natrium – calcium verhouding (Na/Ca).

Dit proefschrift

Het doel van dit onderzoek is om de ontwikkeling van het klimaat tijdens het Holoceen in kaart te brengen. Hiervoor worden afzettingen op de bodem van de Adriatische Zee en de Golf van Tarente bestudeerd. Niet alleen hebben kernen uit deze gebieden de benodigde hoge resolutie, door hun ligging bieden ze bovendien ook informatie over klimaatsveranderingen in de tropen en de meer noordelijkere gebieden en de interactie tussen beide.

Om klimaatsveranderingen te reconstrueren op basis van de chemische samenstelling van het sediment in deze gebieden, moet men eerst begrijpen hoe het huidige sedimentverspreidingssysteem werkt. Tot op heden is er nog niet veel bekend over de exacte herkomst van sediment in onze onderzoeksgebieden en hoe deze sedimenten zich verspreiden in het gebied. In **hoofdstuk 2** van dit proefschrift proberen we meer inzicht te krijgen in deze mechanismen in ons studiegebied door de chemische samenstelling van sedimenten van de bovenste centimeters van de zeebodem te bepalen. Deze resultaten worden vervolgens vergeleken met de chemische samenstelling van monsters genomen in Italiaanse meren en rivieren. Op basis van deze vergelijking blijkt dat sedimenten van een Noord-Italiaanse origine zijn te onderscheiden van sedimenten die een herkomst in Zuid-Italië hebben door middel van de verhouding tussen de sporenelementen cesium en nikkel (Ce/Ni) en tussen zirkoon en chroom (Zr/Cr) in het sediment. Belangrijk is dat deze verhouding los staat van de korrelgrootte van het sediment, en dus het transportmechanisme. De herkomst van organisch materiaal (marien of terrestrisch) kan bepaald worden met behulp van koolstofisotopen en de verhouding tussen koolstof en stikstof (C/N) van het organisch materiaal. Door het combineren van deze resultaten met die van andere studies aan dezelfde monsters blijkt dat:

- sedimenten van noordwestelijk Adriatische origine door de West-Adriatische zeestroom tot aan de oostelijke Golf van Tarente gebracht kunnen worden;

- tijdens het transport door de West-Adriatische zeestroom richting de Golf van Tarente de hoeveelheid materiaal met een meer noordelijke herkomst (Po en andere noordelijke rivieren) afneemt, terwijl het percentage organisch materiaal gevormd in de zee zelf juist toeneemt;

- ongeveer 80 procent van de sedimenten in de oostelijke Golf van Tarente uit

materiaal met een meer noordelijke herkomst bestaat, terwijl de andere 20 procent een meer Zuid-Italiaanse herkomst heeft;

- lokale rivieren de bron van organisch materiaal en sedimenten in de westelijke Golf van Tarente vormen, dit in tegenstelling tot de oostelijke Golf van Tarente.

In **hoofdstuk 3** presenteren we de resultaten van een uitgebreid en gedetailleerd onderzoek naar patronen in de verspreiding van sedimenten in het onderzoeksgebied gedurende de afgelopen 16.000 jaar. Hiervoor werd de elementensamenstelling van 11 kernen uit de Gulf van Tarente, de Zuidelijk Adriatische Zee en de Ionische zee bepaald met behulp van metingen met röntgenstraling (XRF). Op basis van de chemische samenstelling van kernen genomen in de oostelijke Golf van Tarente en de zuidelijke Adriatische Zee en patronen daarin, kan geconcludeerd worden dat beide gebieden door dezelfde factoren worden beïnvloed. Dit in tegenstelling met de patronen geobserveerd in kernen genomen in de westelijke Golf van Tarente en de Ionische Zee die beïnvloed lijken te worden door andere processen. Dateringen met behulp van koolstof-14 en de overeenkomsten in patronen in de chemische samenstelling zijn vervolgens gebruikt om alle kernen in de oostelijke Gulf van Tarente precies te dateren. Met behulp van deze gedateerde kernen en hun chemische samenstelling kunnen vervolgens de veranderingen in omgevingsvariabelen in het onderzoeksgebied sinds de laatste ijstijd worden beschreven. Op basis van deze reconstructie blijkt dat:

- gedurende een warme periode, tijdens het over het algemeen aangenomen koude en droge Jonge Dryas (~12.900-11.500 jaar geleden), er veel regen viel in Zuid-Italië, terwijl Noord-Italië droog bleef;

- sinds zo'n 7.000 jaar geleden de hoeveelheid materiaal dat wordt getransporteerd van de Adriatische Zee naar de Golf van Tarente toeneemt. Deze periode komt overeen met het einde van de periode waarin de laatste sapropel werd gevormd, maar valt ook samen met een stijging van de zeespiegel en de start van de vorming van diep water in de noordelijke Adriatische Zee;

- vanaf circa 6.000 jaar geleden er korte periodes waarneembaar zijn waarin er meer materiaal van terrestrische oorsprong wordt getransporteerd naar de Golf van Tarente. Deze periodes lijken overeen te komen met periodes waarin een meer negatieve NAO regenval in Italië bevorderde.

In **hoofdstuk 4** combineren we de chemische samenstelling van een kern uit de Golf van Tarente met de chemische samenstelling van de kalkschaaltjes van de foraminiferensoorten *Globigerinoides ruber* en *Hyalinea balthica* voor een gedetailleerde klimaatreconstructie van de laatste 3.500 jaar. Regenval in het Middellandse Zeegebied wordt over het algemeen het meeste beïnvloed door het blokkeren van de westenwinden in de zomer door het verschuiven van de zogenaamde Hadley cel. De zuidelijke tak van de subtropische Hadley cel staat bekend als de ITCZ. In de winter wanneer de Hadley cel noordelijker ligt domineren de westenwinden, en dus de NAO, de regenval in het

gebied. Omdat *G. ruber* voornamelijk in de zomer groeit, kan aangenomen worden dat zijn koolstoofisotopensamenstelling veranderingen in zomerregen, en dus de ITCZ, weergeeft. Omdat het water in de Golf van Tarente in de winter beter mengt dan in de zomer, worden de eigenschappen van het bodemwater voornamelijk bepaald door wintercondities. De Na/Ca waarde van de benthische soort *H. balthica* reflecteert daarom veranderingen in het zoutgehalte van de waterkolom in de winter, en dus variabiliteit van de NAO. Zowel de koolstofisotopen van *G. ruber* en de Na/Ca van H. balthica laten cyclische patronen zien met een lengte van enkele honderden jaren gedurende de laatste 3.000 jaar. Hoe het winter- en zomerklimaat zich ten opzichte van elkaar verhouden lijkt echter te variëren. Deze veranderingen worden waarschijnlijk deels gestuurd door variaties in de oppervlaktewatertemperatuur in de Atlantische Oceaan. Als het oppervlaktewater in de Atlantische Oceaan erg warm is of onder invloed van het klimaatfenomeen El Niño wordt het winter klimaat meer beïnvloed door deze oppervlaktetemperaturen. Dit in tegenstelling tot de zomercondities die met veranderingen in de ITCZ samenhangen, en continu beïnvloed worden door de Atlantische Oceaan.

In **hoofdstuk 5** wordt de chemische samenstelling (Mg/Ca, zuurstof- en koolstofisotopen) van individuele kalkschaaltjes van *G. ruber* gebruikt om veranderingen in de seizoenen gedurende de laatste 3.000 jaar te bepalen. Hiervoor worden monsters gebruikt van bepaalde periodes die overeenkomen met AKV's. De resultaten van deze aanpak worden gecombineerd met hoge resolutie (<15 jaar per monster) oppervlaktewaterreconstructies voor zowel het zomer- en winterseizoenen door middel van de eerder genoemde soorten *G. ruber* (zuurstofisotopen) en *H. balthica* (Mg/Ca). Veranderingen in de verschillen tussen het winter- en zomerseizoen zijn voornamelijk merkbaar in veranderingen in neerslag, in tegenstelling tot verschillen in temperatuur. Ondanks de kleine verschillen in temperatuur zijn de winters tijdens de Bronstijd (~1000 V. Chr.) en Kleine IJstijd (~1400-1850) relatief koeler dan gedurende de andere bestudeerde periodes. Echter, terwijl tijdens de Kleine IJstijd een winterachtig, nat en koud klimaat gedurende het hele jaar waarneembaar is, is het tijdens de Bronstijd extreem droog tijdens zowel het zomer- als het winterseizoen. Opvallend is dat deze periode van extreme droogte samenvalt met de val van enkele befaamde beschavingen in het Middellandse Zeegebied.

In **hoofdstuk 6** bestuderen we een gelamineerde kern uit de zuidelijke Adriatische Zee, die gevormd werd tijdens het ontstaan van de laatste sapropel in de oostelijke Middellandse Zee. De diepte van de bodem waar de kern is genomen valt in grensgebied tussen de zuurstofarme bodemwaters en de meer zuurstofrijke oppervlaktewaters ten tijde van de laatste sapropel. Samen met de aanwezigheid van laminaties en de hoge sedimentatiesnelheid maakt dit deze kern geschikt voor een geochemische studie van zuurstofcondities op een zeer hoge resolutie tijdens het vormen van de laatste sapropel. Eerst bepalen we met behulp van geavanceerde technieken, zoals de laser-ICP-MS en micro-XRF, de verschillen in samenstelling tussen de lichte en de donkere sedimentlagen. In de donkere laminiaties worden niet alleen hogere waardes gevonden van het redox-gevoelige element vanadium maar ook pyrieten, die een framboo-

sachtige structuur hebben. Hieruit blijk dat, in tegenstelling tot de lichtere laminaties, de donkere laminaties gevormd zijn tijdens overwegend zuurstofarme condities. De variaties in de kleur van het sediment, van donker en licht, worden vervolgens gebruikt om variaties in zuurstofcondities te reconstrueren. Hieruit blijkt dat deze condities niet alleen variëren op tijdschalen van enkele honderden of tientallen jaren, maar zelfs binnen acht jaar. Vergelijking met andere klimaatreconstructies van deze periode en met recente instrumentele klimaatwaarnemingen laat zien dat de patronen overeenkomen met variaties in het uitbreken van winden van de polen naar het Middellandse Zeegebied. Waarschijnlijk initieerden deze poolwinden het ontstaan van zuurstofrijk diep water in de Adriatische Zee, dat vervolgens mogelijk de rest van de oostelijke Middellandse Zee van zuurstof kon voorzien.

Acknowledgments

A boat does not sail without a crew, just like there is not one person who can finish a PhD without some help (not even Dr. Topper). So **thank you** for your patience, support, (scientific) contributions, help, coffee (cards), cups of tea, time, (small) talk, and company during dancing, eating, sports, etc.

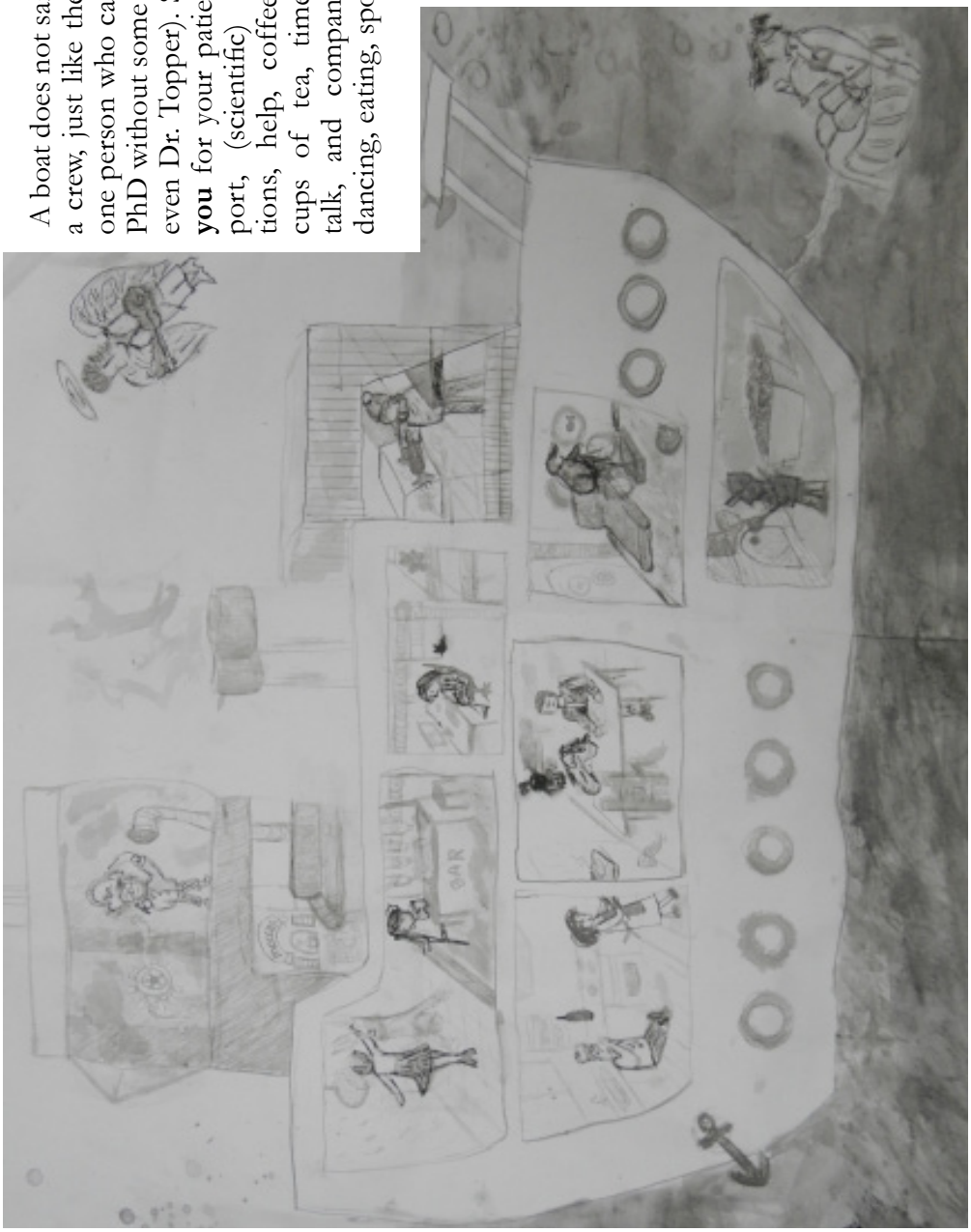

Dank je wel: promoter and co-promoter (Gert en Gert-Jan bedankt voor de unieke kans, jullie eerlijkheid, inzet en interesse), dissertation committee (ik kijk al 4 jaar uit naar die ene moeilijke vraag Jack!), all MOCCHA group members, co-authors, reviewers, lab technicians at UU and the NIOZ, my bachelor students : Joeri, Jessica en Sjoerd, all members of the geochemistry group and other colleagues and students at UU (e.g. Marieke, Emmy, Julia, Lennard, Peter B, Sander, Helen, Joost, Matthias, Nikki, Amir, Alejandra, Amalia (Thank you for being there during that awkward moment in your office), Anne, Iris, Melanie, Peter K, Iana, Tom, Fati, and many more in no particular order), thee drinkers Jos en Els, the running group, en de koffiekaarten van en het nakijken door Mathilde en Alwina, my office mates over the years (Claudia, Jiawang, Hamid, some Spanish people;) en n.b. Rick & Anna zonder jullie geen mexicaanse hoedjes, Arie in een Daphnia pak, snoepjes, of avondjes Derrick!), everybody onboard of the Macchiato, Ristretto é Lungo and Café Cortado cruise (e.g. Sediment trap girls!, the Bulgarian chicks and Spanish Guapa's), my Urbino people (e.g. Robin, Joyce, Itzel, Johan, Nele & Audrey) everyone at Ekko Serveert and Atelier van Wees, my friends (e.g. dLaor, Groepje 1.5, Vera, deWookies, D. & Ca$h, Nadine, Marijke en Eef!), paranimfen and my great family (de beste Mama, de beste broer (Flip), de beste zus (Rochelle),the best Dad, de beste tante (Hella), de beste 'oom' (Peter) & de beste peetoom (Henny) van de wereld).

As I could write another 157 pages thanking people and I would still forget to thank the most important people, I left some space for a handwritten, personal message just for you!:)

(your personal message)

Curriculum Vitae

Marie-Louise Sophie Goudeau was born on the 14th of October, 1983 in Sapulpa, Oklahoma (United States of America). In 1986 the Goudeau family moved to the Netherlands. There, Marie-Louise graduated from secondary school (VWO) at the Scholengemeenschap 'de Goudse Waarden' in Gouda in 2002. Subsequently she started studying 'Biology' at Utrecht University specialising in Biogeology. After obtaining her Bachelor of Science in Biology in 2005, she took a short hiatus from her studies to travel around Southeast- Asia and India. In 2006 she started her master 'Biogeology' at the Earth sciences faculty of Utrecht University. During her masters she studied benthic foraminiferal assemblages from Indo-Pacific coral reefs (Berau and Pulau Seribu, Indonesia) and a coral aquarium (Burgers' Ocean, the Netherlands) under supervison of Sander Ernst and Gert-Jan Reichart (Utrecht University), Willem Renema (Naturalis Biodiversity center) and Max Janse (Burgers' Zoo, Arnhem). Furthermore, she reconstructed primary productivity variabitlity in the Northern Arabian Sea during the Pleistocene using coccolith assemblages as a proxy. This was under supervison of Martin Ziegler, Lucas.J. Lourens (Utrecht University) and Luc Beaufort (CNRS-Cerege, Aix-en-Provence, France). For this study she worked three months at the laboratory of CNRS-Cerege, Aix-en-Provence, France. In 2008 she obtained her masters degree after which she shortly worked as a Junior Palynologist for the GeoBiology group of TNO. In May 2009 she started her PhD under supervision of Prof.Gert J. de Lange and Gert-Jan Reichart at the faculty of Geochemistry of Utrecht University, which resulted in this thesis.